# MICROBIAL INTERACTIONS AND THE ROLE OF ENVIRONMENTAL STRESS IN NATURAL AND SYNTHETIC CONSORTIA

by

Ashley Esther Beck

A dissertation submitted in partial fulfillment
of the requirements for the degree

of

Doctor of Philosophy

in

Microbiology and Immunology

MONTANA STATE UNIVERSITY
Bozeman, Montana

April 2018

# ACKNOWLEDGMENTS

This dissertation would not have been possible without a host of wonderful and supportive people.

- My funding sources: the Molecular Biosciences Program at Montana State University, Pacific Northwest National Laboratory, and the National Science Foundation.
- My adviser, Dr. Ross Carlson: thank you for mentoring me and guiding me through my Ph.D.
- My committee members (Dr. Jeffrey Heys, Dr. Robin Gerlach, Dr. Matthew Fields, and Dr. Seth Walk): thank you for your advice and input in my work.
- My incredible laboratory colleagues, past and present, especially Dr. Kristopher Hunt, Dr. James Folsom, Dr. Heidi Schoen, Dr. Hans Bernstein, Dr. Heejoon Park, and Lee McGill: I am grateful for all I have learned from you.
- My mentors in the Education Department, especially Dr. Tricia Seifert and Dr. Sarah Schmitt-Wilson: thank you for sharing your wisdom.
- My friends, roommates, and family, especially William Moore and Carl Fahlstrom: thank you for dragging me along on outdoor adventures and helping me maintain sanity.

TABLE OF CONTENTS

1. INTRODUCTION .....1

1.1. Environmental Stress and Metabolic Acclimation .....1
1.2. Modeling Metabolism .....2
1.3. Microbial Interactions and Metabolite Exchange .....3
1.4. Synthetic Ecology .....3
1.5. Ecological Theories for Microbial Community Structure .....4
1.6. Combining Theory, *In Silico* Simulations, and *In Vitro*/*In Vivo* Experiments .....5
1.7. Overview of Chapters .....5

2. INTERPRETING AND DESIGNING MICROBIAL COMMUNITIES FOR BIOPROCESS APPLICATIONS, FROM COMPONENTS TO INTERACTIONS TO EMERGENT PROPERTIES .....8

Contribution of Authors and Co-Authors .....8
Manuscript Information Page .....9
2.1. Introduction .....10
2.2. Definitions .....11
2.2.1. Community Components .....13
2.2.2. Interaction Outcomes .....15
2.2.3. Interaction Mechanisms .....16
2.2.4. Emergent Properties .....19
2.3. Ecological Theories for Interpreting and Designing Communities .....20
2.3.1. Maximum Power Principle .....20
2.3.2. Resource Ratio Theory .....21
2.3.3. Resource Allocation Theories: Pareto Surfaces and Metabolic Tradeoff Analysis .....25
2.4. Case Studies of Communities with Interpretation .....31
2.4.1. Case Study: Multilevel Interactions in a Naturally Occurring Phototrophic Community .....33
2.4.1.1. Community Description .....33
2.4.1.2. Interaction Mechanisms .....34
2.4.1.3. Theory Applications .....35
2.4.2. Case Study: Anaerobic Syntrophy in Methanogenic Communities .....36
2.4.2.1. Community Description .....36
2.4.2.2. Interaction Mechanisms .....36
2.4.2.3. Theory Applications .....37
2.4.3. Case Study: Cross-Feeding Chemostat Communities .....38
2.4.3.1. Community Description .....38
2.4.3.2. Interaction Mechanisms .....39
2.4.3.3. Theory Applications .....40

TABLE OF CONTENTS CONTINUED

2.5. Conclusions....41
2.6. Acknowledgments....42

3. MEASURING CELLULAR BIOMASS COMPOSITION FOR COMPUTATIONAL BIOLOGY APPLICATIONS....44

Contribution of Authors and Co-Authors....44
Manuscript Information Page....45
3.1. Abstract....46
3.2. Introduction....47
3.3. Culturing Methods....49
3.3.1. Strains and Media....49
3.3.2. Culture Conditions....50
3.3.3. Dry Weight Determination....51
3.4. Carbohydrate....52
3.4.1. Literature Review....52
3.4.2. Procedure (after Del Don et al., 1994)....54
3.4.2.1. Reagents....54
3.4.2.2. Quantification of Glycogen....54
3.4.2.3. Quantification of Hexoses Excluding Glycogen....55
3.4.2.4. Quantification of Total Carbohydrate....56
3.4.3. Test Results....56
3.5. DNA....58
3.5.1. Literature Review....58
3.5.2. Procedure (after Downs and Wilfinger, 1983)....59
3.5.2.1. Reagents....59
3.5.2.2. Assay....60
3.5.3. Test Results....61
3.6. Lipid....65
3.6.1. Literature Review....65
3.6.2. Procedure (after Bligh and Dyer, 1959)....66
3.6.2.1. Reagents....66
3.6.2.2. Assay....66
3.6.3. Test Results....67
3.7. Protein....69
3.7.1. Literature Review....69
3.7.2. Procedure (after Henderson et al., 2000)....70
3.7.2.1. Reagents....70
3.7.2.2. Assay....71
3.7.3. Test Results....72
3.8. RNA....74

TABLE OF CONTENTS CONTINUED

3.8.1. Literature Review....74
3.8.2. Procedure (after Benthin et al., 1991)....76
3.8.2.1. Reagents....76
3.8.2.2. Assay....76
3.8.3. Test Results....77
3.9. Model Biomass Reaction....78
3.10. Conclusions....83
3.11. Acknowledgments....85
3.12. Appendix A....85

4. STOICHIOMETRIC NETWORK ANALYSIS OF CYANOBACTERIAL ACCLIMATION TO PHOTOSYNTHESIS-ASSOCIATED STRESSES IDENTIFIES HETEROTROPHIC NICHES....89

Contribution of Authors and Co-Authors....89
Manuscript Information Page....90
4.1. Abstract....91
4.2. Introduction....91
4.3. Materials and Methods....97
4.3.1. Photobioreactor Culturing....97
4.3.2. Biomass Composition Determination....98
4.3.3. Model Construction....99
4.4. Materials and Methods....101
4.4.1. Computational BP-1 Metabolic Model and Photobioreactor Biomass Composition Measurement....101
4.4.2. Computational Analysis of Stress Acclimation....104
4.4.2.1. Irradiance and Photosynthetic Electron Flow....105
4.4.2.2. Irradiance, High $O_2$, and Nutrient Limitation....107
4.4.3. Comparison of Computational Predictions with Photobioreactor Physiological Data....110
4.4.4. Comparison of Computational Predictions with Photobioreactor Transcriptomic Data....114
4.4.4.1. Photosynthesis, Photorespiration, and Byproducts....115
4.4.4.2. Central Metabolism and Nutrient Assimilation....118
4.4.5. Stress Acclimation and Photoautotrophic-Heterotrophic Interactions....119
4.5. Discussion....122
4.6. Supplementary Materials....129
4.7. Acknowledgments....129
4.8. Appendix A. Biomass Composition Analytical Methods....130
4.8.1. DNA, After Downs and Wilfinger, 1983....130
4.8.2. Glycogen, After Del Don et al., 1994....131

TABLE OF CONTENTS CONTINUED

4.8.3. Lipid, After Bligh and Dyer, 1959 ..... 132
4.8.4. Protein and Amino Acid Distribution, After Henderson et al., 2000 ..... 133
4.8.5. RNA, After Benthin et al., 1991 ..... 135
4.9. Appendix B. Supplemental Figures ..... 136
4.10. Appendix C. Supplemental Tables ..... 139
4.11. Appendix D. Nitrogen and Iron Limitation ..... 142
4.12. Appendix E. Biomass Yield Comparison ..... 144

5. *ESCHERICHIA COLI* CO-METABOLIZES GLUCOSE AND LACTATE FOR ENHANCED GROWTH ..... 145

Contribution of Authors and Co-Authors ..... 145
Manuscript Information Page ..... 147
5.1. Abstract ..... 148
5.2. Introduction ..... 149
5.3. Results ..... 152
5.3.1. Growth on Glucose is Enhanced in the Presence of Lactate ..... 152
5.3.2. Lactate is Co-metabolized with Glucose ..... 153
5.3.3. Co-metabolism of Lactate Results in Additional Energy Available for Growth ..... 156
5.3.4. Lactate is Preferred Over Acetate as a Carbon and Energy Source ..... 159
5.3.5. Lactate and Acetate Show Different Concentration-Dependent Inhibition Profiles ..... 160
5.4. Discussion ..... 163
5.4.1. Co-metabolism and the Importance of Energy ..... 163
5.4.2. Organic Acid Toxicity ..... 164
5.5. Materials and Methods ..... 165
5.5.1. Bacterial Strains and Culturing Media ..... 165
5.5.2. Batch Culturing Conditions ..... 166
5.5.3. Metabolite Analysis ..... 167
5.5.4. Kinetic Expression Modeling ..... 167
5.6. Supplemental Figures and Tables ..... 169

6. SYNTHETIC CONSORTIA ENGINEERED FOR PUSH AND PULL DYNAMICS SHOW CONDITIONAL OPTIMALITY OVER METABOLIC GENERALIST ..... 185

Contribution of Authors and Co-Authors ..... 185
Manuscript Information Page ..... 186
6.1. Abstract ..... 187
6.2. Introduction ..... 188

TABLE OF CONTENTS CONTINUED

6.3. Methods....191
6.3.1. Culturing Media....191
6.3.2. Strains....192
6.3.3. Batch Culturing....193
6.3.4. Dry Weight and Colony-Forming Unit Correlations....195
6.3.5. Metabolite Analysis....196
6.4. Results....197
6.4.1. Construction of Acetate- and Lactate-Exchanging Consortia....197
6.4.2. Acetate-Exchanging Consortium Outperforms Specialist....199
6.4.3. Lactate-Exchanging Consortium Shows Enhanced Growth Over Specialist and Generalist....202
6.4.4. Application and Interpretation of the Maximum Power Principle....208
6.5. Discussion....211
6.5.1. Mechanism for Improved Consortia Growth....212
6.5.2. Push/Pull System and the Influence of Growth and Production Rates....214
6.5.3. Intersection of Maximum Power Principle and Resource Ratio Theory....215
6.6. Supplemental Figures and Tables....218

7. EPILOGUE....224

7.1. Synopsis....224
7.2. *In Silico* Modeling....225
7.3. *In Vitro* Laboratory Studies....226
7.4. Ecological Theory....227
7.5. Future Directions....228
7.6. Concluding Statement....229
7.7. Additional Publications....229

REFERENCES CITED....231

# LIST OF TABLES

Table Page

2.1. Recent community-relevant review articles categorized by focus .....12

2.2. Representative microbial communities organized by system components.....14

2.3. Representative microbial communities organized by system interaction mechanisms .....17

2.4. Ecological theory studies .....22

2.5. Microbial community *in silico* analysis studies.....28

3.1. Fluorescent plate reader settings for Hoechst DNA assay.....61

3.2. Amino acid analysis HPLC gradient settings .....72

3.3. Amino acid distributions and protein quantification for *E. coli*, *Synechococcus* 7002, and *A. acidocaldarius*.....74

3.4. Summary of average macromolecular composition, based on mass fraction of dry biomass.....79

3.5. Example calculation of DNA macromolecular formula for *A. acidocaldarius* with 61.9% GC content, assuming a polymer length of 1 monomer .....80

3.6. Species-specific biomass reactions for *E. coli*, *Synechococcus* 7002, and *A. acidocaldarius*, without consideration of maintenance energy.....82

4.1. *T. elongatus* BP-1 metabolic model inputs and outputs, including potential reduced carbon byproducts, with corresponding degree of reduction.....103

4.2. Experimentally determined *T. elongatus* BP-1 biomass composition from turbidostat biomass samples grown under an irradiance of 2000 μmol photons $m^{-2}$ $s^{-1}$ .....103

LIST OF TABLES CONTINUED

Table Page

4.3. Comparison between computational predictions of stress acclimations and photobioreactor gene expression data under high versus low irradiance conditions .....115

4.S1. Experimentally measured amino acid distribution from OPA/FMOC derivatization and HPLC fluorescence detection .....139

4.S2. Upregulated BP-1 genes under high versus low irradiance conditions.....140

4.S3. Genes involved in amino acid synthesis pathways found to be upregulated under high irradiance conditions .....141

4.S4. Byproduct yields with respect to BP-1 biomass for pathways that secreted byproducts along the tradeoff curve for irradiance-induced stress and $O_2$/$CO_2$ competition and the corresponding yield of heterotroph biomass .....142

5.1. Major pathway fluxes under different carbon substrates.....159

5.S1. (A) Parameterized inhibition model fits for acetic acid as sole substrate. (B) Parameterized inhibition model fits for acetic acid as a product with glucose as the main substrate. .....172

5.S2. (A) Parameterized inhibition model fits for lactic acid as sole substrate. (B) Parameterized inhibition model fits for lactic acid as a dual substrate with glucose. .....178

5.S3. Matrix of carbon source concentrations used to construct inhibition curves and corresponding growth rates and standard deviations for triplicate biological cultures .....183

6.1. Physiological characterization of generalist and producer/scavenger strains in mono-culture.....198

6.S1. Measurements, calculated rates, and yields across varied initial pH conditions for generalist, producers, and consortia.....222

# LIST OF FIGURES

Figure Page

2.1. Resource investment and economies of scale for enzymatic flux .....32

2.2. Phototrophic community interactions .....35

2.3. Sulfate-reducing bacteria (SRBs)-methanogen anaerobic syntrophy .....37

2.4. Naturally occurring *E. coli* cross-feeding communities .....40

3.1. (A) Representative glucose standard curve for anthrone assay, (B) Carbohydrate mass percentages of dry biomass.....57

3.2. (A) Standard curve with calf thymus DNA, (B) Relationship between dry biomass sample amount and resulting DNA quantity.....64

3.3. (A) Lipid recovery is linear for biomass samples between 10-35 mg dry weight, (B) Lipid mass percentages of dry biomass .....68

3.4. Representative chromatogram from fluorescence detector for amino acid standards .....73

3.5. (A) RNA recovery is linear for biomass samples between 2-8 mg dry weight, (B) RNA mass percentages on a dry biomass basis.....78

3.A1. (A) Biomass-$OD_{730}$ correlation curve determined for *Synechococcus* 7002, (B) Biomass-$OD_{600}$ correlation curve determined for *A. acidocaldarius* .....86

3.A2. (A) Lysis of DNA standard did not significantly influence Hoechst fluorescent response, (B) Washing samples with cell wash solution and freezing samples .....86

3.A3. Autoclaving samples prior to chloroform-methanol lipid extraction did not significantly enhance lipid recovery .....87

3.A4. Correlations between experimentally measured and genome-based amino acid distributions .....88

4.1. Light and dark reactions of photosynthesis .....94

LIST OF FIGURES CONTINUED

Figure Page

4.2. Computational analysis of irradiance and photosynthetic electron flow in cyanobacterium *T. elongatus* BP-1 .....107

4.3. Computational analysis of irradiance-induced stress and $O_2/CO_2$ competition at RuBisCO in cyanobacterium *T. elongatus* BP-1 .....109

4.4. Photobioreactor impact of irradiance on specific growth rate and biomass production efficiency in *T. elongatus* BP-1 continuous culture .....111

4.5. Growth rate-dependent photon absorption rate and maintenance energy in cyanobacterium *T. elongatus* BP-1 .....113

4.6. Cyanobacterium *T. elongatus* BP-1 photorespiration and byproduct secretion pathways with transcriptomic data measured under high versus low irradiance .....117

4.7. Byproduct secretion generates a heterotrophic niche and stimulates a mutually beneficial relationship .....121

4.8. Comparison of computational and experimental $O_2/CO_2$ competition and concentrations at RuBisCO .....126

4.S1. BP-1 amino acid distribution .....136

4.S2. Computational analysis of nutrient availability and $O_2/CO_2$ competition at RuBisCO in cyanobacterium BP-1 .....137

4.S3. Analysis of influence of nitrogen source on photon requirement .....138

5.1. Growth rate and biomass accumulation of *E. coli* on glucose media is enhanced in the presence of lactate .....153

5.2. *E. coli* co-metabolizes glucose and lactate .....155

5.3. *E. coli* converts lactate to acetate .....156

5.4. Simplified pathway schematic for glucose and lactate utilization .....158

5.5. *E. coli* prefers lactate to acetate as a carbon and energy source .....160

LIST OF FIGURES CONTINUED

Figure Page

5.6. Inhibition by lactic and acetic acids with and without glucose as a substrate ....161

5.S1. Culture pH differs when lactate is added to glucose as a substrate ....169

5.S2. Acetate does not contribute to growth when lactate is present ....170

5.S3. Inhibition by culture pH and osmotic pressure ....170

5.S4. Combined inhibition model terms predict culture growth rates under compound stresses ....171

6.1. Synthetic consortia design ....199

6.2. Growth characterization of acetate-exchanging consortium under varying initial pH conditions ....201

6.3. Growth characterization of lactate-exchanging consortium under varying initial pH conditions ....204

6.4. Lactate (A) and acetate (B) accumulation dynamics in the lactate consortium at high initial pH (7.5) and altered producer to scavenger ratios ....208

6.5. Maximum power principle analysis of the different biological systems (generalist, consortia, and producers) ....210

6.6. Conceptual rationale for higher biomass accumulation observed in lactate-exchanging consortium relative to generalist and producer ....214

6.S1. Biomass accumulation and pH profiles over time at varying initial pH conditions ....218

6.S2. Fraction of producer in the lactate- (A) and acetate-exchanging consortia (B) under different initial pH conditions ....220

6.S3. Biomass accumulation (A), pH profiles (B), and fraction of producer (C) in lactate-exchanging consortium at high initial pH 7.5 and altered producer to scavenger ratios ....221

# ABSTRACT

Microbial communities are critical underpinnings of most natural processes, e.g. biogeochemical cycling, and can also be harnessed and engineered for a variety of industrial applications. Despite the abundance of detailed physiological characterization of many individual microorganisms, as well as large data sets describing microbial community composition, the area of interspecies interactions requires further research to truly appreciate and harness the potential of microbial capabilities. Using a combination of *in silico* metabolic modeling and *in vitro* laboratory approaches linked to guiding ecological theories, this dissertation investigates metabolite exchange as a mechanism of interspecies interactions and focuses on the role of environmental stress in mediating interactions. A stoichiometric metabolic network model was constructed for the thermophilic cyanobacterium *Thermosynechococcus elongatus* BP-1 and was analyzed with elementary flux mode analysis to predict metabolic acclimations to light and oxygen, two common environmental stressors in photoautotrophic habitats. High stress levels were predicted to activate organic byproduct secretion pathways, which opens a niche to support growth of heterotrophic partners. To further investigate metabolite exchange in the laboratory, synthetic consortia were designed through genetic engineering and pairing of *Escherichia coli* strains to form metabolically partitioned organic acid cross-feeding systems. These controlled systems were used to investigate the impact of division of labor as well as the effect of byproduct detoxification. Kinetic data from these systems were also applied to interpret ecological theories regarding microbial community structure. Altogether, these studies demonstrate an integrated approach to studying microbial community interactions by combining *in silico* metabolic modeling and *in vitro* laboratory experiments with ecological theory as a basis for interpretation. This dissertation provides insight into rationale for microbial community structure and highlights the role of environmental stress, particularly byproduct inhibition, in driving microbial consortia interactions.

# CHAPTER ONE

# INTRODUCTION

## 1.1. Environmental Stress and Metabolic Acclimation

Every environment, whether natural or industrial, presents some type of stress to the organisms living therein, whether that of scarce resources, a harmful abiotic factor like UV radiation, or competition from another species. Without stress factors placing constraints on metabolic capabilities, the rise of a Darwinian demon, or a super-organism that can optimize all metabolic possibilities, would be observed (Law 1979). Some stress factors are directly associated with metabolic processes themselves: every metabolism has a byproduct, and buildup of these byproducts causes inhibition of growth, both thermodynamically and through specific inhibition mechanisms (e.g. as for acetic acid (Repaske and Adler 1981, Roe, O'Byrne et al. 2002)). These growth- or metabolism-associated stresses present new challenges that individual populations, as well as communities, must manage if they are to survive. These stresses impact organisms at both the macro- and micro-level; however, microorganisms provide more tractable systems for the detailed study of metabolic response to stress.

Environmental variables fluctuate constantly, and, to adapt and thrive in challenging habitats, microorganisms must be prepared with versatile metabolic strategies for deployment when environments change. The metabolic strategies that organisms have evolved to cope with environmental stresses are known as metabolic acclimations. Examples of metabolic acclimation strategies include divergent degradative pathways for

a particular substrate leading to different byproducts, alternative pathway variations with differing levels of efficiency and/or resource investments (e.g. Embden-Meyerhof-Parnas versus Entner Doudoroff pathways), or different regulation patterns in response to stress factors. Assessing metabolic acclimations based on cost in terms of growth efficiency and resource investment can demonstrate the competitiveness of a microorganism and provides a metric for evaluating metabolism from the perspective of natural selection.

## 1.2. Modeling Metabolism

A stoichiometric modeling approach can be used to study microorganisms on a detailed metabolic level and investigate metabolic acclimation strategies under different environmental conditions. The genome sequence provides information on a microorganism's metabolic potential. With the aid of annotation databases, genomic information can be used to reconstruct the possible biochemical reactions participating in metabolism at the stoichiometric level (Maarleveld, Khandelwal et al. 2013, Carlson, Beck et al. 2018). Stoichiometric modeling analysis methods can then be used to probe the possible and optimal physiologies of the microorganism using the resulting genome-scale network model. Flux balance analysis, a common stoichiometric modeling technique, employs hypothesized objective functions to find the optimal pathway for a given set of input and output flux constraints (Orth, Thiele et al. 2010). Elementary flux mode analysis, another stoichiometric modeling technique, decomposes the network into all (simplest) possible pathways into and out of the network and provides a large data set for subsequent analysis (Trinh, Wlaschin et al. 2009). Analyzing the possible

physiologies according to resource investment costs and growth efficiencies (resource allocation analysis) can provide a prediction of ecologically relevant metabolic strategies over varying environmental stress levels (Mori, Hwa et al. 2016).

## 1.3. Microbial Interactions and Metabolite Exchange

Microorganisms almost always exist in communities of interacting populations rather than as single, isolated populations, indicating that there must be benefits to this form of existence upon which natural selection has acted. Modeling techniques can be extended from single-species metabolic studies to gain insight into interspecies interactions in microbial communities. Microbial interactions can take on many different forms (e.g. commensal, ammensal, mutualistic, competitive, and more (Holland and DeAngelis 2009)); however, cooperative metabolite exchange is a common motif of community assembly (Zelezniak, Andrejev et al. 2015). In laboratory culturing of microbial communities, measurement of exchanged compounds can be difficult due to low extracellular concentrations; however, modeling permits testing of possible interactions inferred from mono-culture physiologies as well as prediction of metabolite exchange (Romine, Rodionov et al. 2017).

## 1.4. Synthetic Ecology

*In silico* modeling gains power when combined with *in vitro* or *in vivo* observations. However, natural microbial communities contain incredible complexity and present difficulties when attempting to study specific microbial interactions or extract

basic principles of community organization. Synthetic ecology provides a more tractable way to study microbial communities by simplifying a complex system into fewer components with variables that can be more easily controlled. Specific metabolic pathways or physiologies can be engineered into microorganisms, and strains can be combined in varying permutations to enforce specific interactions and to enable a clearer understanding of community function. The parallels to natural communities allow for extraction of foundational principles, which can then be applied to make predictions about more complex assemblies (Brenner, You et al. 2008, Stenuit and Agathos 2015).

## 1.5. Ecological Theories for Microbial Community Structure

Several ecological theories have been developed based on observation and study of macroscale organisms and ecosystems, but, surprisingly, not as much work has been done to apply and test these theories on microbial systems. Resource ratio theory, resource allocation or tradeoff theory, and the maximum power principle are three major ecological theories that can add depth to the interpretation of microbial community interactions and contribute to our understanding of community assembly. Resource ratio theory poses growth as limited by an organism's ability to acquire limited resources, where the ratio of limiting resources determines the outcome of interspecies interactions in the system (Tilman 1980, de Mazancourt and Schwartz 2010). Resource allocation or tradeoff theory uses economic reasoning to compare efficiencies for simultaneous optimization of multiple limiting resources (Molenaar, van Berlo et al. 2009, Carlson and Taffs 2010). The maximum power principle views overall systems in terms of the rate at

which energy is acquired and postulates that systems with the fastest rate will be favored by natural selection (Lotka 1922, Lotka 1922). Synthetic ecology techniques provide an excellent means by which to test some of these ecological theories in a more controlled environment with quantitative measurements.

## 1.6. Combining Theory, *In Silico* Simulations, and *In Vitro*/*In Vivo* Experiments

Researchers often focus efforts singularly on either *in silico* simulations or laboratory benchwork. However, theory and practice should inform each other and operate in an iterative cycle to maximize the scope and impact of the results. A combination of *in silico* simulations and *in vitro*/*in vivo* experiments, complemented by ecological theory to strengthen the interpretation of the results, forms the design of this dissertation. It is also hoped that others will be inspired to seek greater collaboration between theory, modeling, and laboratory experiments in their own work.

## 1.7. Overview of Chapters

Chapter Two is a literature review written as a chapter for *Biotechnology for Biofuel Production and Optimization* that discusses the fundamentals of microbial interactions and consortia, as well as ecological theories governing consortia interactions and emergent properties. Case studies on consortia found in the literature are used to exemplify interaction mechanisms and illustrate underlying ecological theories.

Chapter Three details analytical methods for experimentally determining microbial biomass composition and provides step-by-step procedures for measuring five

major macromolecules (carbohydrate, DNA, lipid, protein, and RNA). The procedures are tested and optimized using a variety of bacterial species. A detailed description of how to apply the laboratory measurements to a biomass reaction in a metabolic model is also included.

Chapter Four addresses metabolic acclimation in a natural system using a thermophilic cyanobacterium *Themosynechococcus elongatus* BP-1. Metabolic modeling (elementary flux mode analysis) is used with resource cost-based analysis to predict metabolic strategies employed to mitigate light and oxygen stress, two common stresses in photoautotrophic niches. The resulting acclimation strategies are extrapolated to predict cross-feeding interactions with heterotrophic partners. The model predictions are also compared with experimental transcriptomic data for validation.

Chapter Five explores organic acid metabolism and inhibition in *Escherichia coli* and investigates the impact of lactic acid on system productivity as a co-substrate with glucose, a physiology which is not well described in the literature. Growth inhibition of acetic and lactic acids is quantified, and kinetic inhibition expressions were parameterized to fit the data.

Chapter Six addresses metabolic acclimation and environmental stress using a synthetic ecology approach. *E. coli* populations were genetically engineered to generate two tractable organic acid-exchanging consortia, which were used to investigate the principles of metabolic specialization (or division of labor) and organic acid detoxification in microbial communities. The synthetic systems also provide a testing ground for quantifying and interpreting the maximum power principle.

Finally, Chapter Seven concludes the entire body of work, including ramifications of the results, applications, and directions for future research.

# CHAPTER TWO

# INTERPRETING AND DESIGNING MICROBIAL COMMUNITIES FOR BIOPROCESS APPLICATIONS, FROM COMPONENTS TO INTERACTIONS TO EMERGENT POPERTIES

## Contribution of Authors and Co-Authors

Manuscript in Chapter Two

Author: Ashley E. Beck

Contributions: Performed the literature review, synthesized the ideas, wrote the manuscript

Co-Author: Kristopher A. Hunt (contributed equally)

Contributions: Performed the literature review, synthesized the ideas, wrote the manuscript

Co-Author: Hans C. Bernstein

Contributions: Performed the literature review, synthesized the ideas, edited the manuscript

Co-Author: Ross P. Carlson

Contributions: Performed the literature review, synthesized the ideas, wrote the manuscript

Manuscript Information Page

Ashley E. Beck, Kristopher A. Hunt, Hans C. Bernstein, and Ross P. Carlson

Status of Manuscript:
____ Prepared for submission to a peer-reviewed journal
____ Officially submitted to a peer-review journal
____ Accepted by a peer-reviewed journal
_X__ Published in a peer-reviewed journal

Chapter 15 in *Biotechnology for Biofuel Production and Optimization*, Edited by Carrie Eckert and Cong Trinh
Elsevier Publishing
Published January 18, 2016
eBook ISBN: 9780081000533
Hardcover ISBN: 9780444634757

## 2.1. Introduction

Most natural microbial ecosystems are the result of millions of years of natural selection in spatially and temporally dynamic landscapes. These ecosystems possess effective, highly evolved functions and are almost exclusively organized as polymicrobial communities. The study of natural and engineered microbial communities has benefited from new technologies such as increased resolution and throughput of omics measurements, development of new genetic systems for establishing model organisms, advanced cell isolation methods such as flow cytometry and cell sorting (Muller and Nebe-von-Caron 2010), comprehensive databases such as KBase (http://kbase.us), and ever- growing computational power for performing *in silico* experiments such as community-scale metabolic network modeling (Taffs, Aston et al. 2009, Mahadevan and Henson 2012). Interest in using polymicrobial systems for applied bioprocesses stems largely from an effort to mimic and ultimately control the beneficial emergent properties that are often observed in natural ecosystems. These attractive attributes of communities have a potential to enable superior catalytic function compared to traditional monocultures based on simultaneous optimization of multiple tasks, increased productivity, and greater stability.

While the study of applied microbial communities is growing in popularity, the appreciation and use of communities for societal purposes is not new. In fact, applications of microbial communities date back at least 5000 years to early food preservation via lactic acid-producing bacterial communities used for yogurt production (Tamime and Robinson 1999), and evidence suggests that directed biogas production was practiced in Assyria and China going back at least 3000 years (Bond and Templeton

2011). The significance of polymicrobial systems was also observed and tested by the earliest pioneers of modern microbiology. In 1683, Antoine van Leeuwenhoek recorded observations of morphologically distinct “animalcules” collected from oral scrapings and, in 1877, Louis Pasteur tested antagonistic interactions between medically relevant bacteria (Pasteur and Joubert 1877, Dobell 1932, Florey 1946, Korgaonkar, Trivedi et al. 2013).

Numerous reviews reiterate, with overlapping content, the relevance and use of polymicrobial systems for human health, biological circuit synthesis, microbial computing, synthetic ecology, biomass degradation, and a myriad of other biological applications (Table 2.1). This review provides a generalized discussion of ecological foundations useful in understanding polymicrobial systems and highlights classical theories applicable to future microbial community engineering efforts. No attempt is made here to exhaustively outline every relevant study in this rapidly growing field; rather, case studies are selected to epitomize ecological themes and design motifs within the context of the current and future state of polymicrobial bioprocessing.

## 2.2. Definitions

The study of microbial communities has expanded from traditional biological disciplines to include a wide cross section of applied sciences. This broad expansion has resulted in the merging of concepts and terms from classical disciplines including biochemistry, computational biology, ecology, engineering, genetics, and microbiology.

These fields use vernacular with varying connotations; hence, a list of terms is provided with the definitions used here to facilitate a unified discussion.

Table 2.1. Recent community-relevant review articles categorized by focus.

| Focus | Reference |
|---|---|
| Artificial symbiosis | (Momeni, Brileya et al. 2013) |
| Biodegradation | (Mikesková, Novotný et al. 2012) |
| Bioenergy, biomaterials | (Ortiz-Marquez, Do Nascimento et al. 2013) |
| Bioengineering | (Brenner, You et al. 2008) |
| Bioprocess | (Bader, Mast‐Gerlach et al. 2010, Jagmann and Philipp 2014) |
| Bioprocess, experimental and theoretical | (Bernstein and Carlson 2012) |
| Biotechnology, algal biofuels | (Pandhal and Noirel 2014) |
| Cellulose degradation, bioprocess | (Zuroff and Curtis 2012) |
| Cyanobacteria/microalgae and bacteria | (Subashchandrabose, Ramakrishnan et al. 2011) |
| Ecological interactions, symbiosis | (Hussa and Goodrich-Blair 2013) |
| Engineering, bioprocess | (Shong, Diaz et al. 2012) |
| Food fermentations | (Smid and Lacroix 2013) |
| Industrial bioprocessing | (Sabra, Dietz et al. 2010) |
| Microbiome | (Thiele, Heinken et al. 2013) |
| Mining | (Brune and Bayer 2012) |
| Polymicrobial infections | (Murray, Connell et al. 2014) |
| Synthetic biology | (Goers, Freemont et al. 2014) |
| Synthetic biology, bioprocess | (Song, Ding et al. 2014) |
| Synthetic communities | (Großkopf and Soyer 2014) |
| Synthetic ecosystems | (De Roy, Marzorati et al. 2014) |
| Viral interactions | (Roossinck 2011) |

A **microbiological community** is a collection of populations that may be comprised of prokaryotic, eukaryotic, or viral components; definable interactions are not a requirement. A **microbial community** is a microbiological community limited to prokaryotic and eukaryotic populations with no explicit accounting for viruses and no constraints on interactions. However, the ubiquity of viruses suggests that the vast majority of microbial species hosts viruses, and the existence of virus-free microbial

communities is therefore thought to be exceedingly rare. A microbial community exhibiting positive interactions is referred to as a **consortium** (plural consortia) (Madigan, Martinko et al. 2010); some uses of the term are more generic, referring to any interacting community. The origin of community populations can be used to further categorize the system. A **natural community** is defined as a collection of wild-type populations that have interacted in nature on evolutionary time scales. An **artificial community** is a collection of unmodified populations that have been assembled through manual intervention and are not thought to interact in natural habitats. A **synthetic community** is defined as a collection of genetically modified populations, whereas a **semisynthetic community** is a collection of populations with at least one wild-type population and at least one genetically modified population. A review of recent case studies exemplifying these different organizations can be found in Bernstein and Carlson (Bernstein and Carlson 2012).

### 2.2.1. Community Components

Communities are ensembles of populations that serve as the system components. Populations can be classified by phylogenetic and/or phenotypic distinction. **Phylogenetically distinct** community populations are different species that can range across the domains of microbial life and can include viruses. Table 2.2 provides examples of components comprising interacting communities ranging from virus-virus systems to archaeon-eukaryote systems. Virus-virus and host-virus interactions are often overlooked in reviews of applied microbial communities despite their common distribution across most natural systems and their potential to impact engineered systems. These community interactions are not limited to

pathogenicity and can represent a spectrum of interaction outcomes, including mutually beneficial effects as reviewed in Roossinck (Roossinck 2011).

Table 2.2. Representative microbial communities organized by system components.

| Community members | Description | Reference |
|---|---|---|
| Virus-Virus | Enhanced pathogenicity | (López-Ferber, Simón et al. 2003) |
| Virus-Bacterium | Enhanced infectivity of human cells | (Kuss, Best et al. 2011) |
| Virus-Bacterium | Lysis of competitors | (Sandaa, Gómez‐Consarnau et al. 2009) |
| Virus-Eukaryote | Suppression of additional virus infection (HIV) | (Tillmann, Heiken et al. 2001, Ernst, Greer et al. 2014) |
| Virus-Eukaryote | Prevention of diabetes | (Oldstone 1988) |
| Virus-Eukaryote | Thermal stress tolerance | (Márquez, Redman et al. 2007) |
| Bacterium-Bacterium | Cyanobacteria differentiating to fix nitrogen | (Zhang, Laurent et al. 2006) |
| Archaeon-Bacterium | Enhanced function via hydrogen exchange and methanogenesis | (McInerney, Sieber et al. 2009) |
| Bacterium-Eukaryote | Cellulose conversion to value-added biochemicals | (Minty, Singer et al. 2013) |
| Archaeon-Eukaryote | Enhanced cellulose degradation via hydrogen exchange and methanogenesis | (Cheng, Edwards et al. 2009) |

**Phenotypically distinct** populations are not differentiable on the species level but exhibit separate expression patterns that often lead to niche differentiation. An **ecological niche** is the function or location of an organism within an ecosystem. The cyanobacterial strategy of cellular differentiation into specialized nitrogen-fixing heterocysts and vegetative cells is a well-studied example of a single-species population functioning as a community (Kumar, Mella-Herrera et al. 2010). Another example is synthetic or adapted communities of *Escherichia coli* strains with different substrate specificities which can lead to niche partitioning in biofilms (e.g., oxic or anoxic separation) (Rosenzweig, Sharp et al. 1994, Eiteman, Lee et al. 2008, Poltak and Cooper 2011, Bernstein, Paulson et al. 2012). **Biofilms** are polymer-encapsulated microbial populations attached to biological or abiotic surfaces

(Hall-Stoodley, Costerton et al. 2004). Mass transfer typically limits the availability of resources within a biofilm, resulting in spatial heterogeneity which, in turn, leads to phenotypic differentiation (Stoodley, Sauer et al. 2002, Hall-Stoodley, Costerton et al. 2004, Poltak and Cooper 2011).

### 2.2.2. Interaction Outcomes

Community interactions can be classified as one of six outcomes. These interactions may be unidirectional, bidirectional, or of higher order; they can also be obligatory or facultative. Each of the interaction outcome categories presented here is symbolically summarized for a two-population community using "+" to indicate a population benefit, "-" to indicate an adverse effect, and "0" to indicate no effect. In practice, these interaction outcomes are often observed in communities comprised of more than two populations (Holland and DeAngelis 2009).

(1) **Mutualism** (+/+): both populations benefit from the interaction(s). Syntrophy is a specific instance of mutualism associated with the cross-feeding of essential resources between populations (McInerney, Sieber et al. 2009). (2) **Commensalism** (+/0): one population benefits from the interaction(s) while the other is unaffected. (3) **Ammensalism** (-/0): one population is adversely affected by the interaction(s) while the other is unaffected. (4) **Competition/antagonism** (-/-): both populations are negatively affected by the interaction(s), which can be due to functional redundancy or antagonistic interactions. (5) **Parasitism** (+/-): one population benefits and one population is adversely affected by the interaction(s). (6) **Neutralism** (0/0): neither population is affected by the interaction(s); alternatively, there is no interaction between populations. Synthetic ecology,

another scientific field witnessing rapid growth, often attempts to assemble tractable, albeit constrained, systems to test these interaction outcomes (De Roy, Marzorati et al. 2014).

### 2.2.3. Interaction Mechanisms

The mechanisms that mediate known interactions can be divided into three generalized categories: metabolite exchange, physical interaction, and environmental modification. These mechanisms are typically combinatorial and interrelated within natural and engineered microbial communities. **Metabolite exchange** is any transfer of material and/or chemical energy between community populations and requires some combination of active transport (e.g., ABC-type transporters) and/or passive transport (e.g., diffusion). Exchanges of **anabolic resources,** resources used in biosynthetic processes (e.g., amino acids, nucleotides, vitamins, cofactors, and siderophores), are widely distributed among natural systems and represent targets for metabolically engineered polymicrobial systems (Table 2.3) (Wintermute and Silver 2010, Phelan, Liu et al. 2012). Exchanged metabolites can also serve as **catabolic resources**, resources used to produce cellular energy. Examples include electron donors or acceptors (e.g., hydrogen or oxygen, respectively), which are used in biologically mediated redox reactions to facilitate production of energetic molecules like NAD(P)H or ATP.

Table 2.3. Representative microbial communities organized by system interaction mechanisms.

| Interaction mechanism | Community | Description | Reference |
|---|---|---|---|
| Anabolic metabolite exchange | Filamentous anoxygenic phototrophs / cyanobacteria | Vitamin | (Rodionova, Li et al. 2015) |
| Anabolic metabolite exchange | Uncultured marine bacteria | Siderophore | (D'Onofrio, Crawford et al. 2010) |
| Anabolic and catabolic metabolite exchange | Sulfate reducing bacteria / methanogens | Alanine and hydrogen / formate | (Walker, Redding-Johanson et al. 2012) |
| Catabolic metabolite exchange | Sulfate reducing bacteria / methanogens | Hydrogen / formate | (Sieber, McInerney et al. 2012) |
| Catabolic metabolite exchange | Colon microbiota | Acetate cross-feeding | (Falony and De Vuyst 2009) |
| Quorum sensing exchange | Sludge community | Granulation and EPS production | (Tan, Koh et al. 2014) |
| Antibiotic / antimicrobial peptide exchange | *K. pneumoniae* / *E. coli* | Microcin-mediated ammensalism | (De Lorenzo, Martínez et al. 1984) |
| Environment sensing exchange | *Vibrio* pathogen / crustacean hosts | Differential virulence impacts | (Pande, Natrah et al. 2013) |
| Direct physical interaction | Cellulose-fed soil biofilm community | Filamentous structures for electron transfer | (Ishii, Shimoyama et al. 2008) |
| Environmental modulation | Marine phytoplankton community | Hydrogen peroxide scavenging | (Morris, Johnson et al. 2011) |

Exchanged material can serve functions other than anabolic or catabolic roles, such as modulating the behavior of community populations. **Quorum sensing**, a process by which organisms secrete and receive specific soluble metabolites that act as regulatory signals, is associated with a wide variety of natural multicellular functions, including coordinated biofilm formation, microbial pathogenicity, and culture bioluminescence (Waters and Bassler 2005). In addition, quorum sensing has been proposed as a means of interrogating local environments, permitting a feedback mechanism for regulating phenotype (e.g., resource-intensive strategies such as enzyme secretion) (Hense, Kuttler et al. 2007, Decho, Norman et al. 2010). Modulating community population activity can

also be realized through competitive strategies like the exchange of inhibitory or toxic metabolites (Fajardo and Martínez 2008, Hibbing, Fuqua et al. 2010). Secretion of antibiotics and antimicrobial peptides is widely distributed and provides both offensive and defensive mechanisms within some communities.

Direct **physical interactions** between community populations can dictate community structure and function. These interactions are a hallmark mechanism of biofilms (Paerl and Pinckney 1996, Stoodley, Sauer et al. 2002); this physical association can be controlled or constrained by metabolite exchange (Brenner, You et al. 2008). Evidence suggests that direct physical contact between community populations can also be used for the transfer of electrons through materials such as cytochrome-rich extracellular structures, which have been characterized as outer membrane and periplasmic extensions (Pirbadian, Barchinger et al. 2014). Similarly, filamentous cable bacteria in microbial sediment communities permit electron transfer across centimeter-length scales (Pfeffer, Larsen et al. 2012). Direct interpopulation electron transfer remains an active area of investigation.

**Environmental modification** is a mechanism of interaction in which a community population influences the local environment and thereby alters the niche(s) that other populations can inhabit. Modulation often occurs when one population consumes a chemical species (e.g., organic acids, oxygen, or hydrogen sulfide) that inhibits other populations (Kühl and Jørgensen 1992, Carlton and Richardson 1995, Bernstein, Paulson et al. 2012). Table 2.3 provides examples of natural and engineered systems organized by mechanism of interaction.

### 2.2.4. Emergent Properties

A major advantage of polymicrobial systems over traditional monoculture biotechnology is the potential for emergence of higher order properties. **Emergent properties** are attributes that are either not present or increased in magnitude from those properties characteristic of the individual system components. Contrary to many connotations, emergent properties are not always beneficial to a community; however, the discussions here are limited to positive attributes. **Stability** is defined by a community's response to perturbations (Rykiel 1985), although many other interpretations have been used for the concept of ecological stability and related properties such as robustness (Grimm and Wissel 1997). Generally, a stable community returns to its initial state after a small perturbation, while an unstable community does not. Stable community behavior is attributed to the two quantifiable metrics, resistance and resilience (Pimm 1984). **Resistance** is defined as the degree to which community behavior is insensitive to a perturbation, and **resilience** is the rate at which community behavior returns to its original condition (Shade, Peter et al. 2012). An increase in any combination of resistance and resilience is desirable for bioprocessing and often for **ecological fitness**, defined as the ability of an organism to survive and reproduce in an environment. Another set of properties that can emerge from community interactions is productivity and uptake. **Productivity** is defined by the rate at which material is produced; **uptake** is the material consumption rate. Many ecological studies have observed correlations between productivity and diversity (or species richness) (Waide, Willig et al. 1999), although a universally accepted mechanism has not been identified.

## 2.3. Ecological Theories for Interpreting and Designing Communities

Ecologists have historically studied multiscale material and energy flows between populations and their environments. Resource scarcity has influenced fundamental aspects of biological organization, including the elemental and macromolecular composition of microorganisms (Zinn, Witholt et al. 2004, Dekel and Alon 2005, Elser, Acquisti et al. 2011). Hence, theories focused on themes of resource acquisition, resource investment, energetic efficiencies, and tradeoffs have been developed to explain observations of natural phenomena. Fundamental theories help organize observations, describe community behaviors, and enable strategic engineering of community composition or manipulation of environmental factors to improve natural and biotechnological processes (Prosser, Bohannan et al. 2007, Brenner, You et al. 2008, Konopka 2009). The current section details three distinct but complementary ecological theories that provide explanations for the competitive basis of component organization and interaction outcomes found in many natural and engineered communities. These classical theories will remain relevant to ecologists and bioengineers as their respective fields further mature. Table 2.4 outlines some existing studies of microbial communities employing these theoretical concepts.

### 2.3.1. Maximum Power Principle

The maximum power principle describes community interactions based on acquisition of available energy. The maximum power principle asserts that the fitness of biological systems will increase with the rate of available energy harvest, resulting in a

maximization of metabolic power (units of J/s) (Lotka 1922, Lotka 1922, Sciubba 2011). From an evolutionary viewpoint, the principle predicts selection of systems that capture previously unutilized energy sources (Cai, Montague et al. 2006). The ability to acquire available energy from the environment at faster rates leads to enhanced fitness by enabling more energy to be apportioned to survival and reproduction, while reducing available energy for competitors. Interactions between populations that increase the overall metabolic power of a system can lead to coexistence via cooperation (Sciubba 2011) or niche differentiation such as the use of different substrates (Cai, Montague et al. 2006). Additional related postulates have been proposed over the years, including maximization or minimization of entropy (DeLong 2008, Martyushev 2013). Box 2.1 graphically demonstrates interaction outcomes for two populations with different metabolic powers.

### 2.3.2. Resource Ratio Theory

Resource ratio theory is an ecological theory describing resource consumption, competition, and niche partitioning in which interpopulation interactions are defined with respect to shared resources (Tilman 1982, de Mazancourt and Schwartz 2010). These resources are often essential, but hemi-essential and substitutable resources have also been studied (Tilman 1980). Resource ratio theory postulates that the population best capable of depleting a limiting resource while maintaining a positive growth rate will be most competitive. The resource ratio theory has been used to assess outcomes (competitive exclusion or coexistence) between populations competing for shared limiting resources and can predict resource levels that will permit coexistence of multiple populations (Tilman 1980, Tilman 1981, Tilman 1982,

Passarge, Hol et al. 2006). The theory can be consistent with classic chemostat theory, which states that it is possible to sustain multiple stable populations when there are multiple limiting substrates, provided that each population is limited by a different resource (Taylor and Williams 1975, Bull 2010, Brauer, Stomp et al. 2012).

Table 2.4. Ecological theory studies.

| Theory | Community | Description | Reference |
|---|---|---|---|
| Maximum power | Aquatic planktonic microcosms | Effect of pH-controlled light on power acquisition | (Cai, Montague et al. 2006) |
| Maximum power | Two closely-related picocyanobacteria | Stable coexistence due to light partitioning | (Stomp, Huisman et al. 2004) |
| Resource ratio | Competition studies with bacteria, phytoplankton, and zooplankton | Meta-analysis of prediction consistency | (Spijkerman 2007) |
| Resource ratio | Nine phytoplankton species | Competition for nitrogen, phosphorus, and light | (Brauer, Stomp et al. 2012) |
| Pareto/Tradeoff | Three-member hot springs mat community | Community productivity and inhibitory byproduct tradeoffs | (Taffs, Aston et al. 2009) |
| Pareto/Tradeoff | Syntrophic *Geobacter* species | Interspecies electron transfer | (Nagarajan, Embree et al. 2013) |

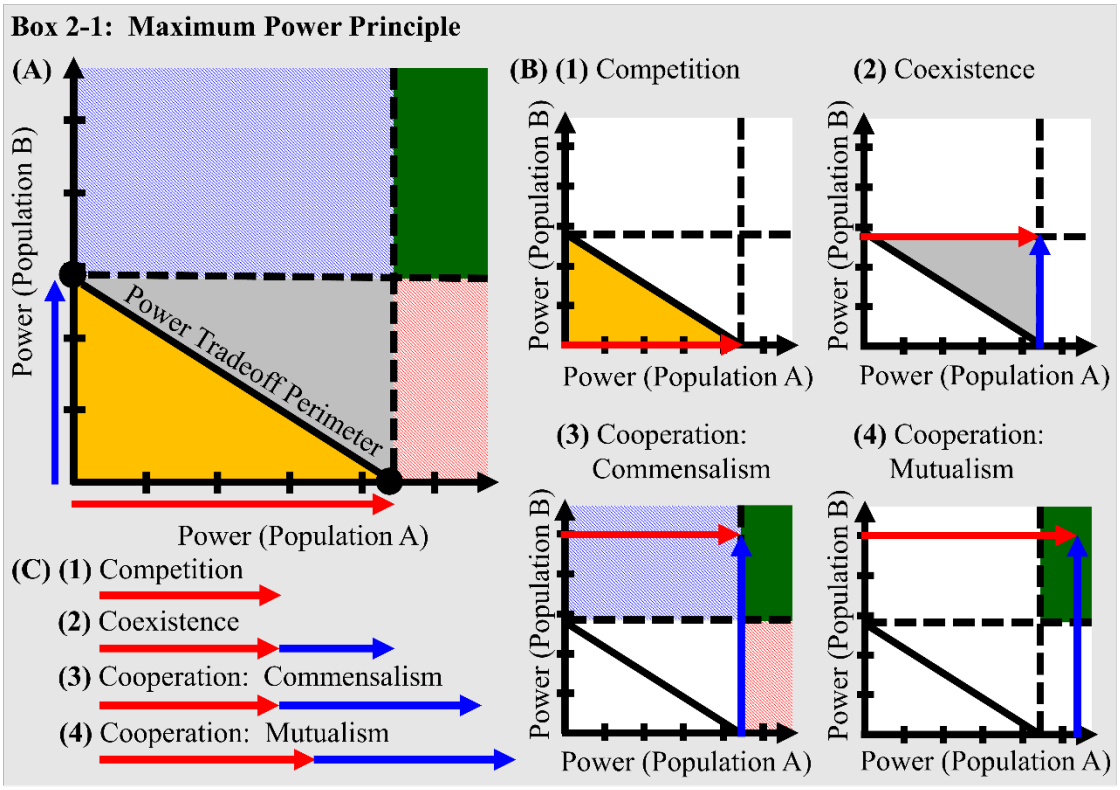


Box 2.1. (A) Graphical representation of key concepts from the maximum power principle. Populations A and B are each characterized by a steady state metabolic power when growing in monoculture (black dots on axes; red and blue arrows represent magnitude of power). The line connecting these two points, the power tradeoff perimeter, represents the partitioning of metabolic power between the two populations. Points within the plot represent the cumulative biological power of the community through summing the individual metabolic powers for populations A and B. The greater the distance from the origin, the higher the total community power, which the theory asserts is more ecologically competitive.
(B) Interaction outcomes interpreted with maximum power principle.
(B1) Populations A and B are competing for resources within the same ecological niche. According to the maximization of power principle, the population with the largest metabolic power will outcompete the other population. Therefore, population A will outcompete population B. Any mixture of two competing populations in the same niche has a total metabolic power that is a non-negative linear combination of the individual metabolic powers and which by definition cannot exceed the power tradeoff perimeter. For unsteady state scenarios, the time-dependent trajectory of community power will shift toward the population that acquires more metabolic power, which will eventually dominate (population A here).
(B2) Coexistence can occur when populations obtain energy from separate resources, allowing each population the potential to achieve its respective maximum power. Total community power may exceed the power tradeoff perimeter but is bounded by the rectangle specified by the magnitude of the individual population maximum metabolic

powers. A neutralistic community exists at the upper right corner, while the edges bounding this region indicate an ammensalistic community in which one population realizes its maximum power and one does not.
(B3) Cooperating populations can exceed the maximum power of neutralistic populations if one population facilitates the acquisition of energy by the other population (e.g., commensal interaction). This results in the total community power exceeding the maximum power attainable by neutralistic populations (boundary of the green region). Parasitic interactions would reduce this gain in community power because the increased energy acquisition of one population occurs at the expense of the other population (red and blue patterned regions indicate parasitism favoring populations A and B, respectively).
(B4) The total community power can exceed a linear combination of the monoculture maximum powers if the populations exhibit a mutualistic relationship. The two populations facilitate acquisition of metabolic energy by each other, placing the community power in the green region. The final magnitude of an unsteady state time-dependent trajectory is unknown without further information about the interaction. Figure adapted from DeLong, 2008.

Resource ratio theory can describe cooperative populations by accounting for mutualistic resource exchange. Cooperating populations that exchange limiting resources can exist in a wider range of resource environments than is possible for either population individually. This scenario describes what has been termed a super-competitor unit (de Mazancourt and Schwartz 2010), a community with the emergent property of enhanced resource utilization that can deplete limiting resources more effectively than the individual monocultures. This ability to survive at reduced resource availabilities highlights an evolutionary advantage of cooperation that has been observed in natural ecosystems (de Mazancourt and Schwartz 2010). Resource ratio theory extended to cooperation is analogous to the economic concept of comparative advantage, where specialization and resource exchange enable enhanced community function (Enyeart, Simpson et al. 2015). Box 2.2 describes a generalized example of resource ratio theory applied to two different populations,

each of which is more effective at depleting a different essential resource (de Mazancourt and Schwartz 2010).

### 2.3.3. Resource Allocation Theories: Pareto Surfaces and Metabolic Tradeoff Analysis

Biological systems from enzymes to communities represent competitive resource allocation (Sterner and Elser 2002). Phenotypic plasticity, the ability to change phenotype with changing environment, can enable different relationships between cellular function and resource allocation. However, phenotypic plasticity requires additional resources for the genes and regulatory systems to express different phenotypes under different environments. This investment cost for phenotypic plasticity may be ecologically justified for populations that persist in spatially and/or temporally dynamic environments (Agrawal 2001).

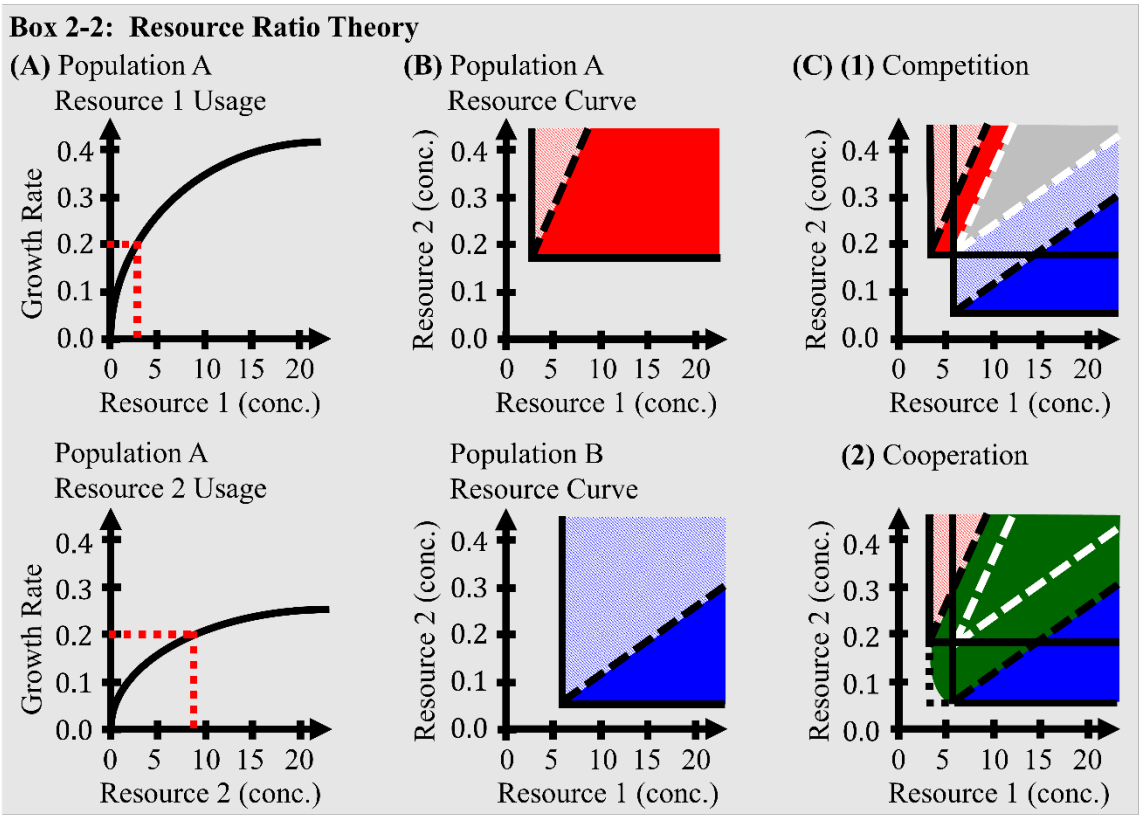


Box 2.2. Graphical representation of resource ratio theory.
(A) Determination of resource requirements. The resource concentrations required to support steady state growth of population A are tabulated using Monod expressions; an analogous set of data for population B is not shown. Resources 1 and 2 are essential for both species (e.g., nitrogen- or phosphorus-containing metabolites). The red dotted lines denote a particular growth rate selected for study with the corresponding resource concentrations required to support steady state growth.
(B) Population growth responses to limiting resources. The minimum requirements for resources 1 and 2 to maintain a steady state growth rate are indicated by the solid black edges for population A (top) and population B (bottom). Population A has a higher affinity for resource 1 and a lower affinity for resource 2 as compared to population B. Thus, populations A and B are more effective at depleting resources 1 and 2, respectively. The shaded areas represent conditions of positive growth for each population. The slope of the dashed line separating the patterned region (resource 1-limited) from the solid region (resource 2-limited) represents the resource ratio requirement (resource 2 per resource 1 necessary for growth). If both resources are initially in excess, the population will maintain positive growth and consume resources as governed by its resource ratio requirement, until its consumption reaches the steady state resource level indicated by the solid lines.
(C) Interaction outcomes.
(C1) Resource ratio theory can describe community interactions by overlaying the properties of the two populations and examining the resulting regions. If populations A and B are competing for resources 1 and 2, the population that can drive the resource concentrations

below the acquisition capability of the other population will dominate the ecological niche. Population A will dominate the community in the red regions due to its superior ability to deplete resource 1, and population B will dominate the community in the blue regions due its superior ability to deplete resource 2. These regions are defined by intersecting the resource ratio requirements of the two populations (white dashed lines). The gray region bounded by the white dashed lines represents an excess of resource 1 for population A and an excess of resource 2 for population B. The excess of resources permits coexistence as there are sufficient resources to support both populations.
(C2) Resource ratio theory can also describe cooperating populations utilizing mutualistic resource exchange. The region of coexistence based on resource trading is expanded from (C1). In the red patterned region, population A is resource 1-limited, leaving no excess resource 1 to trade with population B. Therefore, population A will dominate the community since it is more competitive not to trade with population B. In contrast, to the right of the red patterned region, population A is resource 2-limited and has excess resource 1, making it more competitive to exchange resource 1 with population B for resource 2. Analogous reasoning explains the solid blue region. Additionally, through resource trading, populations A and B are able to exist in a wider range of resource environments than is possible for either population individually (dotted box, lower left). In this region, both resources 1 and 2 are limiting for both populations. Thus, resource exchange is more competitive since neither population can maintain growth under these resource conditions without the other. The rectangular boundary around this extended resource availability region represents an ideal one-to-one trading scenario; however, the shape of this region may take on an ellipsoidal form depending on the costs and relative fluxes of resource exchange.
Figure adapted from de Mazancourt and Schwartz, 2010.

Tradeoff theories analogous to those used in economics have been applied to metabolic systems to assess the competitive use of phenotypic plasticity (Kitano 2010). For many cellular behaviors, a benefit in one objective is realized only at the detriment of another objective. These tradeoffs are postulated to have tamed the “Darwinian demon,” a superspecies that can optimize all objectives simultaneously and which has never been observed in nature or the laboratory (Law 1979). The boundary that describes the tradeoff between resource uses is referred to as the Pareto front, efficiency frontier, or tradeoff surface (Molenaar, van Berlo et al. 2009, Carlson and Taffs 2010, Kitano 2010, Shoval, Sheftel et al. 2012). Analysis of these resource allocation strategies is often paired with

mathematical analysis such as stoichiometric modeling approaches (e.g., elementary flux mode and flux balance analyses) and/or kinetic models (Table 2.5) (Molenaar, van Berlo et al. 2009, Song, Cannon et al. 2014). Phenotypic phase plane analysis and multi-objective optimization have been used in stoichiometric modeling approaches to examine the effects of resource allocation on competitive network function (Edwards, Ramakrishna et al. 2002, Carlson and Srienc 2004, Carlson 2007, Carlson 2009, Oh, Lee et al. 2009, Schuetz, Zamboni et al. 2012). The tradeoff concept can be represented graphically via rates or efficiencies of resource utilization, a measure of cost. Box 2.3 demonstrates a generalized example of a Pareto optimization tradeoff curve for economic costs, with an analogous scenario translated into metabolic terms.

Table 2.5. Microbial community *in silico* analysis studies.

| Focus | Description | Reference |
|---|---|---|
| Review of modeling | Application of genome-scale models to microbial communities | (Mahadevan and Henson 2012) |
| Cyanobacterial mat | Three EFMA modeling approaches | (Taffs, Aston et al. 2009) |
| *Geobacter* electron transfer | Multi-omic modeling | (Nagarajan, Embree et al. 2013) |
| Synthetic microbial ecosystems | Prediction of symbiotic communities via environmental constraints | (Klitgord and Segrè 2010) |
| SRB-methanogen interactions | FBA | (Stolyar, Van Dien et al. 2007) |
| Spatial community dynamics | Reaction-diffusion FBA | (Harcombe, Riehl et al. 2014) |
| Three case studies of OptCom algorithm | Community FBA | (Zomorrodi and Maranas 2012) |
| Consortial studies | Dynamic community FBA | (Hanly and Henson 2011, Hanly, Urello et al. 2012, Zomorrodi, Islam et al. 2014) |

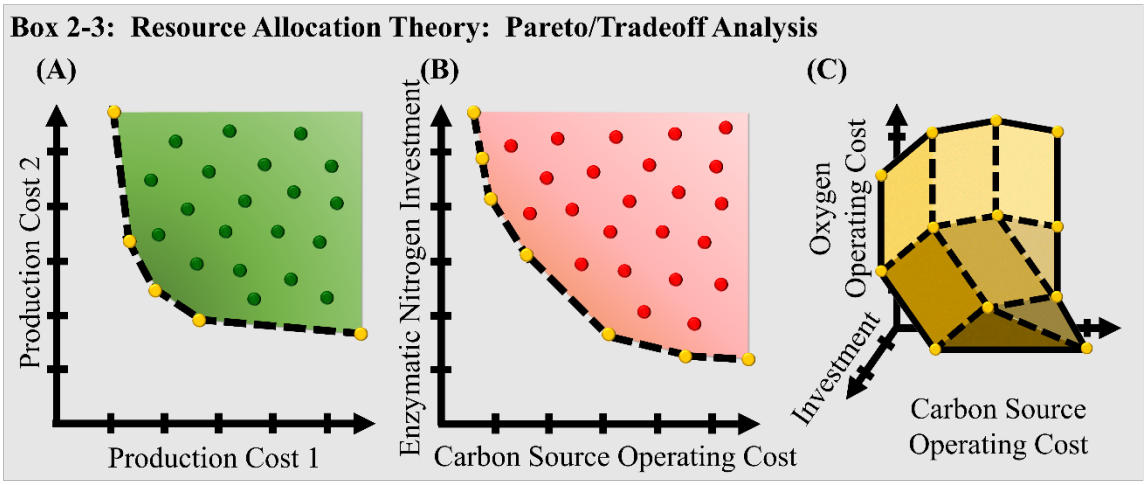


Box 2.3. (A) A generalized Pareto tradeoff surface between two economic costs associated with the production of a good (for instance, the cost of fertilizer and water required to produce a bushel of corn). The plot quantifies the tradeoff between different combinations of cost 1 and cost 2. In the example, the yellow points and the line segments connecting them represent optimal cost minimizing relationships between the variables, while green interior points represent higher-cost alternative strategies.
(B) A metabolic tradeoff surface analogous to a generalized Pareto tradeoff curve between two metabolic costs: (1) the carbon source operating cost, or the amount of carbon source required to synthesize a unit of bioproduct, and (2) enzymatic nitrogen investment, or the amount of nitrogen required to synthesize the enzymes in the utilized pathways. The yellow points represent the continuum of optimal pathways for producing the bioproduct given the objective of minimizing the cost of carbon source or nitrogen investment; interior red points represent less efficient alternative pathways for producing the bioproduct.
(C) Three-dimensional metabolic tradeoff surface considering the requirement for three resources (carbon source, nitrogen investment, and oxygen). The resulting Pareto surface represents the optimal relationship between these three costs for synthesizing a bioproduct.

Single population examples of the predictions from resource allocation tradeoffs include the predicted use of the glyoxylate shunt and the Entner-Doudoroff glycolysis pathway during *E. coli* nutrient-limited growth. These alternative pathways produce less ATP than the citric acid cycle and Embden-Meyerhof-Parnas glycolysis pathway, respectively, but also require fewer anabolic resources, such as nitrogen and carbon, to

synthesize the pathway enzymes as compared to the higher ATP-yielding pathways (Fischer and Sauer 2003, Carlson 2007, Flamholz, Noor et al. 2013).

In addition to modulating metabolic pathways, resource investment transitions are predicted to occur based on allocation of resources to either enzyme or substrate pools. Classic Michaelis-Menten kinetics describe the driving of flux via enzyme ($v_{max} = k_{cat} \cdot [E]$) and substrate pools. These two pools create a continuum of drivers for a single flux, ranging from high relative substrate concentration to high relative enzyme concentrations (Figure 2.1A); these different flux-driving mechanisms are referred to as push- or pull-based mechanisms, respectively (Carlson, Oshota et al. 2012, Valenzuela, Mazurie et al. 2012, Tepper, Noor et al. 2013). The optimal distribution of resources between substrate and enzyme pools can vary depending on the required flux (Figure 2.1A, dotted line). Taking the FumC enzyme as an example, relatively small fluxes are best driven by a substrate-based push mechanism which minimizes overall resource requirements, while higher fluxes are best driven by a pull mechanism in which elevated enzyme concentrations represent a more efficient use of anabolic carbon.

Resource allocation between enzyme and substrate pools can also benefit microbial communities when populations exchange metabolites such as amino acids, vitamins, or nucleotides. Maximization of flux per investment of a valuable resource can be applied to a community exchanging metabolites such as cyanobacterial heterocyst-vegetative cell interactions (Kumar, Mella-Herrera et al. 2010). As a numerical illustration, five interacting populations can each individually support a flux of 50 μM/s through enzyme X, which would require a total substrate and enzyme carbon investment

of 1.51 CmM (millimolar concentration of carbon). Alternatively, one population can specialize in that function and drive a flux of 250 μM/s with a total carbon investment of 4.43 CmM and then exchange the product with the community. The division of labor strategy with product exchange reduces the total community carbon investment requirement by ~41%, neglecting the cost of metabolite exchange. Figure 2.1B demonstrates the general principle of flux as a function of total carbon investment into both enzyme and substrate pools. The net community investment savings continue to improve as the flux magnitude increases. Extrapolating to entire pathways will likely offset the involvement of transport proteins while maintaining resource investment savings. While this economy of scale holds from a purely reaction kinetics basis, additional factors such as diffusion rates and protein synthesis machinery could play substantial roles.

## 2.4. Case Studies of Communities with Interpretation

The maximum power principle, resource ratio theory, and resource allocation theory are useful for developing and interrogating the design principles of microbial communities. The current section provides an analysis of natural and engineered communities with dissection of relevant components, interactions, and theories.

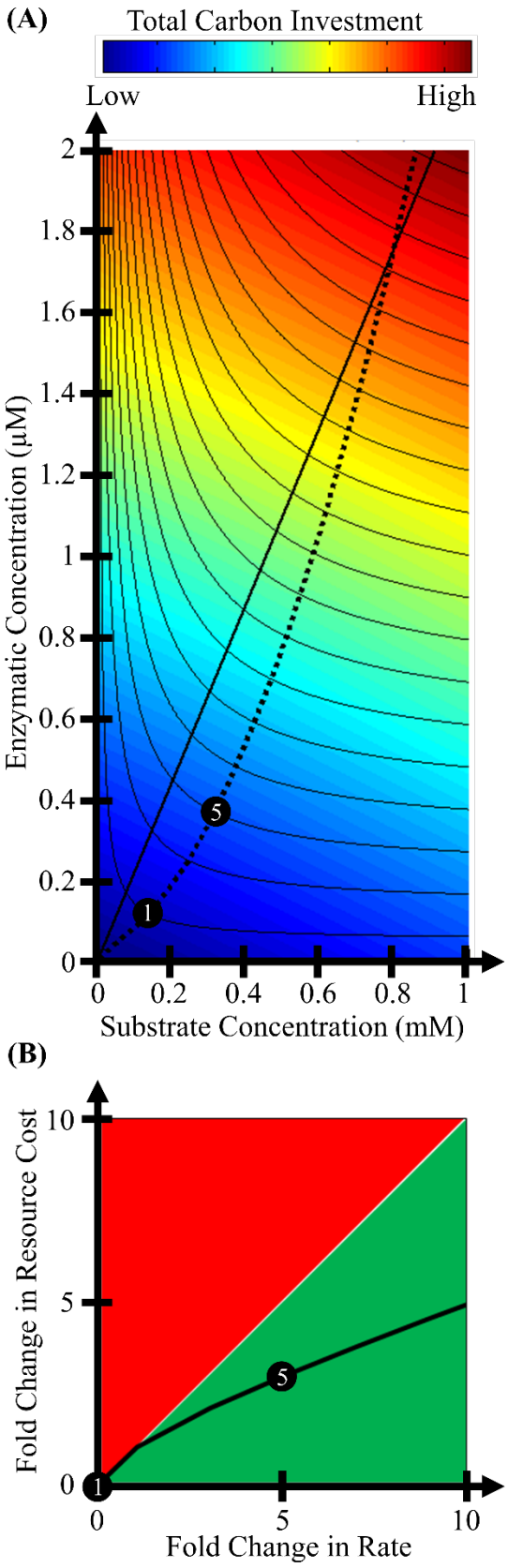
(A)
Total Carbon Investment
Low
High
Enzymatic Concentration (μM)
Substrate Concentration (mM)
0
0.2
0.4
0.6
0.8
1
1.2
1.4
1.6
1.8
2
1
5
(B)
Fold Change in Resource Cost
Fold Change in Rate
0
5
10
1
5

Figure 2.1. Resource investment and economies of scale for enzymatic flux. (A) A target enzymatic flux described by Michaelis-Menten kinetics can be achieved by a continuum of substrate and enzyme concentrations. Thin solid curves depict reaction isoflux lines that increase moving away from the origin. The substrate and enzyme concentrations each have associated resource costs related to the size and composition of the molecules. The total resource investment cost, depicted in color, sums the carbon investment from both the substrate and enzyme pools. The heavy solid line marks equal carbon investment into substrate and enzyme pools. The dotted line represents the minimum total carbon investment for each isoflux line. (B) Relationship between increasing flux and resource investment based on the optimal minimization of investment. Total carbon investment per flux can be higher (red), lower (green), or the same (boundary) at larger fluxes as compared to smaller fluxes. In the example depicted, an increase in flux from 50 mM/s (point 1) to 250 mM/s (point 5) requires only three-fold more resources. This principle can be extrapolated to entire pathways, posing a mechanism for improved resource efficiency with increased specialization, as represented by the economies of scale. (A) Enzyme and substrate calculations used $K_{cat}$=1150 $s^{-1}$ and $K_m$=0.207 mM assuming fumarate and 8800 carbon atoms per functional enzyme (*e.g.* FumC homotetramer).

### 2.4.1. Case Study: Multilevel Interactions in a Naturally Occurring Phototrophic Community

2.4.1.1. Community Description. The naturally occurring phototrophic community "*Chlorochromatium aggregatum*" is comprised of the phototrophic green sulfur bacterium *Chlorobium chlorochromatii* physically attached to the heterotrophic β-proteobacterium *Candidatus* Symbiobacter mobilis (Figure 2.2). This community is typically arranged as 13 green sulfur bacteria surrounding a single central β-proteobacterium and is found in sulfide-containing, oxic-anoxic interfaces of stratified lakes (Overmann, Tuschak et al. 1998, Overmann 2010). The green sulfur bacteria are nonmotile anoxygenic phototrophs which use light energy and electrons from sulfide to fix carbon and nitrogen. The heterotrophic β-proteobacterium is motile and possesses genetic evidence of phototactic and chemotactic capabilities but cannot harvest light energy and has limited respiratory capacities (Liu, Müller et al. 2013). The green sulfur

bacterium, although culturable in the laboratory, is not found free-living in nature, and the β-proteobacterium is unculturable independent of the green sulfur bacteria (Vogl, Glaeser et al. 2006, Liu, Müller et al. 2013).

2.4.1.2. Interaction Mechanisms. "*C. aggregatum*" interacts via a number of mechanisms. First, the green sulfur bacteria exchange anabolic and catabolic metabolites (reduced carbon and nitrogen) with the β-proteobacterium. Metabolite exchange is hypothesized to be bidirectional; the β-proteobacterium may synthesize compounds such as acetate that could be assimilated by the green sulfur bacteria due to limited respiratory capabilities (Liu, Gao et al. 2013). Additionally, the β-proteobacterium and green sulfur bacteria are connected by periplasmic tubules. The direct physical interaction between the bacteria enables the β-proteobacterium to provide community motility toward light and sulfide (Müller and Overmann 2011, Bryant, Liu et al. 2012). These intercellular contacts could also permit exchange of electrons via soluble carriers (Wanner, Vogl et al. 2008), enabling community-wide energy transfer and redox balancing (Liu, Müller et al. 2013).

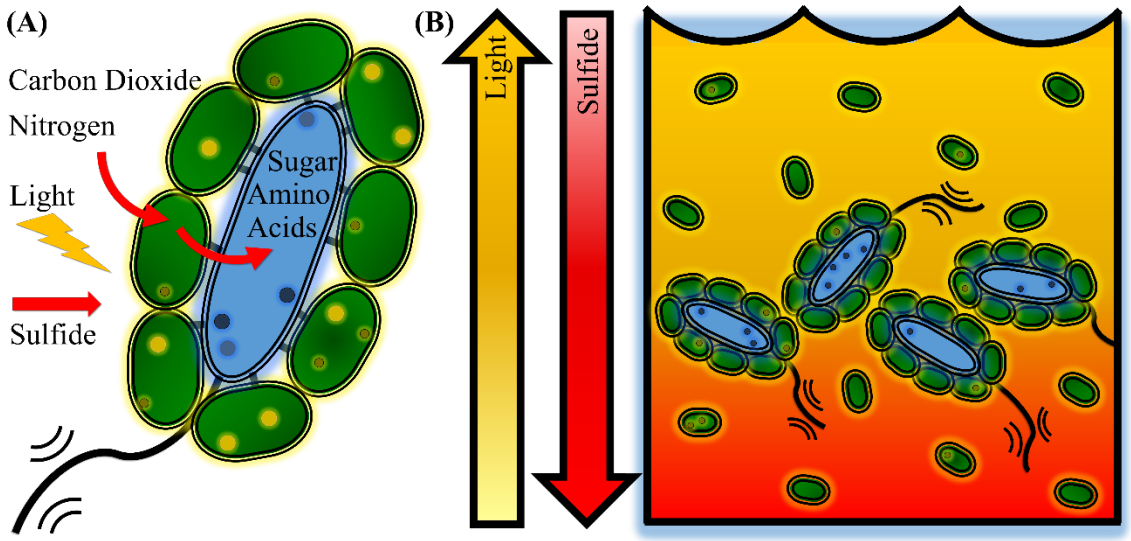


Figure 2.2. Phototrophic community interactions. (A) Green sulfur bacteria fix carbon dioxide and nitrogen from the environment and exchange reduced products with the heterotroph. In return, the heterotroph maintains a flagellum and provides taxis toward light and sulfide, which the green sulfur bacteria require for photosynthesis. (B) In a stratified lake environment, light is more intense at the top of the lake, and sulfide concentration increases toward the bottom. The motile community is able to take advantage of ideal concentrations of both resources, whereas free-living green sulfur bacteria are not able to do so; note that the heterotroph is not able to exist independent of the green sulfur bacteria.

2.4.1.3. Theory Applications. Resource ratio and resource allocation theories provide an evolutionary rationale for the interactions of these two bacteria. In an environment with scarce resources (e.g., light, sulfide, reduced carbon, reduced nitrogen), this cooperative strategy confers a selective advantage (de Mazancourt and Schwartz 2010). The physical interactions and metabolite exchange are consistent with the resource ratio theory concept of a super-competitor unit. The motility contributed by the β-proteobacterium enables a competitive advantage for growth at low sulfide concentrations and lower light intensities via directed movement toward essential resources (Fröstl and Overmann 1998). Additionally, the community configuration

minimizes the associated resource investment costs. The direct physical connection between the bacteria permits 14 cells to benefit from the ability to move actively toward light and sulfide while only one cell needs to maintain the sensing and motility genes, synthesize flagellar proteins, and power flagellar operation (Liu, Müller et al. 2013).

### 2.4.2. Case Study: Anaerobic Syntrophy in Methanogenic Communities

2.4.2.1. Community Description. Methane is a major focus of renewable energy efforts and plays an essential role in ecological food webs. Anaerobic communities produce methane by catabolizing organic feedstocks like biomass via a cascade of cross-feeding microorganisms. Sulfate-reducing bacteria (SRBs) and methanogenic archaea are key members of these anaerobic communities found in aquatic sediments and anaerobic digesters (Offre, Spang et al. 2013). The SRBs oxidize organic acids and produce hydrogen or formate in the absence of alternative electron acceptors. The methanogens catabolize hydrogen and formate for cellular energy, ultimately producing methane as a by-product (Figure 2.3) (Li, McInerney et al. 2011, Meyer, Kuehl et al. 2013).

2.4.2.2. Interaction Mechanisms. Methanogenic communities have a strong requirement for metabolite exchange due to the thermodynamic constraints of hydrogen synthesis (Schink 1997, Thauer, Kaster et al. 2008, Stams and Plugge 2009). Hydrogen partial pressures above a very small critical threshold (~10 Pa) shift the chemical reaction equilibrium from hydrogen synthesis to hydrogen consumption, stalling SRB metabolism in the absence of sulfate. The consumption of hydrogen by methanogens reduces local hydrogen partial pressures below the critical threshold, enabling further SRB catabolism

(Stams and Plugge 2009). The mutualistic interactions can extend further. In addition to providing the methanogens with substrate, the SRBs can also modify the local environment by reducing sulfate to sulfide rather than forming hydrogen. Sulfide is highly reactive with oxygen and reduces the environmental concentrations of oxygen, benefiting the oxygen-inhibited methanogens. In addition, research suggests that SRBs enhance methanogen consumption of hydrogen by exchanging anabolic resources like amino acids (Walker, Redding-Johanson et al. 2012).

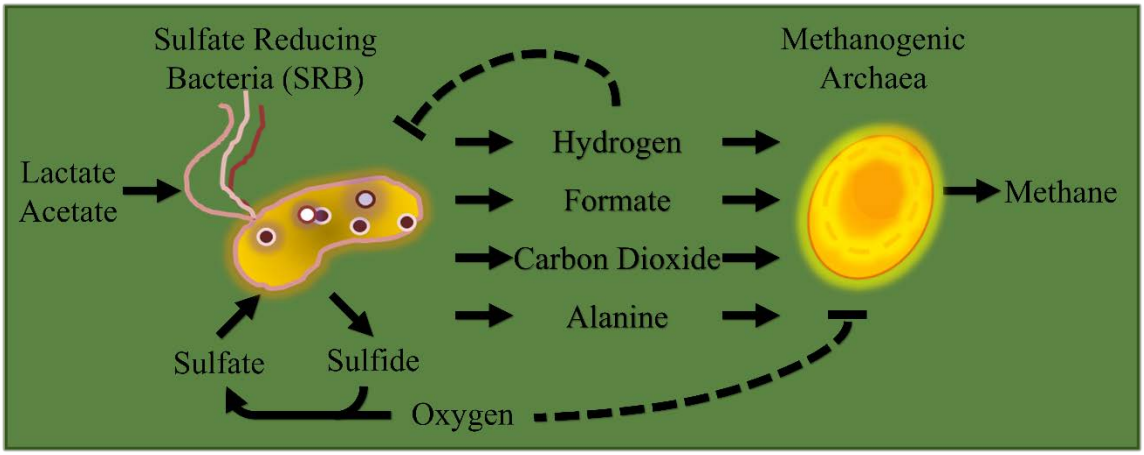


Figure 2.3. Sulfate reducing bacteria (SRBs) – methanogen anaerobic syntrophy. SRBs create a reducing environment conducive to methanogenesis by reducing sulfate to sulfide, which can then abiotically react with oxygen. In the absence of sulfate, SRBs oxidize carbon producing hydrogen and formate; this metabolism becomes unfavorable without a hydrogen sink. Methanogens consume the hydrogen, facilitating SRB oxidation of carbon. SRBs cross feed anabolic resources like amino acids to facilitate methanogen growth, resulting in a larger hydrogen sink.

2.4.2.3. Theory Applications. SRB-methanogen communities are a well-studied example of anaerobic syntrophy (McInerney, Sieber et al. 2009). The cross-feeding of hydrogen, which can also be viewed as an environmental modification interaction, represents a classic example of the maximum power principle by collectively increasing

the potential for energy acquisition from the environment. Metabolite exchange allows the SRBs to consume substrate at higher rates, thus increasing the collective community metabolic power. The exchange of anabolic resources such as amino acids is proposed to facilitate methanogen growth by providing an energetically expensive metabolite, thus increasing methanogen consumption of hydrogen (Walker, Redding-Johanson et al. 2012). The amino acid cross-feeding strategy represents an example of improved function per anabolic resource investment according to resource allocation theory (Figure 2.1B).

The syntrophic interactions of methanogens are not strictly limited to hydrogen-producing SRBs. Hydrogen-producing fermenters, which provide the substrate for SRBs, also benefit from methanogens (Bizukojc, Dietz et al. 2010). Hydrogen transfer has also been observed in communities of hydrogen- producing anaerobic fungi and methanogens, which demonstrate the emergent property of more complete degradation of cellulosic biomass (Cheng, Edwards et al. 2009).

### 2.4.3. Case Study: Cross-Feeding Chemostat Communities

2.4.3.1. Community Description. Culturing a clonal population of *E. coli* in a glucose-limited chemostat for hundreds of generations results in the reproducible formation of multiple, phenotypically distinct *E. coli* populations which cross-feed secondary metabolites (Figure 2.4) (Rosenzweig, Sharp et al. 1994, Treves, Manning et al. 1998, Kinnersley, Wenger et al. 2014). The interacting community consists of three distinct functional populations: a glucose-catabolizing glycerol- and acetate-producing specialist, an acetate-catabolizing specialist, and a glycerol- catabolizing specialist. Both the acetate- and glycerol-catabolizing specialists completely oxidize their respective

substrates. The population functions are based primarily on mutations in gene regulatory sequences, resulting in altered gene expression (Kinnersley, Wenger et al. 2014). For instance, the glucose-catabolizing specialist expresses the high-affinity Mgl sugar transporter and has reduced expression of citric acid cycle enzymes, resulting in acetate and glycerol secretion. This strain, which represents 80% of the community, grown in isolation has a lower specific growth rate and a lower biomass per glucose yield than the parent monoculture; yet the community demonstrates a 15% improvement in biomass per glucose yield. The reproducibility of the interacting consortium suggests that the organization of components and interactions is more competitive and stable than an *E. coli* monoculture in a homogeneous environment like a chemostat.

2.4.3.2. Interaction Mechanisms. The community populations interact through the cross-feeding of catabolic resources. Additionally, consumption of acetate represents an environmental modification interaction that reduces the inhibition of the glucose-catabolizing strain.

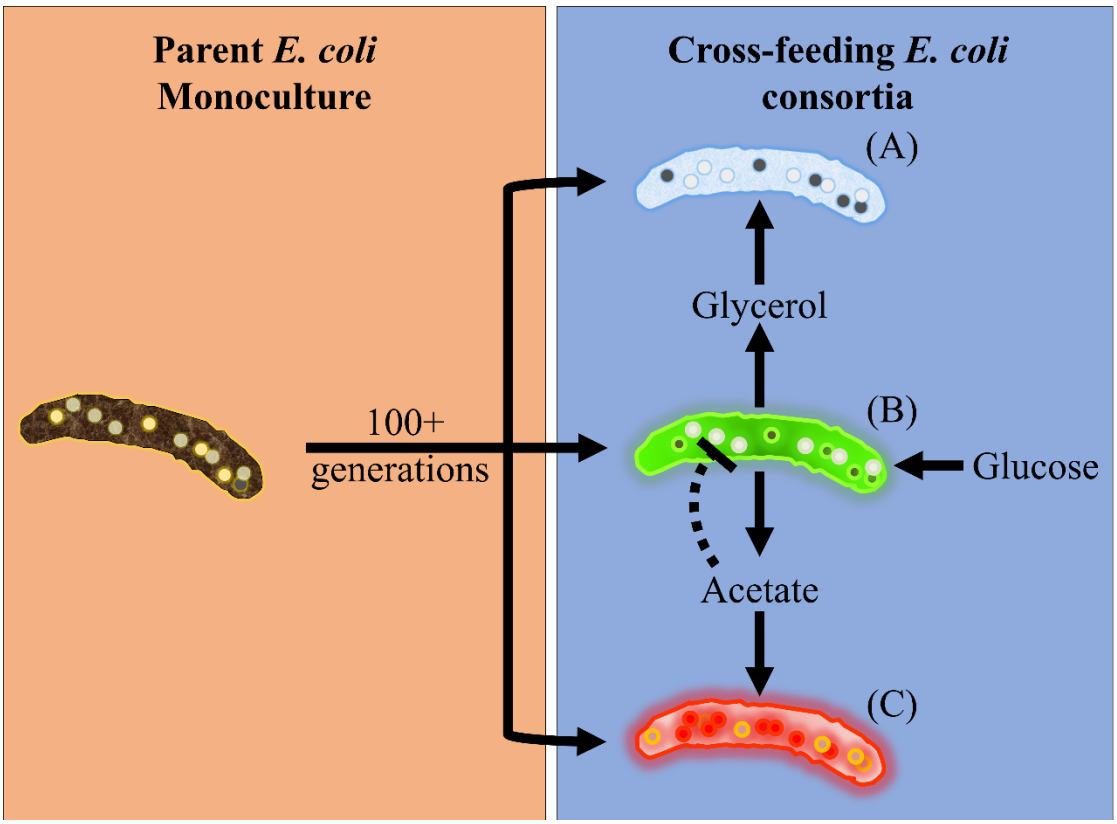


Figure 2.4. Naturally occurring *E. coli* cross-feeding communities. *E. coli* grown long term in glucose-limited chemostats evolve into cross-feeding communities. Community members include a glucose catabolizing specialist that produces acetate and glycerol, an acetate catabolizing specialist and a glycerol catabolizing specialist. The cross-feeding community has a ~15% improvement on biomass per glucose yields as compared to the parent culture and deplete available substrates more completely than the parent culture.

2.4.3.3. Theory Applications. The cross-feeding *E. coli* community highlights key features of the maximum power principle, resource ratio theory, and resource allocation theory. The consortium has a higher metabolic power than the monoculture because inhibitory by-products (e.g., acetate) are removed during growth, allowing for a higher community metabolic rate. The community, as a whole, demonstrates the emergent property of a super-competitor unit defined in resource ratio theory; through metabolite exchange, the community drives the concentrations of carbon-based resources to levels unattainable by the

parent monoculture. The populations also demonstrate an enhanced resource allocation configuration through division of metabolic labor. Each respective population increases expression of enzymes associated with a portion of central metabolism. The glucose-consuming specialist has higher glycolytic expression but lower citric acid cycle fluxes, resulting in the secretion of acetate and glycerol (Rosenzweig, Sharp et al. 1994, Treves, Manning et al. 1998, Kinnersley, Wenger et al. 2014). The strategy is representative of the tradeoff between substrate-driven and enzyme-driven fluxes; driving a reduced number of higher fluxes can be less resource intensive than driving a greater number of smaller fluxes. A synthetic biology analog of the cross-feeding community has been created based on gene deletion rather than altered gene regulation (Bernstein, Paulson et al. 2012). The synthetic system demonstrated improved biomass productivity under batch, chemostat, and biofilm culturing conditions.

## 2.5. Conclusions

The ebbs and flows of scientific efforts build largely on achievements of the predecessors of the modern scientific community. While gaining popularity in recent years, the importance of microbial communities is not new. At this time of renewed interest in a systems-focused future, it is critical to keep a broad view. The early reductionist scientists are to be commended for laying a solid foundation that enables the current trajectory toward systems studies. In fact, reductionist approaches have a bright future because systems cannot be constructed solely on noble postulations but must be

grounded in well-described components. It is not possible to define an emergent property until the basic components and interactions are appropriately catalogued.

A paramount goal and current challenge facing microbial community design is to mechanistically understand the design principles that govern higher order attributes of polymicrobial communities. The definitions presented here lay a foundation for a common language to bridge gaps across varying disciplines and enable greater collaboration between fields studying polymicrobial communities. The three ecological theories discussed—maximum power principle, resource ratio theory, and resource allocation theory—distill a broad range of literature regarding ecological theory into a concise synthesis and highlight the relevance of these theories to community interaction outcomes. The usefulness of these theories is illustrated through application to specific case studies in both natural and engineered environments. The tenets of resource acquisition, concentration, and allocation will remain useful for developing and examining the design principles of microbial communities and guide the future of polymicrobial bioprocess engineering.

## 2.6. Acknowledgments

The development of this work was supported by the National Institutes of Health awards (1U01EB019416-01, P20GM103474) and the Genomic Science Program (GSP), Office of Biological and Environmental Research (OBER), U.S. Department of Energy (DOE), and is a contribution of the PNNL Foundational Scientific Focus Area (Principles of Microbial Community Design) subcontracted to Montana State

University. Ashley E. Beck was supported by the Office of the Provost at Montana State University through the Molecular Biosciences Program. Hans C. Bernstein was supported by the Linus Pauling Distinguished Postdoctoral Fellowship which is a Laboratory Directed Research and Development program at PNNL, operated for the DOE by Battelle Memorial Institute under Contract DE-AC05-76RLO 1830. The content is solely the responsibility of the authors and does not necessarily represent the official views of the National Institutes of Health.

# CHAPTER THREE

# MEASURING CELLULAR BIOMASS COMPOSITION FOR COMPUTATIONAL BIOLOGY APPLICATIONS

## Contribution of Authors and Co-Authors

Manuscript in Chapter Three

Author: Ashley E. Beck

Contributions: Conceived and designed the experiments, performed the experiments, analyzed the data, wrote the manuscript

Co-Author: Kristopher A. Hunt

Contributions: Analyzed the data, edited the manuscript

Co-Author: Ross P. Carlson

Contributions: Conceived and designed the experiments, wrote the manuscript

Manuscript Information Page

Ashley E. Beck, Kristopher A. Hunt, and Ross P. Carlson

Status of Manuscript:
____ Prepared for submission to a peer-reviewed journal
_X__ Officially submitted to a peer-review journal
____ Accepted by a peer-reviewed journal
____ Published in a peer-reviewed journal

Submitted to *Processes*, Methods in Computational Biology Special Issue
Multidisciplinary Digital Publishing Institute
Received January 26, 2018
Revisions Requested February 19, 2018

## 3.1. Abstract

Computational representations of metabolism are increasingly common in medical, environmental, and bioprocess applications. Cellular growth is often an important output of computational biology analyses, and therefore, accurate measurement of biomass constituents is critical for relevant model predictions. There is a distinct lack of detailed macromolecular measurement protocols, including comparisons to alternative assays and methodologies, as well as tools to convert the experimental data into biochemical reactions for computational biology applications. Herein is compiled a concise literature review regarding methods for five major cellular macromolecules (carbohydrate, DNA, lipid, protein, and RNA) with a step-by-step protocol for a select method provided for each macromolecule. Additionally, each method was tested on three different bacterial species, and recommendations for troubleshooting and testing new species are given. Finally, the macromolecular composition measurements are used to construct biomass synthesis reactions with appropriate quality control metrics like elemental balancing for common computational biology methods, including flux balance analysis and elementary flux mode analysis. The current work furthers the computational biology community by reviewing literature regarding a variety of common analytical measurements, developing detailed procedures, testing the methods in the laboratory, and applying the results to metabolic models, all in one publicly available resource.

## 3.2. Introduction

The *in silico* study of metabolism has largely transitioned from a specialty discipline to a mainstream biological approach due to improvements in software usability, increases in computational power, and the accumulation of omics databases. Cellular growth is a critical component of many of these computational biology studies (Pramanik and Keasling 1997, Feist and Palsson 2010, Hunt, Jennings et al. 2016). Understanding the foundation of growth from the level of mass and energy fluxes remains critical for interpretation and integration of *in silico* metabolic models and omics data sets. The macromolecular composition of a cell is one such area of basic knowledge. Macromolecular composition is governed by allocation of resources and can shift depending on cell cycle and specific growth rate (Vrede, Dobberfuhl et al. 2004, White, Drummond et al. 2012).

Constraint-based modeling approaches typically use production of biomass as an objective function, and macromolecular composition dictates the metabolic precursors necessary for growth. Different weightings of macromolecular components in the biomass synthesis reaction can influence results by shifting requirements for precursors (Cankorur-Cetinkaya, Dikicioglu et al. 2017). Often, coefficients are borrowed from literature reported for *Escherichia coli* or an organism similar in physiology or phylogeny to the organism being modeled. However, these values may not be representative of the organism under study. In biotechnology applications, a specific macromolecular component may be targeted, such as lipids extracted for biofuels (Lohman, Gardner et al. 2013) or starch compounds for biochemical production. Accurate quantification of these

components is important for comparison of production potential under different conditions. Additionally, ratios of macromolecule pools, such as protein, DNA, or RNA, from a microbial population can be correlated to important culture properties, including specific growth rate (Bremer and Dennis 1996).

A variety of methods for quantification of any given macromolecule can be found in the literature (e.g. (Herbert, Phipps et al. 1971)). Many of these methods date back several decades, and numerous adaptations have arisen over the years. Selecting and implementing a method with an assurance of valid and accurate results relevant to computational biology applications can present a significant challenge, particularly when testing new organisms. Additionally, not all reported methods have been developed for or tested on prokaryotes, and different organisms may respond differently to treatment conditions. For example, cell wall type may influence the efficacy of reagents or procedures, resulting in a method with varying degrees of efficiency for different types of microorganisms. External factors, such as materials used, can also affect the outcome of an analysis, and specific procedural details not included in publications can hinder reproducibility. A concise collection of information about the variety of existing methods for each macromolecule, including advantages and disadvantages of methods, specific procedural details, and points for potential pitfalls, is a useful resource that is lacking from the published literature.

The current work fills this gap with objectives to: (1) review existing literature regarding methods to measure five major macromolecules (carbohydrate, DNA, lipid, protein, and RNA), (2) develop a select step-by-step protocol for each macromolecule

and test the efficacy on different types of bacterial samples, and (3) demonstrate the application to computational biology by generating biomass synthesis reactions. Three bacterial species were used as test cases in the current work: *E. coli* (gram-negative, mesophilic model laboratory organism), *Synechococcus* sp. PCC 7002 (gram-negative, mesophilic cyanobacterium; *Synechococcus* 7002 hereafter), and *Alicyclobacillus acidocaldarius* (gram-positive, thermophilic acidophile); these microorganisms encompass a range of physiological capabilities and characteristics, including photosynthesis and alicyclic fatty acids. Compiling a literature review in conjunction with laboratory-tested protocols, all within a single source, serves as a useful resource for the computational biology community and should facilitate biomass-related research for other disciplines.

## 3.3. Culturing Methods

### 3.3.1. Strains and Media

*E. coli* str. K-12 substr. MG1655 was grown in standard M9 minimal salts medium (6 g/L $Na_2HPO_4$, 3 g/L $KH_2PO_4$, 1 g/L $NH_4Cl$, 0.5 g/L NaCl), supplemented with 1 mL/L 1 M $MgSO_4 \cdot 7H_2O$ and 10 mL/L trace metals (0.55 g/L $CaCl_2$, 0.10 g $MnCl_2 \cdot 4H_2O$, 0.17 g/L $ZnCl_2$, 0.043 g/L $CuCl_2 \cdot 2H_2O$, 0.06 g/L $CoCl_2 \cdot 6H_2O$, 0.06 g $Na_2MoO_4 \cdot 2H_2O$, 0.06 g/L $Fe(NH_4)_2(SO_4)_2 \cdot 6H_2O$, 0.20 g/L $FeCl_3 \cdot 6H_2O$) (Ausubel, Brent et al. 1992, Bernstein, Paulson et al. 2012).

*Synechococcus* 7002 was grown in A+ synthetic seawater medium (18 g/L NaCl, 0.6 g/L KCl, 1 g/L $NaNO_3$, 5 g/L $MgSO_4 \cdot 7H_2O$, 0.05 g/L $KH_2PO_4$, 0.27 g/L $CaCl_2$, 0.03

g/L $Na_2$ ethylenediaminetetraacetic acid, 0.004 g/L $FeCl_3 \cdot 6H_2O$, 1 g/L Tris pH 8.2), supplemented with 4 mg/L vitamin B12 and 1 mL/L P1 trace metal mix (34.26 g/L $H_3BO_3$, 4.32 g/L $MnCl_2 \cdot 4H_2O$, 0.315 g/L $ZnCl_2$, 0.03 g/L $MoO_3$, 0.003 g/L $CuSO_4 \cdot 5H_2O$, 0.0122 g/L $CoCl_2 \cdot 6H_2O$) (Stevens, Patterson et al. 1973, Ludwig and Bryant 2011).

*A. acidocaldarius* str. acidocaldarius DSM446 was grown in *Bacillus acidocaldarius* medium (BAM) (1 g/L $KH_2PO_4$, 1.5 g/L $(NH_4)_2SO_4$), supplemented with 0.2 g/L $MgSO_4 \cdot 7H_2O$, 0.1 g/L $CaCl_2 \cdot 2H_2O$, and 1 mL/L trace metal mix (10 g/L $FeSO_4 \cdot 7H_2O$, 0.1 g/L $H_3BO_3$, 0.15 g/L $MnSO_4 \cdot H_2O$, 0.18 g/L $ZnSO_4 \cdot 7H_2O$, 0.2 g/L $CuSO_4 \cdot 5H_2O$, 0.3 g/L $Na_2MoO_4 \cdot 2H_2O$, 0.18 g/L $CoCl_2 \cdot 6H_2O$) (modified from Farrand et al. (Farrand, Linton et al. 1983)).

### 3.3.2. Culture Conditions

*E. coli* cultures were grown at 37°C shaking at 150 rpm. Inoculum cultures were prepared in 8 mL of M9 + 10 g/L glucose in disposable culture tubes, inoculated with multiple isolated colonies from an agar plate streaked from a freezer stock, and grown to $OD_{600} < 0.6$ (exponential phase). Optical density was measured using 1 cm path length. Cells were then centrifuged at 4000 rpm for 10 minutes and re-suspended to $OD_{600} \sim 0.05$ in 50 mL of fresh M9 + 1 g/L glucose in 250-mL baffled shake flasks. Cultures were grown to $OD_{600} \sim 0.6$ (exponential phase) and then harvested for analysis (collected in chilled 50-mL polypropylene centrifuge tubes on ice followed by centrifugation).

*Synechococcus* 7002 cultures were grown at 38°C without shaking under continuous light. Inoculum cultures were prepared in 25 mL of A+ media in 250-mL non-

baffled shake flasks, inoculated with multiple isolated colonies from an agar plate (transferred monthly for propagation), and grown to $OD_{730}$ < 0.5. Cells were then centrifuged at 4000 rpm for 10 minutes and re-suspended in 25 or 50 mL of fresh A+ media to an $OD_{730}$ ~0.1. Cultures were grown to $OD_{730}$ 0.4-0.5 and harvested for analysis.

*A. acidocaldarius* cultures were grown at 60°C shaking at 200 rpm. Inoculum cultures were prepared in 50 mL of BAM + 5 g/L glucose in 250-mL baffled shake flasks, inoculated with multiple isolated colonies from an agar plate streaked from a freezer stock, and grown to $OD_{600}$ < 0.6. Cells were then centrifuged at 4000 rpm for 10 minutes and re-suspended to $OD_{600}$ ~0.1 in 50 mL of fresh BAM + 5 g/L glucose. Cultures were grown to $OD_{600}$ ~0.6 and then harvested for analysis.

### 3.3.3. Dry Weight Determination

Optical density was correlated to biomass for each organism to determine amount of dry weight used for macromolecular analyses. Biomass to $OD_{600}$ correlation for *E. coli* of 0.5 g/L cell dry weight per unit $OD_{600}$ was obtained from Folsom, Parker, and Carlson (Folsom, Parker et al. 2014), which used the same strain.

Biomass to $OD_{730}$ correlation for *Synechococcus* 7002 was determined from biomass combined from 50-mL shake flask cultures. Cells were harvested by centrifugation (4000 rpm, 20 minutes, 4°C), re-suspended in A+ media and centrifuged again, and a series of dilutions was prepared. 3 mL of each dilution was aliquoted into pre-dried, pre-weighed aluminum pans, dried at 80°C for 24 h, and weighed on a microbalance with accuracy to 0.001 mg (Mettler Toledo MT5). Pans were dried and

weighed again to confirm stability. The correlation curve is provided in Appendix A (Figure 3.A1A).

Biomass to $OD_{600}$ correlation for *A. acidocaldarius* was determined from biomass grown in a batch fermentor aerated at 1 vessel volume per minute and agitated at 600 rpm. Cells were harvested by centrifugation (6000 rpm, 5 minutes, 4°C), re-suspended in water and centrifuged again, and a series of dilutions was prepared in pre-weighed 50-mL polypropylene centrifuge tubes, which had been dried at 100°C for one week before pre-weighing. Tubes were dried at 100°C for one week and weighed on an analytical balance with accuracy to 0.1 mg. Tubes were dried and weighed again to confirm stability. The correlation curve is provided in Appendix A (Figure 3.A1B).

## 3.4. Carbohydrate

### 3.4.1. Literature Review

Carbohydrates are common cellular energy storage molecules and constituents of cell walls. HPLC methods can be used to separate and quantify specific sugars (ASTM , Lloyd 2011); however, methods for quantifying total carbohydrates were the focus of the current work. Chaplin (Chaplin 1986) reviewed many colorimetric methods for carbohydrate quantification and detailed advantages and disadvantages of each. The phenol sulfuric acid method (Dubois, Gilles et al. 1956, Taylor 1995) is widely used, and the L-cysteine and anthrone methods (Trevelyan and Harrison 1952, Chaplin 1986) are also frequently found in the literature. An issue with many methods is interference from other cellular constituents. For example, protein interferes with measured absorbance in

the phenol sulfuric acid assay (Chaplin 1986). In the L-cysteine assay, pentose, heptose, and deoxy sugars contribute to absorbance, and absorbance stability varies among different carbohydrates. Pentoses also contribute to signal in the anthrone assay, but the absorbance fades rapidly and presents minimal interference. Different hexoses may also produce differential responses in the anthrone assay; for example, mannose produces 55% percent of the measured absorbance intensity of glucose (Trevelyan and Harrison 1952). Minimizing interference from pentoses is a key consideration when selecting assays to avoid measuring nucleotide bases twice in both nucleic acid and carbohydrate assays.

Glycogen is the most common form of carbohydrate storage for bacteria (Beck, Knoop et al. 2012). Glycogen content can indicate cellular responses to changing nutrient conditions; for instance, *E. coli* and *Synechococcus* 7002 have both been found to increase glycogen storage during nitrogen limitation (Vu, Hill et al. 2013, Folsom and Carlson 2015). Glycogen can be precipitated from cells with KOH, but alkalinity causes some degradation of glycogen. An alternative method using sodium sulfate to adsorb and co-precipitate glycogen has been developed for mosquitoes (Van Handel 1985) and adapted to bacterial samples (Del Don, Hanselmann et al. 1994) and was selected for the current study. The anthrone assay was selected for quantification of hexoses due to minimal pentose interference. The method employs sulfuric acid to hydrolyze polysaccharides to glucose monomers. In the presence of anthrone, glucose monomers are converted to hydroxyaldehydes and dehydrated to hydroxymethylfurfurals (Sattler and Zerban 1948), which form blue-green colored complexes with anthrone. The current

study tested the hexose quantification assay on cell pellets, glycogen extracts, and the residue remaining after the glycogen extraction process. The sum of the glycogen extract and residue measurements was compared with the total cell pellet measurement to verify recovery of all cellular carbohydrates. Differentiation between glycogen and other cellular carbohydrates, such as cell wall sugars, can provide useful parameters for metabolic models.

### 3.4.2. Procedure (after Del Don et al., 1994)

#### 3.4.2.1. Reagents.

- Cell pellet (0.5-1 mg dry biomass, fresh or frozen, washed with carbon-free media).
- Anthrone reagent: (per reaction) mix 10 mg anthrone and 250 µL fresh absolute ethanol (anthrone will partially dissolve), add 75% sulfuric acid to a final volume of 5 mL, and stir until anthrone is completely dissolved (Herbert, Phipps et al. 1971). Prepare fresh daily (within 24 hours of use) and store at 4°C.
- 2% sodium sulfate (w/v).
- Methanol.
- Glucose standards (prepare from fresh 1 mg/mL glucose solution). A linear response was observed using 10-250 µg/mL standards (e.g. 10, 50, 90, 130, 170, 210, 250 µg/mL). The limit of detection with anthrone has been previously reported as 5 µg/mL (Del Don, Hanselmann et al. 1994).

#### 3.4.2.2. Quantification of Glycogen.

1. Re-suspend cell pellet in 200 µL 2% sodium sulfate in 2-mL Eppendorf tube.

2. Seal tube with parafilm to prevent cap from popping open and heat for 10 minutes at 70°C (VWR analog heat block).
3. Add 1 mL methanol, and vortex in two 10-second rounds to co-precipitate sodium sulfate and glycogen.
4. Centrifuge for 15 s at 10000 rpm to pellet the precipitate (Eppendorf 5415D microcentrifuge) and decant the supernatant.
5. Wash the precipitate with 1 mL methanol (add methanol, vortex, centrifuge, and decant).
6. Re-suspend the pellet in 1 mL water, transfer to a clean glass test tube, and place on ice to chill.
7. Add 5 mL ice-cold anthrone reagent (mixing is unnecessary).
8. Chill on ice for 5 minutes, vortex briefly to homogenize the solution, and incubate in a boiling water bath for 10 minutes.
9. Place on ice for 5-10 minutes until cool, vortex briefly, and measure absorbance at 625 nm (Genesys 6 spectrophotometer).

Notes: use a neutral reaction (containing no glucose) as the blank. Perform a standard curve with each assay, and treat standards identically to samples with anthrone reagent. Different sources report slightly varying absorbance wavelengths and water bath incubation times; the most widely supported parameters were implemented in the current work.

3.4.2.3. Quantification of Hexoses Excluding Glycogen. Collect the methanol decanted after the precipitation and wash steps (steps 4-5) in an aluminum pan and

evaporate in a fume hood. The methanol contains non-glycogen hexoses, which did not adsorb to and precipitate with sodium sulfate. Re-suspend in 1 mL water, transfer to a clean glass test tube, and place on ice to chill (step 6); then perform the anthrone reaction as in steps 7-9.

3.4.2.4. Quantification of Total Carbohydrate. Skip the glycogen precipitation and wash steps (steps 1-5). Re-suspend the cell pellet in 1 mL water, transfer to a clean glass test tube, and place on ice to chill (step 6); then perform the anthrone reaction as in steps 7-9.

### 3.4.3. Test Results

Assay linearity was observed between 10-250 µg/mL glucose (Figure 3.1A). The sum of the glycogen extract and residue measurements was equivalent to the total carbohydrate measurement for *E. coli*, *Synechococcus* 7002, and *A. acidocaldarius* (Figure 3.1B, $p > 0.05$), indicating that glycogen can be accurately distinguished from other cellular carbohydrates. The glycogen mass percentage obtained for *E. coli* is similar to previously published values measured under carbon limitation (3.6%) (Folsom and Carlson 2015) and in balanced growth (2.5%) (Neidhardt, Ingraham et al. 1990). Previous measurements for *Synechococcus* 7002 estimated 10-12% of dry biomass was carbohydrates under carbon- and light-limited chemostat conditions and 61% of dry biomass was carbohydrates under nitrogen-limited conditions (Vu, Hill et al. 2013). The 17% of dry biomass value measured here falls close to the carbon- or light-limited conditions. No literature comparison was available for *A. acidocaldarius*.

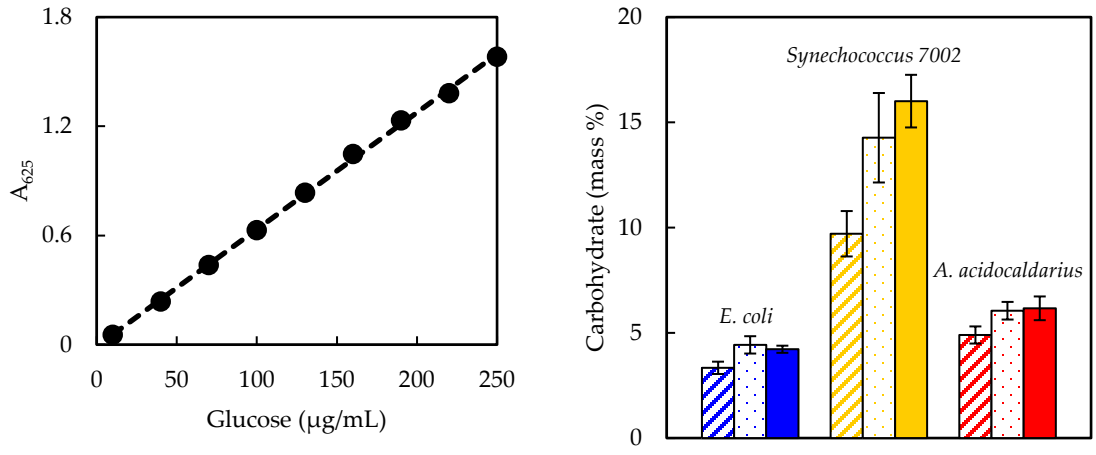


(A) (B)

Figure 3.1. (A) Representative glucose standard curve for anthrone assay. The trendline is described by the equation y = 0.0064x – 0.0082 with $R^2$ value 0.999. (B) Carbohydrate mass percentages of dry biomass measured for *E. coli*, *Synechococcus* 7002, and *A. acidocaldarius*. Striped columns indicate glycogen extract measurements, dotted columns indicate the sum of glycogen extract and residue measurements, and solid columns indicate total carbohydrate measurements. Each column is the average of biological triplicate samples with error bars representing standard deviation.

When testing the anthrone assay on glycogen extract, residue, and total carbohydrate samples, it was found that not all three measurements were captured within the standard curve for the entire set of samples; the residue represented a relatively small proportion of total cellular carbohydrates. Thus, different amounts of biomass were tested for each species to identify a quantity that would place all measurements within the standard curve. 1 mg dry weight was found appropriate for *E. coli* and *A. acidocaldarius*, and 0.5 mg dry weight was used for *Synechococcus* 7002 (i.e. organisms with higher carbohydrate content require less biomass for the assay).

Additionally, the procedure outlined in Del Don et al. (Del Don, Hanselmann et al. 1994) prescribes washing the glycogen pellet with methanol until the pellet is white.

However, in the current work, it was observed that glycogen pellets from cyanobacterial samples remained slightly blue after three successive methanol washes, most likely due to photosynthetic pigments. The anthrone assay was tested on glycogen extracts from *Synechococcus* 7002 samples after one, two, or three washes. The carbohydrate content was not significantly different among the three treatments ($p > 0.05$ for all pair-wise T-tests), indicating that a single wash is sufficient (data not shown).

## 3.5. DNA

### 3.5.1. Literature Review

DNA represents a small but important component of cellular biomass, and its content changes with specific growth rate. For example, slower-growing cells contain more DNA on a cell mass basis than fast-growing cells (Bremer and Dennis 1996, White, Drummond et al. 2012). De Mey et al. (De Mey, Lequeux et al. 2006) provided a summary and comparison of methods for quantifying DNA and RNA. De Mey et al. tested different absorbance, colorimetric, and fluorescence-based assays on purified DNA solutions and reported accuracy and sensitivity for bacteria of differing GC contents (De Mey, Lequeux et al. 2006). UV absorbance is precise but requires a pure sample (for example, from kit extraction) to minimize interference from RNA and protein. Orcinol can be used to quantify DNA colorimetrically, but has differing sensitivities for different nucleic acids and is not as precise for mixtures of DNA and RNA. The diphenylamine assay (Burton 1956) is a commonly used method but has lower sensitivity for low GC content and is not as precise as other mentioned methods (De Mey, Lequeux et al. 2006).

The diphenylamine assay also seems to be sensitive to the purity and preparation of the reagents (Herbert, Phipps et al. 1971). Fluorescence methods for DNA detection are becoming popular (De Mey, Lequeux et al. 2006). Hoechst 33258 is a DNA-intercalating dye and is reported to be biased toward AT content (De Mey, Lequeux et al. 2006). However, cell lysate can be used due to low affinity of the dye for protein and RNA. Thiazole orange is another dye with high sensitivity, but it requires a pure sample and is biased toward GC content (De Mey, Lequeux et al. 2006). Additional fluorescent dyes that require pure sample for good quantification include PicoGreen and RiboGreen (Gorokhova and Kyle 2002).

Considerations when selecting a DNA quantification method include the purity of the sample, interfering substances, and bias toward nucleotide content. Based on these considerations, the Hoechst fluorescent assay was selected for the current study. It is more quantitative than extraction kits and is safer and more precise than the classic diphenylamine method. It is recognized that AT nucleotide bias and the DNA standard used will influence the resulting estimation. Downs and Wilfinger (Downs and Wilfinger 1983) have developed and validated an alkali lysis procedure with subsequent Hoechst quantification of DNA using rat pituitary cells. Downs and Wilfinger showed equivalent accuracy but greater precision than the diphenylamine assay (Downs and Wilfinger 1983).

### 3.5.2. Procedure (after Downs and Wilfinger, 1983)

#### 3.5.2.1. Reagents.

- Cell pellet (0.4-1 mg dry biomass, fresh or frozen).

- Alkali extraction solution: 1 N $NH_4OH$, 0.2% Triton X-100.
- Assay buffer: 100 mM NaCl, 10 mM EDTA, 10 mM Tris, pH 7.0 with HCl.
- Standard buffer: 100 mM NaCl, 10 mM EDTA, 10 mM Tris, pH 7.0 with HCl, 0.025 N $NH_4OH$, 0.005% Triton X-100.
- DNA standards: ~300 µg/mL stock solution calf thymus DNA (Sigma D1501), stored at 4°C. (Concentration was measured with a NanoDrop 1000 spectrophotometer and was verified after several days and again after several weeks to ensure a stable concentration.) Prepare a 100 µg/mL working stock solution with standard buffer. Dilute the working stock into a standard series with standard buffer.
- Hoechst reagent: prepare a 200 µg/mL intermediate Hoechst stock from 10 mg/mL stock solution (Biotium 40044). Prepare a 1 µg/mL Hoechst working stock fresh daily from the intermediate stock with assay buffer. Store solutions at 4°C wrapped in aluminum foil to protect from light.

Note: all solutions were prepared using nuclease-free water.

3.5.2.2. Assay.

1. Re-suspend cell pellet to 50 µL total volume in nuclease-free water in a 2-mL Eppendorf tube.
2. Add 50 µL of alkali extraction solution.
3. Incubate at 37°C for 3 hours (VWR analog heat block).
4. Dilute to 2 mL total volume by adding 1.9 mL assay buffer.

5. Transfer to a 15-mL polypropylene centrifuge tube and centrifuge (3400 rpm, 30 minutes, 4°C).
6. Aliquot 295 µL of Hoechst working reagent in a clear-bottom black 96-well plate (Corning 3603).
7. Add 50 µL of sample to the well (manual mixing via pipette is unnecessary as the plate reader mixes by shaking).
8. Use a fluorescent plate reader (Synergy HT, Gen5 software) to read the wells according to the settings in Table 3.1.

Notes. Perform a standard curve with each assay. Perform three reaction wells of each sample or standard for technical replicates.

Table 3.1. Fluorescent plate reader settings for Hoechst DNA assay.

| Setting | Options |
|---|---|
| Plate type | 96 well plate |
| Set temperature | Setpoint 30°C, preheat before moving to next step |
| Shake | Double orbital 30 s, frequency 180 cpm |
| Read | Fluorescence endpoint, 352 nm excitation, 461 nm emission, bottom optics, gain 100, Xenon flash light source, high lamp energy, normal read speed, 100 ms delay, 10 measurements/data point |

### 3.5.3. Test Results

Downs and Wilfinger's protocol (Downs and Wilfinger 1983) reported using 0.1 µg/mL Hoechst. However, saturation of calf thymus standard DNA was observed with 0.1 µg/mL Hoechst in the current work (Figure 3.2A). More recent protocols (Sigma-Aldrich) have suggested that 1 µg/mL Hoechst dye may be used to detect higher quantities of DNA (up to 10 µg) but may not be as sensitive for lower DNA quantities. Based on standard curves using 0.1 µg/mL and 1 µg/mL Hoechst, 1 µg/mL was selected

for the current work due to its improved detection range (Figure 3.2A). The lowest standard concentration used in the assay was 0.25 µg/mL. Hoechst fluorescent response was determined to be linear up to 40 µg/mL DNA; however, a standard curve up to 10 µg/mL was sufficient to capture sample measurements. Additionally, calf thymus DNA standards were subjected to the lysis procedure to ensure that lysis does not cause loss of DNA. Standard curves showed equivalent fluorescent response regardless of whether or not the lysis procedure was performed, indicating that the lysis step did not influence DNA recovery (Figure 3.A2A, Appendix A). After initial testing, standards were not subjected to the lysis steps along with samples but were subjected only to the Hoechst treatment.

Different quantities of biomass were also tested to ensure that DNA recovery was in the linear range of the assay (Figure 3.2B). DNA recovery from *E. coli* plateaued between 0.5-1 mg biomass. 0.4 mg was selected as an appropriate amount of starting material for *E. coli*, as well as *A. acidocaldarius*. DNA recovery from *Synechococcus* 7002 plateaued around 1.2 mg, and 0.8-1 mg biomass was used for starting material. Organisms with higher DNA content (*E. coli*, *A. acidocaldarius*) required less biomass for the assay. Incubation time in the lysis solution also influenced DNA recovery, with longer incubation times resulting in increased DNA recovery (Figure 3.2C). Downs and Wilfinger (Downs and Wilfinger 1983) developed their assay on mammalian cells, which are more easily lysed, in contrast to bacterial cells. Incubation of *E. coli* samples over a time series of 10, 30, 60, 120, and 180 minutes resulted in about twice the amount of DNA recovered. A similar result was observed for *A. acidocaldarius*. DNA recovery for

*Synechococcus* 7002 samples increased nearly four-fold with longer incubation times. These results highlight the differing sensitivities of different cell types to assay conditions: *E. coli* and *Synechococcus* 7002 are both gram-negative bacteria, but cyanobacteria are known to have thicker cells wall with more peptidoglycan (Hoiczyk and Hansel 2000). *A. acidocaldarius* is a gram-positive bacterium but is adapted to acidophilic environments and may be more sensitive to alkaline conditions. A lysis period of 180 minutes was selected as an adequate incubation time.

Impacts of sample treatment were also investigated with *E. coli*, including freezing of the sample and washing of the cell pellet prior to treatment. Fresh and frozen samples from the same culture were assayed and not found to be significantly different (Figure 3.A2B). Downs and Wilfinger (Downs and Wilfinger 1983) reported washing samples with a cell wash solution (150 mM NaCl, 15 mM citrate, 3 mM EDTA, pH 7.0 with HCl) before performing the lysis step. In the current work, washing the sample with cell wash solution resulted in lower DNA recovery as compared to not washing (Figure 3.A2B) and may indicate cell loss or lysis during the washing process. Extracellular DNA was not expected to comprise a significant proportion of total DNA in the planktonic, exponentially growing samples; however, this may not be the case for all samples, such as biofilm or natural environmental samples.

The DNA percentage of dry biomass obtained for *E. coli* is lower than the value of 3.1% reported in Neidhardt (Neidhardt, Ingraham et al. 1990), while the percentage obtained for *Synechococcus* 7002 is similar to the results reported in Vu et al. (Vu, Hill et al. 2013) measured with the diphenylamine method. Differences in growth rate or growth

phase may contribute to differences in measured percentages. No literature comparison was available for *A. acidocaldarius*.

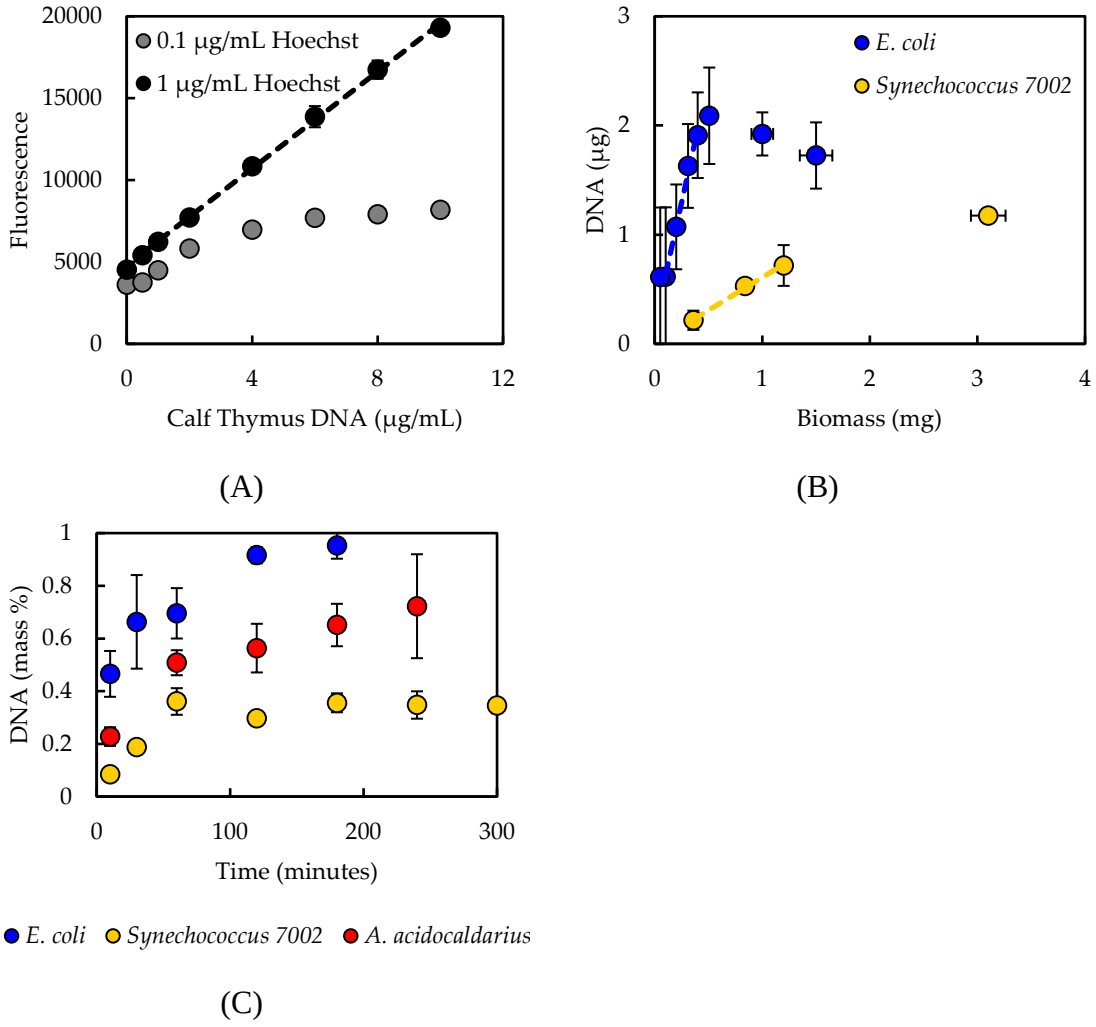


Figure 3.2. (A) Standard curve with calf thymus DNA using 0.1 µg/mL or 1 µg/mL Hoechst reagent. Error bars on the curve with 1 µg/mL Hoechst reagent represent standard deviation of duplicates. The trendline fitting the curve with 1 µg/mL Hoechst reagent is described by the equation $y = 1477x + 4803$ with $R^2$ value 0.999. (B) Relationship between dry biomass sample amount and resulting DNA quantity measured for *E. coli* and *Synechococcus* 7002. Dashed lines designate the linear regions. (C) DNA recovery depends on length of lysis step. Error bars represent standard deviation of 2-8 biological replicates. An incubation period of 180 minutes was selected for the recommended protocol.

## 3.6. Lipid

### 3.6.1. Literature Review

Lipids are essential to cellular membranes and are carbon and energy storage molecules. Measurement of total lipid is commonly performed gravimetrically, with an absorbance-based sulfo-phospho-vanillin assay (Izard and Limberger 2003), or using gas chromatography. A common gravimetric method is the Bligh and Dyer chloroform-methanol extraction (Bligh and Dyer 1959). Other solvents have been used to mitigate the hazards of chloroform, and a variety of modifications to the original Bligh and Dyer procedure exist (Lohman, Gardner et al. 2013). There is debate regarding the performance of these different methods, and methods may vary depending on downstream applications. Much research has been done on lipid extraction from biofuel-producing organisms like algae, and recent testing and comparison of methods have shown microwave extraction with GC analysis to provide optimal results (Lohman, Gardner et al. 2013). However, cyanobacteria synthesize predominantly diacylglycerol lipids as opposed to the triacylglycerol lipids of algae (Sheng, Vannela et al. 2011). Cyanobacterial lipids are also located throughout the cytoplasm in the thylakoid membranes rather than in granular pockets as in algae. Many lipids are also associated with protein and photosynthetic components through hydrogen bonding. Different methods have been tested for the cyanobacterium *Synechocystis* sp. PCC 6803, and the traditional Bligh and Dyer or Folch methods were found to produce optimal results (Sheng, Vannela et al. 2011). Different cell disruption methods have also been tested for *Synechocystis* sp. PCC 6803, and microwave extraction and autoclaving were found to be

the most efficient disruption methods (Sheng, Vannela et al. 2012). The traditional Bligh and Dyer method was selected for the current study for analysis of total cell lipid (Bligh and Dyer 1959).

3.6.2. Procedure (after Bligh and Dyer, 1959)

3.6.2.1. Reagents.

- Cell pellet (10 mg dry biomass, fresh or frozen, washed with carbon-free media).
- Chloroform.
- Methanol.
- Water.

5.2.2. Assay.

1. Re-suspend cell pellet to 0.6 mL total volume with water in a 15-mL polypropylene centrifuge tube.
2. Sequentially add chloroform (0.75 mL) and methanol (1.5 mL) (vortexing between additions is not necessary).
3. Vortex 15 minutes.
4. Sequentially add chloroform (0.75 mL) and water (0.75 mL), vortexing 10-15 seconds after each addition.
5. Centrifuge (4000 rpm, 15 minutes, 20°C).
6. Transfer the lower chloroform phase, which contains the lipids, via micropipette to a pre-weighed aluminum pan.
7. Evaporate the chloroform in a fume hood and weigh after 12, 24, and 36 hours to confirm complete evaporation.

Notes: weights were measured with a Mettler Toledo MT5 microbalance with accuracy to 0.001 mg and were recorded as an average of three measurements. A blank reaction containing 0.6 mL water was also performed as a control.

### 3.6.3. Test Results

Typical protocols for this method recommend a minimum of 30 mg biomass (Lohman, Gardner et al. 2013). However, 30 mg biomass requires a large culture volume. Smaller biomass quantities were tested, and the assay was observed to produce a linear response between 10-35 mg biomass (Figure 3.3A). Thus, 10 mg starting material was used in the current work.

Additional concerns for photosynthetic organisms when selecting an appropriate method for lipid quantification include interference from chlorophyll, which is also extracted by the solvents. Previous work (Archanaa, Moise et al. 2012) suggested that DMSO will remove chlorophyll prior to lipid extraction. DMSO was tested on cyanobacterial samples in the current work by vortexing the cell pellet in 10 mL DMSO, subsequently washing with water (re-suspending, centrifuging, decanting) until the supernatant was colorless, and then following the chloroform-methanol extraction procedure. However, DMSO treatment appeared to remove all lipid signal, resulting in no mass recovered (data not shown); thus, it was recognized that results of this method for cyanobacterial samples will encompass chlorophyll and photosynthetic pigments as well as lipid. Autoclaving samples was also tested as an alternative method of cell disruption for all three species but was not found to significantly improve lipid recovery (Figure 3.A3, Appendix A).

Lipid percentages of dry biomass for all three species are shown in Figure 3.3B. The lipid percentage obtained for *E. coli* is close to the value of 9.1% reported in Neidhardt (Neidhardt, Ingraham et al. 1990), while the measured percentages for *Synechococcus* 7002 are also comparable with previously measured lipid and chlorophyll values by Vu et al. (Vu, Hill et al. 2013) of 8.8%, 5.6%, and 3.8% for carbon-, light-, and nitrogen-limited conditions, respectively. The percentage obtained for *A. acidocaldarius* is similar to a previously published report of 3.6% (Vier, Rogge et al. 1992). Any differences between the current measurements and previously reported values may reflect differences in culturing conditions or the influence of specific procedural details.

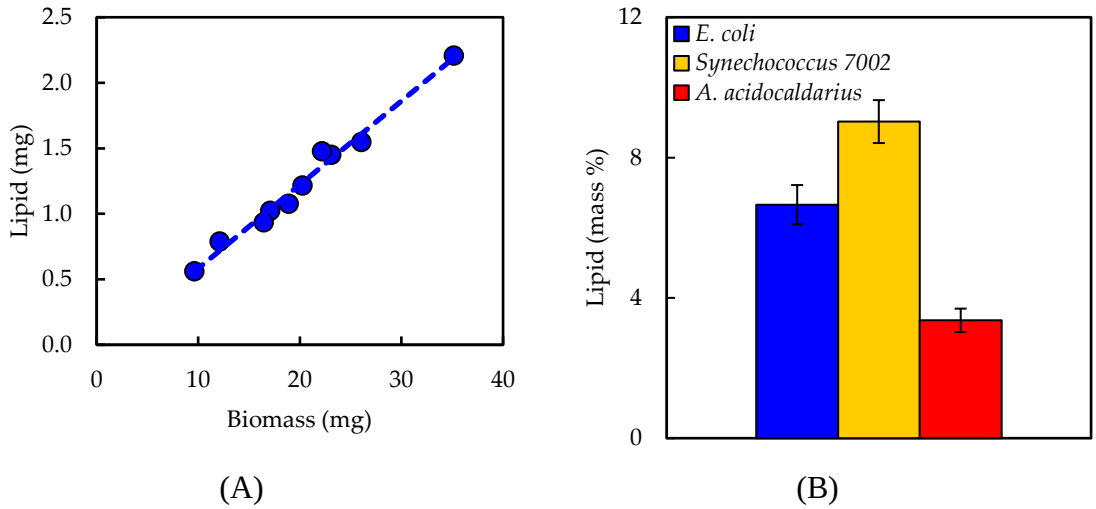


(A) (B)

Figure 3.3. (A) Lipid recovery is linear for biomass samples between 10-35 mg dry weight, measured with *E. coli*. (B) Lipid mass percentages of dry biomass measured for *E. coli*, *Synechococcus* 7002, and *A. acidocaldarius*. Error bars represent standard deviations from 5-9 biological replicates.

Polypropylene centrifuge tubes were used for safety during centrifugation rather than glass tubes, but it was noted that polypropylene is not completely chemically resistant to chloroform and may cause leaching of compounds from the polymer into

chloroform. This error was accounted for by performing a blank reaction (0.6 mL water). The mass of the blank was then subtracted from the mass of the biological sample to obtain the mass of lipid. Additionally, removal of the lower chloroform phase can be difficult to perform reproducibly. Glass Pasteur pipettes were used initially; however, micropipettes with 200-µL tips provided more control over phase removal and yielded more reproducible results.

## 3.7. Protein

### 3.7.1. Literature Review

Protein is typically the largest fraction of bacterial biomass. Many methods have been reported for determining protein quantity, including UV absorption spectroscopy and dye-based assays such as Bradford, Lowry, BCA, and others, of which Noble et al. (Noble, Knight et al. 2007) and Noble and Bailey (Noble and Bailey 2009) provide thorough discussions. UV absorption depends on tyrosine and tryptophan residues and the molar extinction coefficient of the protein under examination, and it requires a highly purified sample. Dye-based assays are influenced by different amino acid distributions and are subject to different interfering compounds as well as variability between proteins. Bovine serum albumin is a commonly used protein standard, but its amino acid sequence may not be representative of the total cellular protein. Amino acid analysis, or hydrolysis of cellular protein followed by derivatization and identification of individual amino acids via HPLC, is an alternative to these methods and is often considered the gold standard for protein analysis (Noble, Knight et al. 2007, Noble and Bailey 2009).

Amino acid analysis was selected for the current study due to improved accuracy and less bias as opposed to UV absorbance or dye-based methods. Some amino acids, such as cysteine and tryptophan, degrade during hydrolysis; special hydrolysis conditions may be used to retain them (Fountoulakis and Lahm 1998), or their proportions may be estimated based on genome codon distribution. Amino acid analysis provides experimental amino acid distribution in addition to total protein quantification, which serve as important parameters for metabolic modeling.

### 3.7.2. Procedure (after Henderson et al., 2000)

#### 3.7.2.1. Reagents.

- Cell pellet (1-3 mg dry biomass, fresh or frozen, washed with carbon-free media).
- 6 M HCl and 6 M NaOH.
- 0.1 M HCl, 0.22 µm filtered.
- Borate buffer: 0.4 N borate, titrate to pH 10.2 with NaOH, 0.22 µm filtered.
- OPA and FMOC derivatizing reagents (Agilent 5061-3335 and 5061-3337).
- Amino acid standard: 1 nmol/mL (Agilent 5061-3330).
- Solvent A: 40 mM sodium phosphate buffer $Na_2HPO_4$, titrate to pH 7.8 with 10 M NaOH, 0.22 µm filtered. (A ratio of different sodium salts can be used to prepare a 40 mM phosphate solution with an initial pH closer to 7.8, e.g. 1:1 molar ratio of $NaH_2PO_4$ and $Na_2HPO_4$.)
- Solvent B: 45:45:10 acetonitrile:methanol:water (v/v/v), 0.22 µm filtered (nylon filter recommended for organic solvents).

#### 3.7.2.2. Assay.

1. Transfer cell pellet to borosilicate HPLC vial with PTFE/silicone cap.
2. Add 50 µL 6 M HCl per mg biomass.
3. Tightly cap the vial and hydrolyze at 105°C for 24 hours (VWR analog heat block).
4. Neutralize to pH 7.0 with 6 M NaOH.
5. Filter with 0.22 µm PVDF centrifugal filters (Millipore UFC30GV00); centrifuge for 5 minutes at 10000 rpm.
6. Transfer filtrate to clean borosilicate HPLC vial, seal with parafilm, and poke a hole in the top (e.g. with a small pipette tip). Place at -80°C to freeze before lyophilizing.
7. Lyophilize for 24 hours (VirTis benchtop lyophilizer).
8. Store at -80°C until HPLC analysis.
9. Re-suspend lyophilized material in 0.1 M HCl, and perform HPLC analysis according to the protocol validated by Agilent Technologies (Henderson, Ricker et al. 2000).

Notes: PVDF was selected as the filter membrane material due to its low protein binding capacity; materials with high protein binding like nylon may affect amino acids. A fluorescence detector or diode array detector can be used for detection. The current work employed an Agilent 1100 HPLC system equipped with autosampler and fluorescence detector (for *A. acidocaldarius* samples) or diode array detector (for *E. coli* and *Synechococcus* 7002 samples). A diode array detector was less sensitive than a fluorescence detector (limit of detection ~100 µM vs. ~2 µM). o-phthalaldehyde (OPA)

reagent with 3-mercaptopropionic acid as a stabilizing agent was used for detection of primary amino acids and 9-fluorenylmethyl chloroformate (FMOC) reagent was used for secondary amino acids. OPA and FMOC reagents were replaced daily in amber vials and were used within 10 days upon opening an ampule. The flow rate was modified from 2 mL/min (Henderson, Ricker et al. 2000) to 1 mL/min to permit increased resolution of peaks (see gradient settings in Table 3.2). The injector program followed the steps described in Henderson et al. (Henderson, Ricker et al. 2000) but did not make use of the optional acetonitrile needle rinse. The integration parameters for collecting the data were set to a slope sensitivity of 1, peak width of 0.04, area reject of 1, and height reject of 0.4, with shoulders off. Amino acids were identified manually in the calibration table, and undesired peaks were discarded (derivatization byproduct peaks at the end of an injection).

Table 3.2. Amino acid analysis HPLC gradient settings.

| Time (min) | % Solvent B |
|---|---|
| 0 | 0 |
| 3.8 | 0 |
| 36.2 | 57 |
| 37.2 | 100 |
| 44.6 | 100 |
| 46.4 | 0 |
| 47 | 0 |

### 3.7.3. Test Results

Upon preparing for HPLC analysis, the lyophilized material was re-suspended in 100 µL 0.1 M HCl per mg biomass hydrolyzed. Different dilutions of the re-suspension were measured to ensure adequate detection of both more abundant and less abundant amino acids. Peak identity was confirmed for each amino acid by testing individual

solutions of each amino acid. A representative chromatogram is shown in Figure 3.4. An internal standard, α-aminobutyric acid, was used in samples and standards alike for peak area normalization across injections. Standard curves were constructed, resulting in linear regressions with fits of 0.99 or greater. The experimental amino acid distribution and total protein quantification for the three bacterial species are shown in Table 3.3. Since cysteine and tryptophan were degraded during hydrolysis and methionine was present in low quantities with high variability (likely oxidized during hydrolysis), the distribution of these three amino acids was calculated according to the percentage found in the protein-coding genes of the genome. Reasonable correlations were observed between the experimentally measured and genome-predicted distributions (Figure 3.A4, Appendix A). Interestingly, leucine content was consistently over-predicted in the genome and under-measured in the laboratory among the three species tested.

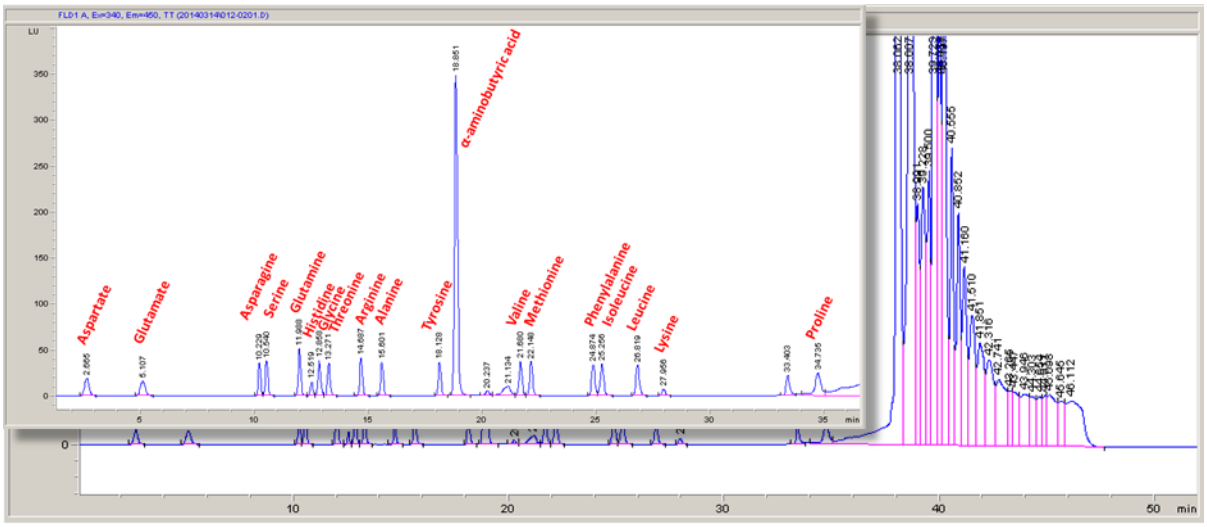


Figure 3.4. Representative chromatogram from fluorescence detector for amino acid standards. The background chromatogram shows the full length of the injection, including the derivatization byproducts eluting at the end. The outset chromatogram labels the individual peaks.

Table 3.3. Amino acid distributions and protein quantification for *E. coli*, *Synechococcus* 7002, and *A. acidocaldarius*. Amino acid mass and mole percentages of total protein are reported as averages of three biological replicates; percent relative standard deviations are in parentheses. HPLC quantification was obtained with a diode array detector for *E. coli* and *Synechococcus* 7002 and a fluorescence detector for *A. acidocaldarius*. Cysteine, methionine, and tryptophan were factored in according to genome-based codon proportions. Asparagine and glutamine were converted to aspartate and glutamate, respectively, during derivatization with OPA. The final row includes the total protein mass percent of cell dry weight, averaged from three biological replicates with standard deviation in parentheses.

| Amino Acid | *E. coli* | | *Synechococcus* 7002 | | *A. acidocaldarius* | |
|---|---|---|---|---|---|---|
| | **Mass %** | **Mole %** | **Mass %** | **Mole %** | **Mass %** | **Mole %** |
| Alanine | 7.1 (3.5) | 10.1 (3.2) | 8.5 (1.4) | 12.0 (1.4) | 8.4 (1.0) | 11.8 (0.9) |
| Arginine | 6.9 (4.9) | 5.0 (4.6) | 8.3 (0.5) | 6.0 (0.6) | 7.7 (1.9) | 5.6 (1.9) |
| Asparagine/Aspartate | 9.9 (1.3) | 9.5 (1.0) | 10.2 (3.3) | 9.7 (3.3) | 10.0 (1.0) | 9.5 (1.0) |
| Cysteine | 1.1 (NA) | 1.2 (NA) | 0.9 (NA) | 1.0 (NA) | 0.9 (NA) | 0.9 (NA) |
| Glutamine/Glutamate | 14.0 (4.9) | 12.1 (4.5) | 14.6 (2.7) | 12.5 (2.6) | 13.2 (0.7) | 11.3 (0.8) |
| Glycine | 6.4 (4.0) | 10.9 (3.6) | 6.1 (3.0) | 10.2 (2.9) | 5.7 (0.3) | 9.6 (0.3) |
| Histidine | 2.0 (4.9) | 1.6 (5.2) | 1.8 (9.7) | 1.4 (9.8) | 2.1 (1.8) | 1.7 (1.8) |
| Isoleucine | 4.9 (6.4) | 4.8 (6.7) | 4.6 (2.8) | 4.4 (3.0) | 4.1 (0.4) | 3.9 (0.5) |
| Leucine | 7.4 (3.3) | 7.2 (2.9) | 9.0 (2.0) | 8.6 (2.0) | 7.6 (0.2) | 7.3 (0.2) |
| Lysine | 6.7 (3.4) | 5.8 (3.1) | 5.3 (0.2) | 4.6 (0.1) | 4.4 (1.1) | 3.8 (1.1) |
| Methionine | 3.2 (NA) | 2.8 (NA) | 2.2 (NA) | 1.9 (NA) | 3.0 (NA) | 2.6 (NA) |
| Phenylalanine | 5.1 (13.3) | 3.9 (13.6) | 5.1 (0.9) | 3.9 (0.7) | 3.6 (0.9) | 2.8 (1.0) |
| Proline | 3.6 (8.2) | 4.0 (8.6) | 4.1 (5.2) | 4.5 (5.3) | 4.3 (0.8) | 4.8 (0.8) |
| Serine | 4.0 (11.3) | 4.9 (11.7) | 4.1 (1.7) | 4.9 (1.6) | 4.7 (0.6) | 5.6 (0.6) |
| Threonine | 4.9 (2.2) | 5.3 (2.0) | 4.9 (0.9) | 5.2 (0.7) | 5.8 (0.4) | 6.2 (0.5) |
| Tryptophan | 2.4 (NA) | 1.5 (NA) | 2.4 (NA) | 1.5 (NA) | 2.6 (NA) | 1.6 (NA) |
| Tyrosine | 3.9 (19.7) | 2.8 (20.0) | 2.5 (10.4) | 1.8 (10.6) | 4.4 (1.0) | 3.0 (1.1) |
| Valine | 6.3 (5.9) | 6.8 (5.5) | 5.4 (0.9) | 5.8 (1.0) | 7.5 (0.5) | 8.1 (0.5) |
| **Total Mass % Protein** | **35.2 (1.3)** | | **27.2 (1.5)** | | **38.5 (2.2)** | |

## 3.8. RNA

### 3.8.1. Literature Review

RNA is a major macromolecule class which contributes to ribosome assembly and cellular information processing. Methods used for quantifying RNA include UV absorbance, orcinol colorimetric reaction, and thiazole orange fluorescent dye (De Mey, Lequeux et al. 2006). UV absorbance is precise but requires a pure sample and is not feasible for a mixture of DNA and RNA. Orcinol is not as precise for RNA or for a

mixture of DNA and RNA, and carbohydrates may also interfere. Thiazole orange has good precision, but fluorescence is biased toward GC content, and it is less sensitive for RNA than for DNA (De Mey, Lequeux et al. 2006). Additionally, kits are available for RNA extraction but focus predominantly on downstream applications such as PCR and RNAseq, and thus remain questionable as quantitative methods. Fluorescent dyes such as RiboGreen and PicoGreen have also been reported for quantifying extracted RNA (Gorokhova and Kyle 2002) but are usually used in combination with kit extractions.

Major concerns in selecting an RNA quantification method include sample purity, accuracy, and bias of nucleotide content. Many studies have used the colorimetric orcinol reaction to quantify RNA after hot perchloric acid extraction. However, Benthin et al. (Benthin, Nielsen et al. 1991) developed an alternative method with the bacterium *Lactobacillus* that utilizes alkali (KOH) lysis in combination with cold perchloric acid extraction, followed by UV absorbance. The method provided similar accuracy to the orcinol reaction but showed improved precision (Benthin, Nielsen et al. 1991). Benthin's KOH-UV method was selected for the current study as a more reliable and safe method, using cold rather than hot perchloric acid, and to eliminate interference from carbohydrates, which occurs in the orcinol reaction. The results can be quantified with UV absorbance using average nucleotide molar extinction coefficients, which eliminates the need to prepare a standard from a different source. This method has been used in metabolic modeling studies to quantify RNA percentage (Imam, Yilmaz et al. 2011, Liao, Huang et al. 2011, Liu, Gao et al. 2013).

3.8.2. Procedure (after Benthin et al., 1991)

3.8.2.1. Reagents.

- Cell pellet (2-8 mg dry biomass, fresh or frozen, washed with carbon-free media).
- $HClO_4$ solutions: 0.5 M, 0.7 M, and 3 M.
- 0.3 M KOH solution.

7.2.2. Assay.

1. Wash cell pellet three times with 3 mL 0.7 M $HClO_4$ to degrade cell walls. Vortex to re-suspend in between washing. Centrifuge 4000 rpm for 10 min at 4°C and decant between washes.
2. Re-suspend pellet in 3 mL 0.3 M KOH to lyse cells.
3. Incubate in a 37°C water bath for 1 hour, shaking at 15-minute intervals.
4. Cool and add 1 mL 3 M $HClO_4$.
5. Centrifuge and decant supernatant into a new 50-mL polypropylene centrifuge tube.
6. Wash pellet twice with 4 mL 0.5 M $HClO_4$ (re-suspend and mix), centrifuge, and decant supernatant into the 50-mL tube. The 0.5 M $HClO_4$ extracts the RNA, while DNA, which is stable even in strong alkali, and protein, which does not solubilize in the alkali, remain in the precipitate.
7. Add 3 mL 0.5 M $HClO_4$ to the collection of extracts to obtain a total volume of 15 mL, and centrifuge once more to remove any non-visible precipitates of $KClO_4$.
8. Measure absorbance at 260 nm against a 0.5 M $HClO_4$ blank.

9. Calculate RNA quantity by assuming 1 unit of absorbance at 260 nm corresponds to 38 µg/mL RNA on average (Carnicer, Baumann et al. 2009).

Notes: quartz cuvettes are commonly used for measuring UV absorbance; but disposable UV cuvettes can also be used (VWR 47727-024, rated to 220 nm and tested for chemical compatibility with concentrated hydrochloric acid). Linearity of the spectrophotometer within the range of sample absorbance should be confirmed by successively diluting the sample with 0.5 M $HClO_4$ and confirming a linear fit to the resulting absorbance measurements. Absorbance at 280 nm can also be measured, and the $A_{260}/A_{280}$ can be calculated to assess RNA purity.

### 3.8.3. Test Results

Benthin et al. (Benthin, Nielsen et al. 1991) recommended using a quantity of biomass corresponding to ~0.4 mg of RNA. ~2 mg and ~8 mg biomass was used for *E. coli* and *Synechococcus* 7002, respectively, based on previous estimates of RNA content (Neidhardt, Ingraham et al. 1990, Vu, Hill et al. 2013). Correlation between biomass and RNA content was tested for *Synechococcus* 7002, and a linear response was observed between 2-8 mg biomass (Figure 3.5A). RNA mass percentages for all three species are shown in Figure 3.5B. The percentage obtained for *E. coli* is similar to the 20.5% value reported in Neidhardt (Neidhardt, Ingraham et al. 1990). The percentage of dry biomass obtained for *Synechococcus* 7002 is higher than the 4.0% average value measured in Vu et al. (Vu, Hill et al. 2013) via the orcinol method but could reflect different growth states. No literature comparison was available for *A. acidocaldarius*.

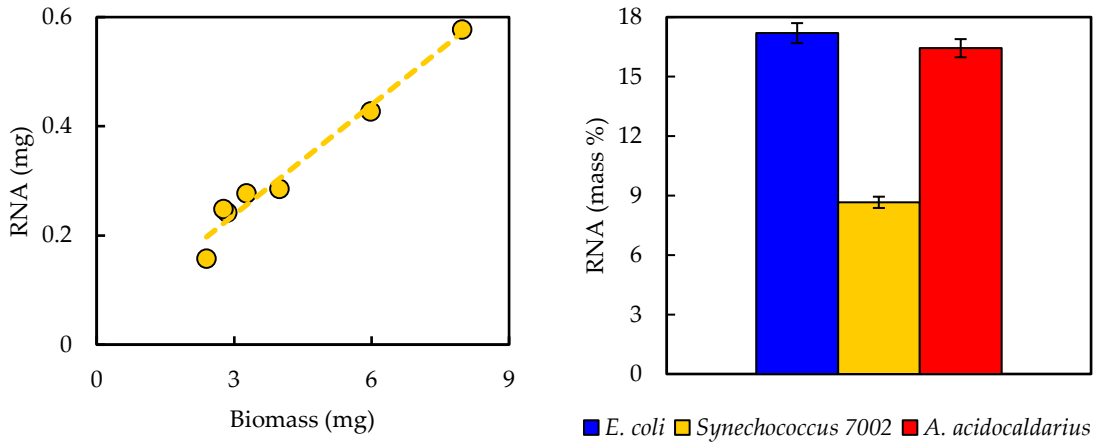


(A) (B)

Figure 3.5. (A) RNA recovery is linear for biomass samples between 2-8 mg dry weight, measured for *Synechococcus* 7002. (B) RNA mass percentages on a dry biomass basis measured for *E. coli*, *Synechococcus* 7002, and *A. acidocaldarius*. Error bars represent standard deviation from three biological replicates.

## 3.9. Model Biomass Reaction

Experimentally measured biomass composition provides a species-relevant basis for representing cellular growth in computational models. The results of the macromolecular assays for *E. coli*, *Synechococcus* 7002, and *A. acidocaldarius* are summarized in Table 3.4. The mass percentages for the five assays do not necessarily sum to 100% of cell dry weight. The reduced mass recovery may be due to loss of biomass during centrifugation and transfer of material while performing the assays. Some bacteria may also possess other storage compounds that are not accounted for in these analyses, such as polyhydroxyalkanoates or polyphosphates. Ash weight typically accounts for 5-10% of cell dry weight (Vanveen and Paul 1979), or perhaps even more for some organisms (e.g. 20-30% ash content has been measured in phytoplankton (Whyte 1987)). To adjust for losses during sample processing, measurements can be

normalized to the total mass recovered such that the sum of biomass recovered from all measurements is 100% (Table 3.4).

Table 3.4. Summary of average macromolecular composition, based on mass fraction of dry biomass, for *E. coli*, *Synechococcus* 7002, and *A. acidocaldarius*; standard deviations are included in parentheses. Column N contains the scaled biomass composition, normalized to the sum of the measurements.

| **Macromolecule** | ***E. coli*** | **N** | ***Synechococcus* 7002** | **N** | ***A. acidocaldarius*** | **N** |
|---|---|---|---|---|---|---|
| Carbohydrate | 4.2 (0.2) | 6.5 | 16.9 (0.1) | 27.2 | 6.2 (0.6) | 9.5 |
| DNA | 1.0 (0.1) | 1.6 | 0.4 (0.0) | 0.6 | 0.7 (0.1) | 1.1 |
| Lipid | 6.7 (0.6) | 10.4 | 9.0 (0.6) | 14.5 | 3.4 (0.3) | 5.2 |
| Protein | 35.2 (1.3) | 54.7 | 27.2 (1.5) | 43.7 | 38.5 (2.2) | 59.0 |
| RNA | 17.2 (0.5) | 26.7 | 8.7 (0.6) | 14.0 | 16.4 (0.5) | 25.2 |
| **Total** | **64.3** | **99.9** | **62.2** | **100** | **65.2** | **100** |

An *in silico* cellular growth reaction is a collection of macromolecular synthesis reactions scaled to account for biomass composition. The macromolecular synthesis reactions are constructed by accounting for the appropriate ratios of the monomers, polymerization energy requirements, and reaction byproducts. Macromolecular monomer distributions are either measured directly, such as the amino acid composition measured here, or can be estimated from appropriate omics data sets or literature. DNA composition is typically estimated from GC content, and RNA composition may be estimated from rRNA-encoding genes; rRNA accounts for approximately 81% of cellular RNA (Neidhardt, Ingraham et al. 1990). Polymer lengths for the macromolecular synthesis reactions can be scaled to a convenient number of monomers, such as 10 or 100, with the appropriate polymerization energy requirements and byproducts. The polymerization energy error introduced with these scaled molecules is assumed minor.

Once formulas for individual macromolecules are calculated, model reactions can be quality control checked for balance of elemental formulas and degree of reduction to ensure adherence to the mass balance constraint required for stoichiometric modeling. Identification of imbalanced reactions can then be further investigated; often the issue can be traced to balancing of redox pairs or hydrolysis products, free protons, and water. Table 3.5 demonstrates the construction of a DNA macromolecule synthesis reaction for *A. acidocaldarius*, including the definition of monomer composition, polymerization energy requirements, and byproducts. The elemental and electron balances are included and validate conservation relationships (Neidhardt, Ingraham et al. 1990). The supplementary material contains a workbook for the major biomass macromolecules that can be modified for different biomass measurements (File 3.S1).

Table 3.5. Example calculation of DNA macromolecular formula for *A. acidocaldarius* with 61.9% GC content, assuming a polymer length of 1 monomer. Polymerization byproducts (diphosphate) are subtracted from the sum of dNTP monomer constituents to obtain the formula for a DNA macromolecule. Overall DNA synthesis reaction is shown in the last row.

| **Monomer** | **Stoichiometry/ Formula** | **C** | **H** | **O** | **N** | **P** |
|---|---|---|---|---|---|---|
| dATP | 0.19/ $C_{10}H_{12}N_5O_{12}P_3$ | 1.91 | 2.29 | 2.29 | 0.95 | 0.57 |
| dCTP | 0.31/ $C_9H_{12}N_3O_{13}P_3$ | 2.79 | 3.71 | 4.02 | 0.93 | 0.93 |
| dGTP | 0.31/ $C_{10}H_{12}N_5O_{13}P_3$ | 3.10 | 3.71 | 4.02 | 1.55 | 0.93 |
| dTTP | 0.19/ $C_{10}H_{13}N_2O_{14}P_3$ | 1.91 | 2.48 | 2.67 | 0.38 | 0.57 |
| Diphosphate | 1/ $HO_7P_2$ | 0.00 | 1.00 | 7.00 | 0.00 | 2.00 |
| DNA molecule | 1/ $C_{9.69}H_{11.19}N_{3.81}O_6P_1$ | 9.69 | 11.19 | 6.00 | 3.81 | 1.00 |
| **0.19 dATP + 0.31 dCTP + 0.31 dGTP + 0.19 dTTP = 1 DNA + 1 diphosphate** | | | | | | |

The overall cell growth reaction has a form analogous to *A* carbohydrate + *B* DNA + *C* lipid + *D* protein + *E* RNA = *1* biomass, where *A*, *B*, *C*, *D*, and *E* are stoichiometric coefficients corresponding to the measured mass fraction. Some biomass reactions may also include additional constituents, such as chlorophyll, salts, and metabolite pools, including vitamins. The coefficients for the macromolecular constituents *A*-*E* are obtained by converting the experimental mass fraction measurements to molar coefficients, thereby yielding the appropriate stoichiometries. The following steps convert experimentally measured mass fractions of macromolecules to molar coefficients for use in the biomass reaction:

1. Mass fractions are recorded as g macromolecule per g cell dry weight (see Table 3.4).
2. The molar mass of each macromolecule representation is tabulated. Multiply the macromolecular formula by the atomic mass of the respective elements, and sum over all elements to obtain g/mol macromolecule.
3. Divide the mass fraction of the macromolecule by its molar mass to obtain mol macromolecule/g cell dry weight. The basis for cell dry weight normalization can be selected as desired; 1, 10, or 100 kg cell dry weight typically results in reasonably scaled coefficients for elementary flux mode and flux balance analyses. 1 kg cell dry weight often provides a convenient basis, as when inputs are scaled to a mM basis in FBA, the resulting output biomass scales to grams.
4. The molar coefficients are incorporated into the biomass reaction. The stoichiometries can be multiplied by the macromolecular formulas and summed

over all the macromolecules to obtain an overall formula for biomass, which allows model output to be analyzed in terms of carbon moles of biomass (Table 3.6). The supplementary material details the macromolecule and biomass calculations for each species, as well as demonstrates a quality control check for balancing mass, charge, electrons, and elemental composition (File 3.S1).

Table 3.6. Species-specific biomass reactions for *E. coli*, *Synechococcus* 7002, and *A. acidocaldarius*, without consideration of maintenance energy. Molar coefficients represent 100 kg dry biomass.

| Species | Biomass Reaction |
|---|---|
| *E. coli* | 5.05 DNA + 8.40 RNA + 5.02 Protein + 13.9 Lipid + 4.03 Glycogen = 1 Biomass |
| *Synechococcus* 7002 | 2.09 DNA + 4.40 RNA + 4.05 Protein + 18.5 Lipid + 16.8 Glycogen = 1 Biomass |
| *A. acidocaldarius* | 3.49 DNA + 7.91 RNA + 5.46 Protein + 6.67 Lipid + 5.86 Glycogen = 1 Biomass |

In addition to the macromolecular constituents that comprise a cell, metabolic models often account for maintenance energy requirements. Maintenance energy is an implicit energy consumption term accounting for a myriad of cellular processes, such as protein turnover and osmotic pressure maintenance. Maintenance energy is typically estimated by fitting the *in silico* model to experimental biomass-on-substrate yield data. For example, experiments correlating substrate consumption rate (for heterotrophs) or photon absorption rate (for photoautotrophs) with growth rate can be used to determine the yield (Carlson and Srienc 2004, Vu, Stolyar et al. 2012). For elementary flux mode analysis applications, a single maintenance energy term, set for a defined growth rate, can be added to the biomass reaction. For flux balance analysis applications, maintenance energy requirements can be broken down into growth and non-growth associated (GAM and NGAM) terms. The supplementary material contains a genome-enabled model constructed for *A. acidocaldarius* (File 3.S2). Calculations fitting maintenance energy to

observed yield data for both glucose and oxygen consumption from Farrand et al. (Farrand, Jones et al. 1983) for both EFMA and FBA application are provided in MATLAB and Excel formats (Files 3.S2 and 3.S3). The specific growth rate-dependent ($\mu$, $h^{-1}$) maintenance energy requirement ($q_{ATP}$) for *A. acidocaldarius* was calculated to be $q_{ATP} = 13.4\mu + 4.2$ mmol cellular energy per g biomass per hour, where GAM was 13.4 mmol cellular energy (phosphodiester bonds) per g biomass and NGAM was 4.2 mmol cellular energy per g biomass per hour. Using multiple data sets to fit the maintenance energy provides a metric of accuracy for the model, as they should provide similar results. The calculated maintenance terms for *A. acidocaldarius* were similar regardless of fitting with glucose or oxygen consumption data (Files 3.S2 and 3.S3).

## 3.10. Conclusions

Computational biology representations of metabolism often include cellular growth reactions necessitating knowledge of biomass composition for accurate predictions. The current work surveyed analytical methods for the five major macromolecules (carbohydrate, DNA, lipid, protein, and RNA), provided step-by-step procedures for a select method for each macromolecule, tested the methods on three different bacterial species, and detailed application of analytical measurements to a computational representation of cellular growth. The literature survey included references to more in-depth reviews for each macromolecule for further exploration and also provided a rationale for the selected method. The three bacterial species used for testing (*E. coli*, *Synechococcus* 7002, and *A. acidocaldarius*) represent a range of physiological

characteristics, including gram-negative and gram-positive, mesophilic and thermophilic, and neutrophilic and acidophilic, as well as chemoheterotrophic and photoautotrophic, which assessed the robustness of the methods. Testing of methods highlighted potential pitfalls and provided guidelines for troubleshooting when testing a new method or when applying a method to new organisms. Based on the current study, recommendations for verifying a new protocol or testing a new organism include ensuring that the test response is linear for both the amount of biomass used and the amount of reagent, testing the standard range, and confirming the effect of any sample pre-treatment steps on standards. It is also important to consider the organism being studied and the downstream application of the measurement (e.g. glycogen vs. total carbohydrate).

The presented methods of experimental measurement and conversion to computational biology reactions need to be integrated with the maturing quality standards for model construction (Le Novere, Finney et al. 2005, Ravikrishnan and Raman 2015). The predicted elemental composition of the synthesized biomass is a relevant metric for the quality of the overall reaction. Average elemental compositions have been measured for a number of common microorganisms and provide a convenient check (Roels 1980). The elemental composition is linked to the biomass degree of reduction, which is an energetic measure of biomass and a critical parameter for computational biology analysis of consortia simulations. The degree of reduction of biomass for an average cell is approximately 4.2 or 4.8 on an $NH_4^+$ or $N_2$ basis, respectively (Roels 1980). These values can shift due to large quantities of cellular storage polymers like polysaccharides or polyhydroxyalkanoates. Additionally, biomass composition is known to shift with growth

rate and culturing stress (Carlson and Srienc 2004, Folsom and Carlson 2015); the provided approach can be used to create culturing condition-specific cellular growth reactions. Altogether, the current work serves as a useful resource for the broader computational biology community, which will enable more accurate representations of biomass synthesis and therefore more accurate metabolism simulations.

## 3.11. Acknowledgments

This work is a contribution of the PNNL Foundational Scientific Focus Area (Principles of Microbial Community Design) subcontracted to Montana State University. A.E.B. was supported by the Office of the Provost at Montana State University through the Molecular Biosciences Program and NSF (DMS-1361240). The authors would also like to thank James Folsom and Zackary Jay for helpful discussions.

## 3.12. Appendix A

Additional data supporting method testing are provided herein.

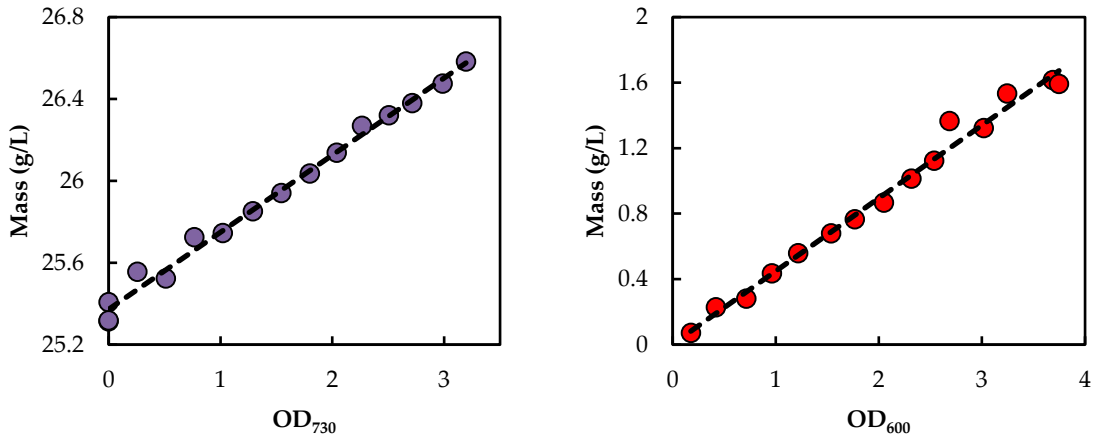


(A) (B)

Figure 3.A1. (A) Biomass-$OD_{730}$ correlation curve determined for *Synechococcus* 7002, described by the equation y = 0.377x + 25.373 with $R^2$ value of 0.991. The average A+ media control ($OD_{730}$ of 0) was 25.347 g/L and was subtracted from the biological samples to obtain biomass values. (B) Biomass-$OD_{600}$ correlation curve determined for *A. acidocaldarius*, described by the equation y = 0.445x + 0.004 with $R^2$ value of 0.987.

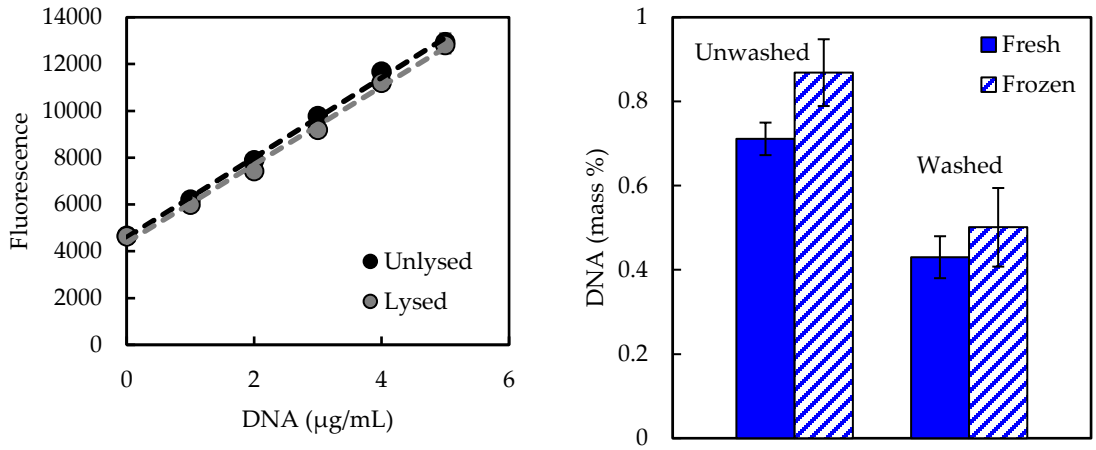


(A) (B)

Figure 3.A2. (A) Lysis of DNA standard did not significantly influence Hoechst fluorescent response. Error bars represent three technical replicates of standard solutions. Neither slopes nor intercepts of the two curves are significantly different ($p > 0.05$, T-tests). (B) Washing samples with cell wash solution resulted in significantly lower DNA recovery from *E. coli* samples ($p < 0.05$, T-test). Freezing samples did not have a significant impact on DNA recovery ($p > 0.05$, T-test).

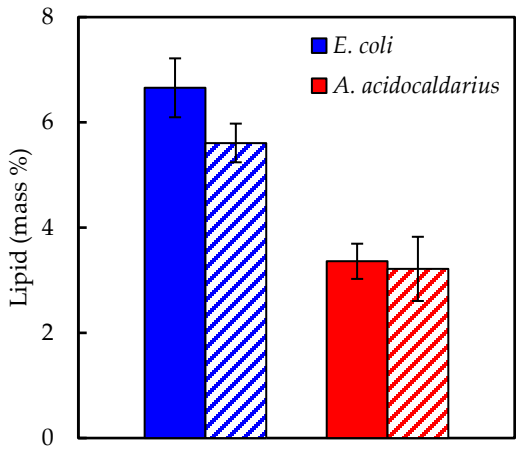


Figure 3.A3. Autoclaving samples prior to chloroform-methanol lipid extraction did not significantly enhance lipid recovery. Solid columns represent unautoclaved samples and striped columns represent autoclaved samples. Lipid recovery was not significantly affected by autoclaving for *A. acidocaldarius* ($p > 0.05$, T-test), whereas lipid recovery was slightly lower for autoclaved *E. coli* samples ($0.05 < p < 0.01$, T-test). n = 9 and 3 for unautoclaved and autoclaved *E. coli* samples, respectively, and n = 6 and 3 for unautoclaved and autoclaved *A. acidocaldarius*, respectively.

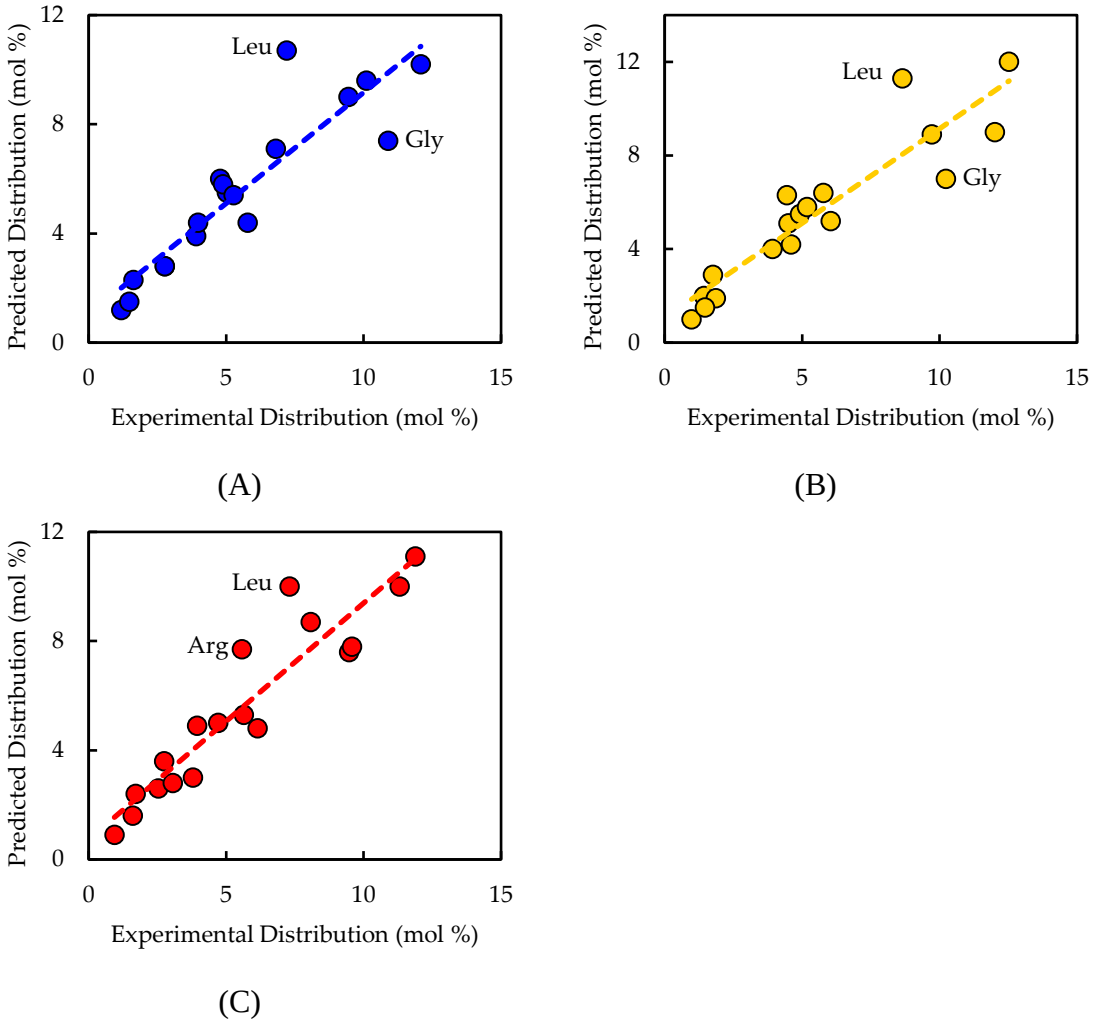


Figure 3.A4. Correlations between experimentally measured and genome-based amino acid distributions for (A) *E. coli* (NCBI reference sequence NC_000913.3; trendline y = 0.81x + 1.04 with $R^2$ value of 0.82), (B) *Synechococcus* 7002 (NCBI reference sequence NC_010475.1; trendline y = 0.81x + 1.07 with $R^2$ value of 0.85), and **(**C**)** *A. acidocaldarius* (NCBI reference sequence NC_013205.1; trendline y = 0.87x + 0.73 with $R^2$ value of 0.87). The two most outlying amino acids are labeled.

# CHAPTER FOUR

# STOICHIOMETRIC NETWORK ANALYSIS OF CYANOBACTERIAL ACCLIMATION TO PHOTOSYNTHESIS-ASSOCIATED STRESSES IDENTIFIES HETEROTROPHIC NICHES

## Contribution of Authors and Co-Authors

Manuscript in Chapter Four

Author: Ashley E. Beck

Contributions: Conceived and designed the experiments, performed the experiments, analyzed the data, wrote the manuscript

Co-Author: Hans C. Bernstein

Contributions: Performed the experiments, contributed reagents/materials/analysis tools

Co-Author: Ross P. Carlson

Contributions: Conceived and designed the experiments, wrote the manuscript

Manuscript Information Page

Ashley E. Beck, Hans C. Bernstein, and Ross P. Carlson

Status of Manuscript:
____ Prepared for submission to a peer-reviewed journal
____ Officially submitted to a peer-review journal
____ Accepted by a peer-reviewed journal
_X__ Published in a peer-reviewed journal

*Processes*, Microbial Community Modeling: Prediction of Microbial Interactions and Community Dynamics Special Issue
Multidisciplinary Digital Publishing Institute
Received April 19, 2017
Revised June 9, 2017
Accepted June 14, 2017
Published June 19, 2017

## 4.1. Abstract

Metabolic acclimation to photosynthesis-associated stresses was examined in the thermophilic cyanobacterium *Thermosynechococcus elongatus* BP-1 using integrated computational and photobioreactor analyses. A genome-enabled metabolic model, complete with measured biomass composition, was analyzed using ecological resource allocation theory to predict and interpret metabolic acclimation to irradiance, $O_2$, and nutrient stresses. Reduced growth efficiency, shifts in photosystem utilization, changes in photorespiration strategies, and differing byproduct secretion patterns were predicted to occur along culturing stress gradients. These predictions were compared with photobioreactor physiological data and previously published transcriptomic data and found to be highly consistent with observations, providing a systems-based rationale for the culture phenotypes. The analysis also indicated that cyanobacterial stress acclimation strategies created niches for heterotrophic organisms and that heterotrophic activity could enhance cyanobacterial stress tolerance by removing inhibitory metabolic byproducts. This study provides mechanistic insight into stress acclimation strategies in photoautotrophs and establishes a framework for predicting, designing, and engineering both axenic and photoautotrophic-heterotrophic systems as a function of controllable parameters.

## 4.2. Introduction

Environmental stresses dictate competitive ecological strategies impacting nutrient and energy flows from the scale of individual cells to ecosystems (Schimel,

Balser et al. 2007, Folsom and Carlson 2015). Cyanobacteria are significant drivers of global nutrient and energy flows, accounting for ~10% of global primary productivity (Rousseaux and Gregg 2014) and forming essential links in carbon and nitrogen biogeochemical cycles (Bullerjahn and Post 2014). Cyanobacteria are also used in wastewater treatment and as bioprocess catalysts for bioproduction of specialty chemicals (Singh, Kate et al. 2005, Abed, Dobretsov et al. 2009). Cyanobacteria are deeply rooted in the tree of life and have adapted competitively to common stressors associated with photosynthesis and are model organisms for examining metabolic acclimation to these stresses.

Photoinhibition is a broad term encompassing different types of photosynthesis-associated stresses including photo-damage by excitation, damage by reactive oxygen species (ROS), and high localized $O_2$ concentrations (Raven 2011). Cyanobacteria can mitigate photo-damage by downregulating synthesis of photosystems, as well as adjusting relative photon absorption at photosystems I and II (PSI, PSII) to modulate ATP and NADPH regeneration (PSII extracts electrons from water which can be used in conjunction with PSI to regenerate NADPH and ATP, while PSI operating alone recycles electrons to regenerate ATP only; see Figure 4.1) (Bailey and Grossman 2008). High excitation can lead to oxidative damage at the photosystems and/or a highly reduced electron transport chain, which may also lead to cellular oxidative damage via ROS. Acclimation strategies include directing excess electrons toward alternative biochemical routes, such as reduction of $O_2$ (by either cellular respiration or the water-water cycle (photoreduction of $O_2$ to water)) or secretion of reduced carbon byproducts. High rates of

oxygenic photosynthesis can also lead to locally high $O_2$ levels (Ward, Bateson et al. 2006, Bernstein, Kesaano et al. 2014), and environments with high concentrations of $O_2$ relative to $CO_2$ can cause additional metabolic stress. Ribulose-1,5-bisphosphate carboxylase oxygenase (RuBisCO) is a dual-functioning enzyme which can react with either $CO_2$ or $O_2$. When RuBisCO reacts with $O_2$, 2-phosphoglycolate is produced, which is either secreted as the inhibitory compound glycolate or catabolized using photorespiration pathways found in cyanobacteria (Eisenhut, Ruth et al. 2008). Cyanobacteria have evolved mechanisms to reduce $O_2$ consumption at RuBisCO, including species-specific enzymes with varying affinities for $CO_2$ and $O_2$, as well as expression of carboxysomes to increase the relative $CO_2$ concentration in the vicinity of RuBisCO (Espie and Kimber 2011, Rae, Long et al. 2013).

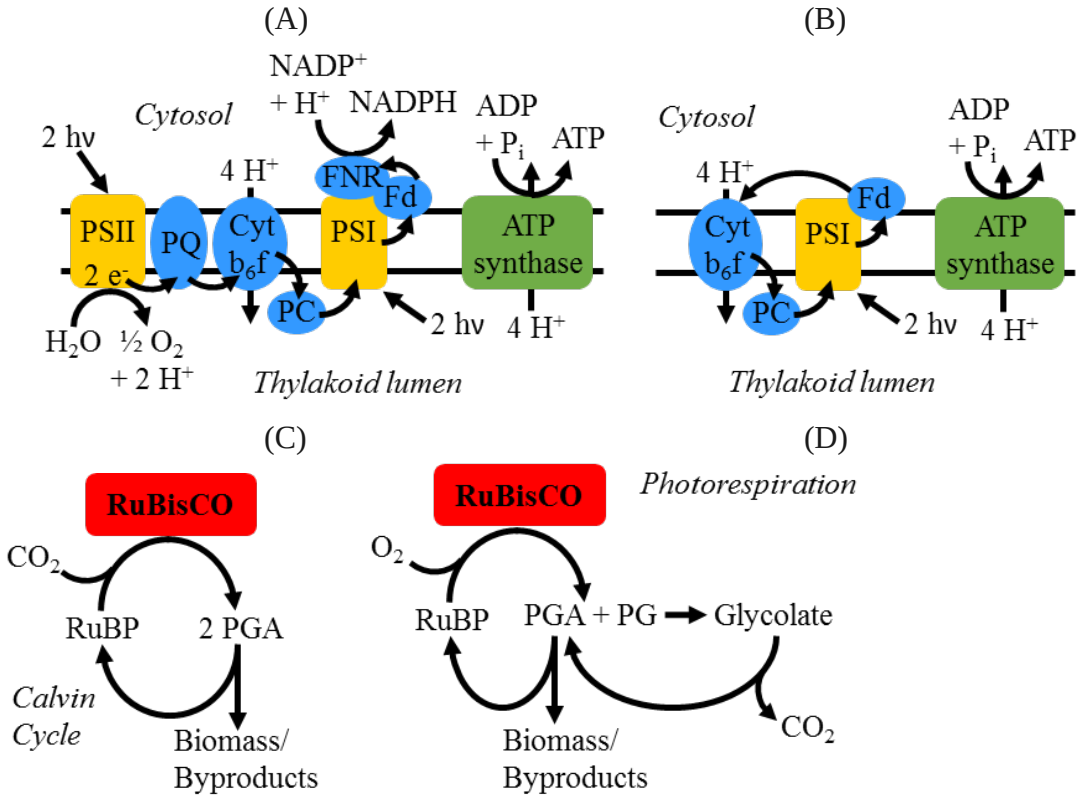


Figure 4.1. Light and dark reactions of photosynthesis. The role of photosystems I and II (PSI and PSII) in linear (A) and cyclic (B) photosynthesis and their relation to production of $O_2$ and regeneration of NADPH and ATP. Linear photosynthesis produces $O_2$ and regenerates both ATP and NADPH, whereas cyclic photosynthesis does not produce $O_2$ and regenerates ATP only. In the dark reactions, the bifunctional RuBisCO enzyme can incorporate inorganic carbon into biomass via the Calvin cycle (C) or can react with $O_2$ (D), resulting in a toxic byproduct and reducing incorporation of carbon into biomass. Abbreviations: hν, photons (photosynthetically active radiation); PQ, plastoquinone/plastoquinol; Cyt $b_6f$, cytochrome $b_6f$; PC, plastocyanin; FNR, ferredoxin-$NADP^+$ reductase; FD, ferredoxin; RuBP, ribulose-1,5-bisphosphate; PGA, 3-phosphoglycerate; PG, 2-phosphoglycolate.

Stoichiometric modeling of metabolism enables prediction and interpretation of system-wide properties of complex metabolic networks, including community-level networks (Llaneras and Pico 2008, Taffs, Aston et al. 2009, Trinh, Wlaschin et al. 2009, Orth, Thiele et al. 2010, Maarleveld, Khandelwal et al. 2013, Henry, Bernstein et al. 2016, Perez-Garcia, Lear et al. 2016). These systems biology approaches, such as flux

balance analysis (FBA) and elementary flux mode analysis (EFMA), use genomic and physiological data to inform the construction of computational representations of metabolism. The application of a steady state assumption simplifies the mass-balanced metabolic reactions into a series of solvable linear equations, reducing the need for difficult-to-measure, condition-dependent enzyme kinetic parameters (Maarleveld, Khandelwal et al. 2013). Whereas FBA uses objective functions such as biomass production to predict an optimal flux distribution under a specific set of conditions, EFMA calculates the complete set of minimal pathways (elementary flux modes, EFMs) through a metabolic network using steady state, reaction reversibility, and indecomposability constraints. Non-negative linear combinations of EFMs define the entire phenotypic solution space of a steady state metabolic network using a single simulation and can be used to examine all possible physiologies in an unbiased manner (Schuster and Hilgetag 1994, Trinh, Wlaschin et al. 2009). Similarities and differences in the output of EFMA versus other stoichiometric modeling techniques can be found in the review by Trinh et al. (Trinh, Wlaschin et al. 2009). The enumerated EFMs can be evaluated by resource allocation theory, which quantitatively assesses the computational phenotypic space according to tradeoffs in consumption of different resources for the production of bioproducts (Carlson 2009, Molenaar, van Berlo et al. 2009, Carlson, Oshota et al. 2012, Beck, Hunt et al. 2016, Mori, Hwa et al. 2016). Previous stoichiometric modeling studies of cyanobacterial metabolism have examined the occurrence of photorespiration as well as irradiance and carbon limitations (Nogales,

Gudmundsson et al. 2012, Vu, Stolyar et al. 2012, Knoop, Grundel et al. 2013, Vu, Hill et al. 2013).

The presented study analyzes metabolic acclimation to photosynthesis-associated stresses in the thermophilic, non-diazotrophic unicellular cyanobacterium *Thermosynechococcus elongatus* BP-1 (hereafter BP-1) and the formation of heterotrophic niches. BP-1 was isolated from the alkaline (pH 8.6) Beppu hot springs in Japan where temperatures range from 50-65°C (Yamaoka, Satoh et al. 1978, Everroad, Otaki et al. 2012). BP-1 is a major primary producer in its native hot springs where it often grows in bacterial mat communities with heterotrophs and is subject to high irradiance, high $O_2$, and low nutrient availability stresses. The objectives of this study were to (i) identify ecologically relevant acclimation strategies to high irradiance, $O_2/CO_2$ competition at RuBisCO, and nutrient limitation at varying degrees using a computational BP-1 stoichiometric model and EFMA combined with resource allocation theory, (ii) analyze BP-1 acclimation to high irradiance through controlled photobioreactors, (iii) compare general computational predictions to specific photobioreactor observations to interpret BP-1 acclimation strategies, and (iv) examine the impact of stress acclimation strategies on the ability of BP-1 to interact with heterotrophic partners. The presented study contributes to the understanding of cyanobacterial metabolism by examining specific photorespiration pathways, relative photon absorption of the photosystems, and byproduct secretion profiles under simultaneous stress conditions of high irradiance and $O_2/CO_2$ competition at RuBisCO, as well as by predicting cross-feeding photoautotrophic-heterotrophic interactions. The computational resource allocation-based

modeling integrated with photobioreactor observations provides a rational basis for interpreting natural cyanobacterial behavior and a framework for controlling cyanobacteria for bioprocess applications.

## 4.3. Materials and Methods

### 4.3.1. Photobioreactor Culturing

*T. elongatus* BP-1 cultures were grown using modified BG-11 (mBG-11) medium (Stanier, Kunisawa et al. 1971, Bernstein, McClure et al. 2017), containing 17.6 mM $NaNO_3$, 0.304 mM $MgSO_4 \cdot 7H_2O$, 0.175 mM $KH_2PO_4$, 0.245 mM $CaCl_2 \cdot 2H_2O$, 0.0028 mM $Na_2EDTA$, and 0.0144 mM $FeCl_3$. A trace metal supplement was added (1 mL/L), comprised of 46.254 mM $H_3BO_3$, 9.146 mM $MnCl_2 \cdot 4H_2O$, 0.772 mM $ZnSO_4 \cdot 7H_2O$, 1.611 mM $Na_2MoO_4 \cdot 2H_2O$, 0.316 mM $CuSO_4 \cdot 5H_2O$, and 0.170 mM $Co(NO_3)_2 \cdot 6H_2O$. Inoculum cultures of BP-1 were initiated from frozen stocks into 150-mL sealed serum bottles filled with 50 mL mBG-11 amended with 15 mM sodium bicarbonate and adjusted to pH 7.5 under $N_2$ headspace containing 10% $CO_2$.

Photobioreactors were operated as turbidostats as described in Bernstein et al. (Bernstein, McClure et al. 2017), similar to Bernstein et al. and Melnicki et al. (Melnicki, Pinchuk et al. 2013, Beliaev, Romine et al. 2014). Reactors were inoculated with exponentially growing inoculum culture to $OD_{730\ nm} = 0.01$. All cultures were grown under continuous light of varying irradiances at 52°C, pH 7.5, and were continuously sparged at 4 L $min^{-1}$ with a 98% $N_2$ and 2% $CO_2$ gas mixture. Incident and transmitted scalar irradiances were measured and used to adjust the turbidostat growth rate. The

specific optical cross section ($\sigma$, $m^2$ (g CDW)$^{-1}$, cell dry weight) was determined according to a previously described method using a light diffuser and spectrophotometer (Shibata, Benson et al. 1954). The specific photon absorption rate was calculated by multiplying the specific optical cross section by the incident irradiance.

4.3.2. Biomass Composition Determination

Macromolecular composition was analyzed from turbidostat biomass samples (pelleted and frozen at Pacific Northwest National Laboratory and then shipped to Montana State University for subsequent analysis) according to the following procedures. DNA was quantified from alkali-lysed solutions with Hoechst 33258 fluorescent dye (Downs and Wilfinger 1983). Glycogen was quantified by co-precipitation with sodium sulfate and detection with anthrone (Del Don, Hanselmann et al. 1994). Lipids were quantified gravimetrically via chloroform-methanol extraction (Bligh and Dyer 1959). Total protein and amino acid distribution were quantified with HPLC fluorescence detection using o-phthalaldehyde (OPA) and 9-fluorenylmethylchloroformate (FMOC) derivatizations of acid-hydrolyzed protein (Henderson, Ricker et al. 2000). Cysteine, methionine, and tryptophan were degraded, and asparagine and glutamine were converted to aspartate and glutamate, respectively, during hydrolysis (Fountoulakis and Lahm 1998); therefore, abundances were predicted from protein-coding gene codon usage. RNA was quantified by lysis with potassium hydroxide, extraction into cold perchloric acid, and measurement of UV absorbance at 260 nm (Benthin, Nielsen et al. 1991). Appendix A contains detailed protocols for each method.

4.3.3. Model Construction

The metabolic network model for BP-1 was constructed in CellNetAnalyzer (Klamt, Saez-Rodriguez et al. 2007, Klamt and von Kamp 2011) from the annotated genome (Nakamura, Kaneko et al. 2002) with the aid of MetaCyc, KEGG, BRENDA, and NCBI databases (Kanehisa, Goto et al. 2012, Schomburg, Chang et al. 2013, Caspi, Billington et al. 2016). Reversible exchange reactions were defined for protons and water. Irreversible exchange reactions defined bicarbonate, magnesium, nitrate, phosphate, photons, and sulfate as possible substrates and $O_2$, acetate, alanine, ethanol, formate, glycolate, lactate, pyruvate, and sucrose as possible byproducts. Biomass was also defined as a product.

Macromolecular synthesis reactions were defined for nucleic acids, glycogen (most common form of cyanobacterial carbohydrate storage (Beck, Knoop et al. 2012)), lipid, and protein. Synthesis reactions utilized two phosphate bonds per nucleic acid monomer, one phosphate bond per glycogen monomer, and four phosphate bonds per protein monomer (Neidhardt, Ingraham et al. 1990). Nucleotide distributions were set based on percent GC content of the genome for DNA and nucleotide sequence of the rRNA genes for RNA. Fatty acid distribution was assigned based on literature values of fatty acid chain and lipid types measured for BP-1 (Miyairi 1995, Maslova, Mouradyan et al. 2004, Petroutsos, Amiar et al. 2014). The amino acid distribution was set using the experimentally measured values in the current study. Macromolecular composition (DNA, glycogen, lipid (including chlorophyll), protein, and RNA) was determined experimentally in the current study (see section 2.2.) and used to set the molar

coefficients in the biomass synthesis reaction, normalized to 1 kg dry biomass (File 4.S1 in the Supplementary Materials). Chlorophyll was also included in biomass synthesis using the mass fraction measured for *Synechococcus* sp. PCC 7002 (Vu, Hill et al. 2013), and the lipid mass fraction was adjusted to reflect the proportion of chlorophyll. The biomass composition was converted into an electron requirement using degree of reduction (moles of electrons per mole of carbon) calculations (Roels 1983) with the assumption that each biosynthetic electron requires two photons (one absorbed at each PSII and PSI). Degree of reduction was calculated with respect to nitrate as a nitrogen source. To estimate photons necessary for ATP regeneration, the phosphate bond requirement for polymerization of monomers into macromolecules was converted into a photon requirement via a stoichiometry of four photons per phosphate bond (one photon absorbed at PSI per proton pumped, with four protons translocated per ATP molecule synthesized). Photon and proton stoichiometries remain active areas of research, and this estimate is recognized as an upper bound considering linear photosynthesis without a Q-cycle (Shikanai, Munekage et al. 2002, Oliver and Atsumi 2014).

All reactions were balanced for elements, charge, and electrons. Thermodynamic considerations were built into the model via reaction reversibilities, based on data from BRENDA (Schomburg, Chang et al. 2013); in the event that data for bacterial species were not available from BRENDA, thermodynamic calculations were performed with eQuilibrator (http://equilibrator.weizmann.ac.il/) to determine physiological reversibility, using a product concentration three orders of magnitude greater than the reactant concentration (Flamholz, Noor et al. 2012, Noor, Bar-Even et al. 2012). Nitrogen

requirements were determined for each reaction by summing the number of nitrogen atoms specified by the enzyme amino acid sequences. Iron requirements were determined for central carbon metabolism and photosynthesis reactions based on metal requirements of similar cyanobacterial species in BRENDA (Schomburg, Chang et al. 2013). For instances of missing or conflicting information in the database, literature values compiled for oxygenic photoautotrophs were used (Raven, Evans et al. 1999). A one-to-one (minimal resource investment) correspondence of enzyme to reaction was used to calculate the total cost per EFM, as it has previously been shown to provide a good approximation of flux distributions in *Escherichia coli* (Carlson 2009, Carlson, Oshota et al. 2012). EFMs were enumerated using EFMtool (Terzer and Stelling 2008). Resource allocation analysis (cost assessment) of the resulting EFMs was performed with MATLAB and Python. The metabolic model with supporting details and CellNetAnalyzer metabolite and reaction input, SBML model version, and documented analysis routines can be found in the Supplementary Materials (Files 4.S1-4).

## 4.4. Results

### 4.4.1. Computational BP-1 Metabolic Model and Photobioreactor Biomass Composition Measurement

The BP-1 computational metabolic model was constructed from the annotated genome (Nakamura, Kaneko et al. 2002). Genetic potential was mapped to enzymes and metabolic reactions which encompassed photosynthesis, central metabolism, and biosynthetic reactions leading to biomass production according to a defined macromolecular composition reaction. Transport reactions were defined for nutrient

uptake and product secretion. Subsequent EFMA resulted in a description of the phenotypic space spanning the range of possible nutrient uptake and product secretion rates, which could then be analyzed for ecologically relevant stress acclimation strategies. The model accounted for 334 metabolism-associated genes which were mapped to 279 metabolites and 284 reactions (File 4.S1 in the Supplementary Materials). Photons were assumed to be within the spectrum of photosynthetically active radiation (PAR; 400-700 nm). A stoichiometrically balanced schematic demonstrating operation of the photosynthetic electron transport chain (linear and cyclic photosynthesis) and carbon flow in the model is shown in Figure 4.1. Nutrient substrates for the model were selected in alignment with the photobioreactor culturing medium. Bicarbonate was modeled as the sole carbon source based on culturing pH while interconversion with $CO_2$ was modeled via the carboxysomal carbonic anhydrase enzyme, and nitrate was modeled as the sole nitrogen source. Two of the three photorespiration pathways possible in cyanobacteria (Eisenhut, Ruth et al. 2008) were identified in BP-1, namely, the C2 cycle and the glycerate pathway. A variety of organic byproducts (Table 4.1) were considered based on previous genomic analysis of BP-1 (Klahn and Hagemann 2011) and culturing studies of related unicellular cyanobacteria (Beliaev, Romine et al. 2014, Kim, Nowack et al. 2015). Secretion of several different amino acids has been observed in BP-1 and related species (Beliaev, Romine et al. 2014, Kim, Nowack et al. 2015, Bernstein, McClure et al. 2017); alanine was included as a representative amino acid byproduct in the current model, closely linked to central metabolism.

Table 4.1. *T. elongatus* BP-1 metabolic model inputs and outputs, including potential reduced carbon byproducts, with corresponding degree of reduction.

| | Compound | Formula | Charge | Degree of Reduction |
|---|---|---|---|---|
| **Inputs** | Carbon dioxide | $CO_2$ | 0 | 0 |
| | Water | $H_2O$ | 0 | 0 |
| | Photons | NA | NA | NA |
| | Nitrate | $NO_3$ | -1 | -8 / -5 / 0 |
| **Outputs** | Molecular oxygen | $O_2$ | 0 | -4 |
| | Biomass | $CH_{1.6}N_{0.2}O_{0.3}P_{0.01}S_{0.005}$ | -0.7 | 4.3 / 5.0 / 6.1[a] |
| | Acetate | $C_2H_3O_2$ | -1 | 4 |
| | Alanine | $C_3H_7NO_2$ | 0 | 4 / 5 / 6.7[a] |
| | Ethanol | $C_2H_6O$ | 0 | 6 |
| | Formate | $CHO_2$ | -1 | 2 |
| | Glycolate | $C_2H_3O_3$ | -1 | 3 |
| | Lactate | $C_3H_5O_3$ | -1 | 4 |
| | Pyruvate | $C_3H_3O_3$ | -1 | 3.3 |
| | Sucrose | $C_{12}H_{22}O_{11}$ | 0 | 4 |

[a] Degree of reduction calculated with respect to ammonia / molecular nitrogen / nitrate. NA, not applicable.

Table 4.2. Experimentally determined *T. elongatus* BP-1 biomass composition from turbidostat biomass samples grown under an irradiance of 2000 μmol photons $m^{-2}$ $s^{-1}$.

| Macromolecule | Mass Percent | Extraction Method/ Analytical Method |
|---|---|---|
| DNA | 0.4 | Alkaline lysis/ Hoechst 33258 fluorescence |
| Glycogen | 2.0 | Sodium sulfate co-precipitation/ Anthrone detection |
| Lipid (including chlorophyll) | 17.4 | Chloroform-methanol/ Gravimetric |
| Protein | 62.0 | Hydrochloric acid hydrolysis/ OPA, FMOC derivatization |
| RNA | 16.3 | Alkaline lysis, perchloric acid/ UV absorbance |
| Total | 98.1 | |

Biomass composition impacts growth and byproducts (Senger 2010), making appropriate composition parameters important for computational growth predictions. BP-

1 macromolecular biomass composition was determined analytically from continuous culture samples and was used to parameterize the model growth reactions. The major measured macromolecule classes (DNA, glycogen, lipid (including chlorophyll), protein, and RNA) summed to 98.1% of cell dry weight (Table 4.2); the remaining 1.9% was assumed to be ash. Protein and lipid/chlorophyll comprised the largest mass fractions of biomass, accounting for 62.0% and 17.4%, respectively. Since protein comprises the largest fraction of biomass, amino acid monomer distribution was also determined analytically (Table 4.S1 in Appendix C) and used to parameterize the model reaction for protein synthesis. A strong correlation was observed between the measured amino acid distribution and the distribution predicted from protein-coding gene sequences (Figure 4.S1 in Appendix B).

### 4.4.2. Computational Analysis of Stress Acclimation

The computational BP-1 metabolic model was decomposed into 4,636,498 unique EFMs using EFMtool (Terzer and Stelling 2008), with ~99.5% producing biomass. Each EFM, as well as any non-negative linear combination of multiple EFMs, represented a mathematically feasible phenotype and possible stress acclimation strategy. Competitive stress acclimation strategies were identified using ecological resource allocation theory. Resource allocation theory analyzes the amount of catabolic or anabolic resource required to synthesize a cellular product, often biomass. Minimizing the requirement of a limiting resource represents a competitive, cost-effective phenotype and is hypothesized to be a probable cellular strategy selected by evolution. When two or more resources are considered simultaneously, a multi-dimensional tradeoff surface is created that quantifies

the utilization relationship between the limiting resources (Carlson 2009, Molenaar, van Berlo et al. 2009, Carlson, Oshota et al. 2012, Beck, Hunt et al. 2016). Biomass-producing EFMs were ranked quantitatively based on efficiency of resource use for biomass production under simulated environmental stresses including high irradiance, $O_2/CO_2$ competition at RuBisCO, and limited availability of dissolved inorganic carbon (DIC) as well as nitrogen or iron. The tradeoff between optimal use of two resources was quantified by simultaneously minimizing the cost of biomass production under two different stress factors. Similar methods have been applied to extend FBA to account for biosynthetic costs (Mori, Hwa et al. 2016), but enumeration of complete EFMs combined with resource allocation theory allows exploration of the entire phenotypic space.

4.4.2.1. Irradiance and Photosynthetic Electron Flow. Photosynthetic electron flow was examined as a function of irradiance-induced stress to interpret relationships between photon absorption and photocatalytic water oxidation. Net $O_2$ production per carbon mole (Cmol) biomass produced was plotted as a function of photons absorbed per Cmol biomass produced, a metric of irradiance-induced stress (Figure 4.2). Each net $O_2$ molecule is the byproduct of four photosynthetically derived electrons extracted from water and requires eight total photons absorbed (Hill and Govindjee 2014); this relationship is reflected in the slope of the upper boundary of the phenotypic cone. Photons absorbed at PSI during cyclic photosynthesis are decoupled from $O_2$ production. Growth phenotypes were analyzed for the ability to direct electrons toward either biomass or reduced byproducts. The EFMs along the lowest boundary of the phenotypic cone in Figure 4.2 represented growth where all electrons were directed to biomass and

no reduced byproducts were secreted, extending up to ~80 mol photons absorbed per Cmol biomass produced. Net $O_2$ production (~1.53 mol $O_2$ per Cmol biomass) at the lowest boundary corresponds to the biomass degree of reduction, ~6.1 mol electrons available to reduce $O_2$ per Cmol biomass (Table 4.1). EFMs with higher net $O_2$ production directed electrons to reduced carbon byproducts, such as formate or acetate.

Biomass-producing EFMs were assessed for photon absorption at PSII relative to PSI to quantify the contribution of the two photosystems to photosynthetic electron flow (Figure 4.2, shaded color bar). A value less than one indicated elevated cyclic photosynthesis, a value greater than one indicated elevated operation of PSII independent of linear photosynthesis (i.e. reduction of $O_2$ through either cellular respiration or the water-water cycle), and a value equal to one indicated linear photosynthesis or, alternatively, equivalent cyclic photosynthesis and $O_2$ reduction. Figure 4.1 provides greater detail on cyclic and linear photosynthesis. An increase in photon absorption at PSII at a fixed net $O_2$ production indicated greater gross production of $O_2$, which was consumed by cellular respiration and/or the water-water cycle. In general, photon absorption at PSII relative to PSI was predicted to increase as irradiance-induced stress increased (Figure 4.2), indicating a greater contribution of PSII to photon absorption at high irradiance.

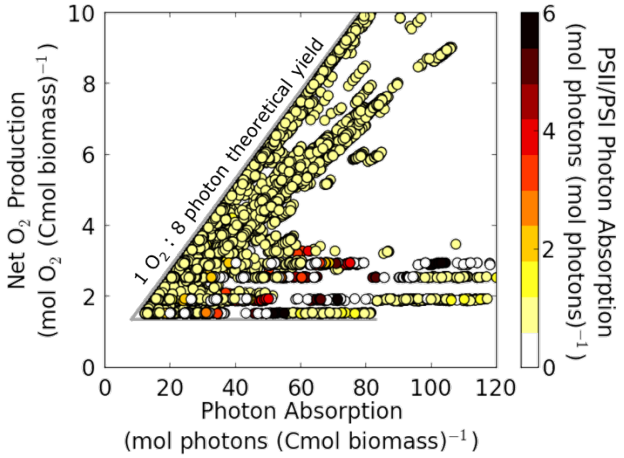


Figure 4.2. Computational analysis of irradiance and photosynthetic electron flow in cyanobacterium *T. elongatus* BP-1. Net $O_2$ production (net mol $O_2$ evolved (Cmol biomass produced)$^{-1}$) is plotted as a function of photon absorption (mol photons absorbed (Cmol biomass produced)$^{-1}$) for biomass-producing EFMs. Each point represents a unique EFM. The slope of the upper boundary of the phenotypic cone indicates maximum net moles of $O_2$ produced per mole of photons absorbed (eight photons required per molecule $O_2$ evolved; theoretical minimum quantum requirement). No byproducts were secreted on the lower boundary of the phenotypic cone minimizing net $O_2$ production per biomass produced; net $O_2$ production along this boundary was a direct result of electrons incorporated into biomass; secreted reduced carbon byproducts were predicted throughout the remaining phenotypic space. Color scale represents the photon absorption at PSII relative to PSI for each EFM (mol photons absorbed at PSII (mol photons absorbed at PSI)$^{-1}$). Relative contribution of PSII was predicted to increase as photon absorption increased. Less than 1% of the EFMs had a PSII/PSI ratio greater than 6 (with maximal value of 20) and were excluded from the plot to represent a more feasible phenotypic space (Kawamura, Mimuro et al. 1979, Vasilikiotis and Melis 1994, Sonoike, Hihara et al. 2001). Modeled biomass production did not include maintenance energy requirements. Points in the plot area shown are representative of 4,371,798 EFMs.

4.4.2.2. Irradiance, High $O_2$, and Nutrient Limitation. Computational BP-1 growth phenotypes were interrogated for stress acclimation strategies under a range of relative $O_2$ to DIC concentrations, represented by $O_2/CO_2$ competition at RuBisCO (Figure 4.3A). The tradeoff curve simultaneously minimizes the cost of biomass production under $O_2/CO_2$ competition (moles $O_2$ per moles $CO_2$ consumed at RuBisCO) and irradiance-induced stress; EFMs on the tradeoff curve (or non-negative linear combinations thereof)

represent optimal predicted growth phenotypes under the combined stresses. Photorespiration, as opposed to secretion of glycolate, was predicted as an essential process on the tradeoff curve except at zero $O_2/CO_2$ competition, and utilization of photorespiration reactions increased with increasing stress. Utilization of the C2 photorespiration cycle was predicted to increase along the tradeoff curve, whereas use of the glycerate pathway remained minimal. Photon absorption at PSII relative to PSI was also predicted to increase along the tradeoff curve. Neither cellular respiration nor the water-water cycle was active along the tradeoff curve, indicating that all photosynthetically derived electrons were directed to either biomass or reduced carbon byproducts. The tradeoff curve was divided into four phenotypic zones based on the suite of byproducts predicted. Zone 1 phenotypes did not secrete reduced byproducts, but as $O_2/CO_2$ competition at RuBisCO increased, more energy from photons was required to mediate the stress as indicated by higher photon absorption per biomass. At high $O_2/CO_2$ competition (~0.8 mol $O_2$ (mol $CO_2$)$^{-1}$), byproduct secretion represented the most resource-efficient acclimation strategy under the combined stresses. Byproduct synthesis effectively consumed photosynthetically derived electrons at the expense of fixed DIC and, conditionally, reduced nitrogen, as seen in the transition in byproducts produced along the tradeoff curve. Formate was predicted to be the most resource-efficient byproduct (zone 2 phenotypes), followed by combinations of formate and amino acids, represented in the model as alanine (zone 3 phenotypes), and acetate and amino acids (zone 4 phenotypes). Secretion of glycolate was not the most competitive use of metabolic potential under the considered stresses. Net $O_2$ production of the tradeoff curve

EFMs quantified the fraction of electrons directed to biomass and reduced byproducts as a function of stress acclimation (Figure 4.3B). A nonlinear increase in net $O_2$ production per Cmol biomass was predicted; the increase in net $O_2$ production correlated with the secretion of reduced byproducts (formate, acetate, and/or alanine).

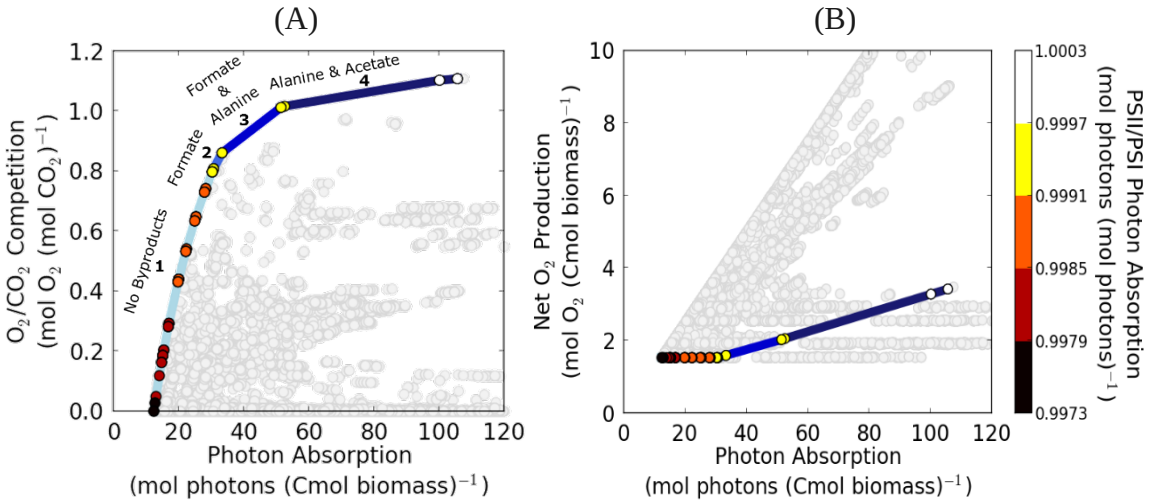


Figure 4.3. Computational analysis of irradiance-induced stress and $O_2/CO_2$ competition at RuBisCO in cyanobacterium *T. elongatus* BP-1. (A) $O_2/CO_2$ competition at RubisCO (mol $O_2$ (mol $CO_2$)$^{-1}$ consumed) as a function of photon absorption (mol photons absorbed (Cmol biomass produced)$^{-1}$) for biomass-producing EFMs are plotted. Each point represents a unique EFM. The tradeoff curve defining competitive strategies between $O_2/CO_2$ competition and irradiance-induced stress was divided into four distinct phenotypic regions based on byproduct secretion behavior, labeled accordingly (intensity of shading increases with increasing stress). The maximum amount of $O_2$ per $CO_2$ consumption at RuBisCO that can be sustained is two to one. Consumption of two $O_2$ molecules followed by photorespiration recycles 2-phosphoglycolate to regenerate the ribulose-1,5-bisphosphate precursor, but loses the single molecule of $CO_2$ that was consumed and thus cannot support biomass production. Points in the plot area shown are representative of 4,457,199 EFMs. (B) Net $O_2$ production (net mol $O_2$ evolved (Cmol biomass produced)$^{-1}$) as a function of photon absorption (mol photons absorbed (Cmol biomass produced)$^{-1}$) for biomass-producing EFMs are plotted. Colored points indicate net $O_2$ production of EFMs on the tradeoff curve in (a). Color scale represents the photon absorption at PSII relative to PSI (mol photons absorbed at PSII (mol photons absorbed at PSI)$^{-1}$). Modeled biomass production did not include maintenance energy requirements. Points in the plot area shown are representative of 4,355,094 EFMs.

In addition to DIC, nitrogen and iron are essential anabolic resources and place constraints on cellular functions such as growth or ATP regeneration (Folsom, Parker et al. 2014). Acclimation to nitrogen- or iron-limited growth, assessed by investment into enzymes, was analyzed in conjunction with $O_2/CO_2$ competition (Figure 4.S2A-B in Appendix B). Increasing $O_2/CO_2$ competition at RuBisCO necessitated an increase in nitrogen and iron investments into metabolic enzymes due to the requirement to process 2-phosphoglycolate. Tradeoff curve analysis of simultaneous acclimation to $O_2/CO_2$ competition and nutrient limitation showed trends similar to those predicted under irradiance-induced stress in Figure 4.3A, and amino acid secretion was again predicted at the highest resource limitation stress. However, under nitrogen limitation, reduced byproduct secretion was required for the most competitive phenotypes over the entire range of resource-limited growth. BP-1 metabolism was predicted to be less robust to nitrogen-limited stress than irradiance-induced stress as indicated by relatively fewer suboptimal EFMs near the tradeoff curve (Figure 4.S2A in Appendix B). Additional details on nitrogen and iron limitation are found in Appendix D. While the majority of EFMs produced biomass, energy-producing EFMs (not producing biomass) also showed similar optimal byproducts under irradiance-induced stress and $O_2/CO_2$ competition (data not shown).

### 4.4.3. Comparison of Computational Predictions with Photobioreactor Physiological Data

The optimal predicted growth phenotypes identified along the tradeoff curve (Figure 4.3A) were compared with data from turbidostat culturing experiments.

Irradiance levels altered both specific growth rate and biomass yield during cultivation. Specific growth rates ranged from 0.06-0.29 $h^{-1}$ at irradiances varying from 200-2000 μmol photons $m^{-2}$ $s^{-1}$ (Figure 4.4A). Specific growth rates increased linearly as a function of incident irradiance below 500 μmol photons $m^{-2}$ $s^{-1}$. Above 500 μmol photons $m^{-2}$ $s^{-1}$, irradiance became saturating, possibly inhibitory, and specific growth rate approached a maximum at 1800-2000 μmol photons $m^{-2}$ $s^{-1}$. Conversely, biomass yield per photon absorbed had a maximum at low irradiance (200-300 μmol photons $m^{-2}$ $s^{-1}$) and decreased nonlinearly as a function of incident irradiance (Figure 4.4B). Irradiance-induced stress at 2000 μmol photons $m^{-2}$ $s^{-1}$ reduced the biomass production efficiency by more than 50% compared to low irradiance conditions. The decrease in biomass per photon yield is consistent with predicted acclimation strategies, as is the nonlinear relationship between stress and biomass growth efficiency (Figure 4.3).

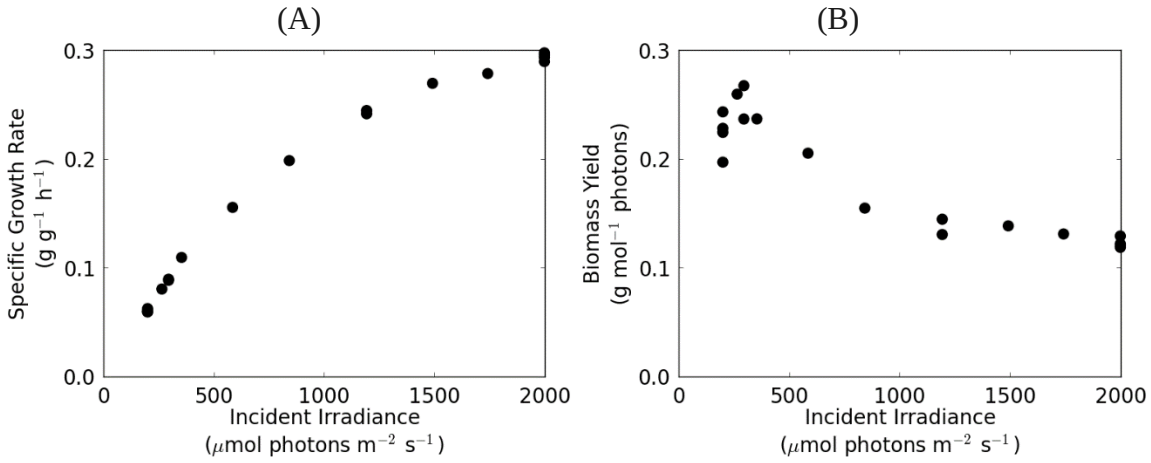


Figure 4.4. Photobioreactor impact of irradiance on specific growth rate and biomass production efficiency in *T. elongatus* BP-1 continuous culture. (A) Photobioreactor measurement of BP-1 specific growth rate (g CDW (g CDW)$^{-1}$ $h^{-1}$) as a function of incident irradiance (μmol photons $m^{-2}$ $s^{-1}$). CDW, cell dry weight. (B) Photobioreactor measurement of BP-1 biomass yield (g CDW (mol photons absorbed)$^{-1}$) as a function of incident irradiance (μmol photons $m^{-2}$ $s^{-1}$).

BP-1 maintenance energy requirements were estimated by analyzing specific photon absorption rate as a function of specific growth rate (Figure 4.5). The non-growth associated maintenance energy requirement (0.16 mol photons $(g\ CDW)^{-1}\ h^{-1}$) was estimated by extrapolating the specific photon absorption rate data to a zero growth rate. Photon requirements for growth can be partitioned into the cellular energy required to (1) reduce nutrients such as DIC and nitrate into biomass monomers and (2) polymerize monomers into macromolecules. The photon requirement to reduce nutrient substrates, including bicarbonate and nitrate, to biomass monomers was calculated using the experimentally measured biomass composition. Macromolecular synthesis reactions in the model incorporated the energy cost of phosphate bonds required to polymerize monomers.

Photon requirement per Cmol biomass increased nonlinearly at higher growth rates (Figure 4.5), which corresponded to higher incident irradiance and represented successively increasing irradiance-induced stress and reduced biomass production efficiency. The difference between the photon requirement for biomass and the experimentally measured photon requirement is hypothesized to be the photon requirement for growth-associated maintenance energy, including tasks such as general protein repair, enzyme turnover, and maintenance of gradients, or other drains such as non-photochemical quenching of absorbed photons (Kirilovsky 2007, Bailey and Grossman 2008, Rochaix 2011, Muramatsu and Hihara 2012). Additionally, the repair and recycling of PSII due to increased photoinactivation at high irradiance requires a large investment of nitrogen and poses a significant limitation on growth (Li, Brown et al.

2015, Murphy, Roodvoets et al. 2017). The implications of nitrogen source degree of reduction were also factored into maintenance energy calculations. A comparison of the effects of different nitrogen sources on the photon requirement is shown in Figure 4.S3 in Appendix B. Molecular nitrogen and ammonia required fewer photons per biomass since they are more reduced than nitrate. Nitrate may be a preferred nitrogen source for photoautotrophs under high irradiance conditions, likely because it represents a possible sink for electrons which can buffer over-reduced photosynthetic machinery.

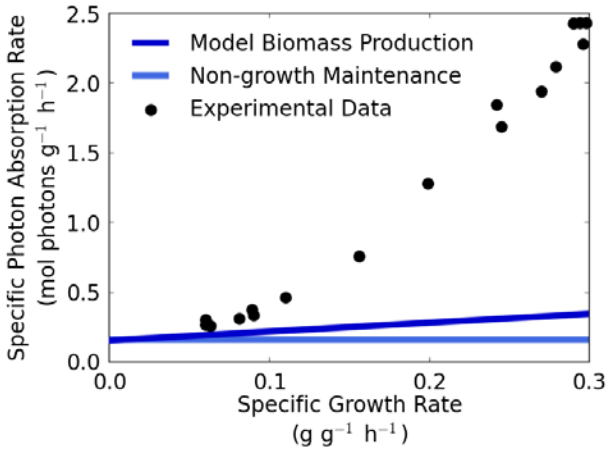


Figure 4.5. Growth rate-dependent photon absorption rate and maintenance energy in cyanobacterium *T. elongatus* BP-1. Specific photon absorption rate (mol photons absorbed (g CDW)$^{-1}$ h$^{-1}$) is plotted as a function of specific growth rate (g CDW (g CDW)$^{-1}$ h$^{-1}$) for experimental BP-1 turbidostat cultures (black circles). Specific photon absorption rate is dependent on specific growth rate (μ) according to the equation $0.16e^{9.47\mu}$ determined from an exponential regression of the photobioreactor data. The non-growth associated maintenance energy requirement was extrapolated from a specific growth rate of zero (light blue line). Measured photon absorption rates are contrasted with calculated requirements for biomass synthesis, including polymerization (dark blue line). CDW = cell dry weight.

### 4.4.4. Comparison of Computational Predictions with Photobioreactor Transcriptomic Data

The optimal predicted growth phenotypes identified along the tradeoff curve (Figure 4.3A) were compared with previously published BP-1 transcriptomic data (Bernstein, McClure et al. 2017). The transcriptomic data were analyzed for differentially expressed genes (two-fold or greater difference) between high and low irradiance conditions (2000 versus 200 μmol photons $m^{-2}$ $s^{-1}$). A change in expression of two-fold or greater was observed for 1147 genes. Differentially expressed genes were examined according to metabolic pathways and compared with the pathways utilized in the predicted optimal stress acclimation phenotypes. Consistencies and inconsistencies between predicted and observed metabolic functionalities were grouped into six categories (Table 4.3) and are discussed in detail below.

Table 4.3. Comparison between computational predictions of stress acclimations and photobioreactor gene expression data under high versus low irradiance conditions (Bernstein, McClure et al. 2017). Metabolic functionalities were predicted from competitive pathways along the optimal tradeoff curve for irradiance-induced stress and $O_2/CO_2$ competition (Figure 4.3A), and observations were made from gene expression data comparing change in transcripts from high to low irradiance (2000 versus 200 μmol photons $m^{-2}$ $s^{-1}$) (Bernstein, McClure et al. 2017).

| | **Prediction** | **Observation** |
|---|---|---|
| 1. Photosystem contribution | • Increased PSII photon absorption relative to PSI | • Upregulation of PSII-associated genes<br>• No change in PSI-associated genes |
| 2. Photorespiration pathways | • Use of photorespiration<br>• Increase in photorespiration with higher $O_2/CO_2$ competition<br>• Primarily C2 cycle, minimal glycerate pathway usage | • Transcription of photorespiration genes<br>• Upregulation of C2 cycle genes<br>• No change in glycerate pathway genes |
| 3. Byproduct secretion | • Production of reduced byproducts<br>• Formate and acetate production<br>• Amino acid (alanine) secretion at highest stress | • Upregulation of formate, acetate, and sucrose synthesis genes<br>• Upregulation of amino acid synthesis pathway and transporter genes |
| 4. Glycolysis | • Increased use of lower portion of glycolysis | • Upregulation of genes in lower portion of glycolysis |
| 5. TCA cycle | • No change in TCA cycle use | • Upregulation of TCA cycle genes leading to synthesis of α-ketoglutarate |
| 6. Nitrate and sulfate assimilation | • Increased nitrate uptake in pathways that secrete amino acid byproducts<br>• No change in sulfate uptake | • Upregulation of nitrate uptake and assimilation genes<br>• Upregulation of sulfate uptake and assimilation genes |

4.4.4.1. Photosynthesis, Photorespiration, and Byproducts. The predicted increase in photon absorption at PSII relative to PSI (Figure 4.3A) was reflected in the transcriptomic data (Bernstein, McClure et al. 2017) showing upregulation of genes coding for several PSII subunit and repair genes but no upregulation of PSI-associated genes (Table 4.S2 in Appendix C). The increase in transcript level could be due to increased photon absorption, or it could reflect an increased turnover of PSII, which has been reported during culturing at high irradiance (Li, Brown et al. 2015, Murphy,

Roodvoets et al. 2017). A relative increase in photon absorption at PSII would suggest an increased relative contribution of PSII to photosynthetic electron flow under irradiance-induced stress. Photorespiration was a predicted strategy under high irradiance and $O_2/CO_2$ competition, corresponding to upregulation of photorespiration pathway genes observed in the transcriptomic data (Bernstein, McClure et al. 2017). Predicted pathways indicated preferential utilization of the C2 photorespiration cycle as opposed to the glycerate pathway, and transcriptomic data (Bernstein, McClure et al. 2017) indicated upregulation of C2 cycle genes with no change in expression of glycerate pathway genes (Figure 4.6). Byproduct secretion was predicted as a competitive strategy at high irradiance and $O_2/CO_2$ competition. Irradiance, nitrogen investment, and iron investment analyses in conjunction with $O_2/CO_2$ competition all predicted amino acid secretion as a resource-efficient strategy at the highest combined stress conditions (Figures 4.3A, 4.S2). These predictions corresponded with observations of upregulated genes for synthesis pathways of organic compounds such as acetate and formate (Figure 4.6), as well as for more than 50 amino acid synthesis pathway and transporter genes (Table 4.S3 in Appendix C). Altogether, these parallels with the transcriptomic data (Bernstein, McClure et al. 2017) suggest increased electron flow into the system, increased photorespiration, and reprocessing of salvaged carbon into other byproducts with greater degree of reduction (Table 4.1) at higher irradiance.

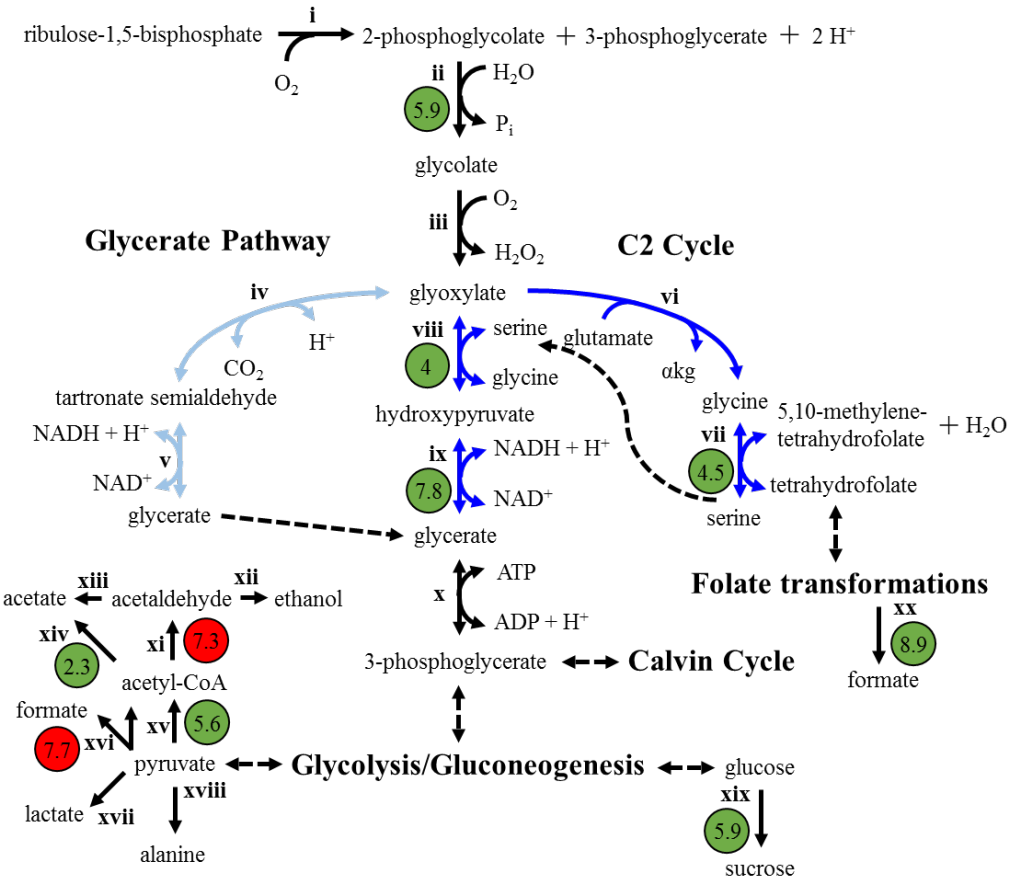


Figure 4.6. Cyanobacterium *T. elongatus* BP-1 photorespiration and byproduct secretion pathways with transcriptomic data measured under high versus low irradiance. Genome-based photorespiration routes (C2 cycle, dark blue, and glycerate pathway, light blue) and byproduct secretion pathways included in the BP-1 model are illustrated. Green circles represent upregulated gene expression measured under high irradiance (2000 versus 200 µmol photons $m^{-2}$ $s^{-1}$), and red circles represent downregulated gene expression (Bernstein, McClure et al. 2017). Numbers indicate fold change for each gene. Enzymes coded in Roman numerals are: i, ribulose-1,5-bisphosphate carboxylase oxygenase; ii, phosphoglycolate phosphatase; iii, glycolate oxidase; iv, glyoxylate carboligase; v, tartronate semialdehyde reductase; vi, glycine transaminase; vii, serine hydroxymethyltransferase; viii, serine-glyoxylate transaminase; ix, glycerate dehydrogenase; x, glycerate 3-kinase; xi, acetaldehyde dehydrogenase; xii, alcohol dehydrogenase; xiii, succinate-semialdehyde dehydrogenase; xiv, acetyl-CoA synthetase; xv, pyruvate dehydrogenase; xvi, formate acetyltransferase; xvii, lactate dehydrogenase; xviii, alanine dehydrogenase; xix, sucrose phosphate synthase and sucrose phosphate phosphatase; xx, formyltetrahydrofolate deformylase. Other abbreviations: αkg, α-ketoglutarate.

4.4.4.2. Central Metabolism and Nutrient Assimilation. Several glycolysis genes were observed to be upregulated under high irradiance conditions (Bernstein, McClure et al. 2017), primarily genes involved in the lower portion of glycolysis after glyceraldehyde-3-phosphate (glyceraldehyde-3-phosphate dehydrogenase, phosphoglycerate kinase, phosphoglycerate mutase, enolase, and pyruvate kinase) (Table 4.S2 in Appendix C). Tradeoff curve analysis of the EFMs under high irradiance and $O_2/CO_2$ competition predicted that utilization of the reactions catalyzed by these enzymes increased with increasing stress except for glyceraldehyde-3-phosphate dehydrogenase. Both glyceraldehyde-3-phosphate and 3-phosphoglycerate intersect the Calvin cycle and glycolysis; thus, increased use of the lower portion of glycolysis suggested funneling of glyceraldehyde-3-phosphate from the Calvin cycle into glycolysis to produce pyruvate, which may be used to synthesize byproducts such as formate, acetate, and amino acids. Several TCA cycle genes were also observed to be upregulated under high irradiance conditions, predominantly genes catalyzing reactions up to the synthesis of α-ketoglutarate, from which several amino acids are synthesized (Table 4.S2 in Appendix C). Tradeoff curve analysis of the EFMs under high irradiance and $O_2/CO_2$ competition predicted no change in utilization of any TCA cycle reactions. The BP-1 model utilized alanine as a representative amino acid which could be secreted as a byproduct; alanine is synthesized via pyruvate. However, if the computational model was modified to allow secretion of amino acids that are synthesized via TCA cycle intermediates, such as glutamate, it would lead to predictions of increases in some TCA cycle fluxes.

Finally, the transcriptomic data (Bernstein, McClure et al. 2017) showed upregulation of genes involved in both nitrate and sulfate uptake and assimilation under high irradiance conditions (Table 4.S2 in Appendix C). Tradeoff curve analysis of the EFMs under high irradiance and $O_2$/$CO_2$ competition predicted increased use of the nitrate uptake reaction for strategies that secreted amino acids; conversely, no change in use of the sulfate uptake reaction was predicted. Reduction of nitrate to ammonia for amino acid synthesis represents an effective strategy for using excess electrons from the photosynthetic electron transport chain, consuming 8 moles of electrons per mole of nitrate reduced. Thus, at high irradiance and $O_2$ production, secretion of amino acids represents an economical stress acclimation strategy. Similarly, sulfate reduction also consumes 8 moles of electrons per mole of sulfate reduced to hydrogen sulfide, which is used in synthesis of cysteine and methionine. Permitting secretion of cysteine or methionine in the computational model would lead to predictions of increased sulfate uptake. Altogether, comparison of the predicted competitive strategies with transcriptomic data under high irradiance (Table 4.3) suggests overall consistency of the computational model with photobioreactor observations.

### 4.4.5. Stress Acclimation and Photoautotrophic-Heterotrophic Interactions

BP-1 acclimation to a variety of culturing stresses was predicted to result in secretion of reduced carbon byproducts including organic acids and amino acids (Figures 4.3A, 4.S2A-B; illustrated in Figure 4.7A). These byproducts represent a nutritional niche for heterotrophs. Photoautotrophic-heterotrophic cross-feeding could represent a mutually

beneficial mechanism for buffering a photoautotroph from environmental stresses. Consumption of reduced carbon byproducts by the heterotroph would relieve potential inhibitory organic acid stress, as well as maximize the efficiency of total resource usage by the community (illustrated in Figure 4.7B). Cross-feeding of byproducts could also promote growth of the photoautotroph through consumption of $O_2$ by an aerobic heterotroph, thus decreasing local $O_2$ concentrations and lowering $O_2/CO_2$ competition. The amount of heterotroph able to be supported by secreted byproducts was predicted as a function of stress using published heterotrophic biomass per byproduct yields (Goldberg, Rock et al. 1976, Luttik, vanSpanning et al. 1997, Seifritz, Frostl et al. 1999, Nagpal, Chuichulcherm et al. 2000, Edwards, Ibarra et al. 2001, Janssen and Hugenholtz 2003, Hunt, Jennings et al. 2016) (see File 4.S5 in the Supplementary Materials for calculations) (Figure 4.7C). The predicted amount of heterotrophic biomass that can be supported by BP-1 through cross-feeding of byproducts increased as stress increased due to higher byproduct yields at higher stress levels, as well as the varying heterotrophic biomass yields on different byproducts (Table 4.S4 in Appendix C). The cross-feeding was also predicted to reduce local $O_2$ levels, which was calculated based on heterotrophic biomass $O_2$ requirements (Figure 4.7D, File 4.S5 in the Supplementary Materials).

The predicted ratio of heterotroph to photoautotroph as a function of stress acclimation was compared to published photobioreactor co-culture data of BP-1 with the aerobic heterotroph *Meiothermus ruber* str. A (Bernstein, McClure et al. 2017). Experiments reported heterotroph to photoautotroph ratios of ~1:10 (Bernstein, McClure et al. 2017). This ratio, with some variation accounting for cell size differences between

the two populations, falls within the range of heterotroph to photoautotroph ratios predicted at modest culturing stress (Figure 4.7C). These predictions considered autotrophic-heterotrophic interactions based on secreted carbon and not necessarily nitrogen source. Additional analysis of potential cross-feeding based on nitrogen or iron limitation can be found in Appendix B (Figure 4.S2C-F).

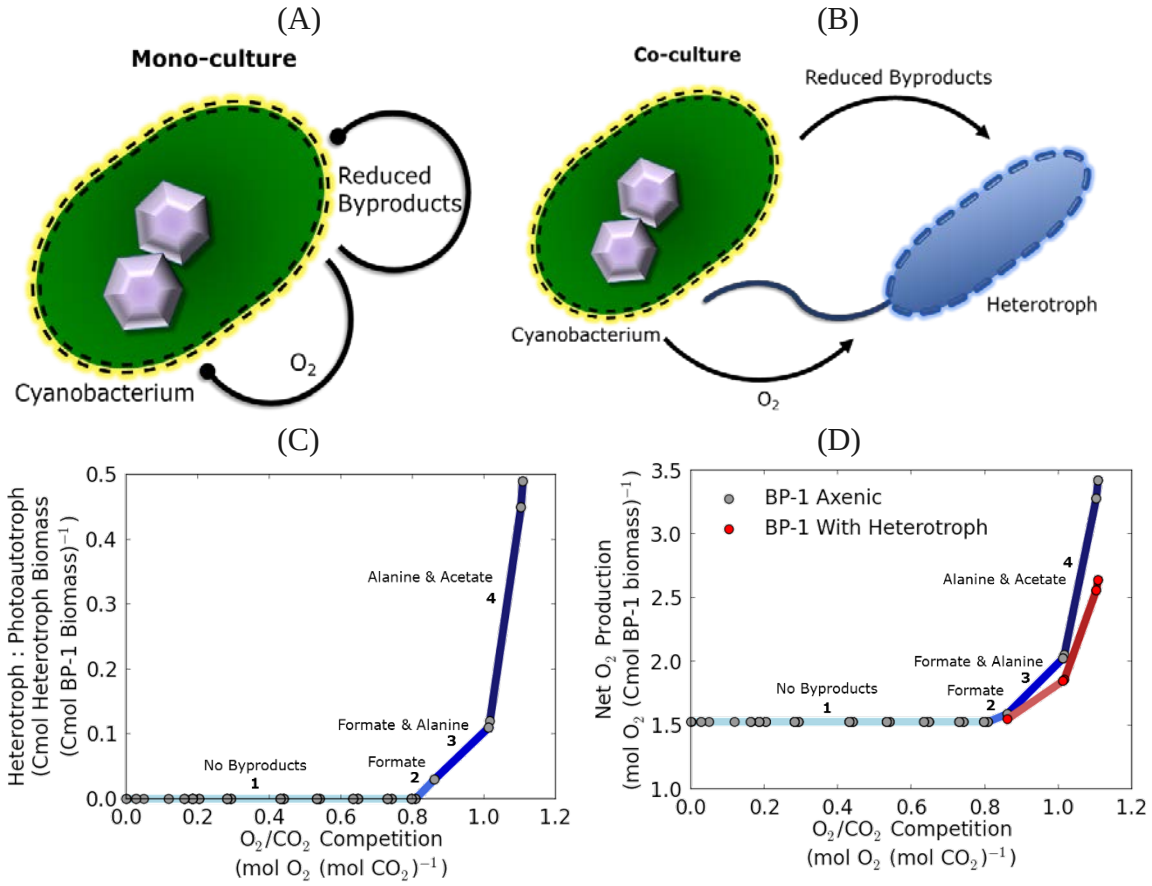


Figure 4.7. Byproduct secretion generates a heterotrophic niche and stimulates a mutually beneficial relationship. (A) Cyanobacterium BP-1 produces $O_2$ and reduced carbon compounds as metabolic byproducts during environmental stress, both of which are inhibitory to BP-1 growth. (B) The presence of reduced byproducts and $O_2$ forms a nutritional niche for heterotrophic organisms, which relieves inhibition for BP-1. (C) Heterotrophic biomass yield per BP-1 biomass (Cmol $Cmol^{-1}$) is presented as a function of $O_2/CO_2$ competition at RuBisCO (mol $O_2$ (mol $CO_2$)$^{-1}$ consumed) for the EFMs forming the optimal tradeoff with irradiance-induced stress. (D) Presence of a heterotroph lowers net $O_2$ production per Cmol BP-1 biomass as a function of $O_2/CO_2$ competition

(mol $O_2$ (mol $CO_2$)$^{-1}$ consumed) for the EFMs forming the optimal tradeoff with irradiance-induced stress, which reduces $O_2$ inhibition. The distinct phenotypic regions defined by the tradeoff between $O_2$/$CO_2$ competition and irradiance-induced stress are labeled according to byproduct secretion patterns as in Figure 4.3A.

## 4.5. Discussion

Computational modeling was integrated with photobioreactor analyses to identify and interpret, from a systems perspective, the inferred mechanisms that underpin cyanobacterial acclimation to irradiance-associated stress. The combined results of this study show how different cyanobacterial systems, such as the photosynthetic apparatus and central carbon metabolism, can respond to environmentally induced stresses. Photobioreactor steady state growth of BP-1 showed decreased biomass production efficiency at high irradiance (Figure 4.4B), indicating that electrons were partitioned into non-biomass-producing alternative metabolic routes. Examination of transcriptomic data (Bernstein, McClure et al. 2017) comparing high to low irradiance conditions identified upregulation of genes involved in PSII operation, photorespiration, organic acid synthesis, and amino acid synthesis, among other pathways (Figure 4.6, Tables 4.S2, 4.S3). Interrogation of BP-1 metabolic pathways with EFMA and resource allocation theory under conditions of high irradiance, high $O_2$, and limited nutrient availability provided a theoretical explanation for utilization of these pathways. Evolution has selected phenotypes which allocate limiting resources competitively. The origin of the stresses is the imbalance in resource acquisition which is manifested as a resource limitation. Acclimation to the resource stresses resulted in the secretion of reduced byproducts in a behavior analogous to classic overflow metabolism in heterotrophs. The

byproduct-secreting phenotypes represent a competitive and economical response to the stress (Folsom and Carlson 2015). It is worth noting that photobioreactor observations and computational predictions for BP-1 are in general agreement with the transcriptional patterns and physiological trends observed in the closely related *Synechococcus* sp. PCC 7002 (Bernstein, McClure et al. 2016). The predicted byproduct secretion profiles furthermore control nutrient niches for proximal heterotrophic partners (Figure 4.7). In some cases, heterotrophic consumption of the byproducts represents a mutually beneficial interaction in that byproduct removal prevents accumulation of byproducts to a degree that represents an additional stress. This mutually beneficial interaction template likely plays a significant role in the many reported occurrences of photoautotrophic-heterotrophic consortia (Paerl and Pinckney 1996, Paerl, Pinckney et al. 2000, Cole, Hutchison et al. 2014). In fact, cross-feeding between BP-1 and the aerobic heterotroph *M. ruber* str. A has been both predicted by genome-scale modeling and observed in a laboratory setting (Henry, Bernstein et al. 2016, Bernstein, McClure et al. 2017).

The computational analyses investigated several metabolic acclimations to photosynthesis-associated stresses that apply broadly to photoautotrophs, including photosystem utilization and photorespiration strategies, the nature of reduced carbon byproducts, and the severity of $O_2$/$CO_2$ competition at RuBisCO. PSII was predicted to increase in photon absorption relative to PSI as irradiance increased (Figure 4.3), supported by transcriptomic data (Bernstein, McClure et al. 2017) (Tables 4.3, 4.S2). Increased relative photon absorption of PSII under higher irradiance is also reported in the literature from studies with the mesophilic cyanobacterium *Synechocystis* sp. PCC

6803 and is hypothesized to aid in reducing overall electron transport (Sonoike, Hihara et al. 2001). Additionally, increased utilization of the C2 photorespiration cycle at high irradiances may intersect with byproduct secretion strategies and contribute to amino acid synthesis as a resource-efficient strategy at high irradiances. Photorespiration permits salvage of carbon from unusable RuBisCO oxygenation byproducts; this carbon may be directed toward other byproduct pathways. The C2 photorespiration cycle requires more enzymatic steps and thus more biosynthetic resources (e.g. nitrogen) than the glycerate pathway, but links into glycine-serine interconversion and amino acid synthesis pathways.

Formate is the least reduced organic byproduct considered in the model (Table 4.1). It is predicted to be a more competitive byproduct secretion strategy at intermediate irradiance-induced stress and $O_2/CO_2$ competition, releasing a minimal quantity of electrons in the form of reduced carbon byproducts and retaining the remaining electrons for biomass (Figure 4.3). Alanine is predicted to be a competitive byproduct at high stress levels due to its high degree of reduction (Table 4.1). At high electron load (supported by high rates of oxygenic photosynthesis) and high $O_2/CO_2$ competition, alanine synthesis consumes more electrons per Cmol, resulting in a more efficient redox sink (Figure 4.3). Alanine was selected in this study as a representative amino acid; however, amino acids with higher nitrogen content, such as arginine, histidine, or lysine, would serve as even more effective electron sinks when nitrate is the nitrogen source. Genes involved in synthesis pathways for several amino acids beside alanine (Table 4.S3 in Appendix C) were identified as upregulated under high irradiance conditions in the transcriptomic data

(Bernstein, McClure et al. 2017). Additionally, qualitative measurements from BP-1 steady state cultures have identified a variety of amino acids in the extracellular environment, including glutamate, isoleucine, leucine, lysine, phenylalanine, serine, threonine, and valine (Bernstein, McClure et al. 2017).

Experimental assessment of $O_2/CO_2$ competition and actual concentrations of $O_2$ and $CO_2$ at the active site of RuBisCO *in vivo* is challenging. The specificity factor, a kinetic constant describing the relative affinity of RuBisCO for $CO_2$ versus $O_2$ ($v_c/v_o = SF\,[CO_2]/[O_2]$) (Gubernator, Bartoszewski et al. 2008), has been measured for a variety of phototrophs and is typically obtained from enzyme extracts. Falkowski and Raven (Falkowski and Raven 2007) compiled a list of specificity factors from a variety of organisms, including cyanobacteria, algae, and plants, and estimated $v_o/v_c$ ratios under assumptions of air equilibrium at 25°C. These experimental estimates were compared with the predicted $v_o/v_c$ values from the BP-1 model irradiance tradeoff curve (Figure 4.8A(A)). The variation in values within and among different types of organisms highlights the diversity of RuBisCO enzyme properties, which organisms are thought to have optimized over time based on different selective pressures (Tcherkez, Farquhar et al. 2006, Savir, Noor et al. 2010). However, the experimental estimates do not account for the optimal temperature environment of the organism, the confounding influence of photosynthetic $O_2$ evolution, or effects of the carbon-concentrating mechanism, which may also be influenced by pH (Mangan, Flamholz et al. 2016).

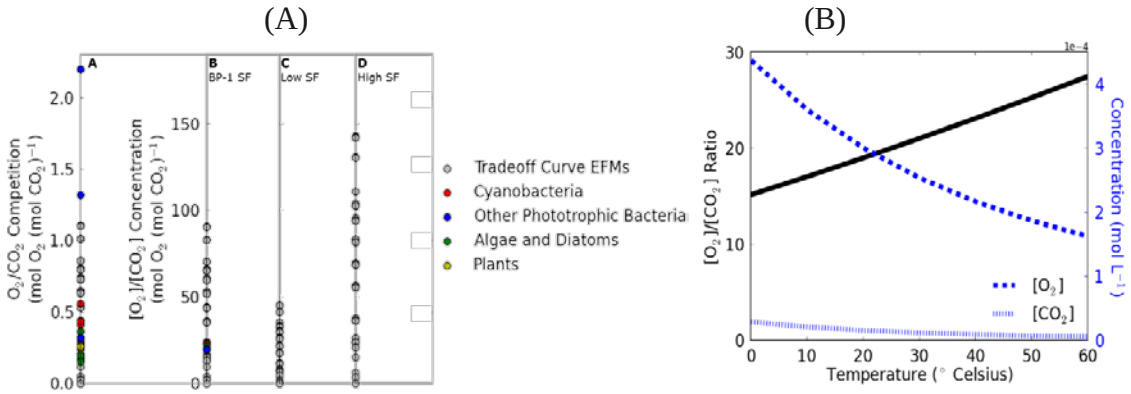


Figure 4.8. Comparison of computational and experimental $O_2/CO_2$ competition and concentrations at RuBisCO. (A) Predicted $O_2/CO_2$ competition values (mol $O_2$ (mol $CO_2$)$^{-1}$ consumed at RuBisCO) from the irradiance tradeoff curve in Figure 4.3A are shown in gray (A). Experimental $O_2/CO_2$ values for a variety of organisms calculated at air equilibrium and 25°C (Falkowski and Raven 2007) are overlaid in color. Predicted $O_2/CO_2$ competition values (gray points) were converted to relative $O_2/CO_2$ concentrations around RuBisCO by multiplying by the specificity factor (SF). The experimentally measured SF for BP-1 of 82 (Gubernator, Bartoszewski et al. 2008) was used for conversion in (B). Experimental data points from Falkowski and Raven (colored points) were converted to $O_2/CO_2$ concentrations via the respective SF of each organism (Falkowski and Raven 2007). Comparison of the BP-1 SF with lower and higher SF values is visualized using a lower SF of 41 (representative of *Synechococcus* sp.) (C) and a higher SF of 129 (representative of a red alga) (D). A lower SF indicates that lower relative $O_2/CO_2$ concentrations result in higher $O_2/CO_2$ competition ratios, whereas a higher SF indicates that an organism is more tolerant of higher relative $O_2/CO_2$ concentrations. (B) Temperature affects the relative propensity of RuBisCO for oxygenation. Dashed and dotted blue curves represent $O_2$ and $CO_2$ concentrations in aqueous phase at equilibrium with atmospheric concentrations, calculated using Henry's law constants from Sander (Sander 2015). The black curve represents the ratio of the $[O_2]$ to $[CO_2]$ curves, showing that the relative proportion of $O_2$ increases with elevated temperature. Calculations are provided in File 4.S6.

The specificity factor can be used to convert predicted $O_2/CO_2$ competition values to local relative $O_2/CO_2$ concentrations around RuBisCO (Gubernator, Bartoszewski et al. 2008), thereby permitting extension of stoichiometric modeling into the kinetic realm. Equivalent relative $O_2/CO_2$ competition values convert to different relative concentrations depending upon the magnitude of the specificity factor. Values for mesophilic cyanobacteria range from 45 to 70, and higher plants have an average value

around 100 (Gubernator, Bartoszewski et al. 2008). Figure 4.8A(B-D) shows the effect of varying the specificity factor on the $O_2/CO_2$ concentrations necessary to achieve the predicted $v_o/v_c$ values along the irradiance tradeoff curve in Figure 4.3A; relative concentrations are lowered with a smaller specificity factor and raised with a higher specificity factor. A higher specificity factor indicates a greater tolerance to stress from $O_2/CO_2$ competition. *In vivo* measurements of oxygenation and carboxylation rates are sparse in the literature, particularly for microbial species; Taffs et al. (Taffs, Aston et al. 2009) calculated a range of 3-7% oxygenation based on measurements of extracellularly secreted glycolate (Bateson and Ward 1988), but these values are likely an underestimate considering glycolate may be salvaged through the complete photorespiration pathway rather than excreted (Figure 4.3). Isotopic labeling studies of cyanobacteria also provide experimental data, but extrapolation of $v_c/v_o$ ratios should be exercised with caution. Studies have shown operation of photorespiration even under high $CO_2$ (5%) conditions (Huege, Goetze et al. 2011). Another study has presented both modeling and experimental validation of the necessity of photorespiration even under saturating $CO_2$ conditions, positing that high $CO_2$ stimulates high photosynthetic rates to provide adequate energy for carbon fixation, which thereby leads to increased $O_2$ production levels (Yokota, Iwaki et al. 1987). Additionally, elevated temperatures have been shown to enhance oxygenation due to both changes in the specificity of RuBisCO and the different solubilities of $O_2$ and $CO_2$ (Jordan and Ogren 1984) (Figure 4.8B). Experimental data on $v_o/v_c$ values is variable and dependent on the conditions under which the measurements were made. However, an environmental scenario with low $O_2/CO_2$ ratios

may indicate that greater priority is placed on minimizing $O_2/CO_2$ competition than on minimizing photon absorption cost particularly under high irradiance conditions, e.g. $O_2/CO_2$ competition is a stronger driver of stress acclimation. Byproduct production and existence of heterotrophic partners is observed in experimental cyanobacterial systems, suggesting that byproduct production is an effective strategy for managing electrons from excess photon absorption. Instead, the cell may be simultaneously optimizing for other stresses such as biosynthetic nutrient investment like nitrogen or iron (Figure 4.S2).

The systems-level analysis provided by this study indicated that the suite of metabolic carbon and electron sinks (i.e. secreted byproducts and biomass) is dependent upon environmental stressors. Pathway utilization and resource investments were co-dependent upon irradiance, $O_2/CO_2$ competition at RuBisCO, and DIC, nitrogen, and iron levels. These results provided novel insight into ecologically competitive metabolic strategies that cyanobacteria use to acclimate to environmental conditions. Physiological and transcriptomic (Bernstein, McClure et al. 2017) data paralleled the predictions, providing an additional level of support to the stoichiometric modeling predictions. It is noted that the stoichiometric model does not account for kinetic constraints, regulatory effects, or other aspects of thermodynamics beside reaction reversibilities (Gerstl, Jungreuthmayer et al. 2015, Peres, Jolicoeur et al. 2017), which may account for some of the differences between predictions and data and represents an avenue for further development. Finally, analysis of predicted optimal growth phenotypes was extended to make inferences about the nature of photoautotrophic-heterotrophic interactions and provide a theoretical basis for examining community composition. Taken holistically, this

work presents a synergistic experimental and theoretical approach for understanding metabolic acclimation and provides a new level of insight into how different cyanobacterial systems, such as the photosynthetic apparatus and central carbon metabolism, coordinate and respond to environmental stresses that influence resource allocation.

## 4.6. Supplementary Materials

The following are available online at www.mdpi.com/2227-9717/5/2/32/s1, File 4.S1: Model Reactions and Supporting Information, File 4.S2: SBML Model Version, File 4.S3: MATLAB Analysis Routines, File 4.S4: Python Graphics Routines, File 4.S5: Heterotroph Niche Calculations, File 4.S6: Solubility Calculations.

## 4.7. Acknowledgments

This work is a contribution of the PNNL Foundational Scientific Focus Area (Principles of Microbial Community Design) subcontracted to Montana State University. Ashley E. Beck was supported by the Office of the Provost at Montana State University through the Molecular Biosciences Program and NSF (DMS-1361240). Hans C. Bernstein was supported by the Linus Pauling Distinguished Postdoctoral Fellowship which is a Laboratory Directed Research and Development program at PNNL, operated for the DOE by Battelle Memorial Institute under Contract DE-AC05-76RLO 1830. The authors would like to acknowledge and thank Alexander Beliaev, Lye Meng Markillie, Eric Hill, Ryan McClure, and Margaret Romine for assisting with the culturing, RNA

sequencing, and genome annotation activities that helped support this study and Reed Taffs for primary MATLAB algorithm development. The authors would also like to thank Kristopher Hunt, Zackary Jay, Heidi Schoen, Lee McGill, and William Moore for critical reading of the manuscript.

## 4.8. Appendix A. Biomass Composition Analytical Methods

### 4.8.1. DNA, After Downs and Wilfinger, 1983

50 µL of frozen cell pellet equivalent to approximately 1.5 mg of biomass (dry weight) was re-suspended in 50 µL of alkali extraction solution (1 N $NH_4OH$, 0.2% Triton X-100 with nuclease-free water) in 2-mL Eppendorf tubes. Tubes were incubated at 37°C for 10 minutes in a block heater. After 10 minutes, samples were diluted to 2 mL total volume with assay buffer (100 mM NaCl, 10 mM EDTA, 10 mM Tris, pH 7.0 with HCl, nuclease-free water) and transferred to 15-mL Falcon tubes for centrifugation (2500 xG, 30 minutes, 4°C). Calf thymus DNA standards were prepared by making a DNA stock solution in nuclease-free water about 300 µg/mL (stored at 4°C). Exact concentration was measured with a NanoDrop 1000 spectrophotometer. The standard solution was diluted to a working stock of 100 µg/mL with standard buffer, or assay buffer containing the same concentration of alkali extraction solution as the diluted samples (100 mM NaCl, 10 mM EDTA, 10 mM Tris, pH 7.0 with HCl, 0.025 N $NH_4OH$, 0.005% Triton X-100). The DNA working stock was then diluted into a standard series with standard buffer (1-5 µg/mL). 50 µL of sample or standard were added to a black 96-well plate with clear bottom. 295 µL of Hoechst working reagent was added to each well.

Hoechst working reagent was prepared fresh daily from an intermediate stock of 200 µg/mL by diluting to 1 µg/mL with assay buffer. The intermediate stock was prepared from a 10 mg/mL stock solution by diluting to 200 µg/mL with nuclease-free water. Stock solutions and working stocks were stored at 4°C wrapped in aluminum foil to protect from light. The wells were then read in a Synergy fluorescent plate reader using the following settings: (plate type) 96 well plate; (set temperature) setpoint 30°C, preheat before moving to next step; (shake) double orbital 30 s, frequency 180 cpm; (read) fluorescence endpoint, 352 nm excitation, 461 nm emission, bottom optics, gain 100, Xenon flash light source, high lamp energy, normal read speed, 100 ms delay, 10 measurements/data point. Three reaction wells of sample or standard were performed for each sample or standard. The concentration of the samples was determined based on the average of the three standard calibration curves.

4.8.2. Glycogen, After Del Don et al., 1994

Anthrone reagent was prepared fresh daily according to Herbert et al. (Herbert, Phipps et al. 1971) and stored at 4°C. Frozen cell pellet (-80°C) was thawed and divided into three equal parts by mass in 2-mL Eppendorf tubes, approximately 0.5 mg dry weight. Each aliquot was re-suspended in 200 µL 2% sodium sulfate (w/v). Eppendorf tubes were sealed with parafilm and heated for 10 minutes at 70°C in a block heater. After heating, 1 mL methanol was added to each tube and vortexed to co-precipitate glycogen and sodium sulfate. The precipitate was pelleted by centrifuging for 15 s at 10,000 rpm. The precipitate was washed with 1 mL methanol, until the pellet was white, to remove impurities. Pellets were then re-suspended in 1 mL reverse osmosis water and

transferred to clean glass test tubes and placed on ice to chill. 5 mL of ice-cold anthrone reagent was added to each test tube. After adding reagent, tubes were chilled on ice for 5 minutes, vortexed gently to homogenize the solution, and transferred to a boiling water bath for 10 minutes. Tubes were then returned to ice for 5-10 minutes until cool, vortexed gently to mix contents, and absorbance at 625 nm was read with a Genysys spectrophotometer using a reagent blank. A glucose standard curve (10-190 µg/mL) was treated identically with anthrone reagent.

For total carbohydrate quantitation, the cell pellet aliquot was re-suspended in 1 mL reverse osmosis water and transferred to a clean glass test tube, and the anthrone procedure deailed above was followed. For quantitation of other cellular carbohydrates, the residual methanol from the extraction and washings were collected in an aluminum pan and evaporated, re-suspended in 1 mL reverse osmosis water, and the anthrone procedure detailed above was followed.

4.8.3. Lipid, After Bligh and Dyer, 1959

Frozen cell pellet (10 mg) was re-suspended to 0.6 mL using Milli-Q water in a 15-mL polypropylene centrifuge tube. Chloroform (0.75 mL) and methanol (1.5 mL) were sequentially added, adhering to the 1:2:0.8 chloroform:methanol:water volume ratio recommended by Bligh and Dyer. The mixture was vortexed 15 minutes at speed setting 3 using a VWR vortex mixer. Chloroform (0.75 mL) and Milli-Q water (0.75 mL) were sequentially added, vortexing 10-15 seconds at speed setting 7 after each addition. Upon centrifugation (4000 rpm, 15 minutes, 20°C), the lower chloroform phase, containing lipids, chlorophyll, and pigments, was transferred via micropipette to an aluminum pan

that had been pre-dried at room temperature and pre-weighed. The liquid was evaporated in a fume hood and weighed at three different time intervals following evaporation. Weights were measured with a Mettler Toledo MT5 microbalance with accuracy to 0.001 mg and recorded as an average of three measurements. It was noted that chloroform may leach compounds from polypropylene materials; thus a blank reaction using 0.6 mL Milli-Q water was used and its weight was subtracted from the biological sample weight.

### 4.8.4. Protein and Amino Acid Distribution, After Henderson et al., 2000

Amount approximately equivalent to 3 mg of frozen cell pellet was transferred to borosilicate HPLC vials with PTFE/silicone caps. 50 µL 6 M HCl per mg biomass was added to each vial. The vials were tightly capped and hydrolyzed at 105°C for 24 hours using a block heater. After 24 hours, the samples were then neutralized with 6 M NaOH to pH 7.0 and filtered with 0.22 µm PES spin filter in microfuge for 5 minutes at 10,000 rpm. Samples were then placed at -80°C to freeze before lyophilizing for 24 hours (specifications of lyophilizer). After lyophilization samples were placed at -80°C until HPLC analysis. HPLC analysis was performed according to the following protocol validated and published by Agilent Technologies (Henderson, Ricker et al. 2000) using an Agilent 1100 HPLC equipped with fluorescence detector. Borate buffer was 0.4 N borate, pH 10.2 with NaOH; o-phthalaldehyde (OPA) reagent, fluorenylmethylchloroformate (FMOC) reagent, and amino acid standards were obtained from Agilent. OPA and FMOC reagents were replaced daily in amber vials. Upon opening a vial of reagent, analyses were performed within 10 days. Solvent A was 40

mM sodium phosphate buffer (using 1:1 ratio of $NaH_2PO_4$ and $Na_2HPO_4$), pH 7.8 with NaOH, 0.2 µm filtered. Solvent B was 45:45:10 acetonitrile:methanol:water (v/v/v), 0.2 µm filtered. The pump rate was 1 mL/min, 47 minutes per injection, with gradient settings as follows:

| Time (min) | % Solvent B |
|---|---|
| 0 | 0 |
| 3.8 | 0 |
| 36.2 | 57 |
| 37.2 | 100 |
| 44.6 | 100 |
| 46.4 | 0 |
| 47 | 0 |

The flow rate was halved and the timing was doubled from the procedure reported in the Agilent technical note to improve resolution and reduce wear on equipment. The column thermostat was set at 40°C, and the autosampler thermostat was set at 4°C. The fluorescence detector settings were as followed, to switch from OPA- to FMOC-derivatized amino acids:

| Time (min) | Ex/Em (nm) | PMT Gain |
|---|---|---|
| 0 | 340/450 | 10 |
| 30 | 266/305 | 9 |

The injection program was as follows:

| Step | Instruction |
|---|---|
| Step 1 | Draw 2.5 µL from vial 1 (borate buffer) |
| Step 2 | Draw 0.5 µL from sample |
| Step 3 | Mix 3 µL in air, max speed, 2x |
| Step 4 | Wait 0.5 min |
| Step 5 | Draw 0 µL from vial 2 (needle wash) |
| Step 6 | Draw 0.5 µL from vial 3 (OPA) |
| Step 7 | Mix 3.5 µL in air, max speed, 6x |
| Step 8 | Draw 0 µL from vial 2 (needle wash) |
| Step 9 | Draw 0.5 µL from vial 4 (FMOC) |
| Step 10 | Mix 4 µL in air, max speed, 6x |
| Step 11 | Draw 32 µL from vial 5 (water) |
| Step 12 | Mix 18 µL in air, max speed, 2x |
| Step 13 | Inject |
| Auxiliary settings | Drawspeed = 200 µL/min |
| | Ejectspeed = 600 µL/min |
| | Draw position = 0.0 mm |

The integration parameters for collecting the data were set according to the following parameters.

| Parameter | Value |
|---|---|
| Slope Sensitivity | 1 |
| Peak Width | 0.04 |
| Area Reject | 1 |
| Height Reject | 0.4 |
| Shoulders | OFF |

4.8.5. RNA, After Benthin et al., 1991

Samples were thawed and washed three times with 3 mL 0.7 M $HClO_4$ for degradation of cell walls, vortexing to re-suspend in between washing and centrifuging at 4000 rpm for 10 min at 4°C. The pellet was then re-suspended in 3 mL 0.3 M KOH to lyse the cells and was incubated in a 37°C water bath for 1 hour, shaking at 15-minute intervals. After 1 hour, samples were cooled and 1 mL 3 M $HClO_4$ was added for neutralization. The solution was centrifuged at the same specifications as before, and the

supernatant was poured off into a new centrifuge tube. The pellet was washed twice with 4 mL 0.5 M $HClO_4$, centrifuged, and supernatant added to the new tube. 0.5 M $HClO_4$ extracts the RNA, while DNA, which is stable even in strong alkali, and protein, which does not solubilize in the alkali, remain in the precipitate. The collection of extracts was made up to a volume of 15 mL by adding 3 mL 0.5 M $HClO_4$ and was centrifuged once more to remove any non-visible precipitates of $KClO_4$. Upon final centrifugation, absorbance was measured at 260 nm against a 0.5 M $HClO_4$ blank for each wavelength using disposable UV cuvettes rated to 220 nm. Linearity of the spectrophotometer was confirmed within that range by successively diluting the sample twice with 0.5 M $HClO_4$ and confirming a linear fit to the three measured absorbances at 260 nm. Calculation of RNA quantity was performed by assuming 1 unit of absorbance at 260 nm corresponds to 38 µg/mL RNA on average (Carnicer, Baumann et al. 2009).

## 4.9. Appendix B. Supplemental Figures

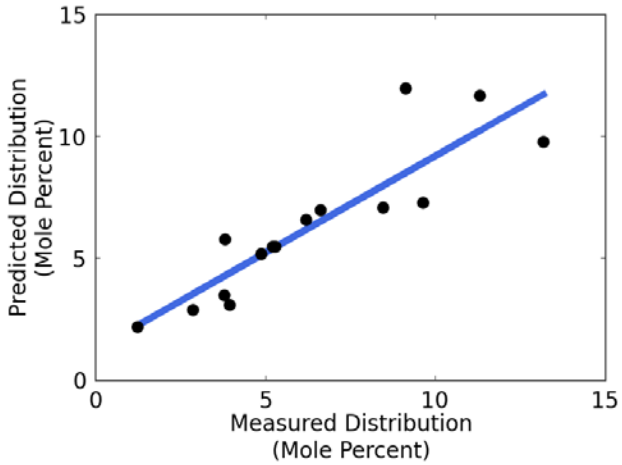


Figure 4.S1. BP-1 amino acid distribution. Correlation between the predicted amino acid distribution (based on protein-coding gene sequences) and the experimentally measured distribution. Cysteine, methionine, and tryptophan are excluded from the correlation due

to degradation during hydrolysis of the biomass samples to extract the protein. The equation of the best-fit linear trendline is y = 0.79x + 1.29 with $R^2$ = 0.79.

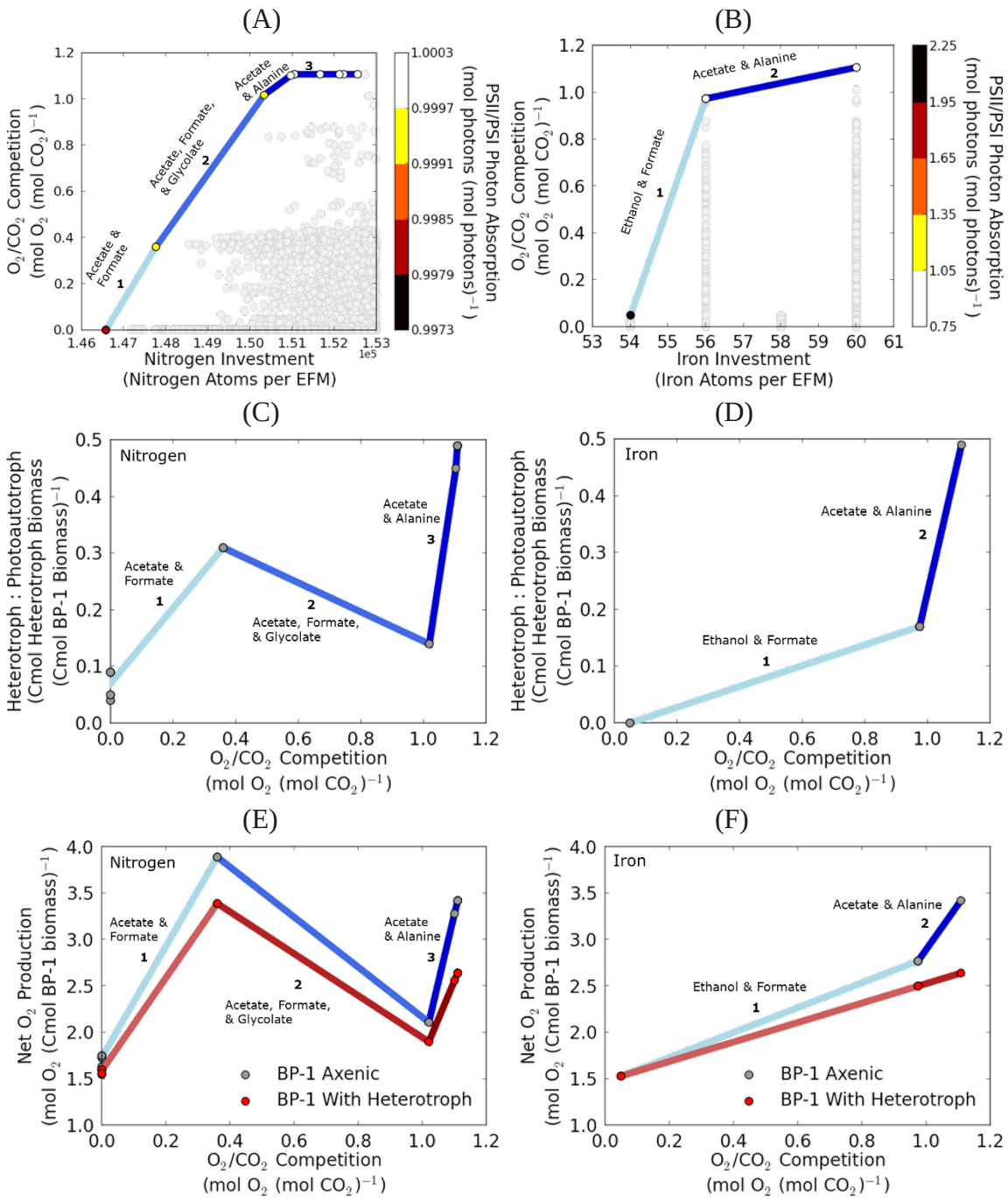


Figure 4.S2. Computational analysis of nutrient availability and $O_2/CO_2$ competition at RuBisCO in cyanobacterium BP-1. (A) Nitrogen availability. $O_2/CO_2$ competition (mol $O_2$ (mol $CO_2$)$^{-1}$ consumed at RuBisCO) as a function of nitrogen investment (nitrogen

atoms per EFM) for biomass-producing EFMs. The tradeoff curve defining competitive strategies between $O_2/CO_2$ competition and nitrogen limitation was divided into three distinct phenotypic regions based on byproduct secretion, labeled accordingly (intensity of shading increases with increasing stress levels). Points in the plot area are representative of 1,430,252 EFMs. (B) Iron availability. $O_2/CO_2$ competition (mol $O_2$ (mol $CO_2$)$^{-1}$ consumed at RuBisCO) as a function of iron investment (iron atoms per EFM, considering only photosynthetic and central metabolism reactions) for biomass-producing EFMs. The tradeoff curve defining competitive strategies between $O_2/CO_2$ competition and iron limitation was divided into two distinct phenotypic regions based on byproduct secretion, labeled accordingly (intensity of shading increases with increasing stress levels). Color scale represents the photon absorption at PSII relative to PSI for EFMs on the tradeoff curve (mol photons absorbed at PSII mol$^{-1}$ photons absorbed at PSI). Each point represents a unique EFM. Modeled biomass production did not include maintenance energy requirements. Points in the plot area are representative of 4,615,500 EFMs. (C-D) Heterotrophic biomass yield per BP-1 biomass (Cmol Cmol$^{-1}$) is presented as a function of $O_2/CO_2$ competition at RuBisCO (mol $O_2$ (mol $CO_2$)$^{-1}$ consumed) for the EFMs forming the optimal tradeoffs with nitrogen and iron availability, respectively. (E-F) Presence of a heterotroph lowers net $O_2$ production per Cmol BP-1 biomass as a function of $O_2/CO_2$ competition (mol $O_2$ (mol $CO_2$)$^{-1}$ consumed) for the EFMs forming the optimal tradeoffs with nitrogen and iron availability, respectively, which reduces $O_2$ inhibition. The distinct phenotypic regions defined by the tradeoff between $O_2/CO_2$ competition and nutrient availability stress are labeled according to byproduct secretion patterns as in panels a-b.

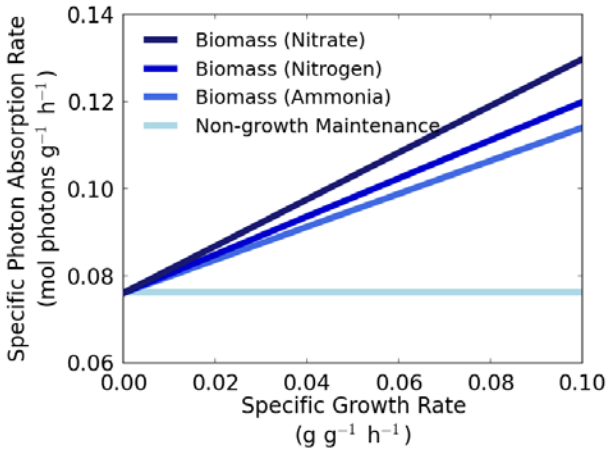


Figure 4.S3. Analysis of influence of nitrogen source on photon requirement. Comparison of the impact of various nitrogen sources on the theoretical specific photon absorption rate necessary for biomass production. Photon absorption rates (mol photons absorbed g$^{-1}$ CDW h$^{-1}$) were calculated using the BP-1 experimentally measured biomass composition. Ammonia is a completely reduced form of nitrogen, whereas and molecular nitrogen and nitrate are less reduced forms and require successively more energy for reduction to be assimilated into biomass, causing an increase in the specific photon absorption rate.

Nitrate serves as the most effective sink for excess electrons from the photosynthetic electron transport chain.

## 4.10. Appendix C. Supplemental Tables

Table 4.S1. Experimentally measured amino acid distribution from OPA/FMOC derivatization and HPLC fluorescence detection. Amino acids are abbreviated according to IUPAC 1-letter convention; average mole percent of two separately hydrolyzed samples and percent relative standard deviation are reported.

| Amino Acid | Mole % | % RSD |
|---|---|---|
| Q/E | 13.1 | 0.16 |
| N/D | 10.1 | 0.07 |
| L | 9.4 | 0.08 |
| A | 9.2 | 0.24 |
| R | 8.5 | 0.96 |
| V | 6.1 | 0.97 |
| I | 5.4 | 0.29 |
| G | 5.0 | 0.02 |
| F | 4.9 | 0.15 |
| T | 4.9 | 0.07 |
| K | 4.5 | 1.96 |
| Y | 4.1 | 0.01 |
| S | 4.0 | 0.08 |
| P | 3.4 | 1.21 |
| H | 1.5 | 0.14 |

Table 4.S2. Upregulated BP-1 genes under high versus low irradiance conditions (2000 versus 200 μmol photons $m^{-2}$ $s^{-1}$) (Bernstein, McClure et al. 2017) involved in photosystem II (PSII), carbon-concentrating mechanism (CCM), Calvin cycle carbon fixation, glycolysis, TCA cycle, oxidative phosphorylation (OP), and nitrate and sulfate uptake and assimilation. For each pathway, upregulated genes are listed in the left column with corresponding fold change in the right column.

| **PSII** | | **CCM** | | **Calvin** | | **Glycolysis** | |
|---|---|---|---|---|---|---|---|
| *psbA3* | 42.0 | *ccmK1* | 2.5 | *gap2* | 5.3 | *eno* | 4.6 |
| *psbP* | 4.3 | *ccmK2* | 2.1 | *gapA* | 4.5 | *gap2* | 5.3 |
| *psbX* | 3.3 | *ccmK3* | 2.6 | *glpX* | 6.6 | *gapA* | 4.5 |
| *psbQ* | 2.7 | *ccmM* | 2.5 | *pgk* | 2.1 | *gmpA* | 6.4 |
| *psb29* | 2.6 | *tlr0311* | 2.4 | *prkB* | 13.4 | *gpmI* | 5.4 |
| *psb32* | 4.1 | | | *rpiA* | 16.2 | *pfkA* | 2.3 |
| | | | | *tpiA* | 5.2 | *pgk* | 2.1 |
| | | | | | | *pyk* | 3.5 |
| | | | | | | *tpiA* | 5.2 |

| **TCA** | | **OP** | | **Nitrate** | | **Sulfate** | |
|---|---|---|---|---|---|---|---|
| *acnB* | 2.2 | *atpC* | 2.2 | *narM* | 2.3 | *cysA* | 2.5 |
| *fumC* | 3.2 | *atpD* | 5.2 | *nirA* | 3.4 | *cysC1* | 3.9 |
| *gltA* | 4.7 | *atpE* | 2.2 | *ntcB* | 4.9 | *cysH* | 4.6 |
| *idh3* | 6.3 | *atpF* | 2.9 | *nrtA* | 2.2 | *cysQ* | 3.1 |
| *sdhC* | 2.0 | *atpG* | 3.2 | *nrtD* | 2.5 | *met3* | 8.5 |
| | | *atpH* | 2.8 | *tll1357* | 3.1 | | |
| | | *cydB* | 3.6 | | | | |
| | | *ndh* | 2.0 | | | | |
| | | *ndhA* | 6.3 | | | | |
| | | *ndhB* | 4.4 | | | | |
| | | *ndhC* | 6.1 | | | | |
| | | *ndhD3* | 13.2 | | | | |
| | | *ndhE* | 4.7 | | | | |
| | | *ndhF3* | 2.4 | | | | |
| | | *ndhG* | 3.0 | | | | |
| | | *ndhH* | 2.2 | | | | |
| | | *ndhI* | 4.9 | | | | |
| | | *ndhJ* | 6.6 | | | | |
| | | *ndhK* | 3.1 | | | | |
| | | *ndhL* | 4.9 | | | | |
| | | *ndhM* | 13.1 | | | | |
| | | *ndhN* | 9.8 | | | | |
| | | *ppa* | 3.6 | | | | |
| | | *sdhC* | 2.0 | | | | |

Table 4.S3. Genes involved in amino acid synthesis pathways found to be upregulated under high irradiance conditions (2000 versus 200 µmol photons $m^{-2}$ $s^{-1}$) (Bernstein, McClure et al. 2017). Amino acids are abbreviated according to IUPAC 1-letter convention and number of nitrogen atoms follows in parentheses. For each amino acid, upregulated genes are listed in the left column with corresponding fold change in the right column.

| R (4) | | N/D (2/1) | | C (1) | | Q (2) | | H (3) | | I/L/V (1/1/1) | | K (2) | |
|---|---|---|---|---|---|---|---|---|---|---|---|---|---|
| *argB* | 3.0 | *asnB* | 2.5 | *cysE* | 4.0 | *glnA* | 3.6 | *hisA* | 3.4 | *avtA* | 2.8 | *dapA* | 2.9 |
| *argC* | 4.8 | *ansA2* | 3.0 | | | | | *hisB* | 3.9 | *cimA* | 2.5 | *dapB* | 4.5 |
| *argD* | 2.5 | *aspB* | 2.7 | | | | | *hisIE* | 6.7 | *ilvE* | 5.6 | *dapF* | 4.1 |
| *argG* | 14.0 | | | | | | | *hisG* | 2.3 | *leuB* | 6.0 | *dapL1* | 4.0 |
| *argH* | 4.4 | | | | | | | *hisF* | 2.0 | *leuC* | 2.9 | *lysA* | 3.3 |
| *argJ* | 4.0 | | | | | | | | | | | *lysC* | 2.1 |

| M (1) | | F/W/Y (1/2/1) | | P (1) | | S (1) | | T (1) | | Transporters | |
|---|---|---|---|---|---|---|---|---|---|---|---|
| *metE* | 12.9 | *aroA* | 9.2 | *proB* | 6.7 | *glyA* | 4.5 | *thrA* | 2.6 | *tlr1046* | 2.2 |
| | | *aroB* | 4.3 | | | *serA* | 7.8 | *thrB1* | 3.7 | *tlr1067* | 3.4 |
| | | *aroC* | 4.3 | | | | | *thrCII* | 6.3 | *tll1105* | 2.4 |
| | | *aroE* | 2.4 | | | | | | | *tlr1120* | 16.5 |
| | | *trpA* | 2.6 | | | | | | | *tlr1121* | 3.6 |
| | | *trpB* | 2.5 | | | | | | | *tlr1151* | 2.3 |
| | | *trpC* | 2.2 | | | | | | | *tll1318* | 2.7 |
| | | *trpE* | 4.1 | | | | | | | *tlr1592* | 2.1 |
| | | *trpF* | 2.3 | | | | | | | | |
| | | *tyrAa* | 2.4 | | | | | | | | |

Table 4.S4. Byproduct yields with respect to BP-1 biomass for pathways that secreted byproducts along the tradeoff curve for irradiance-induced stress and $O_2/CO_2$ competition and the corresponding yield of heterotroph biomass. Heterotroph yield was obtained via substrate consumption costs estimated from the literature for the respective byproducts (Cmol per Cmol heterotroph biomass): 4.53 for formate (Goldberg, Rock et al. 1976), 2.66 for alanine (Hunt, Jennings et al. 2016), and 2.61 for acetate (Edwards, Ibarra et al. 2001). Photons absorbed per BP-1 are reported in mol $Cmol^{-1}$, $O_2/CO_2$ competition is reported in mol $mol^{-1}$, and yields are reported in Cmol $Cmol^{-1}$.

| **Photons absorbed per BP-1 biomass** | **$O_2/CO_2$ competition** | **Formate per BP-1 biomass** | **Alanine per BP-1 biomass** | **Acetate per BP-1 biomass** | **Heterotroph biomass per BP-1 biomass** |
|---|---|---|---|---|---|
| 33.26 | 0.86 | 0.13 | NA | NA | 0.03 |
| 51.36 | 1.01 | NA | 0.30 | NA | 0.11 |
| 52.44 | 1.02 | NA | 0.31 | 0.01 | 0.12 |
| 100.05 | 1.10 | NA | 0.84 | 0.36 | 0.45 |
| 105.55 | 1.11 | NA | 0.90 | 0.40 | 0.49 |

## 4.11. Appendix D. Nitrogen and Iron Limitation

Nitrogen is a major component of protein but is often scarce in the environment (Elser, Bracken et al. 2007). Ecologically competitive acclimation to increased $O_2/CO_2$ competition as a function of pathway nitrogen requirement is shown in Figure 4.S2A in Appendix B; the tradeoff surface defines three phenotypic regions according to byproduct secretion. The EFM at the lower left corner of the plot represents nitrogen-limited cyanobacterial growth under low $O_2/CO_2$ competition; byproduct secretion is predicted even at the lowest nitrogen stress. With increasing $O_2/CO_2$ competition and nitrogen investment, BP-1 is predicted to secrete a number of reduced carbon compounds along the tradeoff surface, including acetate, formate, glycolate, and under the highest stress, the amino acid alanine. Production of byproducts is predicted to achieve the most efficient nitrogen utilization while simultaneously minimizing $O_2/CO_2$ competition.

EFMs on the nitrogen tradeoff surface exclusively use the C2 photorespiration cycle whereas the glycerate pathway is not used (Figure 4.S2A in Appendix B), similar to the result for irradiance-induced stress in Figure 4.3A. Also similar to the result for irradiance-induced stress, relative PSII/PSI photon absorption increases along the tradeoff surface, with greater relative photon absorption at PSII at higher $O_2/CO_2$ competition and higher nitrogen investment (Figure 4.S2A in Appendix B).

Biologically available iron is often limiting in microbial habitats due to low solubility, which is exacerbated at elevated pH (Johnson, Kanao et al. 2012). Figure 4.S2B in Appendix B predicts acclimation to increased $O_2/CO_2$ competition as a function of pathway iron investment. Two phenotypic regions of byproduct secretion were defined by the tradeoff surface, including combinations of ethanol, formate, and acetate, and finally alanine under the highest stress. Under low iron, relative PSII/PSI photon absorption decreases along the tradeoff surface as $O_2/CO_2$ competition and iron investment increase, showing a reversed trend compared with irradiance-induced stress and nitrogen investment. Analogous to the result for irradiance-induced stress in Figure 4.3A, the C2 cycle is the predominant photorespiration strategy as $O_2/CO_2$ competition increases. At low $O_2/CO_2$ competition, the relative PSII/PSI photon absorption is nearly twice that at high $O_2/CO_2$ competition (the scale shows much greater variability than the scale for light stress or nitrogen investment in Figures 4.3A and 4.S3A) and again indicates higher gross $O_2$ and ATP production. Additionally, as compared to the tradeoff surface in Figure 4.3A, the responses to nitrogen and iron limitation are less robust; fewer suboptimal pathways exist in close proximity to the tradeoff surface.

## 4.12. Appendix E. Biomass Yield Comparison

The physiological light response experiments allowed for comparison of photon costs for synthesizing BP-1 biomass with results reported in previously published studies for *Cyanothece* sp. ATCC 51142 and the green alga *Chlamydomonas reinhardtii* (Kliphuis, Klok et al. 2012, Vu, Stolyar et al. 2012). This comparison is of interest because experimental photon requirement values are relatively uncommon. The photon cost per biomass for BP-1 was about three times higher than the costs for these two organisms. This result may be due to the thermophilic nature of the organism and/or higher maintenance costs incurred by alkaline habitats. The nonlinear increase observed in the overall experimental photon absorption rate as growth rate increases (Figure 4.5) may correspond to increased cellular stress with higher maintenance energy requirements or greater thermal dissipation at higher irradiances. For example, higher irradiance may necessitate increased repair of photosystem proteins or a greater proportion of light may be lost to inefficiency (Falkowski and Raven 2007). These experiments and simulations demonstrate the wide range of irradiances under which BP-1 is capable of growing, stimulating interest in the metabolic strategies microbes such as this thermophilic cyanobacterium use to manage the daily fluctuations in irradiance and the accompanying stresses.

# CHAPTER FIVE

## *ESCHERICHIA COLI* CO-METABOLIZES GLUCOSE AND LACTATE FOR ENHANCED GROWTH

### Contribution of Authors and Co-Authors

Manuscript in Chapter Five

Author: Ashley E. Beck

Contributions: Conceived and designed the experiments, performed the experiments, analyzed the data, wrote the manuscript

Co-Author: Kathryn Pintar

Contributions: Performed the experiments

Co-Author: Diana Schepens

Contributions: Performed the experiments

Co-Author: Ashley Schrammeck

Contributions: Performed the experiments

Co-Author: Tim Johnson

Contributions: Analyzed the data

Co-Author: Alissa Bleem

Contributions: Performed the experiments

Co-Author: Hans C. Bernstein

Contributions: Conceived and designed the experiments

Co-Author: Tomas Gedeon

Contributions: Conceived and designed the experiments

Co-Author: Jeffrey J. Heys

Contributions: Conceived and designed the experiments

Co-Author: Ross P. Carlson

Contributions: Conceived and designed the experiments

Manuscript Information Page

Ashley E. Beck, Kathryn Pintar, Diana Schepens, Ashley Schrammeck, Tim Johnson, Alissa Bleem, Hans C. Bernstein, Tomas Gedeon, Jeffrey J. Heys, and Ross P. Carlson

Status of Manuscript:
_X__ Prepared for submission to a peer-reviewed journal
____ Officially submitted to a peer-review journal
____ Accepted by a peer-reviewed journal
____ Published in a peer-reviewed journal

Prepared for submission to *Applied and Environmental Microbiology*

## 5.1. Abstract

Microbial physiology is governed by substrate availability, and preference for different carbon sources may provide microorganisms with advantages in certain environments. Organic acids play a major role in the metabolisms of many microorganisms, acting as substrates, inhibitors, or at times both. Though much is known about the physiology and metabolism of *Escherichia coli*, catabolite repression (or preferential sequential consumption of substrates) has been investigated mainly in the context of glucose with other hexose or pentose sugars. This study investigates the effect of lactic and acetic acids as both substrates and inhibitors in the presence of glucose. It was observed that lactic acid in the presence of glucose enhanced growth rate and biomass accumulation over glucose alone. Metabolite analyses revealed co-consumption of glucose and lactic acid with concurrent increase in acetic acid production. Conversion of lactate to acetate increases energy available to the cell, thereby promoting enhanced growth. Additionally, the inhibitory effects of lactic and acetic acids as both substrates and products were quantified, and kinetic inhibition expressions were developed to describe the effect on growth. A range of functions was tested to determine the best fitting model, including development of a dual substrate inhibition model to describe growth on glucose and lactic acid. Altogether, this work provides insight into a novel feature of *E. coli* metabolism and highlights the importance of energy production in driving metabolism, as well as presents detailed quantification of organic acid toxicity under minimal media conditions.

## 5.2. Introduction

Carbon source availability dictates microbial growth characteristics, and microorganisms typically demonstrate a preference for substrates that promote fast and efficient growth (Gorke and Stulke 2008). Additionally, environmental conditions often favor excretion of organic acid waste byproducts like acetic and lactic acids, either as a natural byproduct of substrate degradation (e.g. cellulolytic microorganisms) or during overflow metabolism (Carlson, Beck et al. 2018). High concentrations of organic acids are inhibitory to growth, yet many organic acids can also serve as carbon and energy sources. In conjunction with environmental factors, such as pH and osmotic pressure, these stresses act in concert to influence microbial growth, shape microbial community interactions, and alter byproduct production efficiency in industrial settings.

Understanding substrate metabolism and preference for different carbon sources is essential to understanding the physiology of microorganisms and predicting growth in different environments. *Escherichia coli* is one of the most well-studied bacteria and has become biotechnologically important in recent years due to its applications in recombinant protein production, vaccine development, and enzyme synthesis. Conventional knowledge of catabolite repression in *E. coli* states that glucose is the preferred, most efficient carbon source, and if glucose is present, genes for synthesis of enzymes to consume other carbon sources will be repressed (Bettenbrock, Fischer et al. 2006, Deutscher 2008, Gorke and Stulke 2008). Most of this work has been elucidated via study of growth with glucose and lactose or other sugars, e.g. (Inada, Kimata et al. 1996). Studies in other microbial species have demonstrated analogous features, though

glucose may not always be the preferred carbon source (Rojo 2010, Romero-Rodriguez, Rocha et al. 2017). Although organic acids can serve as potential carbon substrates, relatively little is known about the catabolism of organic acids along with glucose in the context of catabolite repression, and research regarding organic acids has predominantly focused on inhibitory effects (Warnecke and Gill 2005).

When glucose is in excess, carbon flux into *E. coli* may exceed the capacity of the TCA cycle and other aerobic metabolic pathways, even in cultures operating at the maximum specific oxygen uptake rate (Hollywood and Doelle 1976, Reiling, Laurila et al. 1985, Han, Lim et al. 1992, Farmer and Liao 1997). The secretion of acetate is proposed to regenerate $NAD^+$ consumed during glycolysis and to reprocess coenzyme A using the pyruvate oxidase (PoxB) and phosphotransacetylase/acetate kinase (Pta-AckA) enzymatic reactions (Doelle, Ewings et al. 1982, Dittrich, Bennett et al. 2005, Wolfe 2005); this process also generates ATP (Ingledew and Poole 1984, Han, Lim et al. 1992). This overflow metabolism has also been characterized by repression of acetyl-CoA synthetase (Acs) activity, as triggered by carbon catabolite repression (Valgepea, Adamberg et al. 2010). The rate at which acetate forms is directly related to the rate at which cells grow, and as much as 15% of glucose flux may be directed toward acetate formation (Holms 1996, Eiteman and Altman 2006). Production of acetate inhibits *E. coli* growth as product concentration increases: the protonated form of acetate, acetic acid, is lipophilic and therefore capable of passing through the cell membrane (Repaske and Adler 1981). Once inside the cell, acetic acid dissociates and releases $H^+$ ions, which increase intracellular pH and uncouple the proton motive force (Repaske and Adler

1981). Acetic acid has also been shown to cause toxicity by disrupting methionine biosynthesis (Roe, O'Byrne et al. 2002). *E. coli* has the ability to "switch" metabolic pathways to import and utilize acetate upon depletion of other extracellular carbon sources (i.e. glucose) (Nystrom and Neidhardt 1993, Wolfe 2005). Lactic acid can also increase intracellular pH, uncoupling the proton motive force, and has been shown to damage the outer membrane of gram-negative bacteria and permeabilize the cell (Alakomi, Skytta et al. 2000).

The current study expands upon fundamental principles of carbon catabolite repression and organic acid inhibition with the objectives to (i) investigate lactic and acetic acid metabolism in *E. coli* and understand catabolite repression when glucose is present, (ii) quantify the inhibitory effects of lactic and acetic acids, and (iii) develop model inhibition terms to describe growth when lactic or acetic acids serve as product or substrate. Catabolite repression has historically been studied in terms of glucose and other hexose sugars as carbon sources (e.g. lactose). However, to the authors' knowledge, no studies have investigated the impact of organic acids on growth with glucose in *E. coli* or quantified the inhibitory effects of organic acids using a minimal medium. Herein, experimental data is presented that supports co-metabolism of glucose and lactate. Metabolic pathways for the utilization of these two carbon sources suggest that available energy is increased via co-metabolism. Parameterized models describing inhibition of lactic and acetic acids are also proposed with accompanying experimental data, which provide fundamental quantification of the two organic acids as both a substrate and

inhibitory byproduct, as well as enable predictive capacity for growth under multiple stresses.

## 5.3. Results

### 5.3.1. Growth on Glucose is Enhanced in the Presence of Lactate

*E. coli* showed increased growth rates when growing on glucose in the presence of low concentrations of lactate (9-45 mM lactate; 0.006-0.032 mM protonated lactic acid) as compared to growing on glucose alone, indicating that the presence of lactic acid enhances growth up to a threshold level before inhibition takes effect (Figure 5.1A). Addition of acetate did not produce an analogous result (Figure 5.1A). Growth was characterized in detail for 56 mM glucose + 27 mM lactate, a condition that showed one of the highest improvements in growth rate, to further investigate dual substrate catabolism. In addition to faster growth, *E. coli* also accumulated more biomass during batch growth on glucose + lactate than on glucose alone (Figure 5.1B). Moreover, the increase in biomass accumulation demonstrated an additive effect: biomass concentration with growth on glucose + lactate was equivalent to the sum of biomass concentrations with growth on glucose alone and lactate alone, respectively (average 2.3 g/L biomass). Correspondingly, the culture pH remained higher during batch growth on glucose + lactate than on glucose alone (Supplemental Figure 5.S1), indicating net consumption of protons from the extracellular medium via uptake of lactate. Growth on glucose in the presence of acetate was also investigated; however, no improvement in growth rate or biomass accumulation was observed (Figure 5.1B).

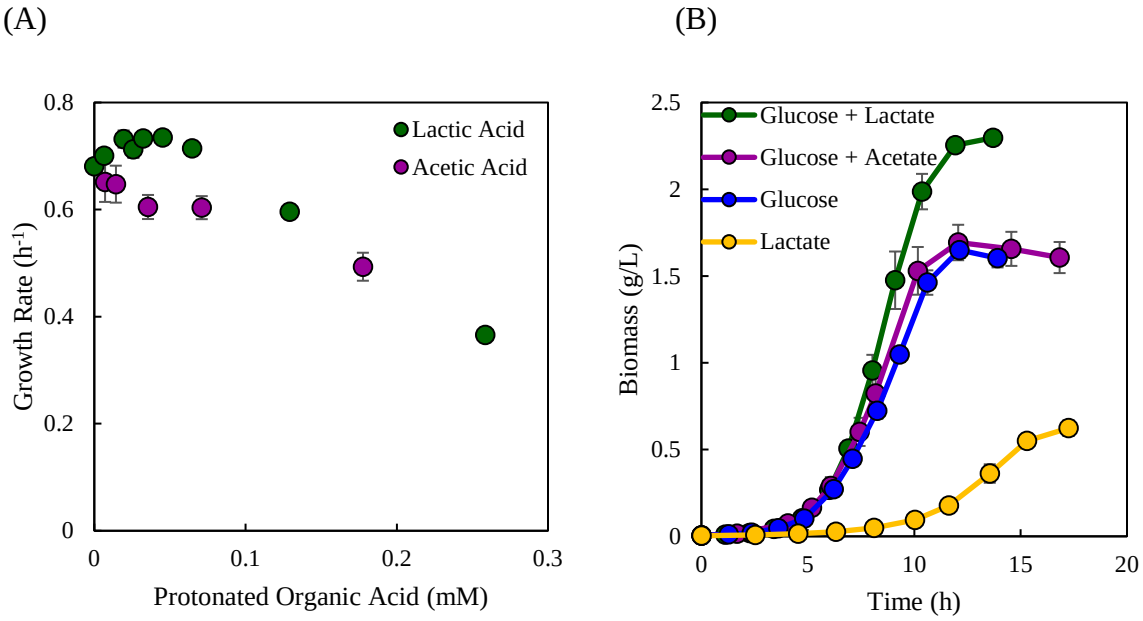


Figure 5.1. Growth rate and biomass accumulation of *E. coli* on glucose media is enhanced in the presence of lactate. (A) Growth rate of *E. coli* on 56 mM glucose as a function of protonated lactic (green) or acetic (purple) acid concentration. Growth rate increases initially with the addition of lower concentrations of lactic acid; in contrast, growth rate only decreases in response to acetic acid. (B) Comparison of batch growth of *E. coli* on different carbon sources: 56 mM glucose + 27 mM lactate (0.019 mM protonated lactic acid; green), 56 mM glucose + 1 mM acetate (0.007 mM protonated acetic acid; purple), 56 mM glucose (blue), and 27 mM lactate (yellow). Lines represent interpolation between data points. Each point represents the average of biological triplicates with error bars indicating standard deviation.

### 5.3.2. Lactate is Co-metabolized with Glucose

Glucose and lactate concentrations decreased simultaneously during batch growth on glucose + lactate, indicating co-consumption (Figure 5.2A). Equivalent amounts of glucose were consumed regardless of the presence of lactate in the medium (33.0 mM glucose consumed during growth on glucose alone compared to 33.9 mM glucose consumed during growth on glucose + lactate, $p = 0.28 > 0.05$). The time-dependent glucose consumption profiles between the two conditions were virtually identical (Figure 5.2B). The amounts of lactate consumed during batch growth on lactate alone and on

glucose + lactate were also similar but were slightly higher when lactate was the sole substrate (27.0 mM compared to 25.1 mM, $p = 0.01 < 0.05$), supporting additive consumption of the amounts of the two carbon substrates. Although nearly the same amount of lactate was consumed, lactate was depleted sooner when glucose was present, i.e. the time frame of consumption shifted earlier (Figure 5.2C).

Specific rates of substrate consumption varied, however; specific uptake rate of glucose was slightly faster when glucose was the sole substrate than when lactate was also present (9.1 compared to 7.2 mmol glucose / g biomass / h, $p = 0.05$), whereas specific uptake rate of lactate was much faster when lactate was the sole substrate than when glucose was also present (17.5 compared to 4.7 mmol lactate / g biomass / h, $p << 0.05$).

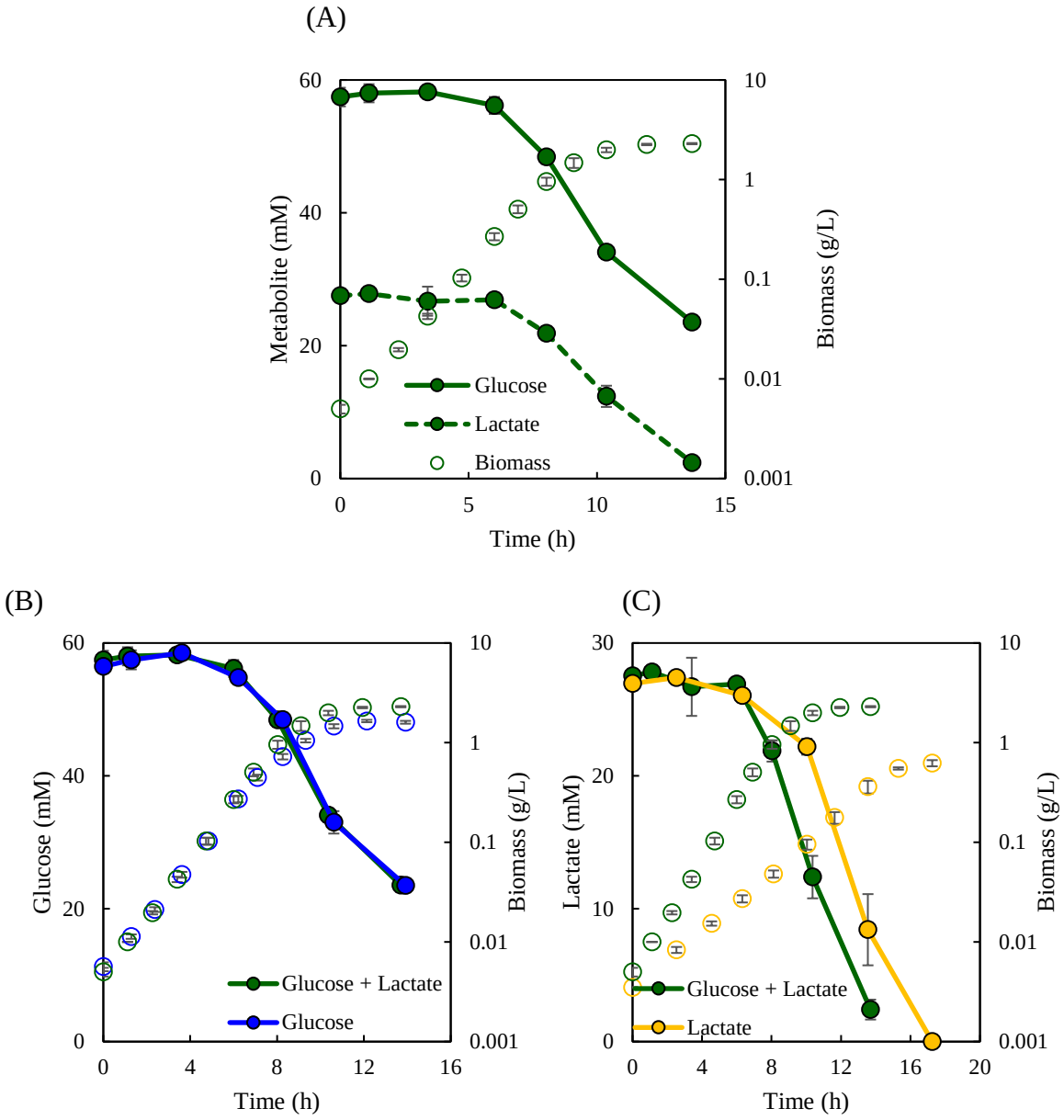


Figure 5.2. *E. coli* co-metabolizes glucose and lactate. (A) Simultaneous decrease (co-consumption) of glucose and lactate during batch growth on 56 mM glucose + 27 mM lactate. (B) Equivalent glucose consumption during batch growth on 56 mM glucose + 27 mM lactate (green) and 56 mM glucose alone (blue). (C) Similar patterns of lactate consumption during batch growth on 56 mM glucose + 27 mM lactate (green) and 27 mM lactate alone (yellow). Lactate was depleted sooner when glucose was present. Lines represent interpolation between data points. Open circles show growth over time for the respective conditions. Each point represents the average of biological triplicates with error bars indicating standard deviation.

### 5.3.3. Co-metabolism of Lactate Results in Additional Energy Available for Growth

Acetate accumulated to a higher concentration in exponential phase during growth on glucose + lactate than on glucose alone (Figure 5.3), though the final concentration was virtually equivalent between the two conditions. Correspondingly, the specific acetate production rate was also higher for growth on glucose + lactate than on glucose alone (4.0 compared to 2.6 mmol acetate / g biomass / h, $p << 0.05$). Furthermore, during growth on lactate alone, acetate accumulated as a byproduct (Figure 5.3) with a specific production rate of 7.8 mmol acetate / g biomass / h, supporting use of the Pta-AckA reactions even when lactate was the sole carbon source.

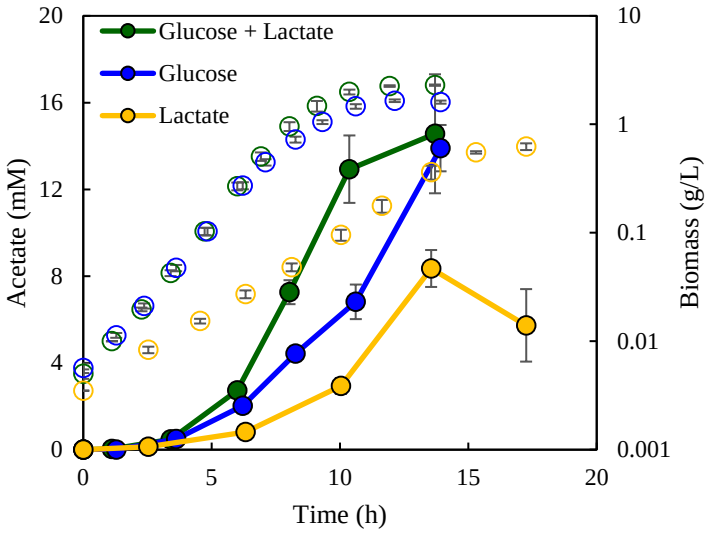


Figure 5.3. *E. coli* converts lactate to acetate. Acetate accumulation during batch growth on 56 mM glucose + 27 mM lactate (green), 56 mM glucose alone (blue), and 27 mM lactate alone (yellow). Acetate accumulated to a higher concentration in exponential phase when lactate was available than on glucose alone. Acetate was also produced when lactate was the sole carbon source. Lines represent interpolation between data points. Open circles show growth over time for the respective conditions. Each point represents the average of biological triplicates with error bars indicating standard deviation.

Increased acetate production when lactate was present with glucose indicated that lactate was being used to provide additional energy for the cell. Lactate, once processed to pyruvate via lactate dehydrogenase (Dld or LldD), can be converted to acetate via the pyruvate dehydrogenase complex and Pta-AckA-catalyzed reactions, which generate one ATP per acetate produced (Figure 5.4). Using the metabolite and biomass measurements, specific glucose and lactate consumption and acetate production rates were calculated during exponential growth and were correlated to fluxes through glycolysis (glucose consumption), LldD (lactate consumption) and Pta-AckA (acetate production) pathways (Table 5.1). These three fluxes were also used to estimate the flux through the TCA cycle by converting to pyruvate equivalents and subtracting production from consumption. Finally, using the measured inputs and outputs, an electron balance was calculated and used to estimate flux through $O_2$ as the terminal electron acceptor.

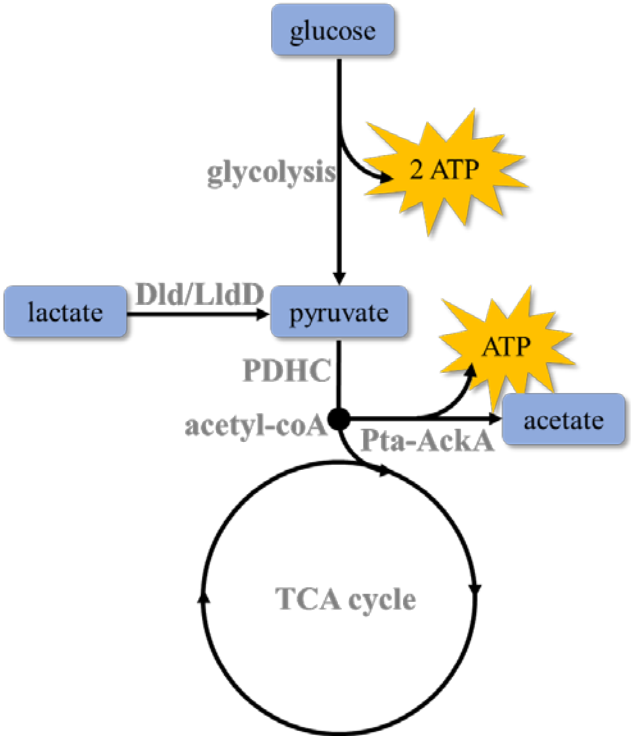


Figure 5.4. Simplified pathway schematic for glucose and lactate utilization. One molecule of glucose is processed through glycolysis to produce two pyruvate molecules, yielding two molecules of ATP, while one molecule of lactate is converted to one pyruvate molecule via lactate dehydrogenase (Dld or LldD). Pyruvate can then be processed to acetyl-CoA by the pyruvate dehydrogenase complex (PDHC) and enter the TCA cycle or be converted to acetate through the Pta-AckA enzymes, which results in one additional ATP molecule.

Table 5.1. Major pathway fluxes under different carbon substrates. Glycolysis flux was estimated via specific glucose consumption rate, LldD flux was estimated via specific lactate consumption rate, and Pta-AckA was estimated via specific acetate production rate. TCA cycle flux was estimated by subtracting the Pta-AckA flux from the pyruvate equivalents obtained via glycolysis and LldD flux and assuming that the remainder entered the TCA cycle, and $O_2$ flux was estimated by calculating the electron balance and assuming electrons unaccounted for in biomass or organic byproducts were consumed by $O_2$ as the terminal electron acceptor. Rates were calculated over the entire exponential growth phase. Values represent the average over three biological replicates with standard deviation.

| **Pathway** | **Carbon Source Condition** | | | | | |
|---|---|---|---|---|---|---|
| | **Glucose** | **Glucose + Lactate** | **Glucose + Acetate** | **Glucose + Lactate + Acetate** | **Lactate** | **Lactate + Acetate** |
| **Glycolysis** (mmol glucose / g biomass / h) | 9.1 ± 0.4 | 7.2 ± 0.4 | 9.4 ± 0.3 | 8.0 ± 0.2 | NA | NA |
| **LldD** (mmol lactate / g biomass / h) | NA | 4.7 ± 0.4 | NA | 3.6 ± 0.2 | 17.5 ± 0.8 | 17.2 ± 0.2 |
| **Pta-AckA** (mmol acetate / g biomass / h) | 2.6 ± 0.2 | 4.0 ± 0.3 | 3.0 ± 0.2 | 4.9 ± 0.7 | 7.8 ±1.5 | 7.2 ± 0.1 |
| **TCA cycle** (mmol acetyl-CoA / g biomass / h) | 15.6 ± 0.5 | 15.1 ± 0.7 | 15.8 ± 0.4 | 14.8 ± 0.8 | 9.7 ± 1.7 | 10.1 ± 0.2 |
| **$O_2$** (mmol $O_2$ / g biomass / h) | 25.6 ± 2.7 | 23.0 ± 2.7 | 25.3 ± 1.5 | 24.3 ± 0.2 | 22.4 ± 4.8 | 23.2 ± 0.7 |

### 5.3.4. Lactate is Preferred Over Acetate as a Carbon and Energy Source

When both lactate and acetate were available as carbon substrates (without glucose), lactate was consumed prior to acetate; in fact, consumption of acetate was not observed until stationary phase (Figure 5.5). Additionally, no difference in time-dependent biomass accumulation or pH profile was observed between growth on lactate + acetate and lactate alone, indicating that acetate was not being utilized as a carbon or

energy source during exponential growth (Supplemental Figure 5.S2). This observation supports lactate as a preferred substrate over acetate and as a more efficient carbon and energy source.

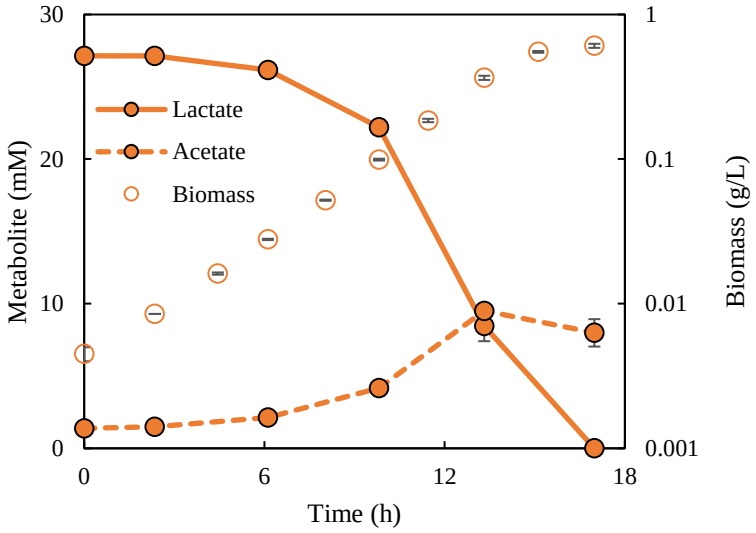


Figure 5.5. *E. coli* prefers lactate to acetate as a carbon and energy source. Lactate is consumed while acetate is net accumulated rather than consumed during batch growth with 27 mM sodium lactate + 1 mM sodium acetate, indicating that lactate is preferred over acetate as a carbon and energy source. Lines represent interpolation between data points. Open circles show growth over time. Each point represents the average of biological triplicates with error bars indicating standard deviation.

### 5.3.5. Lactate and Acetate Show Different Concentration-Dependent Inhibition Profiles

Lactate and acetate are two common organic acid byproducts resulting from overflow metabolism and are secreted under different nutrient stress conditions (Folsom and Carlson 2015). Given the observed difference in substrate preference, the inhibitory effects of both organic acids were investigated by examining the growth rate over a range of lactate or acetate concentrations, both as the sole substrate and with glucose as the main substrate. *E. coli* showed distinctly different growth responses to the concentration

of protonated lactic and acetic acids (Figure 5.6). Lactic acid exhibited a sharper inhibition curve whereas growth rate with acetic acid decreased more gradually as a function of concentration. However, the shape of the inhibition curves was similar regardless of whether the organic acid served as the sole substrate or as a product with glucose as the main substrate.

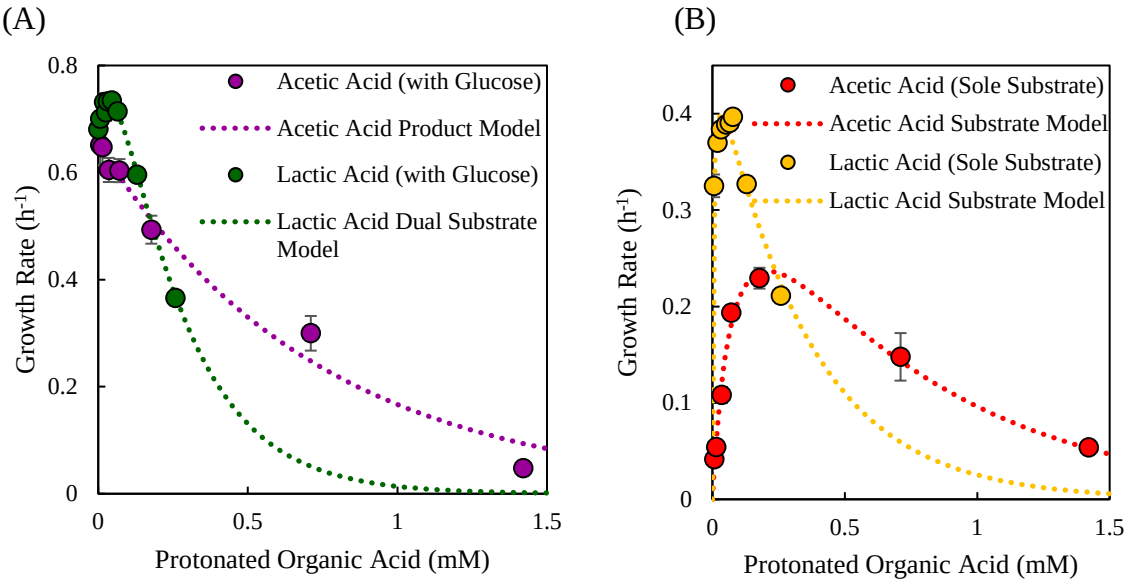


Figure 5.6. Inhibition by lactic and acetic acids with and without glucose as a substrate. (A) Growth of *E. coli* on 56 mM glucose with varying concentrations of lactic (green) or acetic (purple) acids. Dotted lines represent best-fit inhibition models:

(1) $\mu = \mu_{max}\left[\left(\frac{G}{K_g+G}\right)+\left(\frac{L}{K_l+L}\right)\right]e^{-\alpha L}$ for lactic acid, where $\mu$ is growth rate ($h^{-1}$), $G$ is concentration of glucose (= 56 mM), $L$ is concentration of protonated lactic acid (mM), and parameters $\mu_{max}$ = 0.767 $h^{-1}$, $K_g$ = 7.051 mM, $K_l$ = 0.115 mM, and $\alpha$ = 4.6 $mmol^{-1}$,

(2) $\mu = \mu_c\left(\frac{G}{K_G+G}\right)e^{-KA}$ for acetic acid, where $\mu$ is growth rate ($h^{-1}$), $G$ is concentration of glucose (= 56 mM), $A$ is concentration of protonated acetic acid (mM), and parameters $\mu_c$ = 0.974 $h^{-1}$, $K_G$ = 27.29 mM, and $K$ = 1.365 mM.

(B) Growth of *E. coli* on varying concentrations of lactic (yellow) or acetic (red) acids as the sole carbon substrate. Dotted lines represent best-fit inhibition models:

$\mu = \mu_c\left(\frac{OA}{K_G+OA}\right)e^{-\frac{OA}{K_I}}$ for both lactic and acetic acids, where $\mu$ is growth rate ($h^{-1}$) and $OA$ is concentration of protonated organic acid (mM). For lactic acid,

parameters $\mu_c$ = 0.485 $h^{-1}$, $K_G$ = 0.0034 mM, and $K_I$ = 0.339 mM, and for acetic acid, parameters $\mu_c$ = 0.470 $h^{-1}$, $K_G$ = 0.0948 mM, and $K_I$ = 0.669 mM. Experiments were performed at an initial pH of 7.0. When accounting for the different pKa's of lactic and acetic acids (3.86 and 4.76, respectively), the proportions of protonated and de-protonated forms were different for the same concentration of lactic and acetic acid (e.g. a smaller proportion of the total measured lactate is in the protonated form as compared to acetate due to its lower pKa). A data point with growth rate closer to zero was not performed for lactic acid due to the high concentration of sodium lactate required to achieve a higher concentration of the protonated form, which would substantially increase the osmotic pressure. Each point represents the average of at least three biological replicates with error bars indicating standard deviation.

A variety of kinetic expressions for modeling inhibitory compounds (Han and Levenspiel 1988) were tested against the experimental data for lactic and acetic acids to determine the best-fitting expression. The most appropriate fit was selected and is shown with the experimental data in Figure 5.6, while the results of all tested expressions can be found in Supplemental Tables 5.S1 and 5.S2. Existing models found in the literature (Han and Levenspiel 1988) fit well for acetic acid as a substrate and product and for lactic acid as a substrate but did not fit the data well for lactic acid as a product; both glucose and lactate were being utilized as substrates, and the model expressions were not designed to reflect this property. A dual substrate expression was incorporated with an inhibition term to model the data and resulted in an improved fit (Figure 5.6, Supplemental Tables 5.S1 and 5.S2).

Finally, pH and osmotic pressure were investigated as additional environmental parameters that impose stress on a system. Examining pH as a variable allowed to distinguish between pH as a factor independent from organic acid production, which also contributes to changes in pH. Growth rate decreased sharply at low pH whereas growth rate was minimally affected by increasing osmotic pressure (Supplemental Figure 5.S3).

Results from parameterizing inhibition expressions were combined into a predictive model for growth under multiple environmental pressures. The model was compared with a data set measured for *E. coli* growth with glucose and acetic acid under different pHs (pH 6.0 and 5.0) and was observed to match reasonably well (Supplemental Figure 5.S4).

## 5.4. Discussion

The current study provides insight into a novel feature of *E. coli* metabolism that has not yet been thoroughly detailed in the literature. *E. coli* was shown to co-consume lactate along with glucose in batch growth. This strategy is proposed to provide more cellular energy for faster growth and higher biomass accumulation. Inhibition from both lactic and acetic acids was quantified, and distinct concentration-dependent inhibition effects were shown for each. Inhibition terms were fitted to each data set to model the growth, and a novel modeling term was developed to describe growth on glucose and lactate by combining dual substrate limitation with inhibition expressions. The inhibition models developed for different variables can be combined to predict growth under multiple simultaneous stressors.

### 5.4.1. Co-metabolism and the Importance of Energy

Co-utilization of organic acids along with sugars like glucose is not well described in the literature. However, co-utilization of glucose and lactate has also been observed in *Staphylococcus aureus* and is thought to provide energy more efficiently than utilization of acetate (Ferreira, Manso et al. 2013); this metabolic strategy makes the organism competitive in its environment. This phenotype is analogous to the

experimental observations in *E. coli* in the current work. A previous study of *E. coli* growth on mixed substrate media (glucose, glycerol, galactose, lactate, and maltose) demonstrated catabolite repression effects at higher growth rates but not at lower growth rates in continuous culture, an observation that was hypothesized to be related to intracellular density (Zhou, Vazquez et al. 2013). However, the current work supports glucose and lactate co-consumption during batch growth when cells are growing at their maximum growth rate, a difference which could be due to the presence of additional substrates or the different culturing conditions. Maximization of ATP production rate has been postulated to be an important driver of microbial evolution (Pfeiffer and Bonhoeffer 2004). The conversion of lactate to acetate, both with and without glucose present, suggests the importance of the additional energy gained via the production of acetate to the overall metabolism (Figure 5.4, Table 5.1).

### 5.4.2. Organic Acid Toxicity

Previous studies have correlated organic acid inhibition effects (decrease in growth rate) to the concentration of protonated acid, for example, comparing the effects of lactic acid and 3-hydroxypropionic acid in *E. coli* str. W (Chun, Yunxiao et al. 2014). Several other common organic acids were also investigated, and acetate was reported to be more toxic than other organic acids, including lactic acid. However, in the current study, even when protonated free acid concentration was accounted for, lactic acid resulted in more intensive growth inhibition than acetic acid, with growth rate decreasing more quickly at lower acid concentrations.

The presented work expands the horizon of knowledge on the well-studied bacterium *E. coli* and highlights the complexity of metabolism and physiology within a single organism, notwithstanding the great diversity among phylogenetic lineages. Extending our understanding of this model organism will enable improved engineering of industrial processes and will translate conceptually to understanding other organisms. For example, bioprocess applications may consider adding an optimal amount of lactic acid as a supplement to increase biomass and desired product production. Further research into dual or multiple substrate metabolism will be useful to test additional scenarios of mixed substrates and the effect on growth rate and efficiency for different organisms. Additionally, most kinetic models have been developed using a single substrate approach; modeling approaches considering multiple substrates, simultaneous substrate and inhibitor, and improving inhibition expressions will enable better predictions of growth responses to either undesired or desired byproduct accumulation. As suggested by the benefit in energy *E. coli* obtained from co-utilizing lactate with glucose in the present study, energy production rate should be examined as an important component driving metabolism.

## 5.5. Materials and Methods

### 5.5.1. Bacterial Strains and Culturing Media

*Escherichia coli* str. K-12 substr. MG1655 was used for all culturing experiments. Cultures were grown in M9 media supplemented with 10 mL/L of trace metal stock solution (Ausubel, Brent et al. 1992, Bernstein, Paulson et al. 2012). Media was amended

with the desired carbon source(s): 10 g/L (56 mM) glucose and/or varying concentrations of sodium acetate or sodium lactate. Supplemental Table 5.S3 contains a comprehensive list of conditions tested to construct inhibition curves. Media components and stock solutions were autoclaved or filter sterilized. Media was filter sterilized after adjusting the initial pH to 7.0 (or desired pH, as in Supplemental Figures 5.S3-S4) with HCl.

5.5.2. Batch Culturing Conditions

Inocula were prepared from fresh overnight cultures grown in 7 mL M9 with appropriate carbon source(s) in disposable culture tubes. The same carbon source concentration(s) were used for the inocula as for the experimental condition except for organic acid substrate experiments. For experiments with lactate as the only substrate, inocula were grown with 3 g/L (27 mM) sodium lactate and then transferred to the experimental media. For experiments with acetate as the only substrate, inocula were grown with the same acetate concentration as used in the experiment but were spiked with 1 g/L LB to facilitate faster inoculum growth. Cells were collected by centrifugation (3700 rpm, 8 min, 25°C, Eppendorf 5810 R, 15 amp version) and re-suspended in an equal volume of fresh growth media. Sterile 250-mL baffled Erlenmeyer shake flasks filled with 50 mL M9 media containing appropriate carbon source(s) were inoculated with 1 mL of prepared inoculum to $OD_{600}$ ~0.010. Shake flasks were incubated at 37°C and agitated at 150 rpm. Triplicate shake flasks were run for each experimental condition. Samples were taken aseptically every 1-2 hours or approximately each doubling time and $OD_{600}$ was measured as a proxy for biomass. Growth rate was calculated by plotting $OD_{600}$ against time and fitting the exponential growth phase data with logistic regression

in Excel to obtain an equation of the form $y = ae^{bx}$. The growth rate was found by taking the natural logarithm of the coefficient $b$. The number of data points included in the regression was adjusted until the maximum growth rate was obtained, retaining at least four points in the calculation and excluding the first data point (measured at the time of inoculation). The growth rate was calculated for each individual replicate, and the triplicates were averaged for each experimental condition.

### 5.5.3. Metabolite Analysis

Glucose, lactate, and acetate concentrations were measured with high-performance liquid chromatography (HPLC) analysis. Samples were aliquoted aseptically, filtered (0.45 µm), and stored at -20°C until analysis. An Agilent 1200 HPLC with Bio-Rad HPX-87H column was used for analysis. Filtered (0.22 µm) 5 mM sulfuric acid served as the mobile phase with the column operating at 45°C. Glucose was detected with a refractive index detector with heater set at 40°C. Lactate and acetate were detected with a variable wavelength detector set at 210 nm. Standards and samples were prepared in 1:1 (v:v) ratio with 2X mobile phase containing 1 g/L fucose as an internal standard. RID signal was normalized to the internal standard, and concentrations were quantified using standard calibration curves.

### 5.5.4. Kinetic Expression Modeling

Models of microbial reaction kinetics are essential to the fundamental principles of microbial growth. Monod proposed that reaction rate is ultimately limited by a single substrate, and the kinetics may be expressed as

$$\mu = k\frac{XS}{S+C_M},$$

where $\mu$ is the specific growth rate of cells, $k$ is the reaction rate constant, $X$ is the cell concentration, $S$ is the substrate concentration, and $C_M$ is the Monod constant (Monod, 1949). For purposes of this study, an equation more similar to Michaelis-Menten kinetics was used:

$$\mu = \frac{\mu_{max}S}{S+k_m},$$

where $k_m$ is the half-saturation constant. An essential feature of microbial growth rate is that growth becomes saturated at high $S$, eventually reaching a point at which $\mu$ is equal to $\mu_{max}$. At low substrate concentrations, reaction rate has an approximate linear dependence on $S$. However, microbial growth kinetics is a complicated process, often involving multiple inhibition effects. Thus, a variety of methods have sought to account for inhibition terms. A compendium of possible kinetic expressions to describe the inhibition effect of organic acids were identified (Han and Levenspiel 1988) and examined against the lactate and acetate inhibition data both with and without glucose. Additionally, dual substrate models were explored to improve model fit for data with both glucose and lactate present in the media (Lendenmann and Egli 1998), given the observation of co-consumption of the two compounds. Equations and parameters were defined in Python and the data were fit using the curve_fit function. Goodness-of-fit was assessed both visually and with the chisquare function in SciPy.

## 5.6. Supplemental Figures and Tables

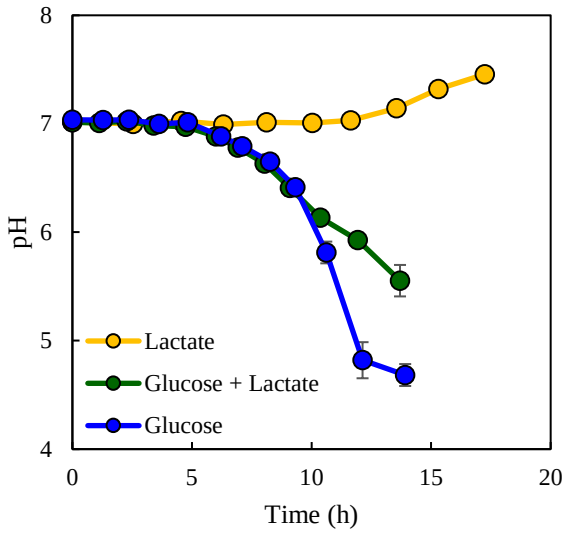


Supplemental Figure 5.S1. Culture pH differs when lactate is added to glucose as a substrate. Comparison of pH during batch growth with 27 mM lactate (yellow), 56 mM glucose + 27 mM lactate (green), and 56 mM glucose (blue). Growth on glucose alone resulted in lower pH than when lactate was added to the medium with glucose due to consumption of protons from the extracellular medium. Lines represent interpolation between data points. Each point represents the average of biological triplicates with error bars indicating standard deviation.

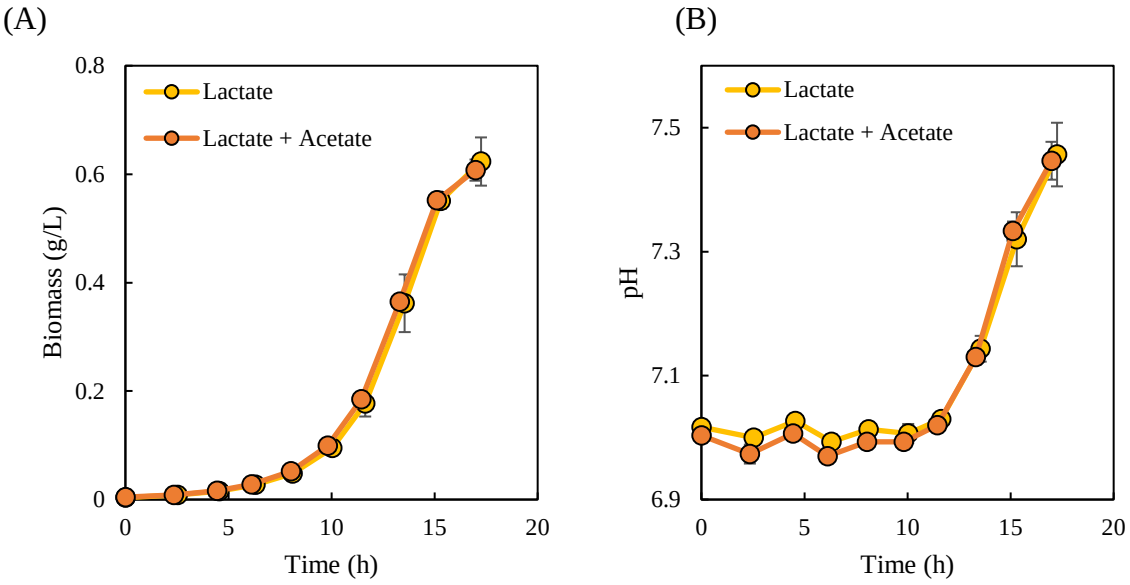


Supplemental Figure 5.S2. Acetate does not contribute to growth when lactate is present. Comparison of biomass production (A) and pH (B) during batch growth on 27 mM lactate (yellow) and 27 mM lactate + 1 mM acetate (orange). Virtually no difference was observed between the two growth conditions, suggesting that acetate does not contribute to growth when lactate is present as a carbon/energy source. Lines represent interpolation between data points. Each point represents the average of biological triplicates with error bars indicating standard deviation.

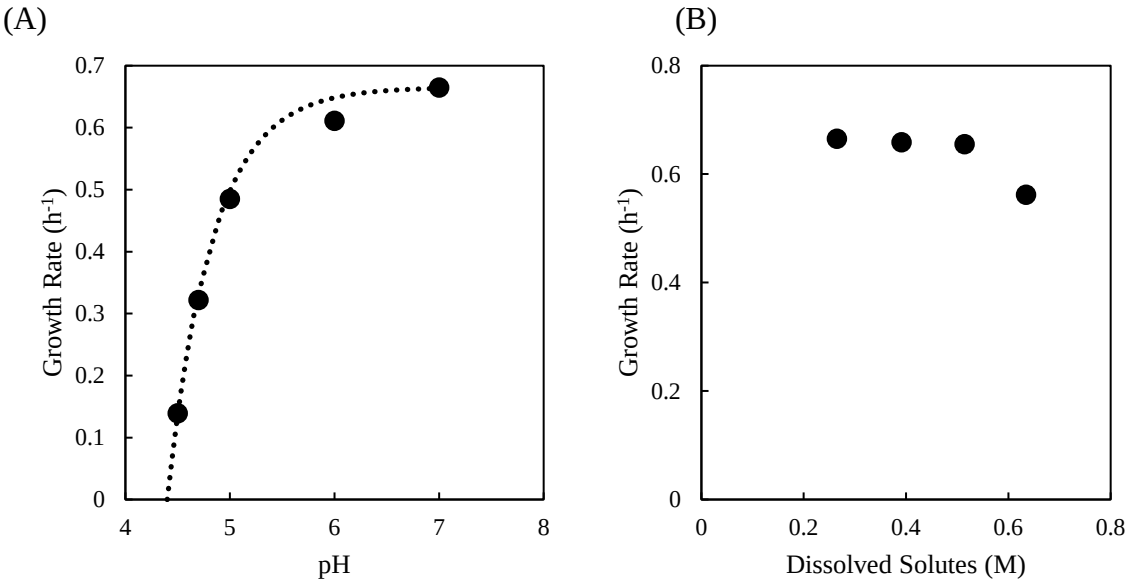


Supplemental Figure 5.S3. Inhibition by culture pH and osmotic pressure. (A) Growth rate decreases steeply at low pH. Dotted line represents best-fit model using the method

of Han and Levenspiel: $\mu = \mu_{max}\left(1 - \frac{H}{H^*}\right)$, where $\mu$ is growth rate ($h^{-1}$), $H$ is concentration of $H^+$ (M), and parameters $\mu_{max}$ = 0.665 $h^{-1}$ and $H^*$ = $10^{-4.4}$ M (the critical threshold for $H^+$ concentration above which growth is not possible). (B) Growth rate is minimally affected by increasing osmotic pressure. Growth was tested at 1X, 1.5X, 2X, and 2.5X the concentration of M9 medium components (converted to concentration of dissolved solutes with Visual MINTEQ 3.1). Growth rate remained unaffected until 2.5X medium concentration.

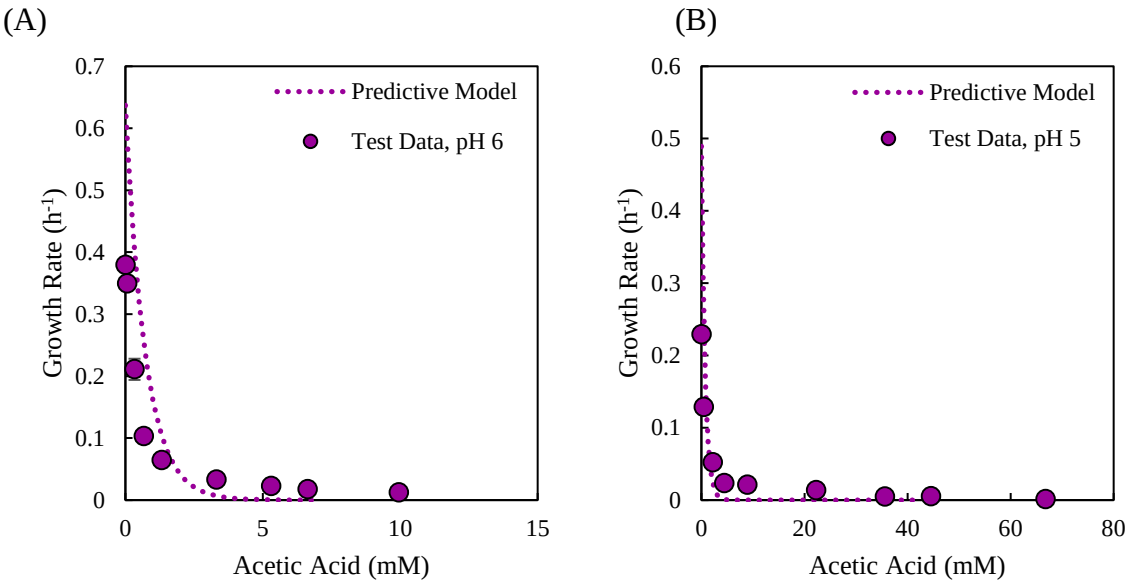


Supplemental Figure 5.S4. Combined inhibition model terms predict culture growth rates under compound stresses. Inhibition terms for acetic acid as a product (Figure 5.6) and pH (Supplemental Figure 5.S3) were combined into a single equation and tested against data sets with varying acetic acid concentrations at pH 6 (A) and pH 5 (B). The dotted lines represent the model equation $\mu = \mu_c\left(\frac{G}{K_G+G}\right)\left(1 - \frac{H}{H^*}\right)e^{-KA}$, where $\mu$ is growth rate ($h^{-1}$), $G$ is concentration of glucose (= 56 mM), $H$ is concentration of $H^+$ (M), $A$ is concentration of protonated acetic acid (mM), and parameters $\mu_c$, $K_G$, $K$, and $H^*$ are as noted in Figure 5.6 and Supplemental Figure 5.S3. Experiments used 2X M9 medium composition, but the effect of osmotic pressure was deemed negligible according to Supplemental Figure 5.S3B and was not added to the model.

Supplemental Table 5.S1. (A) Parameterized inhibition model fits for acetic acid as sole substrate. (B) Parameterized inhibition model fits for acetic acid as a product with glucose as the main substrate. Model equations can be found in (Han and Levenspiel 1988).

**A. Single Substrate (Acetic Acid Only)**

**A1.**

Andrews and Noack

$$\mu = \mu_c \left( \frac{1}{1 + \frac{K_G}{A} + \frac{A}{K_I}} \right)$$

$$\mu_c = 0.702\ h^{-1}$$
$$K_G = 0.165\ mM$$
$$K_I = 0.168\ mM$$

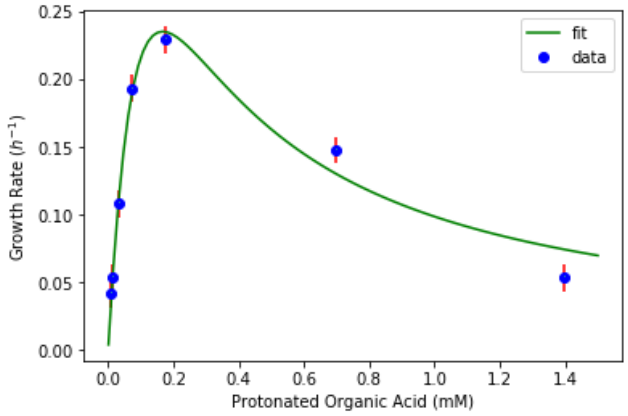


**A2.**

Webb

$$\mu = \mu_c \left( \frac{A\left(1 + \frac{K_G}{K_I}\right)}{K_G + A + \frac{A^2}{K_I}} \right)$$

$$\mu_c = 0.354\ h^{-1}$$
$$K_G = 0.165\ mM$$
$$K_I = 0.168\ mM$$

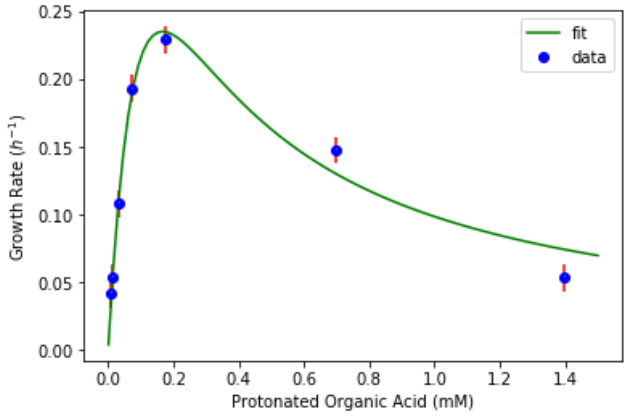


**A3.**

Yano and co-workers

$$\mu = \mu_c \left( \frac{1}{1 + \frac{K_G}{A} + \frac{A}{K_I} + \left(\frac{A}{K_I}\right)^2} \right)$$

$$\mu_c = 0.428\ h^{-1}$$
$$K_G = 0.165\ mM$$
$$K_I = 0.168\ mM$$

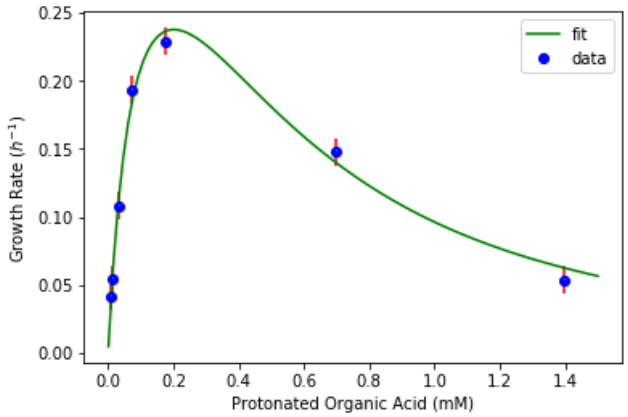

**A4.**

Aiba and co-workers

$$\mu = \mu_c \left(\frac{A}{K_G + A}\right) e^{-\frac{A}{K_I}}$$

$$\mu_c = 0.470\ h^{-1}$$
$$K_G = 0.0948\ mM$$
$$K_I = 0.669\ mM$$

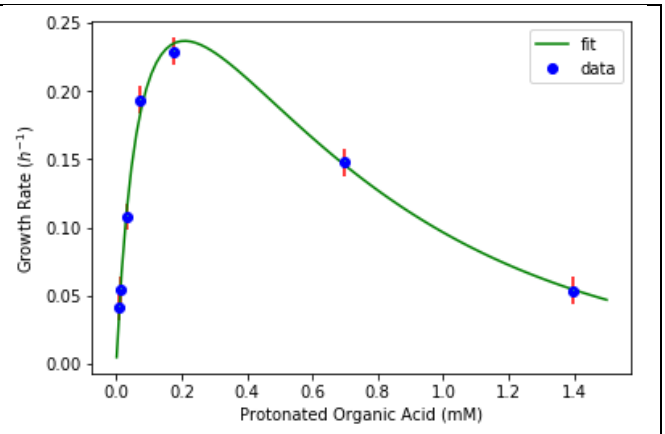


**A5.**

Tessier-Type

$$\mu = \mu_c \left[e^{-\frac{A}{K_I}} - e^{-\frac{A}{K_G}}\right]$$

$$\mu_c = 0.316\ h^{-1}$$
$$K_G = 0.0649\ mM$$
$$K_I = 0.850\ mM$$

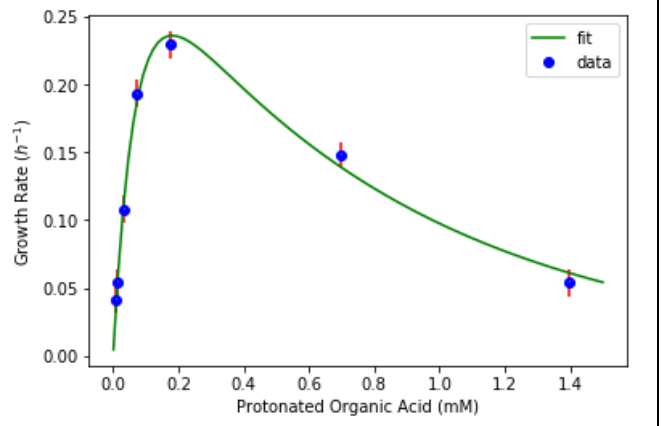


**A6.**

Webb (with σ)

$$\mu = \mu_c \left(\frac{A}{A + K_G\left(1 + \frac{\sigma}{K_I}\right)}\right) e^{1.17\sigma A}$$

$$\mu_c = 0.470\ h^{-1}$$
$$K_G = 0.462\ mM$$
$$K_I = 1.608\ mM$$
$$\sigma = -1.278\ mM$$

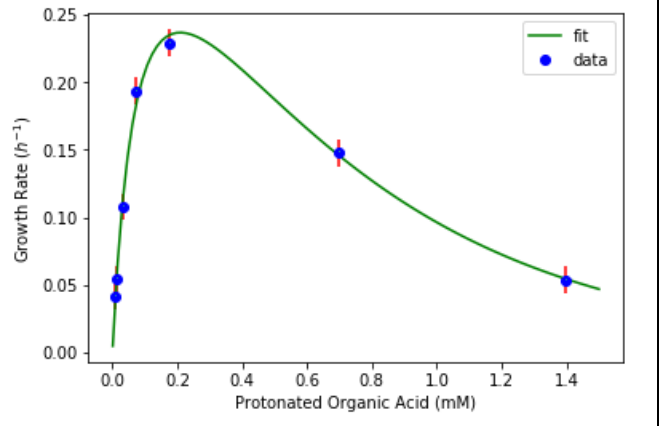

**A6.**

Wayman and Tseng

$$\mu = \mu_c \left(\frac{A}{K_G + A}\right), A < A'$$

$$\mu = \mu_c \left(\frac{A}{K_G + A}\right) - K_I(A - A'), \quad A > A'$$

$$A' = 0.139\ mM$$
$$\mu_c = 0.301\ h^{-1}$$
$$K_G = 0.065\ mM$$
$$K_I = 0.633\ mM$$

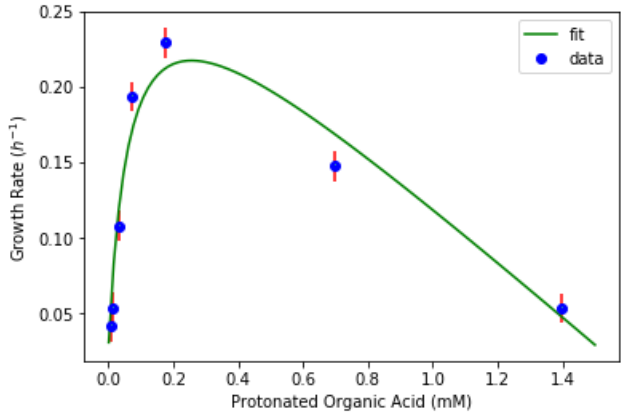


**A7.**

Classic model

$$\mu = \mu_c \left(\frac{A}{K_A + A}\right)\left(\frac{K_I}{K_I + A}\right)$$

$$\mu_c = 0.883\ h^{-1}$$
$$K_A = 0.166\ mM$$
$$K_I = 0.166\ mM$$

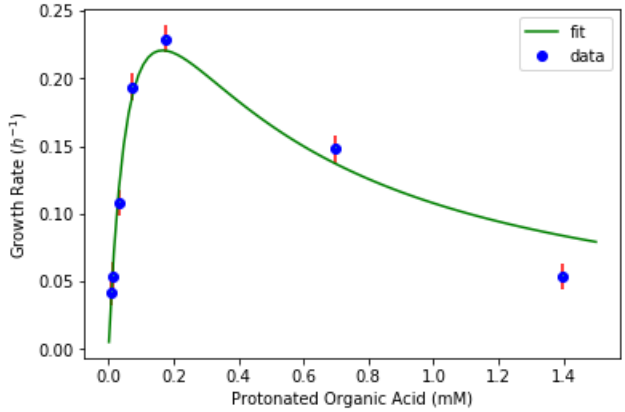


**B. Multiple Substrate (Acetic Acid and Glucose)**

**B1.**

Dagley and Hinshelwood

$$\mu = \mu_c \left(\frac{G}{K_G + G}\right)(1 - KL)$$

$$\mu_c = 0.173\ h^{-1}$$
$$K_G = -40.06\ mM$$
$$K = 1.365\ mM$$

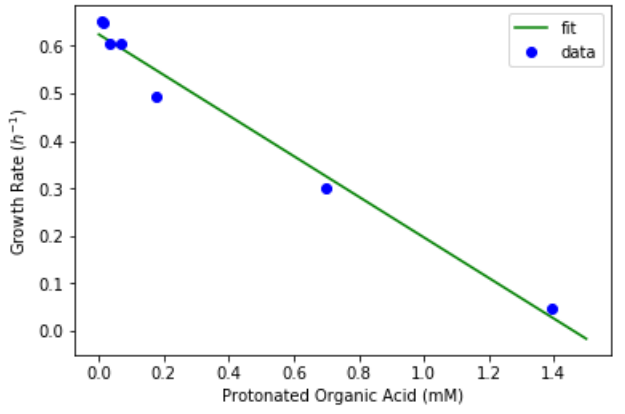

**B2.**

Holzberg and co-workers

$$\mu = \mu_c - K(L - K_I)$$

$$\mu_c = 1.249\ h^{-1}$$
$$K = 0.428\ mM$$
$$K_I = -1.462\ mM$$

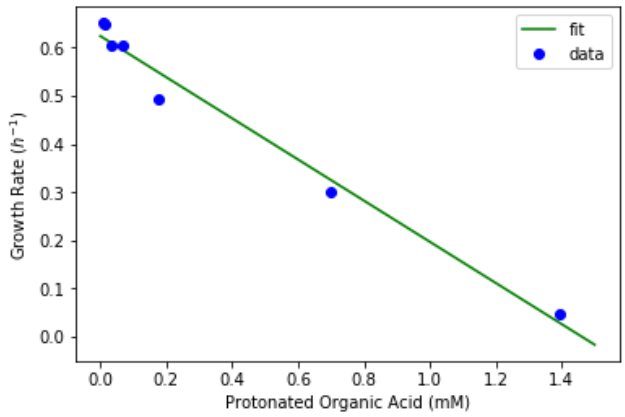


**B3.**

Ghose and Tyagi

$$\mu = \mu_c \left(1 - \frac{A}{A^*}\right)\left(\frac{G}{K_G + G}\right)$$

$$\mu_c = 0.765\ h^{-1}$$
$$K_G = 12.506\ mM$$
$$A^* = 1.461\ mM$$

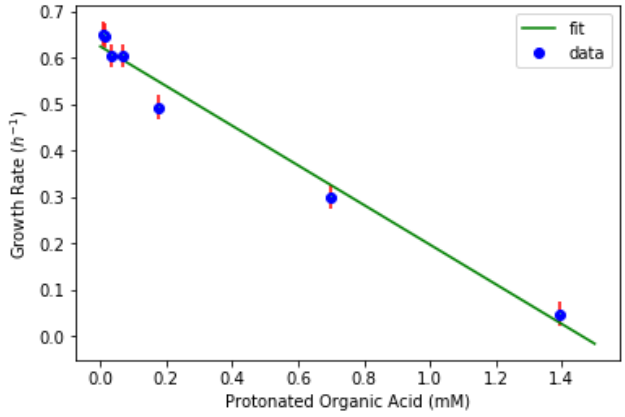


**B4.**

Aiba and co-workers

$$\mu = \mu_c \left(\frac{G}{K_G + G}\right) e^{-KA}$$

$$\mu_c = 0.974\ h^{-1}$$
$$K_G = 27.29\ mM$$
$$K = 1.365\ mM$$

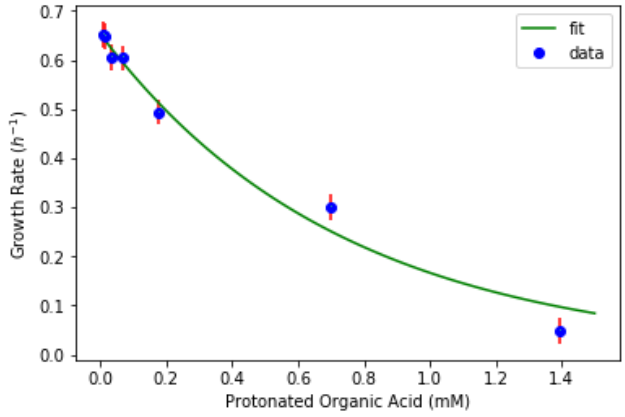

**B5.**

Jerusalimsky and Neronova

$$\mu = \mu_c \left(\frac{G}{K_G + G}\right)\left(\frac{K_I}{K_I + A}\right)$$

$$\mu_c = 678\ h^{-1}$$
$$K_G = 0.0032\ mM$$
$$K_I = 0.405\ mM$$

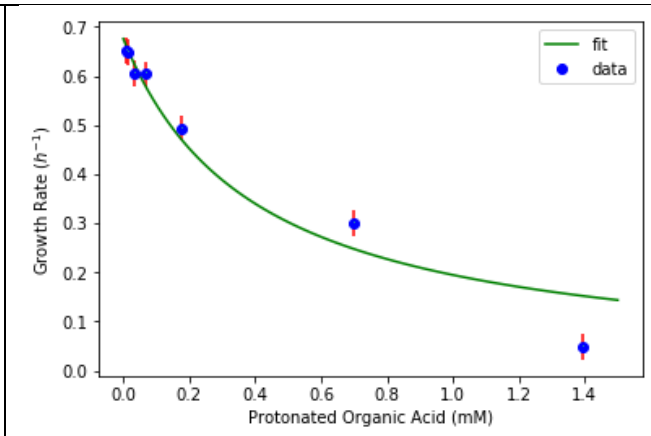


**B6.**

Aiba and co-workers dual substrate derivative

$$\mu = \left[\mu_G \left(\frac{G}{K_G + G}\right) + \mu_L \left(\frac{L}{K_L + L}\right)\right] e^{-\alpha L}$$

$$\mu_G = 0.702\ s^{-1}$$
$$\mu_L = 0.781\ s^{-1}$$
$$K_G = 1.735\ mM$$
$$K_L = 0.117\ mM$$
$$\alpha = 4.62\ mM^{-1}$$

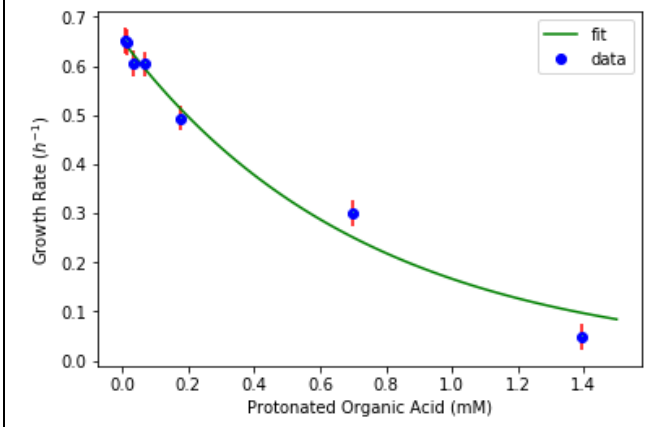


**B7.**

Aiba and co-workers dual substrate derivative (single μ)

$$\mu = \mu_c \left[\left(\frac{G}{K_G + G}\right) + \left(\frac{L}{K_L + L}\right)\right] e^{-\alpha L}$$

$$\mu_c = 0.781\ s^{-1}$$
$$K_G = 8.222\ mM$$
$$K_L = 0.117\ mM$$
$$\alpha = 4.62\ mM^{-1}$$

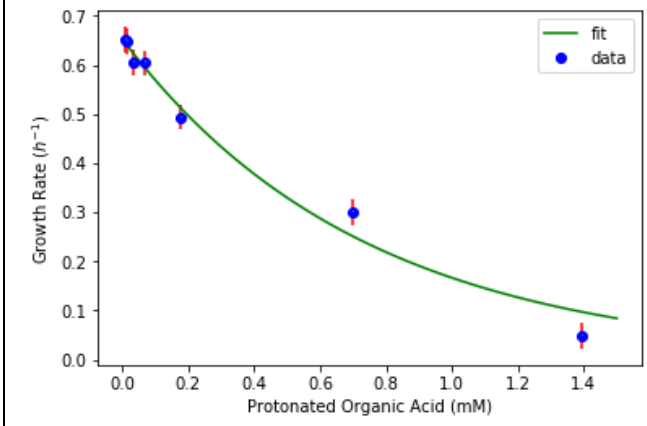

**B8.**

Classic model dual substrate derivative

$$\mu = \left[\mu_G\left(\frac{G}{K_G + G}\right) + \mu_L\left(\frac{L}{K_L + L}\right)\right]\left(\frac{K_I}{K_I + L}\right)$$

$$\mu_G = 0.679\ s^{-1}$$
$$\mu_L = 1.266\ s^{-1}$$
$$K_G = 0.882\ mM$$
$$K_L = 0.08637\ mM$$
$$K_I = 0.08639\ mM$$

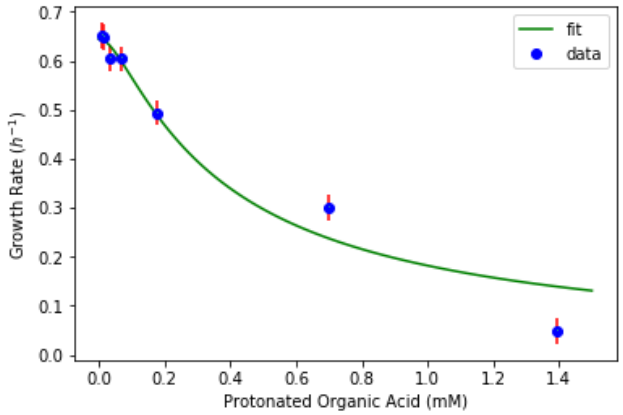


**B9.**

Classic model dual substrate derivative (single μ)

$$\mu = \mu_c\left[\left(\frac{G}{K_G + G}\right) + \left(\frac{L}{K_L + L}\right)\right]\left(\frac{K_I}{K_I + L}\right)$$

$$\mu_c = 0.791\ s^{-1}$$
$$K_G = 27.37\ mM$$
$$K_L = 0.0737\ mM$$
$$K_I = 0.1007\ mM$$

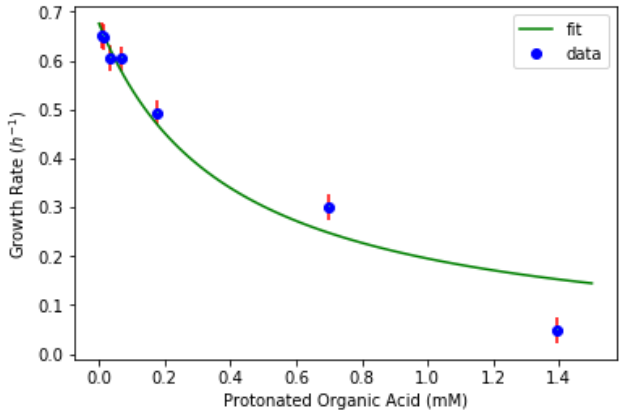

Supplemental Table 5.S2. (A) Parameterized inhibition model fits for lactic acid as sole substrate. (B) Parameterized inhibition model fits for lactic acid as a dual substrate with glucose. Model equations can be found in (Han and Levenspiel 1988).

| **A. Single Substrate (Lactic Acid Only)** | |
|---|---|
| **A1.**<br>Andrews and Noack<br>$$\mu = \mu_c \left( \frac{1}{1 + \frac{K_G}{L} + \frac{L}{K_I}} \right)$$<br>$\mu_c = 0.504 h^{-1}$<br>$K_G = 0.0038\ mM$<br>$K_I = 0.23\ mM$ | 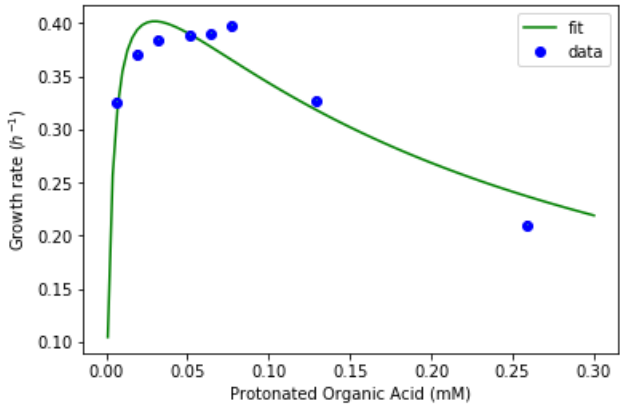 |
| **A2.**<br>Webb<br>$$\mu = \mu_c \left( \frac{L\left(1 + \frac{K_I L}{K_s}\right)}{K_G + L + \frac{L^2}{K_s}} \right)$$<br>$\mu_c = 0.461\ h^{-1}$<br>$K_G = 0.0028\ mM$<br>$K_I = -3.7 * 10^6\ mM$<br>$K_S = 1.8 * 10^6\ mM$ | 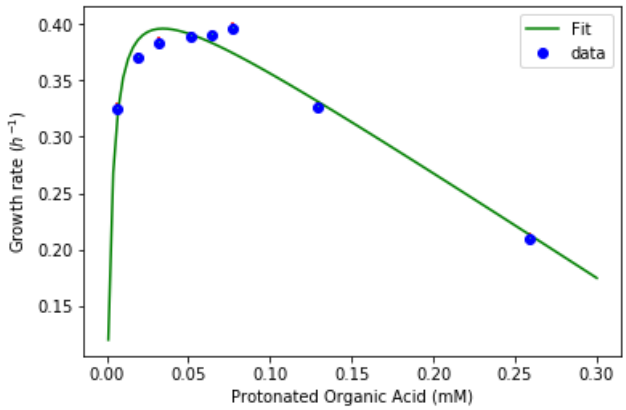 |
| **A3.**<br>Yano and co-workers<br>$$\mu = \mu_c \left( \frac{1}{1 + \frac{K_G}{L} + \frac{L}{K_I} + \left(\frac{L}{K_I}\right)^2} \right)$$<br>$\mu_c = 0.474\ h^{-1}$<br>$K_G = 0.0032\ mM$<br>$K_I = 0.388\ mM$ | 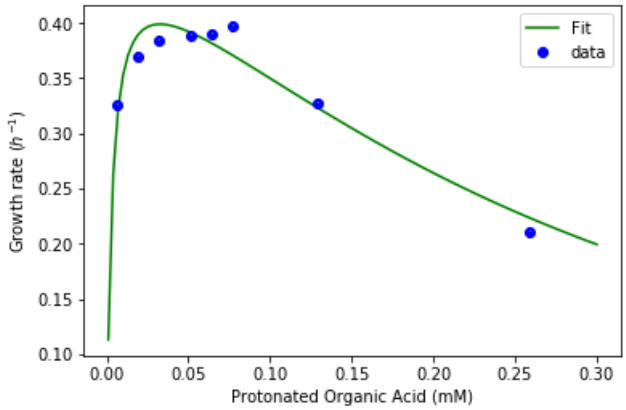 |

**A4.**

Aiba and co-workers

$$\mu = \mu_c \left(\frac{L}{K_G + L}\right) e^{-\frac{L}{K_I}}$$

$\mu_c = 0.485\ h^{-1}$
$K_G = 0.0034\ mM$
$K_I = 0.339\ mM$

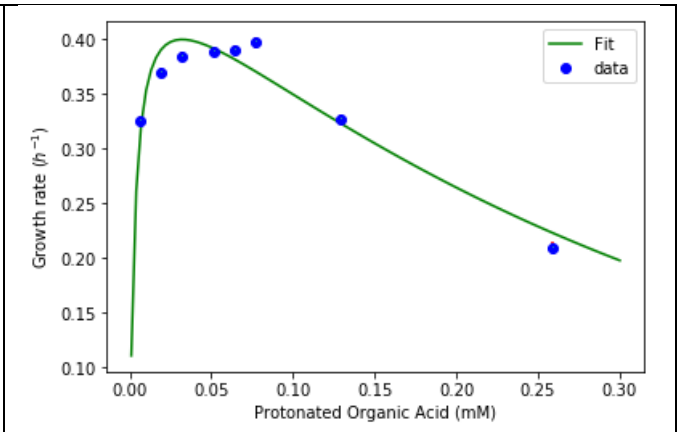


**A5.**

Tessier-Type

$$\mu = \mu_c \left[e^{-\frac{L}{K_I}} - e^{-\frac{L}{K_G}}\right]$$

$\mu_c = 0.433\ h^{-1}$
$K_G = 0.0047\ mM$
$K_I = 0.419\ mM$

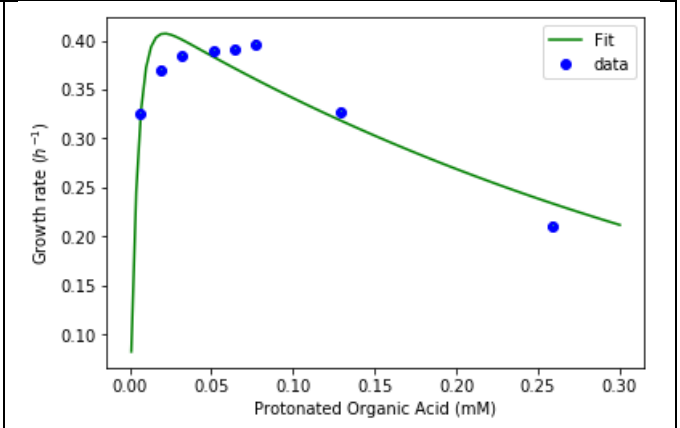


**A6.**

Webb (with σ)

$$\mu = \mu_c \left(\frac{L}{L + K_G\left(1 + \frac{\sigma}{K_I}\right)}\right) e^{1.17L\sigma}$$

$\mu_c = 0.485\ h^{-1}$
$K_G = -0.0001\ mM$
$K_I = 0.081\ mM$
$\sigma = -2.524\ mM$

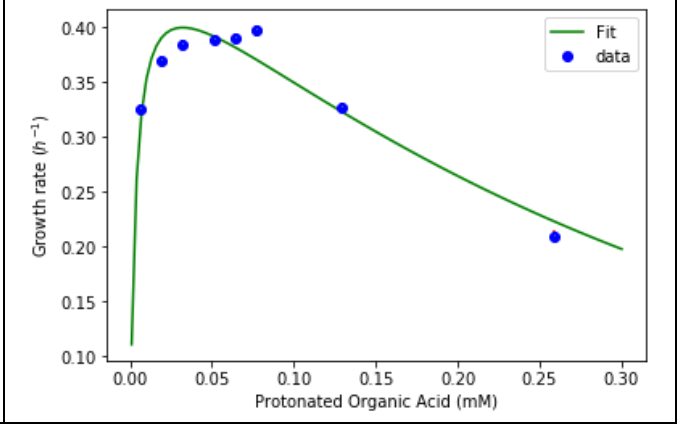

**A7.**

Wayman and Tseng

$$\mu = \mu_c \left(\frac{L}{K_G + L}\right), L < L'$$

$$\mu = \mu_c \left(\frac{L}{K_G + L}\right) - K_I(L - L'), \quad L > L'$$

L' = 0.078 mM

$\mu_c = 0.393\ h^{-1}$

$K_G = 0.0038\ mM$

$K_I = 2.46\ mM$

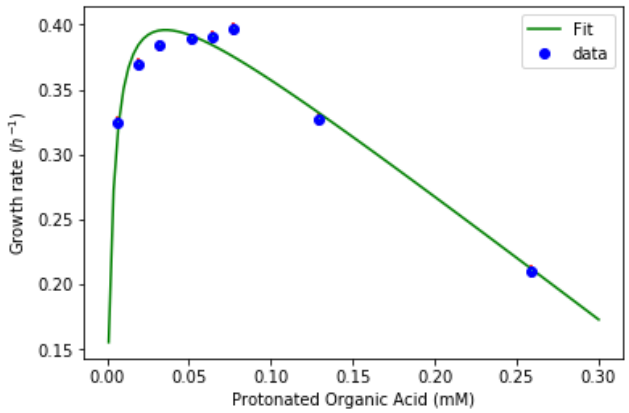


**A8.**

Classic Model

$$\mu = \mu_c \left(\frac{L}{L + K_L}\right)\left(\frac{K_I}{K_I + L}\right)$$

$\mu_c = 0.513\ h^{-1}$

$K_L = 0.0039\ mM$

$K_I = 0.229\ mM$

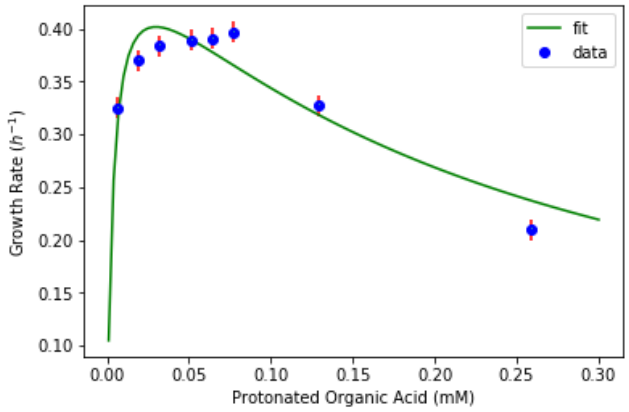


**B. Multiple Substrate (Lactic Acid and Glucose)**

**B1.**

Dagley and Hinshelwood

$$\mu = \mu_c \left(\frac{G}{K_G + G}\right)(1 - KL)$$

$\mu_c = 0.751\ h^{-1}$

$K_G = 0.0047\ mM$

$K = 1.794\ mM$

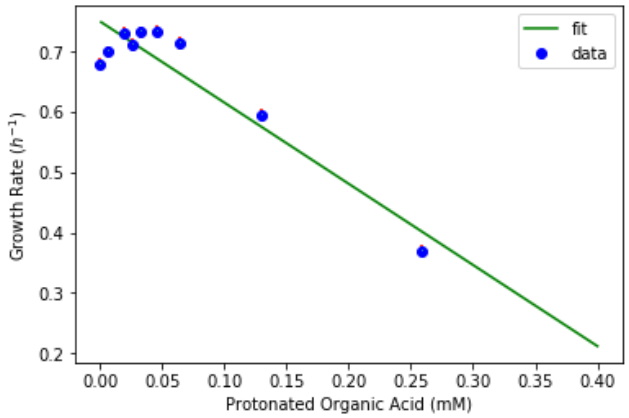

**B2.**

Holzberg and co-workers

$$\mu = \mu_c - K(L - K_I)$$

$$\mu_c = 0.3196\ h^{-1}$$
$$K = 1.347\ mM$$
$$K_I = 0.320\ mM$$

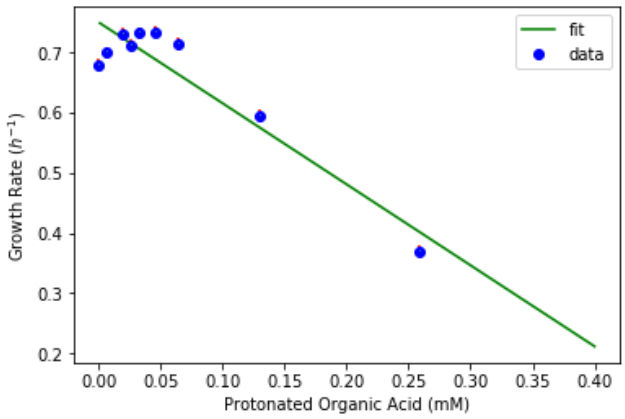


**B3.**

Ghose and Tyagi

$$\mu = \mu_c \left(1 - \frac{L}{L^*}\right)\left(\frac{G}{K_G + G}\right)$$

$$\mu_c = 0.756\ h^{-1}$$
$$K_G = 0.176\ mM$$
$$L^* = 0.557\ mM$$

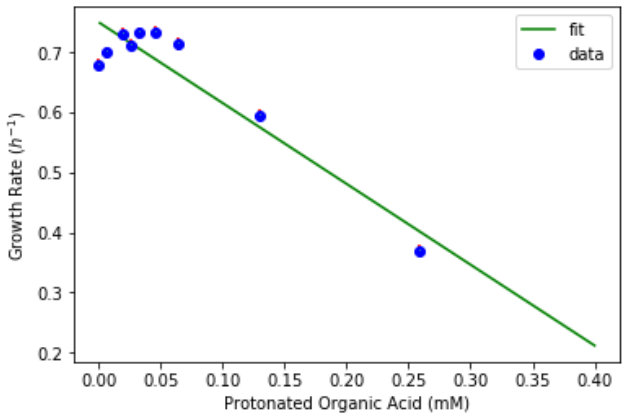


**B4.**

Aiba and co-workers

$$\mu = \mu_c \left(\frac{G}{K_G + G}\right) e^{-KL}$$

$$\mu_c = 0.768\ h^{-1}$$
$$K_G = 0.950\ mM$$
$$K = 2.184\ mM$$

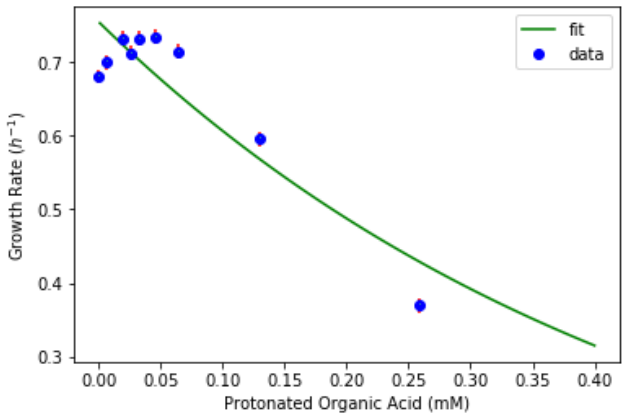

**B6.**

Jerusalimsky and Neronova

$$\mu = \mu_c \left(\frac{L}{K_G + L}\right)\left(\frac{K_I}{K_I + L}\right)$$

$$\mu_c = 0.757\ h^{-1}$$
$$K_G = 0.0041\ mM$$
$$K_I = 0.391\ mM$$

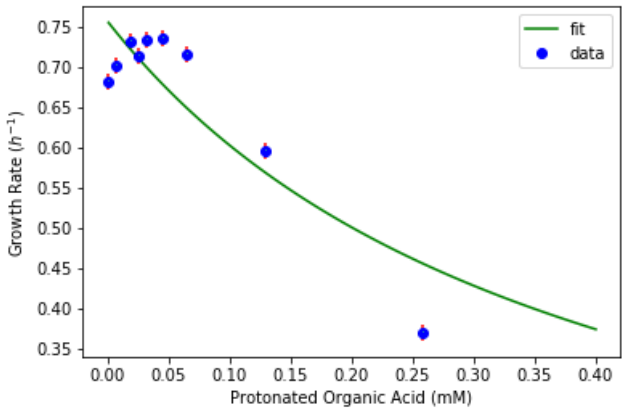


**B7.**

Aiba and co-workers dual substrate derivative (single µ)

$$\mu = \mu_c \left[\left(\frac{G}{K_G + G}\right) + \left(\frac{L}{K_L + L}\right)\right] e^{-\alpha L}$$

$$\mu_c = 0.7812\ h^{-1}$$
$$K_G = 8.222\ mM$$
$$K_L = 0.117\ mM$$
$$\alpha = 4.62\ mM^{-1}$$

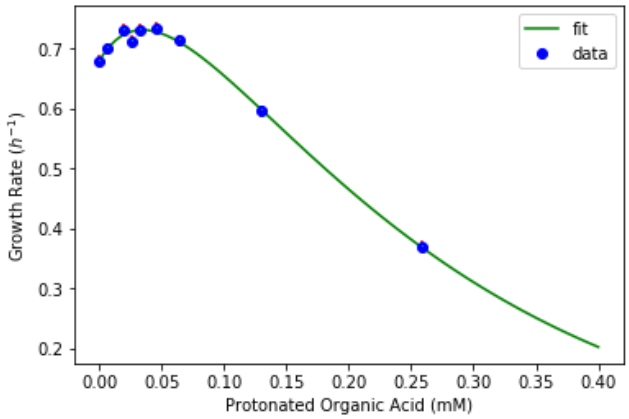


**B8.**

Classic model dual substrate derivative (single µ)

$$\mu = \mu_c \left[\left(\frac{G}{K_G + G}\right) + \left(\frac{L}{K_L + L}\right)\right]\left(\frac{K_I}{K_I + L}\right)$$

$$\mu_c = 0.999\ h^{-1}$$
$$K_G = 27.37\ mM$$
$$K_L = 0.0737\ mM$$
$$K_I = 0.1007\ mM$$

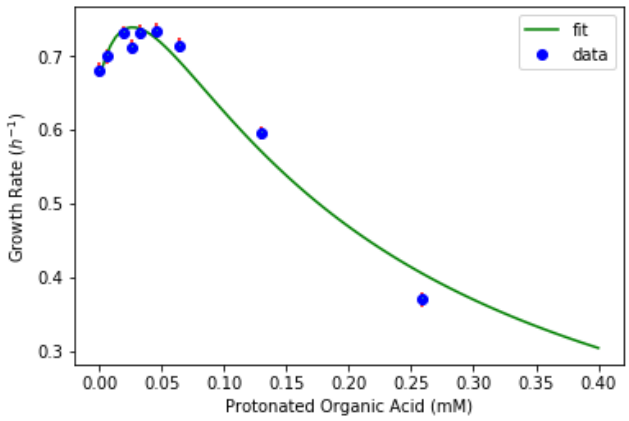

Supplemental Table 5.S3. Matrix of carbon source concentrations used to construct inhibition curves and corresponding average growth rates and standard deviations for triplicate biological cultures.

| Carbon source concentration (mM (g/L)) | | | Growth Rate | S.D. |
|---|---|---|---|---|
| **Glucose** | **Sodium Lactate** | **Sodium Acetate** | | |
| **Lactate Dual Substrate Inhibition** | | | | |
| 56 (10) | 0 (0) | | 0.681 | 0.014 |
| 56 (10) | 9 (1) | | 0.700 | 0.009 |
| 56 (10) | 27 (3) | | 0.732 | 0.016 |
| 56 (10) | 36 (4) | | 0.712 | 0.016 |
| 56 (10) | 45 (5) | | 0.733 | 0.009 |
| 56 (10) | 62 (7) | | 0.735 | 0.006 |
| 56 (10) | 89 (10) | | 0.714 | 0.005 |
| 56 (10) | 178 (20) | | 0.596 | 0.009 |
| 56 (10) | 357 (40) | | 0.366 | 0.005 |
| **Lactate Substrate Inhibition** | | | | |
| | 9 (1) | | 0.325 | 0.012 |
| | 27 (3) | | 0.370 | 0.004 |
| | 45 (5) | | 0.384 | 0.007 |
| | 71 (8) | | 0.389 | 0.004 |
| | 89 (10) | | 0.390 | 0.003 |
| | 107 (12) | | 0.397 | 0.002 |
| | 178 (20) | | 0.327 | 0.003 |
| | 357 (40) | | 0.211 | 0.002 |
| **Acetate Product Inhibition** | | | | |
| 56 (10) | | 1 (0.1) | 0.652 | 0.037 |
| 56 (10) | | 2 (0.2) | 0.647 | 0.035 |
| 56 (10) | | 6 (0.5) | 0.605 | 0.022 |
| 56 (10) | | 12 (1) | 0.604 | 0.022 |
| 56 (10) | | 30 (2.5) | 0.493 | 0.026 |
| 56 (10) | | 122 (10) | 0.300 | 0.032 |
| 56 (10) | | 244 (20) | 0.048 | 0.005 |
| **Acetate Substrate Inhibition** | | | | |
| | | 1 (0.1) | 0.042 | 0.006 |
| | | 2 (0.2) | 0.054 | 0.006 |
| | | 6 (0.5) | 0.108 | 0.008 |
| | | 12 (1) | 0.194 | 0.008 |
| | | 30 (2.5) | 0.229 | 0.011 |
| | | 122 (10) | 0.148 | 0.025 |
| | | 244 (20) | 0.054 | 0.006 |
| **Acetate Product Inhibition, pH 6.0** | | | | |

| | | | | |
|---|---|---|---|---|
| 111 (20) | | 0 (0) | 0.380 | 0.010 |
| 111 (20) | | 1 (0.1) | 0.350 | 0.002 |
| 111 (20) | | 6 (0.5) | 0.211 | 0.017 |
| 111 (20) | | 12 (1) | 0.103 | 0.001 |
| 111 (20) | | 24 (2) | 0.064 | 0.002 |
| 111 (20) | | 61 (5) | 0.033 | 0.006 |
| 111 (20) | | 98 (8) | 0.023 | 0.002 |
| 111 (20) | | 122 (10) | 0.018 | 0.003 |
| 111 (20) | | 183 (15) | 0.013 | 0.003 |
| **Acetate Product Inhibition, pH 5.0** | | | | |
| 111 (20) | | 0 (0) | 0.229 | 0.002 |
| 111 (20) | | 1 (0.1) | 0.129 | 0.002 |
| 111 (20) | | 6 (0.5) | 0.052 | 0.003 |
| 111 (20) | | 12 (1) | 0.024 | 0.002 |
| 111 (20) | | 24 (2) | 0.021 | 0.003 |
| 111 (20) | | 61 (5) | 0.014 | 0.009 |
| 111 (20) | | 98 (8) | 0.005 | 0.004 |
| 111 (20) | | 122 (10) | 0.005 | 0.004 |
| 111 (20) | | 183 (15) | 0.001 | 0.001 |

# CHAPTER SIX

## SYNTHETIC CONSORTIA ENGINEERED FOR PUSH AND PULL DYNAMICS SHOW CONDITIONAL OPTIMALITY OVER METABOLIC GENERALIST

### Contribution of Authors and Co-Authors

Manuscript in Chapter Six

Author: Ashley E. Beck

Contributions: Conceived and designed the experiments, performed the experiments, analyzed the data, wrote the manuscript

Co-Author: Ross P. Carlson

Contributions: Conceived and designed the experiments

Manuscript Information Page

Ashley E. Beck and Ross P. Carlson

Status of Manuscript:
_X__ Prepared for submission to a peer-reviewed journal
____ Officially submitted to a peer-review journal
____ Accepted by a peer-reviewed journal
____ Published in a peer-reviewed journal

## 6.1. Abstract

Metabolite exchange is a common organizational motif of microbial communities. Waste byproducts of one species can often serve as substrates for another species, thereby introducing co-dependent relationships. Relief of toxic byproduct accumulation also creates a reciprocal benefit for the producer species. Synthetic biology provides a way to investigate microbial interactions in a more controlled environment. This study constructs and analyzes the properties of synthetic organic acid-exchanging *Escherichia coli* consortia with a producer-scavenger specialist food chain design. Lactate- and acetate-exchanging consortia were each constructed via genetic engineering and strain selection, and the effect of pH stress on productivity of the consortia as compared to producer or generalist (wild-type) monoculture strains was examined. The acetate-exchanging consortium showed enhanced growth over the producer monoculture but not over the generalist, whereas the lactate-exchanging consortium performed better than both the producer monoculture and the generalist. The growth kinetics of the producer and scavenger specialists played an important role in modulating the overall consortium dynamics: the acetate-exchanging consortium represented a “push” system where the scavenger struggled to keep up with byproduct production, while the lactate-exchanging consortium represented a “pull” system where the scavenger consumed byproduct nearly as fast as it was produced. Finally, the quantifications from the synthetic consortia provided a testing ground for applying maximum power principle theory to examine system energetics from a fitness perspective.

## 6.2. Introduction

Microorganisms in the environment almost always coexist in communities rather than as single-species populations. Despite the competitive “eat or be eaten” survival philosophy (or “nature red in tooth and claw” according to Tennyson (Harcombe 2010)), natural selection has selected for communities of multiple species that often cooperate with one another, indicating that benefits derived from sharing resources must outweigh the costs. Although large-scale data sets characterizing the composition of microbial communities in different environments are common, principles of microbial community assembly, organization, and structure are still not well known, leaving much to be learned about how microbial interactions form within a community as well as how the environment influences interactions.

Metabolite exchange serves as an important basis of community organization. Every metabolism converts a substrate to some type of metabolic byproduct, and byproducts are thermodynamically inhibitory to the forward driving of metabolism and are sometimes toxic, especially in high concentration. Often the byproducts of one species’ metabolism can be used as a substrate by another species and simultaneously relieve byproduct inhibition, setting up interdependent interactions between species in a community. Understanding why microorganisms may secrete certain metabolites as byproducts over others under different environmental conditions is useful to understanding natural community structures and can aid in industrial community design. Metabolite exchange often entails metabolic specialization in a particular pathway, or division of labor among species in a community. Understanding the benefits of

cooperation is of recent interest in the literature and has been investigated both with models and in laboratory experiments (e.g. (Mee, Collins et al. 2014, Germerodt, Bohl et al. 2016)).

Natural microbial communities are complex and often contain thousands of species that interact in different ways. Synthetic systems can be designed to simplify the system to a few species with well-defined functionalities. These more tractable systems illuminate basic properties and mechanisms of interaction, which can then be extrapolated to better understand the role and function of microbial communities in natural systems and industrial bioprocesses. Synthetic ecology has been used to examine spatial structuring, cross-feeding, and competition in microbial communities. Synthetic communities have been tested in a variety of applications, for example, simultaneous utilization of different sugars, enhanced conversion of cellulose to biofuels, and quorum sensing (Brenner, You et al. 2008, Johns, Blazejewski et al. 2016), as well as more advanced applications, such as integrating plant capabilities within microorganisms to enhance biofuel production (Georgianna and Mayfield 2012).

The ability to carefully control many variables with synthetic communities that usually cannot be controlled in the natural environment provides an excellent means to test community ecology theories. Many ecological principles have been developed to describe systems at the macro-scale but are often difficult to test quantitatively in the natural world. For example, the maximum power principle is a compelling ecological theory initially developed by Lotka (Lotka 1922, Lotka 1922) to describe community organization and the role of natural selection. The principle states that populations or

communities of populations that can obtain available energy at a faster rate will be favored by natural selection (Lotka 1922, Lotka 1922). Over the years, there has been some ambiguity regarding the interpretation of obtaining energy; different meanings have been proposed, such as (1) solely acquisition of energy, thereby removing its availability to competing populations, and (2) efficiency of usage of the acquired energy (Sciubba 2011, Martyushev 2013). Thus, there is a need for well-defined systems that can be used to measure energy inputs and outputs in a rigorous, quantitative way to further investigate the formulation and interpretation of this principle. Another ecological principle relevant to the structure of microbial communities is that of resource ratio theory, which states that populations that can more effectively deplete limiting resources will be most competitive (Tilman 1980). This theory can also be extended to multiple populations, leading to the concept of a "super-competitor unit" where a community can more effectively deplete resources than a single population (de Mazancourt and Schwartz 2010).

The presented study constructs and analyzes the properties of synthetic *Escherichia coli* communities. The objectives of the study were to: (i) design different organic acid-exchanging synthetic consortia and examine the effect of pH stress on consortia productivity, (ii) quantify the impact of metabolic specialization by comparison of organic acid-exchanging consortia with the generalist *E. coli* from which the consortia members were derived, and (iii) apply the maximum power principle and interpret various thermodynamic extensions thereof. The metabolism of *E. coli* was partitioned into two non-overlapping functionalities by selecting or designing genetically engineered

organisms and pairing producer strains that produced either lactate or acetate with a scavenger that was unable to consume glucose as a carbon/energy source but consumed the organic acid as a carbon/energy source. The presented study uses synthetic consortia to improve understanding of community metabolic function and extend the predominantly qualitative maximum power principle to microbial communities in a quantitative manner. This advance in fundamental understanding can be applied to designing consortia for industrial bioprocessing and broadens our understanding of natural microbial community interactions in global nutrient cycling and other environmental processes.

## 6.3. Methods

### 6.3.1. Culturing Media

Conventional M9 medium (Ausubel, Brent et al. 1992) contained 6 g/L $Na_2HPO_4$, 3 g/L $KH_2PO_4$, 1 g/L $NH_4Cl$, and 0.5 g/L NaCl. After autoclaving, 1 mL/L 1 M $MgSO_4 \cdot 7H_2O$ solution was added along with 1 mL/L trace metals solution, containing (per L): 0.73 g $CaCl_2 \cdot 2H_2O$, 0.10 g $MnCl_2 \cdot 4H_2O$, 0.17 g $ZnCl_2$, 0.043 g $CuCl_2 \cdot 2H_2O$, 0.06 g $CoCl_2 \cdot 6H_2O$, 0.06 g $Na_2MoO_4 \cdot 2H_2O$, and 0.24 g $FeCl_3 \cdot 6H_2O$. Carbon source (glucose, sodium acetate, or sodium lactate) was added to achieve the desired concentration from a filter sterilized stock solution. The pH of the medium was adjusted if necessary with HCl or NaOH and the medium then filter sterilized. Conventional M9 medium was modified to ensure carbon limitation at 5 g/L glucose by increasing nitrogen, iron, and sulfate content. Modified M9 medium contained 2.5 g/L $NH_4Cl$, 1.5

mL/L 1 M $MgSO_4 \cdot 7H_2O$, and an additional 2.4 mg/L $FeCl_3 \cdot 6H_2O$. For experimental conditions, phosphate buffering capacity was minimized to allow a more direct observation of organic acid production. Low phosphate modified M9 medium contained 0.9 g/L $Na_2HPO_4$ in place of 6 g/L $Na_2HPO_4$ and 3 g/L $KH_2PO_4$.

6.3.2. Strains

Mutant strains were derived from *E. coli* str. K-12 substr. MG1655, which served as the wild-type generalist strain for comparison.

The lactate producer strain, *E. coli* str. ECOM4LA, was obtained from the Palsson group (Portnoy, Scott et al. 2010). The strain was designed to prevent oxygen uptake through deletions of all three terminal oxidases (*cbdAB*, *cydAB*, and *cyoABCD*), as well as deletion of the quinol monooxygenase *ygiN*. Oxygen consumption is reduced nearly 60-fold so as to be considered negligible, and the strain ferments glucose to produce high yields of lactate (Portnoy, Scott et al. 2010). The strain was received in a frozen glycerol stock. Growth of the initial stock was found to be slow, possibly due to sensitivity to freeze-thaw cycles. Thus, the frozen stock was serially passaged by transferring during exponential phase to fresh conventional M9 media containing 4 g/L glucose. Samples were tested for growth rate periodically, and serial passaging was continued until growth rate plateaued (≈120 generations).

The acetate producer, *E. coli* str. 409, was constructed from *E. coli* str. 307G100, which was designed in a previous study to prevent acetate consumption and increase acetate production via *aceA*, *ldhA*, and *frdA* deletions (Bernstein, Paulson et al. 2012). An additional deletion (*atpF*) was added to *E. coli* str. 307G100 using P1 viral

transduction with the KEIO mutant library according to the protocol outlined in Bernstein and Carlson (Bernstein and Carlson 2014). The resulting kanamycin resistance gene replacement was cured with a pFTA plasmid transformation (Bernstein and Carlson 2014). *E. coli* str. 409 was designed to function similarly to the homoacetate fermenting strain reported in Causey et al. (Causey, Zhou et al. 2003), where disruption of oxidative phosphorylation requires the cell to generate energy via substrate-level phosphorylation, resulting in high quantities of acetate. The *atpF* gene deletion was confirmed with PCR (forward primer 5'-GTTATGGGTCTGGTGGATGC-3', reverse primer 5'-CGAACACCAAAGTGTAGAACGC-3'), and physiological studies were performed to verify increased acetate production by *E. coli* str. 409.

The scavenger strain, *E. coli* str. 403, was previously constructed in Bernstein et al. (Bernstein, Paulson et al. 2012) to prevent glucose consumption by blocking the glucose phosphotransferase uptake system and phosphorylation of glucose via *ptsG*, *ptsM*, *glk*, and *gcd* deletions. This strain does not grow readily on glucose as the sole carbon source but is able to metabolize glucose at a slow base rate, whereas lactate and acetate are readily consumed in the presence of oxygen.

### 6.3.3. Batch Culturing

All cultures were grown at 37°C in a shaking incubator (Barnstead|Lab-Line MaxQ 5000, A-class) at 150 rpm. Frozen stock vials prepared from the same culture were used for all experiments. *E. coli* MG1655 and producer strain inocula were grown with 5 g/L glucose as the carbon source, and scavenger strain inocula were grown with either 1 g/L sodium acetate or 2.8 g/L sodium lactate. Disposable test tubes containing 5 mL

modified M9, pH 7.0, were inoculated from frozen stock and incubated until optical density at 600 nm ($OD_{600}$) reached 0.2 – 0.4. Cultures were transferred into 25 mL modified M9, pH 7.0, in 250-mL borosilicate glass baffled shake flasks to an initial $OD_{600}$ ≈0.010 and grown until $OD_{600}$ reached 0.2 – 0.4. Sufficient culture for inoculation was aliquoted into 15-mL Falcon tubes and pelleted at 4000 rpm for 10 minutes at 20°C (Eppendorf 5810 R, 15 amp version). Cells were washed in an equal volume of low phosphate modified M9 containing 5 g/L glucose to remove metabolic byproducts and excess phosphate and were pelleted again. 100-mL batch cultures of low phosphate modified M9 containing 5 g/L glucose were inoculated to an initial $OD_{600}$ ≈0.020. 500-mL borosilicate glass baffled shake flasks with silicone sponge closures were used to allow gas exchange with minimal evaporation. Consortia cultures were inoculated to an initial $OD_{600}$ ≈0.020 of producer and scavenger each.

Flasks were sampled aseptically approximately every doubling time; total culture volume was not reduced more than 20% by the end of the experiment. $OD_{600}$ and pH were measured, and culture supernatant was frozen at -20°C for subsequent metabolite analysis. For consortia experiments, samples were also analyzed for producer and scavenger populations. Samples were serially diluted 1:10 in phosphate buffered saline (PBS; 42.5 mg/L $KH_2PO_4$ and 405.5 mg/L $MgCl_2 \cdot 6H_2O$) and drop plated (10 10-µL drops using a Rainin EDP2 pipette) on selective conventional M9 agar after the method of Herigstad et al. (Herigstad, Hamilton et al. 2001). Selective plates contained 15 g/L Noble agar (Affymetrix) to eliminate bacterial growth on carbon source contaminants available in the agar. The scavenger was selected for with either 1 g/L sodium lactate or 1

g/L sodium acetate, and the producer was selected for with 1 g/L glucose. In the lactate consortia experiments, both scavenger and producer were able to grow on glucose due to the slower growth rate of the producer and the high yield of lactate. Therefore, the producer proportion of the population was estimated by subtracting the scavenger counts on lactate agar from the total population (producer and scavenger) counts on glucose agar. Experiments were performed with triplicate flasks for each condition along with an un-inoculated control flask carried through the entire inoculation and sampling procedure.

### 6.3.4. Dry Weight and Colony-Forming Unit Correlations

Correlation of $OD_{600}$ to cell dry weight (CDW) was determined for the producer and scavenger strains separately. Producer strains were grown in conventional M9 containing 4 g/L glucose, and the scavenger strain was grown in conventional M9 containing 2.8 g/L lactate. Exponentially growing cultures were harvested on ice, pelleted at 4000 rpm for 20 minutes at 4°C in 50-mL Falcon tubes, re-suspended in an equal volume of carbon-free M9 to minimize lysis of cells, and pelleted again. The cultures were combined and concentrated into one tube, and a series of 12 dilutions ranging from $OD_{600}$ 0.25 – 2.5 was made using carbon-free M9 as the diluent. $OD_{600}$ of each dilution was measured and recorded, and 5 mL of each dilution was aliquoted into a pre-dried and pre-weighed aluminum pan. Three aluminum pans contained 5 mL carbon-free M9 as a media control. Pans were placed in a drying oven at 80°C for 24 h and weighed. Samples were dried for an additional 24 h and weighed again to ensure that samples were completely dry. Biomass concentration was calculated from the difference in mass.

Correlation curves were constructed by setting the mass of the media control as zero and adjusting the sample masses accordingly. The CDW correlation for *E. coli* MG1655 was obtained from Folsom et al. (Folsom, Parker et al. 2014).

Colony-forming unit (CFU) to $OD_{600}$ correlation curves were constructed in a similar manner. Exponentially growing cultures were harvested and a series of eight dilutions was made, ranging from $OD_{600}$ 0.010 – 0.275 for *E. coli* str. ECOM4LA and 0.010 – 1.1 for *E. coli* str. 403. $OD_{600}$ was measured and recorded, and each dilution was serially diluted 1:10 in PBS and drop plated on LB agar (Herigstad, Hamilton et al. 2001). Plates were incubated overnight, and counts from countable dilutions (3-30 colonies within a drop) were recorded, from which CFU/mL values were back-calculated.

6.3.5. Metabolite Analysis

Glucose consumption and organic acid secretion were monitored via high-performance liquid chromatography (HPLC). Cells were pelleted from samples and supernatant was frozen at -20°C until analysis, before which samples were filtered (0.45 μm) and prepared 1:1 (v/v) with 2x mobile phase containing fucose as an internal standard. An Agilent 1200 HPLC instrument was used with filtered (0.22 μm) 5 mM sulfuric acid as the mobile phase. Samples were stored in a chilled (4°C) autosampler during the run, and 20-μL sample injections were run on a Bio-Rad HPX-87H column operated at 45°C. Glucose was detected with refractive index detector (RID) with heater set at 40°C, and concentrations were normalized by fucose. Organic acids acetate and lactate were detected with variable wavelength detector (VWD). Significant levels of

formate and succinate were not detected in the samples. Concentrations were quantified using calibration curves with limit of detection at 0.1 mM.

## 6.4. Results

### 6.4.1. Construction of Acetate- and Lactate-Exchanging Consortia

Organic acid-exchanging consortia were constructed by pairing synthetically designed producer and scavenger specialists. Genetically engineered specialists were derived from *Escherichia coli* K-12 MG1655, which served as the metabolic generalist reference strain. Two different organic acid producer specialists were each paired with an organic acid scavenger specialist: *E. coli* str. 409 (*ΔaceA ΔldhA ΔfrdA ΔatpF*) (constructed in the current work) produces high quantities of acetate from glucose catabolism, *E. coli* str. ECOM4LA (*ΔcbdAB ΔcydAB ΔcyoABCD ΔygiN*) (Portnoy, Scott et al. 2010) produces high quantities of lactate, and *E. coli* str. 403 (*ΔptsG ΔptsM Δglk Δgcd*) (Bernstein, Paulson et al. 2012) is unable to consume glucose but oxidizes organic acids. Strains were characterized individually in M9 media to compare the physiological features of the different specialists (Table 6.1). The generalist showed the highest growth rate and had a lower organic byproduct yield than the producers. The acetate and lactate producer specialists showed differential growth rates and byproduct yields, with the lactate producer growing slower but producing a higher percentage of organic byproducts. The scavenger also showed varied growth rates depending upon the organic acid carbon source, growing faster on lactate than on acetate.

Table 6.1. Physiological characterization of generalist and producer/scavenger strains in mono-culture. Measurements were obtained from growth on conventional M9 medium containing 4 g/L glucose (for generalist and producer specialists) or 1 g/L sodium acetate or 2.8 g/L sodium lactate (for scavenger specialist).

| | **Generalist** (*E. coli* K-12 MG1655) | **Acetate Producer** (*E. coli* str. 409) | **Lactate Producer** (*E. coli* str. ECOM4LA) | **Scavenger** (*E. coli* str. 403) |
|---|---|---|---|---|
| **Carbon source** | Glucose | Glucose | Glucose | Acetate / Lactate |
| **Growth rate** | 0.65 $h^{-1}$ | 0.54 $h^{-1}$ | 0.24 $h^{-1}$ | 0.14 / 0.41 $h^{-1}$ |
| **Byproduct yield (per g glucose)** | 0.05 g acetate | 0.34 g acetate | 0.87 g lactate | NA |

Notes: the scavenger is capable of growth on glucose but only at a very low rate (0.016 $h^{-1}$). The lactate producer accumulates minor amounts of acetate (< 0.06 g/L) and succinate (< 0.12 g/L) in addition to lactate during stationary phase, which aligns with results reported in Portnoy et al., 2010.

Pairing of the producer and scavenger strains partitioned metabolic processes between two distinct populations (Figure 6.1). The producer specializes in glycolysis and excretes organic acid fermentation byproducts, whereas the scavenger specializes in the TCA cycle for oxidation of organic acids and depends on the producer for its carbon and energy source. This pairing creates a uni-directional metabolite exchange analogous to a food chain that also allows for quantification of the benefit derived from byproduct detoxification performed by the scavenger. Media with limited buffering capacity was used to compare the performance of the different systems. Low buffering capacity makes the effect of organic acid production more readily apparent by influencing pH and is more representative of natural systems. A range of initial pH conditions (6.0 – 7.5) was explored to further investigate the effect of pH as a stressor on the consortia.

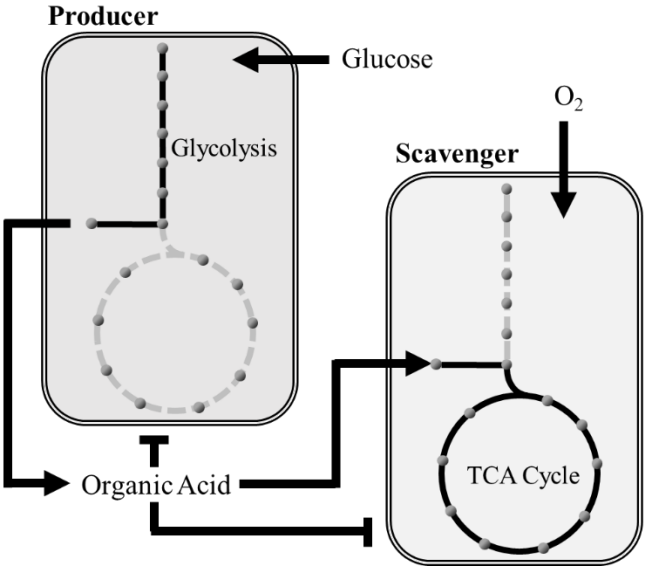


Figure 6.1. Synthetic consortia design. Producer operates glycolysis (highlighted in black) to ferment glucose, producing organic acid byproducts (acetic or lactic acids). Scavenger consumes organic acids as a carbon and energy source via the TCA cycle (highlighted in black).

### 6.4.2. Acetate-Exchanging Consortium Outperforms Specialist

Batch growth of the acetate-exchanging consortium at varying initial pH showed a pH-dependent response in productivity. Highest biomass accumulation occurred at initial pH 7.5, whereas highest growth rate occurred at initial pH 7.0 (Figure 6.2A). Under each initial condition, pH successively decreased over time to an endpoint range of 4.1 – 4.5. (Supplemental Figure 6.S1 compiles time-dependent biomass and pH data for all the conditions, and Supplemental Table 6.S1 provides calculated yields and rates.) Highest acetate production rate and yield occurred at initial pH 7.0, but highest acetate accumulation occurred at initial pH 7.5 due to the larger change in pH before reaching the endpoint pH value. Selective plating of the producer and scavenger revealed an average of 52% producer at the end of the experiments, with lower percentages of producer in the

lower initial pH experiments (6.0 and 6.5) (Supplemental Figure 6.S2). Extracellular metabolite analysis revealed that the scavenger did not re-consume all of the acetate produced by the end of growth under any of the conditions. Biomass accumulation per $H^+$ produced served as a measure of the effect of pH stress on growth. Lower biomass per $H^+$ was observed with decreasing pH, indicating that pH stress lowers the biomass accumulation (Figure 6.2B).

In general, the acetate-exchanging consortium properties were enhanced over those of the acetate producer. The consortium accumulated more biomass per $H^+$ than the producer at each initial pH condition (Figure 6.2B), indicating a greater tolerance to pH stress. The consortium manifested a slower growth rate than the producer (Supplemental Table 6.S1), which is due to the slower growth rate of the scavenger on acetate as compared to the producer (Table 6.1). The consortium accumulated more biomass in total, except under the initial pH 7.0 condition, with the largest increase (1.6-fold enhancement) at initial pH 7.5 (Figure 6.2C). The consortium also accumulated lower quantities of acetate and consumed less total glucose than the producer (except under the initial pH 6.0 condition) but exhibited a higher biomass yield than the producer under each initial condition (Figure 6.2C). Greater than two-fold enhancement in biomass yield over the producer was observed at initial pH 7.0. The combined increase in biomass yield and decrease in byproduct accumulation indicate improved efficiency of the system via addition of the scavenger.

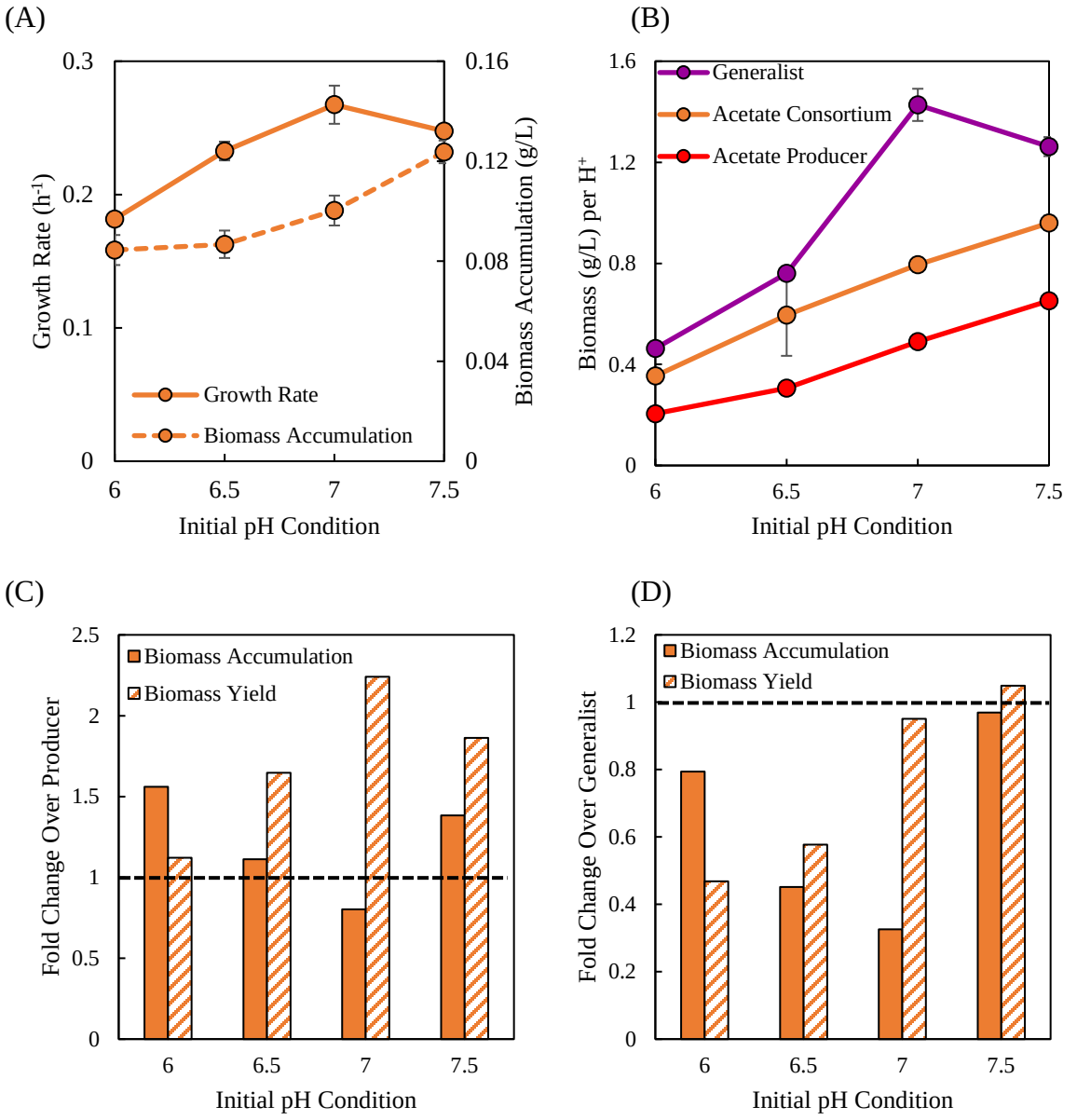


Figure 6.2. Growth characterization of acetate-exchanging consortium under varying initial pH conditions. (A) Growth rate and total biomass accumulation of the acetate-exchanging consortium as a function of initial pH: growth rate decreased at initial pH values diverging from neutral, and total biomass accumulation decreased with decreasing initial pH. (B) Tolerance to pH stress of the acetate-exchanging consortium, acetate producer, and generalist, as measured by biomass yield per $H^+$ produced. The acetate-exchanging consortium was better able to tolerate pH stress than the acetate producer but was not as effective as the generalist. (C) Comparison of total biomass accumulation and biomass yield between acetate-exchanging consortium and acetate producer, as expressed by fold change in measurements (consortium/producer): the consortium showed generally

improved characteristics over the producer. The dashed line shows the relative values for the producer. (D) Comparison of total biomass accumulation and biomass yield between acetate-exchanging consortium and generalist, as expressed by fold change in measurements (consortium/generalist): the consortium in general performed less well than the generalist. The dashed line shows the relative values for the generalist.

The acetate-exchanging consortium did not, however, provide enhanced properties over those of the generalist. The generalist grew faster and accumulated more biomass in total as well as per $H^+$ (Figure 6.2B,D); however, the biomass yields of the consortium and generalist were equivalent at higher initial pH conditions. The acetate consortium also accumulated more byproducts than the generalist, indicating that the addition of the scavenger to the acetate producer specialist in a 1:1 cell ratio was not sufficient to alleviate stress from acetate in comparison to the generalist system.

### 6.4.3. Lactate-Exchanging Consortium Shows Enhanced Growth Over Specialist and Generalist

Batch growth of the lactate-exchanging consortium showed highest productivity at neutral pH. Both growth rate and biomass accumulation attained maximal value at initial pH 7.0 (Figure 6.3A). As with the acetate-exchanging consortium, pH decreased continuously over time to an endpoint range of 3.9 – 4.2, with the exception of the initial pH 7.5 condition. An interesting system recovery phenomenon was observed when culture growth began at initial pH 7.5: culture pH decreased during exponential growth to ~4.9 but thereafter reversed direction and raised to ~6.8. Growth curve data and calculated rates for all of the conditions are provided in Supplemental Figure 6.S1 and Supplemental Table 6.S1. Selective plating of the producer and scavenger showed an average of 3% producer toward the end of growth; however, producer proportions

remained slightly higher throughout the initial growth phase in the initial pH 7.5 condition than for the other conditions (Supplemental Figure 6.S2). Extracellular metabolite analysis revealed nearly complete consumption of lactate by the end of exponential growth for initial conditions pH 6.0 – 7.0 (< 0.2 mM remaining); the remainder was consumed during stationary phase. Under the initial pH 7.5 condition, lactate successively decreased after early exponential phase as the pH rose, leaving < 0.7 mM remaining by the end of growth. As with the acetate consortium, lower biomass per $H^+$ was observed with decreasing pH (Figure 6.3B), again indicating that pH stress inhibits biomass accumulation.

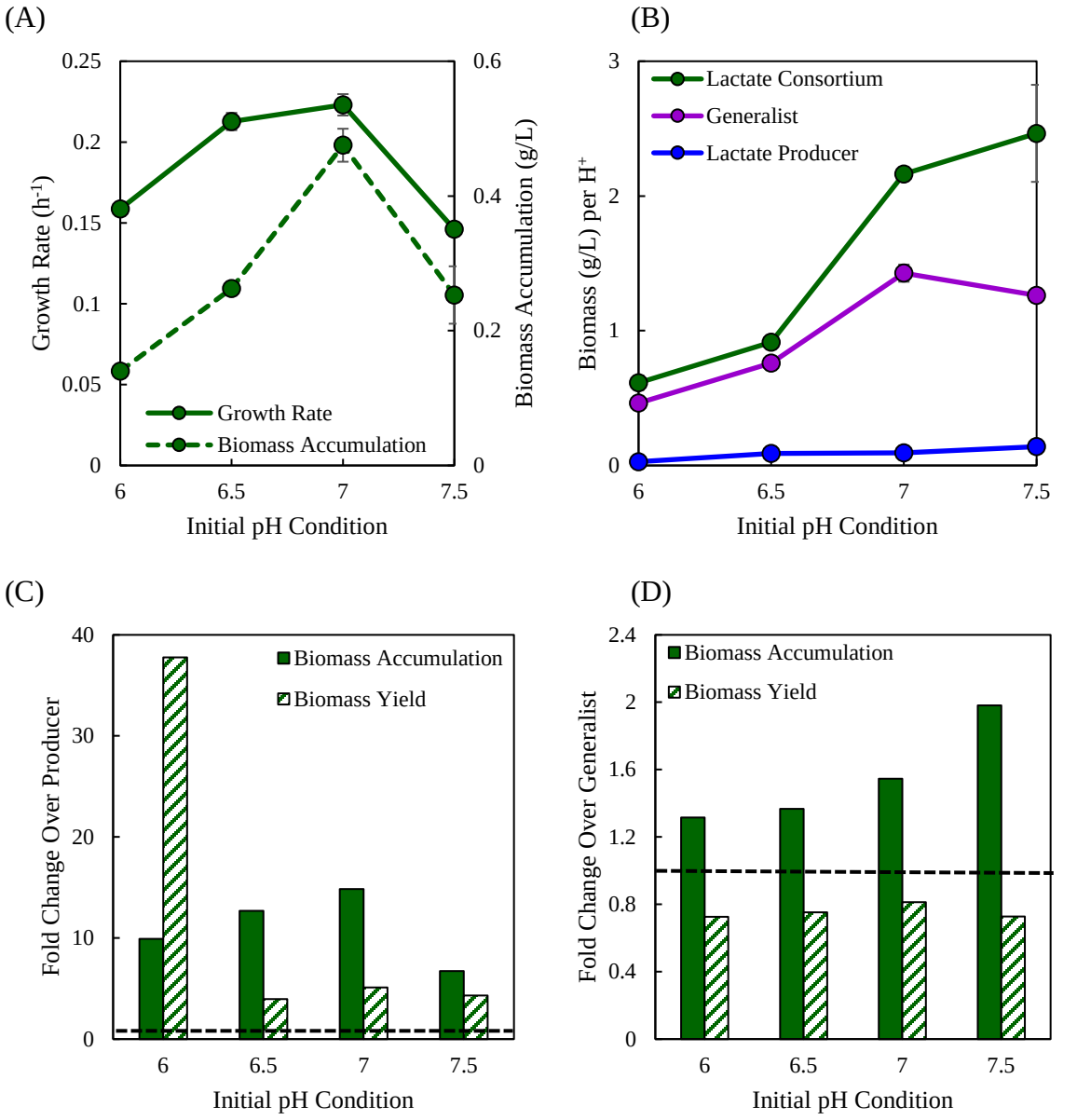


Figure 6.3. Growth characterization of lactate-exchanging consortium under varying initial pH conditions. (A) Growth rate and total biomass accumulation of the lactate-exchanging consortium as a function of initial pH: both growth rate and biomass accumulation decreased at initial pH values diverging from neutral. (B) Tolerance to pH stress of the lactate-exchanging consortium, lactate producer, and generalist, as measured by biomass yield per $H^+$ produced. The lactate-exchanging consortium was better able to tolerate pH stress than either the lactate producer or the generalist. (C) Comparison of total biomass accumulation and biomass yield between lactate-exchanging consortium and lactate producer, as expressed by fold change in measurements (consortium/producer): the consortium showed greatly improved characteristics over the

producer. The dashed line shows the relative values for the producer. (D) Comparison of total biomass accumulation and biomass yield between lactate-exchanging consortium and generalist, as expressed by fold change in measurements (consortium/generalist): the consortium showed improved biomass accumulation over the generalist while exhibiting slightly lower biomass yields. The dashed line shows the relative values for the generalist.

Productivity of the lactate-exchanging consortium was enhanced over that of the lactate producer under every initial pH condition. The consortium exhibited greater tolerance to pH stress as evidenced by higher biomass accumulation per $H^+$ over the producer (Figure 6.3B). Conversely from the acetate consortium, the lactate consortium manifested a faster growth rate than the producer alone (Supplemental Table 6.S1) due to the faster growth rate of the scavenger on lactate as compared to the growth rate of the producer (Table 6.1). The consortium accumulated more biomass in total (Figure 6.3C), with nearly 15-fold increase over the producer at initial pH 7.0, and also did not accumulate any byproducts. The consortium was capable of consuming more glucose than the producer, and the consortium also showed higher biomass yield with four- to five-fold increase over the producer under most initial pH conditions (Figure 6.3C). The high amount of lactate excreted by the producer severely limited biomass accumulation with low biomass produced even under neutral pH conditions, which was greatly exacerbated under pH stress (Supplemental Figure 6.S1). The degree of relative enhancement between the consortium and producer was much greater for the lactate-exchanging system than for the acetate-exchanging system.

The lactate-exchanging consortium showed increased tolerance to pH stress over the generalist. While the generalist grew faster and exhibited a higher biomass yield than

the consortium, the consortium was capable of consuming more glucose in total and accumulating more biomass in total and per $H^+$ than the generalist (Figure 6.3B,D), with nearly 1.8-fold increase in biomass accumulation over the generalist. The addition of the scavenger to the lactate producer specialist in a 1:1 cell ratio allowed for complete re-consumption of organic byproducts and alleviation of stress from byproduct toxicity above that of the generalist.

The pH trajectory showed surprising patterns in the lactate-exchanging consortium under certain conditions, unlike any of the other systems. Whereas batch growth conditions at initial pH 6.0, 6.5, and 7.0 showed consistent patterns of monotonic decrease in pH until stationary phase, growth at initial pH 7.5 showed a similar sharp decrease in pH during early exponential growth but experienced a sudden reversal in the direction of pH change with subsequent gradual rise in pH and growth thereafter (Supplemental Figure 6.S1). A traditional stationary phase was not observed in the time maintained.

An analogous response was triggered by altering the ratio of lactate producer and scavenger. For altered ratio experiments, the producer was inoculated to the same level as in 1:1 experiments, while the amount of scavenger inoculum was adjusted to achieve the desired ratio; this procedure allowed a constant lactate production rate across conditions and isolated the effect of the scavenger. Increasing the relative producer to scavenger ratio (to compensate for the faster growth rate of the scavenger) demonstrated a reversal in pH trajectory after early exponential phase for both 10:1 and 100:1 producer to scavenger initial ratios (Supplemental Figure 6.S3). Interestingly, when the relative

amount of scavenger was increased (1:2 producer to scavenger ratio), the reversal in pH trajectory was still observed. Whereas no lactate accumulation was observed (or minimal transient accumulation at most) in the initial pH 6.0, 6.5, and 7.0 conditions, lactate accumulated in the initial pH 7.5 and altered ratio conditions and was subsequently depleted (Figure 6.4). Interestingly, the lactate production and consumption patterns followed very similar patterns among the initial pH 7.5, 10:1, and 100:1 ratio experiments, while about half as much lactate accumulated in the 1:2 ratio experiment. Additionally, acetate also accumulated during the initial pH 7.5 and altered ratio experiments (Figure 6.4). The scavenger is postulated to convert lactate into acetate, which may then be re-consumed later for growth. Finally, the composition of the consortia showed dominance of the scavenger toward the end of growth. However, the 1:2 ratio condition showed slightly higher producer proportions near the end of growth than the other conditions (Supplemental Figure 6.S3).

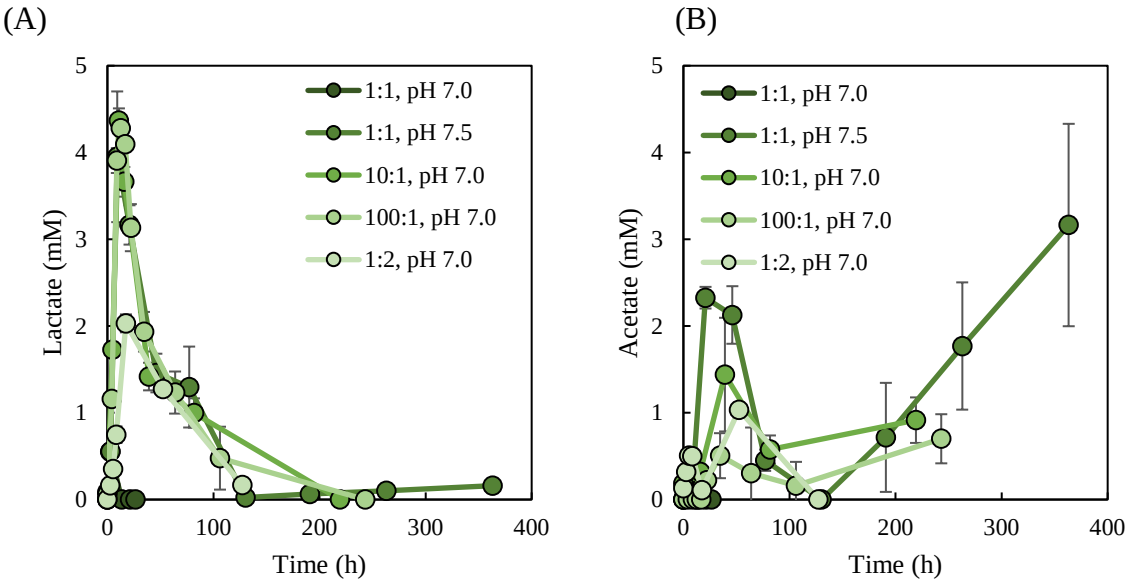


Figure 6.4. Lactate (A) and acetate (B) accumulation dynamics in the lactate consortium at high initial pH (7.5) and altered producer to scavenger ratios.

### 6.4.4. Application and Interpretation of the Maximum Power Principle

The maximum power principle as formulated by Lotka states that the system capable of capturing energy at the fastest rate will be the most favorable arrangement and will be selected under natural selection (Lotka 1922, Lotka 1922). The batch growth data acquired in the current study was used to test this theoretical principle against the division of labor arrangement synthetically engineered in the consortia. Specifically, the detailed measurements made under batch growth scenarios allowed for exploration of the concept of rate of energy "capture" (e.g. acquisition of energy or efficiency of use of the acquired energy).

Power acquisition can be estimated for microbial communities by calculating substrate consumption rates. For the batch experiments presented in the current work, specific glucose uptake rates were calculated and converted to gross power acquisition

rates via the heat of combustion value for glucose. For both the acetate and lactate scenarios, the producers exhibited higher glucose consumption rates than either the generalist or the respective consortia (Figure 6.5A). Despite having the highest gross power acquisition rates, the high organic acid byproduct accumulation made the producers less productive overall in terms of growth.

Rather than interpreting the maximum power principle based on power acquisition (glucose consumption rate) alone, an alternative method for quantifying power consumption is through power utilization by examining energy flow in the system. Figure 6.5B shows the comparison between systems when the rate of energy storage in biomass is subtracted from gross power acquisition (obtained by converting both specific glucose consumption rates and growth rates into power quantities). The remainder represents energy that was either converted to organic byproducts or lost to the environment (e.g. heat transfer processes). The lactate-exchanging consortium showed a smaller value than the generalist or lactate producer (Figure 6.5B), indicating more efficient power utilization. The acetate-exchanging consortium also showed a smaller value than the acetate producer, but larger than the generalist, analogous to the trends observed in section 6.3.2.

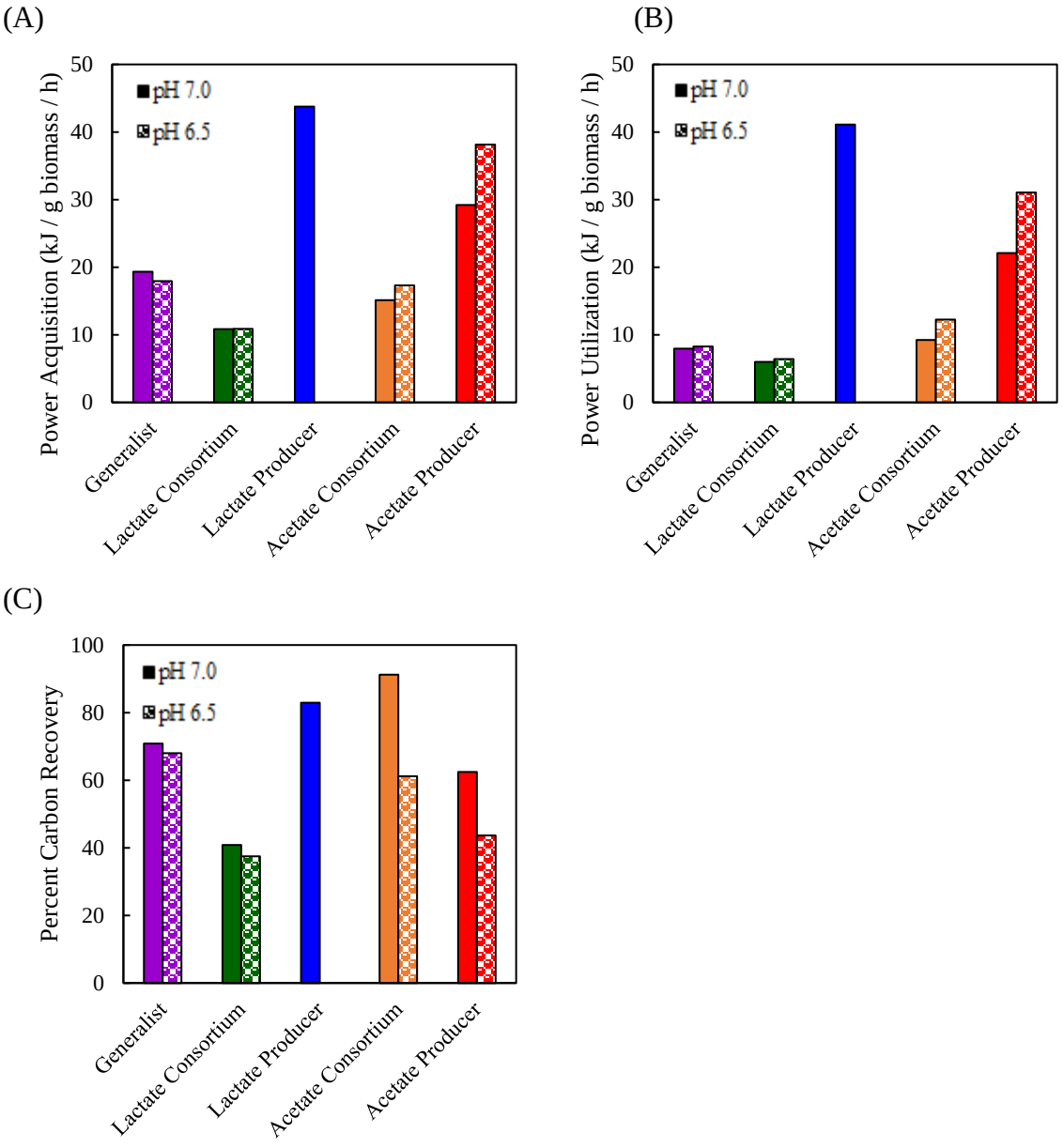


Figure 6.5. Maximum power principle analysis of the different biological systems (generalist, consortia, and producers). (A) Power acquisition was highest by the producers and lowest by the consortia. Glucose consumption rate was calculated over exponential phase and converted to power acquisition via the heat of combustion of glucose. (B) Power utilization was lower for the consortia than for the producers, and power utilization for the lactate-exchanging consortia was lower than for the generalist, indicating more efficient use of acquired energy. Power utilization was calculated by converting the growth rate over exponential phase into the rate of energy storage into biomass via the heat of combustion of biomass and subtracting this quantity from the power acquisition values calculated in (A). This metric represents the efficiency of usage

of acquired power: a lower value indicates that less total power was directed into waste byproducts or lost to the environment. (C) Percent carbon recovery was lower for the lactate-exchanging consortium than for the lactate producer or generalist (indicating that carbon was more completely oxidized), whereas percent carbon recovery for the acetate-exchanging consortium was in fact greater than the producer due to higher acetate yield. Percent carbon recovery was calculated by balancing carbon inputs and outputs in the system. Glucose carbon completely oxidized to $CO_2$ was not measured and represents the unrecovered portion of the carbon balance. Solid columns indicate initial pH 7.0, and dotted columns indicate initial pH 6.5. No value is shown for the lactate producer for the initial pH 6.5 condition due to low consumption of glucose. Each column represents the median value of biological triplicates.

Examination of the carbon balance provides another metric for comparison among the systems (Figure 6.5C). Carbon entered the system only in the form of glucose, and carbon outputs were measured in the form of biomass and organic byproducts. The remainder of the input carbon not accounted for in biomass and other byproducts is assumed to be oxidized completely to $CO_2$. The lactate-exchanging consortium exhibited a lower percent carbon recovery than both the generalist and the lactate producer, showing that carbon was utilized more efficiently in this system (Figure 6.5C). The acetate-exchanging consortium, however, showed a higher percent carbon recovery than the acetate producer, likely due to the higher product yield in the consortium (Supplemental Table 6.S1).

## 6.5. Discussion

The presented work designs and characterizes synthetic *E. coli* communities with the goal to investigate the benefits of division of labor and metabolite exchange in a controlled environment. The resulting lactate- and acetate-exchanging consortia both showed enhancements in growth over producer mono-cultures, demonstrating the

effectiveness of byproduct detoxification. Additionally, the two consortia each showed different growth characteristics compared to the metabolic generalist wild-type *E. coli*. The lactate-exchanging consortium exhibited no accumulation of organic byproducts and was more tolerant of pH stress than the generalist whereas the acetate-exchanging consortium accumulated byproducts to a greater degree than the generalist, showing the importance of selecting species with appropriate uptake/secretion rates and yields in industrial consortia design or tuning kinetic parameters with genetic engineering to obtain an optimal pairing. A previous study has also shown enhanced biomass yield and lower byproduct accumulation in a genetically engineered acetate-exchanging *E. coli* consortium using similar strains, 307G100 and 403G100 (Bernstein, Paulson et al. 2012). The 307G100 acetate-producing strain had a lower acetate yield than the 409 acetate-producing strain constructed in the current work (but higher than the generalist), showing that byproduct production yields may play an important role in consortia efficiencies and outcomes. Finally, the experimental data obtained in the current work can be used to investigate foundational ecological theories such as the maximum power principle and resource ratio theory.

### 6.5.1. Mechanism for Improved Consortia Growth

Principles of effective microbial partnership can be derived from the differences in growth and byproduct accumulation between the generalist and the lactate- and acetate-exchanging consortia. Figure 6.6 presents a conceptual diagram illustrating the effect of byproduct detoxification in the minimal medium batch systems studied in the current work. Each of the systems (generalist, consortia, producers) showed an endpoint

pH around 4-4.5 regardless of the initial pH. Organic acid production lowered the pH of the medium during growth due to dissociation into $H^+$ ions. Additionally, consumption of ammonium (the sole nitrogen source) for growth also contributed to acidification of the medium due to $H^+$ release when incorporating ammonia. Thus, biomass production itself contributed to reaching the pH threshold. In the case of the lactate producer, for example, the high amount of lactate drove the majority of the pH decrease, allowing for only a small amount of biomass production before reaching the pH threshold. The generalist produced some acetate, as well, but to a much lesser degree, allowing for more biomass production. The lactate-exchanging consortium, however, did not accumulate any organic byproducts, allowing for more biomass production than either the producer or the generalist before reaching the pH threshold. Conversely, the acetate-exchanging consortium accumulated more organic acid than the generalist, which led to lower productivity. Furthermore, the interacting variables of the biomass yields/growth rates of producer and scavenger and the production/consumption rates of lactate, which influence the proportional contributions of $H^+$ to the medium, may be driving the different dynamics observed in the altered ratio conditions for the lactate-exchanging consortium (Figure 6.4, Supplemental Figure 6.S3). Although organic acid and biomass production and nitrogen content of biomass are known measurements, other cellular reactions consuming and producing protons prevented direct calculation of the relative proportions of $H^+$ contribution from the experimental data.

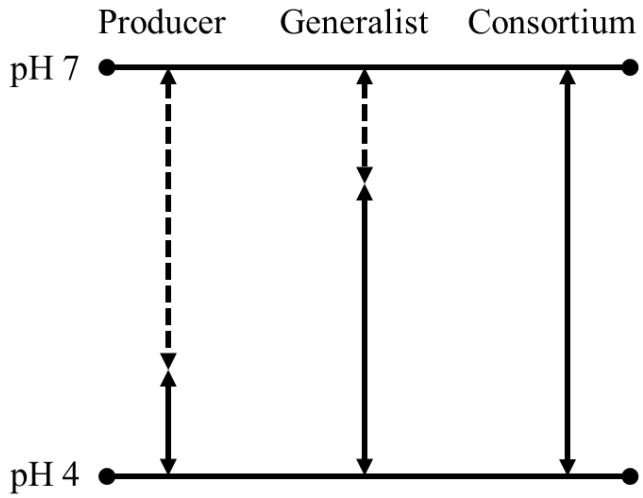


Figure 6.6. Conceptual rationale for higher biomass accumulation observed in lactate-exchanging consortium relative to generalist and producer. Dashed line represents acid production that contributes to pH reduction. Solid line represents reduction in pH due to ammonia consumption, which is required for biomass production. The consortium is able to produce more biomass before reaching the pH threshold due to re-consumption of organic acids by the scavenger.

### 6.5.2. Push/Pull System and the Influence of Growth and Production Rates

On a cellular basis, the difference in growth rates and production capacities of the acetate and lactate producers resulted in a “push” or “pull” system. The relatively faster growth rate of the acetate producer combined with the relatively slower growth rate of the scavenger on acetate resulted in a build-up of acetate which eventually toxified the consortium before the scavenger was able to consume it in a batch system. The producer, forming the dominant portion of the consortium, effectively “pushed” acetate on the scavenger. In contrast, the relatively slower growth rate of the lactate producer combined with the relatively faster growth rate of the scavenger on lactate resulted in a system where the scavenger “pulled” lactate from the producer. The initial build-up of lactate

was quickly depleted by the scavenger, which dominated the community by the end of batch growth.

### 6.5.3. Intersection of Maximum Power Principle and Resource Ratio Theory

The maximum power principle and resource ratio theory are two complementary ecological theories describing community structure. Maximum power principle relates the ability of species to consume energy to community arrangement (e.g. greater power consumption is more competitive, and the system will be arranged according to power consumption by the community rather than by an individual species). Resource ratio theory relates instead to the ability of species to most effectively consume limiting resources; thus, affinity for scarce nutrients plays a large role in determining the outcome of competition according to resource ratio theory. Relatively few rigorous empirical studies on these theories have been performed in microbial communities, in particular with regard to the maximum power principle. Cai et al. (Cai, Montague et al. 2006) examined adaptation of aquatic microcosms where energy was defined as light input, and DeLong (DeLong 2008) estimated metabolic rates of bacteria-feeding protozoa from previously published studies and examined maximum power principle predictions; however, the authors could not find any existing studies using defined substrate consumption and byproduct production rates to quantify the energetics of the maximum power principle.

Based on the analysis of substrate uptake and growth rates among the generalist, producer, and consortia systems in the current work, it was found that power acquisition

alone (measured in terms of glucose consumption rate) was not the best measure for system fitness, as the producers, which had the highest glucose consumption rate, also showed the lowest biomass productivity. However, when power channeled directly into biomass was accounted for by subtracting this quantity from the power consumed in glucose, this formulation was an accurate reflection of the biomass productivity observed in the systems, with the lactate-exchanging consortium showing less power diverted to other channels than the generalist or producer. The maximum power principle is then suggested to operate according to efficiency of power utilization rather than mere power acquisition itself. In conjunction with the consortia interpretation by the maximum power principle, the improved efficiency of the lactate-exchanging consortium is also supported by resource ratio theory. As an alternative to the classic competitive exclusion principle, it has been proposed that cooperating populations can exchange resources that they are each capable of utilizing more efficiently and thereby more completely deplete total resources to inhabit niches that are unavailable to either population on its own (de Mazancourt and Schwartz 2010). In the current work, the lactate-exchanging consortium was able to drive resource concentration lower than the generalist (more total glucose is consumed) (Supplemental Table 6.S1), making it a “super-competitor unit” (de Mazancourt and Schwartz 2010) in comparison to the metabolic generalist.

The presented work demonstrates the usefulness of synthetically designed consortia to study microbial interactions and uncover principles behind organizational structures of microbial communities, such as metabolic specialization and division of labor. The experimental data obtained are also integrated with ecological theories, and the

synthetic consortia are used to interpret possible evolutionary outcomes in natural systems. In application to industrial bioprocess, this study highlights the importance of the kinetic properties of microorganisms when designing consortia, as well as the influence of the initial proportion of populations on the system trajectory. There is much room to continue exploring the design of synthetic communities, extending to more complex arrangements and multiple partnerships and types of interactions. Additionally, the incorporation of ecological theory adds a rich dimension of the rationale behind microbial community organization that will continue to inform our understanding of natural microbial processes as well as application and engineering of microbial processes in industry.

## 6.6. Supplemental Figures and Tables

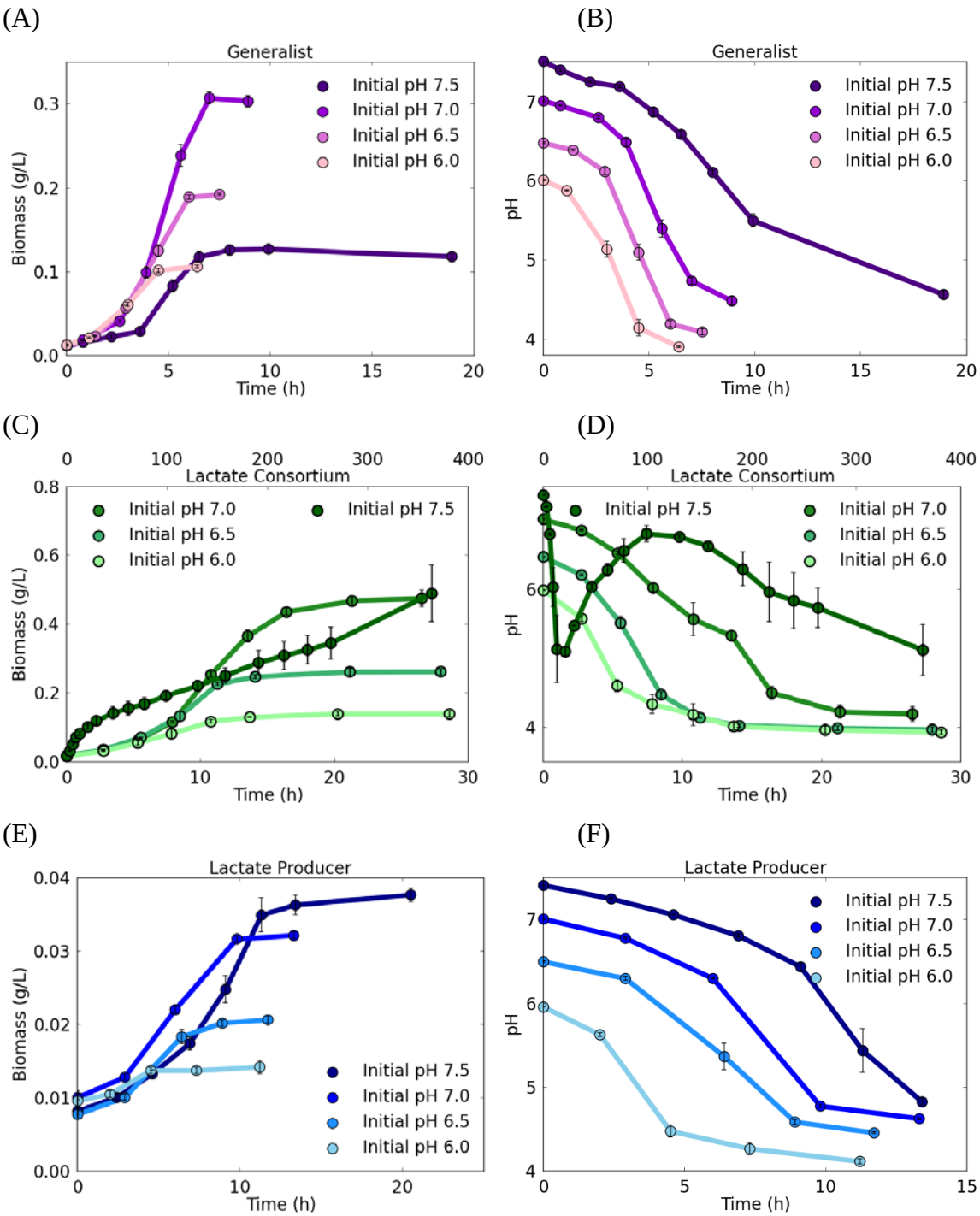

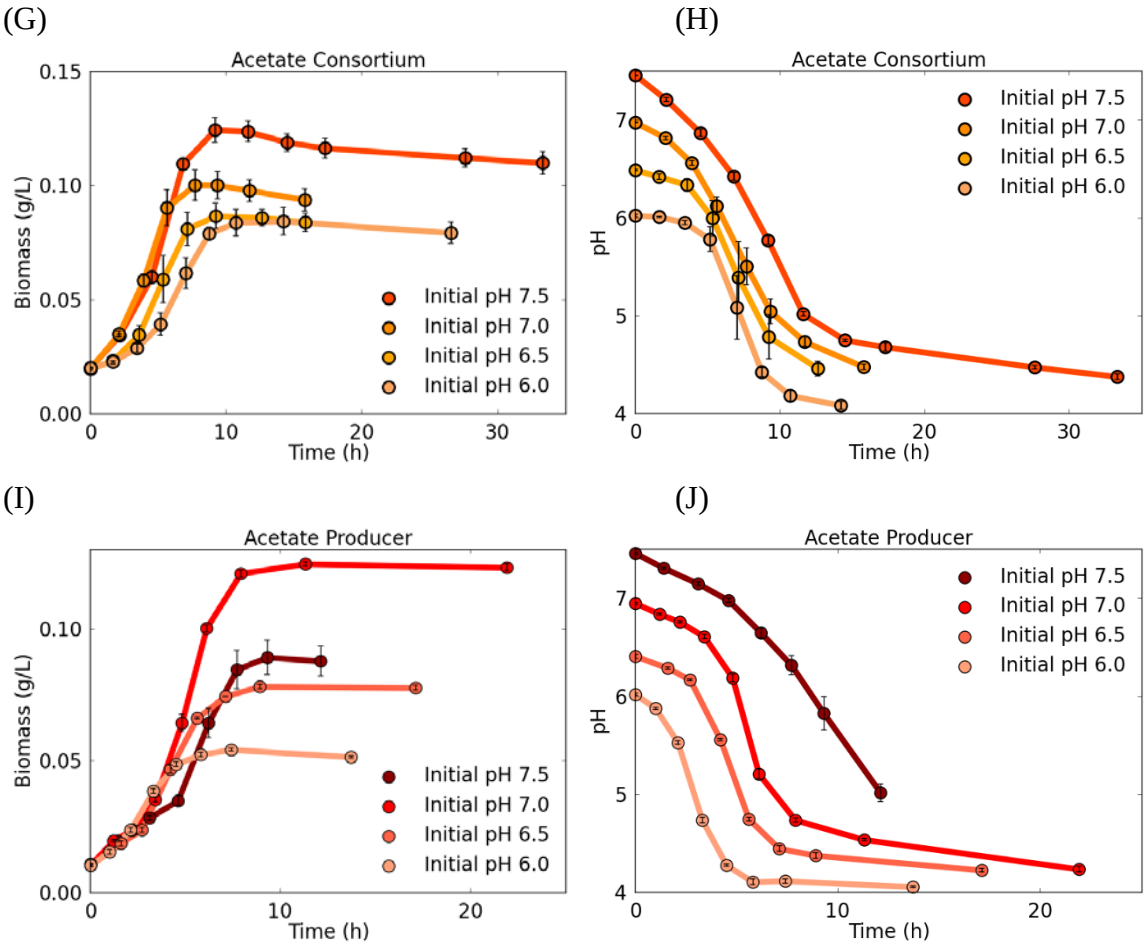


Supplemental Figure 6.S1. Biomass accumulation and pH profiles over time at varying initial pH conditions for the generalist (A-B), lactate-exchanging consortium (C-D), lactate producer (E-F), acetate-exchanging consortium (G-H), and acetate producer (I-J). The secondary x-axis in (C-D) indicates the time scale for the initial pH 7.5 condition.

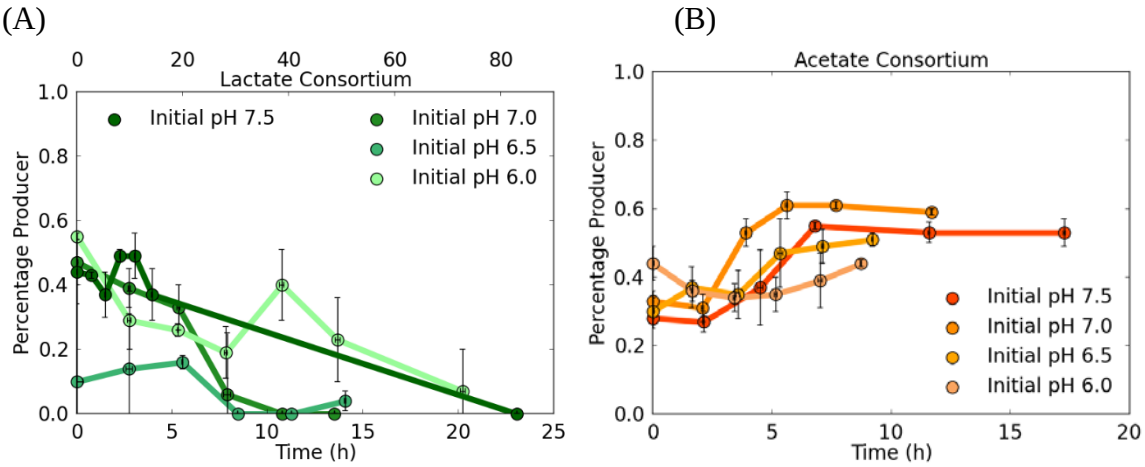


Supplemental Figure 6.S2. Fraction of producer in the lactate- (A) and acetate-exchanging consortia (B) under different initial pH conditions. (Graphs can be viewed as representing the fraction of producer below the curve and the fraction of scavenger above the curve.) The secondary x-axis in (A) indicates the time scale for the initial pH 7.5 condition.

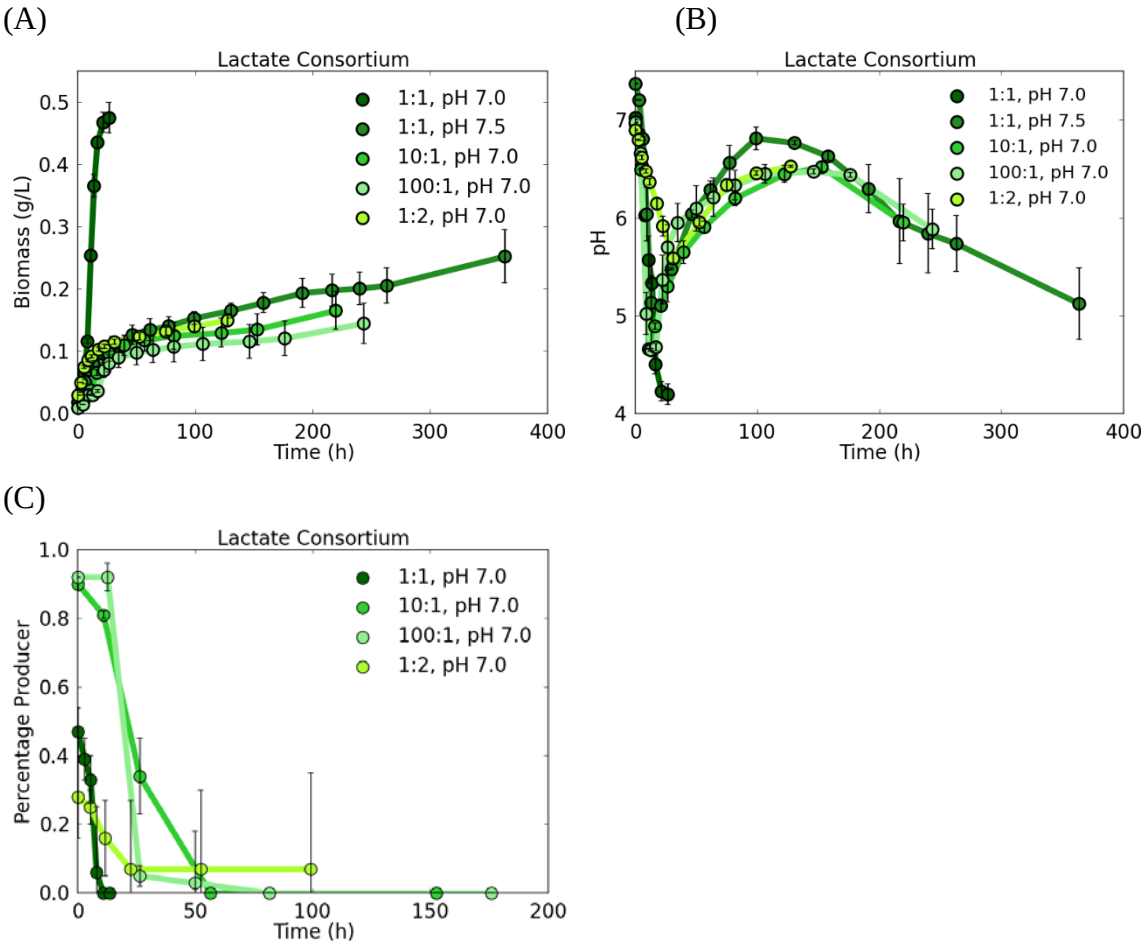


Supplemental Figure 6.S3. Biomass accumulation (A), pH profiles (B), and fraction of producer (C) in lactate-exchanging consortium at high initial pH 7.5 and altered producer to scavenger ratios.

Supplemental Table 6.S1. Measurements, calculated rates, and yields across varied initial pH conditions for generalist, producers, and consortia. Rates and yields are calculated over exponential growth phase.

| pH | Generalist | | Lactate Producer | | Lactate Consortium | | Acetate Producer | | Acetate Consortium | |
|---|---|---|---|---|---|---|---|---|---|---|
| **Average growth rate ($h^{-1}$)** | | | | | | | | | | |
| **7.5** | 0.37 | (0.01) | 0.14 | (0.01) | 0.15 | (0.00) | 0.23 | (0.02) | 0.25 | (0.00) |
| **7.0** | 0.53 | (0.01) | 0.13 | (0.01) | 0.22 | (0.01) | 0.34 | (0.01) | 0.27 | (0.01) |
| **6.5** | 0.45 | (0.00) | 0.17 | (0.00) | 0.21 | (0.01) | 0.33 | (0.01) | 0.23 | (0.01) |
| **6.0** | 0.46 | (0.01) | 0.11 | (0.00) | 0.16 | (0.00) | 0.33 | (0.01) | 0.18 | (0.00) |
| **Biomass yield (g CDW produced (g glucose consumed)$^{-1}$)** | | | | | | | | | | |
| **7.5** | 0.32 | (0.08) | 0.05 | (0.01) | 0.23 | (0.13) | 0.18 | (0.02) | 0.33 | (0.19) |
| **7.0** | 0.42 | (0.03) | 0.07 | (0.04) | 0.34 | (0.04) | 0.18 | (0.01) | 0.40 | (0.21) |
| **6.5** | 0.39 | (0.01) | 0.07 | (0.04) | 0.29 | (0.02) | 0.14 | (0.01) | 0.22 | (0.02) |
| **6.0** | 0.56 | (0.31) | 0.01 | | 0.40 | (0.06) | 0.23 | (0.01) | 0.26 | (0.03) |
| **Substrate consumption rate (mmol glucose (g CDW produced)$^{-1}$ $h^{-1}$)** | | | | | | | | | | |
| **7.5** | 6.70 | (1.46) | 14.96 | (3.68) | 4.13 | (1.87) | 7.32 | (0.76) | 4.96 | (2.20) |
| **7.0** | 6.99 | (0.60) | 12.70 | (5.27) | 3.63 | (0.45) | 10.59 | (0.97) | 4.36 | (1.92) |
| **6.5** | 6.44 | (0.16) | 19.47 | (16.89) | 4.05 | (0.33) | 13.43 | (0.81) | 5.80 | (0.68) |
| **6.0** | 5.60 | (2.73) | 55.63 | | 2.21 | (0.27) | 7.94 | (0.71) | 3.90 | (0.34) |
| **Product production rate (mmol product produced (g CDW produced)$^{-1}$ $h^{-1}$)** | | | | | | | | | | |
| **7.5** | 7.04 | (0.24) | 25.84 | (0.45) | 10.88 | (2.42) | 9.41 | (0.73) | 7.42 | (0.25) |
| **7.0** | 3.60 | (0.13) | 24.57 | (0.79) | NA | NA | 13.21 | (0.84) | 8.63 | (0.33) |
| **6.5** | 3.75 | (0.13) | 28.68 | (1.17) | NA | NA | 10.63 | (0.33) | 5.74 | (0.78) |
| **6.0** | 3.46 | (0.13) | 21.22 | (1.00) | NA | NA | 8.87 | (0.24) | 2.68 | (0.64) |
| **Product/biomass selectivity (g product produced (g CDW produced)$^{-1}$)** | | | | | | | | | | |
| **7.5** | 1.13 | (0.02) | 16.79 | (0.43) | 6.84 | (1.56) | 2.38 | (0.04) | 1.77 | (0.08) |
| **7.0** | 0.40 | (0.02) | 17.16 | (0.20) | NA | NA | 2.28 | (0.06) | 1.91 | (0.09) |
| **6.5** | 0.49 | (0.02) | 15.06 | (0.77) | NA | NA | 1.91 | (0.02) | 1.45 | (0.16) |
| **6.0** | 0.44 | (0.02) | 17.07 | | NA | NA | 1.58 | (0.06) | 0.87 | (0.23) |
| **Product yield (g product produced (g glucose consumed)$^{-1}$)** | | | | | | | | | | |
| **7.5** | 0.36 | (0.10) | 0.89 | (0.19) | 1.45 | (0.45) | 0.42 | (0.03) | 0.60 | (0.36) |
| **7.0** | 0.17 | (0.02) | 1.15 | (0.66) | NA | NA | 0.41 | (0.02) | 0.78 | (0.45) |
| **6.5** | 0.19 | (0.01) | 1.13 | (0.68) | NA | NA | 0.26 | (0.02) | 0.32 | (0.02) |
| **6.0** | 0.24 | (0.12) | 0.18 | | NA | NA | 0.37 | (0.03) | 0.23 | (0.05) |
| **Total glucose consumed (mmol glucose consumed)** | | | | | | | | | | |
| **7.5** | 1.86 | (0.44) | 2.71 | (0.78) | 12.42 | (1.98) | 2.03 | (0.27) | 1.50 | (0.67) |
| **7.0** | 2.89 | (0.35) | 1.85 | (0.78) | 5.38 | (0.80) | 2.48 | (0.18) | 0.92 | (0.44) |
| **6.5** | 2.37 | (0.03) | 0.90 | (0.75) | 3.61 | (0.26) | 1.93 | (0.14) | 1.44 | (0.26) |
| **6.0** | 0.98 | (0.51) | 1.67 | | 1.19 | (0.18) | 0.79 | (0.05) | 1.20 | (0.11) |

| | | | | | | | | | | |
|---|---|---|---|---|---|---|---|---|---|---|
| **Maximum biomass concentration (g CDW $L^{-1}$)** | | | | | | | | | | |
| **7.5** | 0.13 | (0.01) | 0.04 | (0.00) | 0.25 | (0.04) | 0.09 | (0.01) | 0.12 | (0.00) |
| **7.0** | 0.31 | (0.01) | 0.03 | (0.00) | 0.48 | (0.02) | 0.12 | (0.00) | 0.10 | (0.01) |
| **6.5** | 0.19 | (0.00) | 0.02 | (0.00) | 0.26 | (0.01) | 0.08 | (0.00) | 0.09 | (0.01) |
| **6.0** | 0.11 | (0.00) | 0.01 | (0.00) | 0.14 | (0.01) | 0.05 | (0.00) | 0.08 | (0.01) |
| **Biomass yield per net H+ produced (g CDW (mol $H^+$)$^{-1}$)** | | | | | | | | | | |
| **7.5** | 1.26 | (0.04) | 0.14 | (0.01) | 0.42 | (0.12) | 0.65 | (0.03) | 0.96 | (0.03) |
| **7.0** | 1.43 | (0.06) | 0.09 | (0.00) | 2.16 | (0.02) | 0.49 | (0.01) | 0.79 | (0.01) |
| **6.5** | 0.76 | (0.01) | 0.09 | (0.01) | 0.91 | (0.01) | 0.31 | (0.00) | 0.60 | (0.16) |
| **6.0** | 0.46 | (0.02) | 0.03 | (0.00) | 0.61 | (0.05) | 0.21 | (0.00) | 0.35 | (0.03) |

# CHAPTER SEVEN

# EPILOGUE

## 7.1. Synopsis

This dissertation employs a broad suite of methodological approaches across natural and synthetic systems to investigate foundational principles of microbial community interactions, focusing on metabolic acclimation to environmental stress. The interconnected themes of metabolite exchange and relief of byproduct inhibition were found to be two important underpinnings of interspecies interactions in both the natural and the synthetic systems studied. The thermophilic cyanobacterium *Thermosynechococcus elongatus* BP-1 was predicted to use byproduct secretion as a metabolic acclimation strategy in response to high light and oxygen conditions, two common stresses associated with photoautotrophs. Additionally, heterotrophic partners were predicted to occupy a niche for growth using the organic byproducts as carbon and energy sources, as well as consuming photosynthetically produced oxygen for respiration, thereby relieving oxygen inhibition for the cyanobacteria. Paralleling the photoautotrophic primary producer system, synthetic microbial consortia of genetically engineered producer and scavenger *Escherichia coli* strains examined the benefits of metabolic specialization, metabolite exchange, and byproduct detoxification. When producer and scavenger strains with complementary kinetic capabilities (production, consumption, and growth rates) were paired, the consortia demonstrated enhanced growth over the metabolic generalist. The physiological capabilities of *E. coli* were also

investigated in greater detail to show conversion of lactate to acetate under aerobic conditions. Further, application of the maximum power principle provided a framework with which to analyze the energetics of the system.

## 7.2. *In Silico* Modeling

Stoichiometric metabolic network modeling permits detailed exploration of complex microbial systems where little experimental data may be available, using only genomic or metagenomic information. Elementary flux mode analysis enumerates all (simplest) possible network pathways, and the physiological space can subsequently be analyzed according to ecologically relevant variables. Resource investment considering nutrients of interest can be applied (e.g. nitrogen or iron), and efficiencies of growth or desired metabolite production can be computed. As in Chapter Four, predictions regarding possible interactions with other species can be made even without the construction of a second model (e.g. relative amount of heterotroph supported), though the field is working toward community model analysis (Zomorrodi and Maranas 2012, Zomorrodi, Islam et al. 2014). In fact, recent computational work pairing *T. elongatus* BP-1 with the aerobic heterotroph *Meiothermus ruber* str. A has begun to examine interspecies interactions in this co-culture (Henry, Bernstein et al. 2016). As the number of computational models published in the literature continues to increase, calls for attention to standards in modeling rigor are aptly suited (Ravikrishnan and Raman 2015), and the detailed methodological description of how to convert experimental measurements into a model biomass reaction in Chapter Three seeks to address this need.

Additionally, the importance of understanding the biochemistry of underlying metabolic reactions in a model as well as the particular physiology of the organism being studied, rather than relying solely on automated model building tools, cannot be over-emphasized.

## 7.3. *In Vitro* Laboratory Studies

The macromolecular biomass composition methods detailed in Chapter Three provide important parameters for *in silico* models, as specific procedural details are often not included in the literature. Integration of experimental data with *in silico* modeling should be continued and expanded. Computational methods for integration of large omics data sets with models is in the forefront of the literature (Hyduke, Lewis et al. 2013). To achieve this goal in Chapter Four, transcriptomics and photobioreactor data were used in conjunction with metabolic modeling to verify model predictions.

Engineering microbial community interactions through synthetic ecology is also on the forefront of research in microbial ecology. Interacting consortia can be engineered artificially by co-culturing individual organisms with different physiological capabilities for a desired result or can also be engineered via genetic manipulations, as was used in Chapter Six. This approach maintains a constant genetic basis across the consortium and thus eliminates regulatory issues or quorum sensing responses to different species; instead, desired gene pools are partitioned into different populations to obtain the resulting functionality. However, it remains important to carefully consider the design and intended outcome of synthetic consortia to ensure that findings are indeed relevant and can be extrapolated to natural microbial communities (Yu, Krause et al. 2016).

## 7.4. Ecological Theory

Ecological theory is important for explanation of why microbial communities exhibit a particular function; a theoretical framework lends credence and rationale to observations of the functions themselves and/or the mechanisms (Prosser, Bohannan et al. 2007). With regard to resource cost-based analysis for *in silico* modeling, efficiency of growth under light and oxygen stress provided a good correlation with the experimental data; however, this assumption may not be valid for every scenario depending upon the organism and type of environment being modeled. For example, energy or a certain limiting nutrient may play a greater role in determining metabolic acclimations.

The synthetic ecology study in Chapter Six illuminated different ways that the maximum power principle may be interpreted and provides insight into assessing the interpretations. Power acquisition alone may not be enough to determine the outcome of the system, as was seen in the result of producers having the highest power acquisition, yet inhibition from byproduct accumulation prohibited them from having the most effective growth. When system power was analyzed according to utilization by subtracting the rate of energy storage in biomass, the net power of the systems reflected the trends in growth observed among the producers, consortia, and generalist, e.g. the lactate-exchanging consortium, which accumulated the highest biomass, also utilized power the most efficiently.

## 7.5. Future Directions

A variety of directions exists for future studies to extend the work presented in this dissertation, in addition to some of the broader ideas mentioned in the three previous sections. Regarding the thermophilic cyanobacterial system in Chapter Four, further exploration of the role of oxygen stress will elucidate the role and impact of the heterotroph in the system. Further experiments to complement the modeling predictions of oxygen consumption by aerobic respiration on the part of the heterotroph will quantify the benefit of byproduct detoxification on the overall productivity of the cyanobacteria.

Regarding the genetically engineered organic acid-exchanging consortia, the influence of initial producer to scavenger ratio warrants further exploration, as well as the type of culturing environment. Culturing in a steady state environment like a chemostat will provide more insight into the optimal carrying capacity of the populations, stability of the interactions, and robustness to perturbations. Additionally, a biofilm environment, in which the effects of the organic acid byproduct are intensified due to spatial constraints and lower diffusion rates, will provide another way to examine the effect of byproduct detoxification and may show different effects between lactic and acetic acids than planktonic conditions. Initial work developing an ordinary differential equation-based model to describe the growth kinetics of the two populations is already underway and can be used to explore system dynamics *in silico* and to specifically probe the source of $H^+$ acidifying the medium (organic acid production or ammonium consumption). Finally, future work designing a system where the nitrogen source is less likely to contribute to

acidification, e.g. nitrate, will provide more direct experimental measurements by removing the substantial effect of biomass production on pH change.

## 7.6. Concluding Statement

Microbial community interactions form the basis of most ecological processes and are also extremely important in industry. Environmental stress plays a critical role in metabolic acclimation, drives microbial community structure, and furthermore shows the dependencies or co-dependencies different populations may have. Integration of *in silico* modeling, *in vitro* laboratory data, and ecological theory provides a template for impactful research and highlights the multi-faceted aspects of the story of microbial interactions. Lastly, as we seek to understand how microbial communities work, how they impact the world, and how we impact them, let us use our knowledge wisely, with respect, and to do good rather than simply exploit for our own benefit.

## 7.7. Additional Publications

Additional works in concert with this dissertation, but not included as individual chapters, are found in the following citations:

Schepens, D., Beck, A. E., Heys, J. J., Gedeon, T., & Carlson, R. P. (2017). The benefits of resource partitioning and division of labor in microbial consortia. In P. Amar, F. Kepes, & V. Norris (Eds.), *Advances in systems and synthetic biology* (pp. 137-148). EDP Sciences Publishing.

Carlson, R. P., Beck, A. E., Phalak, P., Fields, M. W., Gedeon, T., Hanley, L., Harcombe, W. R., Henson, M. A., & Heys, J. J. Competitive resource allocation to metabolic pathways contributes to overflow metabolisms and emergent properties in cross-feeding consortia. *Biochemical Society Transactions*, 2018. DOI: 10.1042/BST20170242

Schepens, D., Carlson, R. P., Heys, J. J., Beck, A. E., & Gedeon, T. Role of resource allocation and transport in emergence of cross-feeding in microbial consortia. Prepared for submission to *PLoS Computational Biology*.

# REFERENCES CITED

Abed, R. M. M., S. Dobretsov and K. Sudesh (2009). "Applications of cyanobacteria in biotechnology." Journal of Applied Microbiology **106**(1): 1-12.

Agrawal, A. A. (2001). "Phenotypic plasticity in the interactions and evolution of species." Science **294**(5541): 321-326.

Alakomi, H. L., E. Skytta, M. Saarela, T. Mattila-Sandholm, K. Latva-Kala and I. M. Helander (2000). "Lactic acid permeabilizes gram-negative bacteria by disrupting the outer membrane." Applied and Environmental Microbiology **66**(5): 2001-2005.

Archanaa, S., S. Moise and G. K. Suraishkumar (2012). "Chlorophyll interference in microalgal lipid quantification through the Bligh and Dyer method." Biomass & Bioenergy **46**: 805-808.

ASTM E1758-01, Standard method for the determination of carbohydrates by HPLC. 2003 Annual Book of ASTM Standards. Philadelphia, PA, American Society for Testing and Materials, International. **11.05**.

Ausubel, F. M., R. Brent, R. E. Kingston, D. D. Moore, J. G. Seidman, J. A. Smith and K. Struhl, Eds. (1992). Short Protocols in Molecular Biology. New York, Greene Publishing Associates and John Wiley & Sons.

Bader, J., E. Mast-Gerlach, M. Popović, R. Bajpai and U. Stahl (2010). "Relevance of microbial coculture fermentations in biotechnology." Journal of applied microbiology **109**(2): 371-387.

Bailey, S. and A. Grossman (2008). "Photoprotection in cyanobacteria: Regulation of light harvesting." Photochemistry and Photobiology **84**(6): 1410-1420.

Bateson, M. M. and D. M. Ward (1988). "Photoexcretion and fate of glycolate in a hot-spring cyanobacterial mat." Applied and Environmental Microbiology **54**(7): 1738-1743.

Beck, A. E., K. A. Hunt, H. C. Bernstein and R. P. Carlson (2016). Interpreting and designing microbial communities for bioprocess applications, from components to interactions to emergent properties. Biotechnology for biofuel production and optimization. C. E. Eckert and C. T. Trinh. Amsterdam, Elsevier**:** 407-432.

Beck, C., H. Knoop, I. M. Axmann and R. Steuer (2012). "The diversity of cyanobacterial metabolism: Genome analysis of multiple phototrophic microorganisms." BMC Genomics **13**.

Beliaev, A. S., M. F. Romine, M. Serres, H. C. Bernstein, B. E. Linggi, L. M. Markillie, N. G. Isern, W. B. Chrisler, L. A. Kucek, E. A. Hill, G. E. Pinchuk, D. A. Bryant, H. S. Wiley, J. K. Fredrickson and A. Konopka (2014). "Inference of interactions in cyanobacterial-heterotrophic co-cultures via transcriptome sequencing." ISME Journal **8**(11): 2243-2255.

Benthin, S., J. Nielsen and J. Villadsen (1991). "A simple and reliable method for the determination of cellular RNA content." Biotechnology Techniques **5**(1): 39-42.

Bernstein, H. C. and R. P. Carlson (2012). "Microbial consortia engineering for cellular factories: In vitro to in silico systems." Computational and Structural Biotechnology Journal **3**(4).

Bernstein, H. C. and R. P. Carlson (2014). Design, Construction, and Characterization Methodologies for Synthetic Microbial Consortia. Engineering and Analyzing Multicellular Systems: Methods and Protocols. L. Sun and W. Shou. **1151:** 49-68.

Bernstein, H. C., M. Kesaano, K. Moll, T. Smith, R. Gerlach, R. P. Carlson, C. D. Miller, B. M. Peyton, K. E. Cooksey, R. D. Gardner and R. C. Sims (2014). "Direct measurement and characterization of active photosynthesis zones inside wastewater remediating and biofuel producing microalgal biofilms." Bioresource Technology **156**: 206-215.

Bernstein, H. C., R. S. McClure, E. A. Hill, L. M. Markillie, W. B. Chrisler, M. F. Romine, J. E. McDermott, M. C. Posewitz, D. A. Bryant, A. E. Konopka, J. K. Fredrickson and A. S. Beliaev (2016). "Unlocking the constraints of cyanobacterial productivity: Acclimations enabling ultrafast growth." Mbio **7**(4).

Bernstein, H. C., R. S. McClure, V. Thiel, N. C. Sadler, Y. M. Kim, W. B. Chrisler, E. A. Hill, D. A. Bryant, M. F. Romine, J. K. Jansson, J. K. Fredrickson and A. S. Beliaev (2017). "Indirect interspecies regulation; transcriptional and physiological responses of a cyanobacterium to heterotrophic partnership." mSystems **2**(2): e00181-00116.

Bernstein, H. C., S. D. Paulson and R. P. Carlson (2012). "Synthetic *Escherichia coli* consortia engineered for syntrophy demonstrate enhanced biomass productivity." Journal of Biotechnology **157**(1): 159-166.

Bettenbrock, K., S. Fischer, A. Kremling, K. Jahreis, T. Sauter and E. D. Gilles (2006). "A quantitative approach to catabolite repression in *Escherichia coli*." Journal of Biological Chemistry **281**(5): 2578-2584.

Bizukojc, M., D. Dietz, J. Sun and A.-P. Zeng (2010). "Metabolic modelling of syntrophic-like growth of a 1, 3-propanediol producer, *Clostridium butyricum*, and a methanogenic archeon, *Methanosarcina mazei*, under anaerobic conditions." Bioprocess and biosystems engineering **33**(4): 507-523.

Bligh, E. G. and W. J. Dyer (1959). "A rapid method of total lipid extraction and purification." Canadian Journal of Biochemistry and Physiology **37**(8): 911-917.

Bond, T. and M. R. Templeton (2011). "History and future of domestic biogas plants in the developing world." Energy for Sustainable Development **15**(4): 347-354.

Brauer, V. S., M. Stomp and J. Huisman (2012). "The nutrient-load hypothesis: Patterns of resource limitation and community structure driven by competition for nutrients and light." The American Naturalist **179**(6): 721-740.

Bremer, H. and P. P. Dennis (1996). "Modulation of chemical composition and other parameters of the cell by growth rate." *Escherichia coli* and *Salmonella*: Cellular and molecular biology **2**(2): 1553-1569.

Brenner, K., L. C. You and F. H. Arnold (2008). "Engineering microbial consortia: A new frontier in synthetic biology." Trends in Biotechnology **26**(9): 483-489.

Brune, K. D. and T. Bayer (2012). "Engineering microbial consortia to enhance biomining and bioremediation." Frontiers in microbiology **3**: 203.

Bryant, D. A., Z. Liu, T. Li, F. Zhao, A. M. G. Costas, C. G. Klatt, D. M. Ward, N.-U. Frigaard and J. Overmann (2012). Comparative and functional genomics of anoxygenic green bacteria from the taxa *Chlorobi*, *Chloroflexi*, and *Acidobacteria*. Functional genomics and evolution of photosynthetic systems, Springer**:** 47-102.

Bull, A. T. (2010). "The renaissance of continuous culture in the post-genomics age." Journal of industrial microbiology & biotechnology **37**(10): 993-1021.

Bullerjahn, G. S. and A. F. Post (2014). "Physiology and molecular biology of aquatic cyanobacteria." Frontiers in Microbiology **5**.

Burton, K. (1956). "Study of the conditions and mechanism of the diphenylamine reaction for the colorimetric estimation of deoxyribonucleic acid." Biochemical Journal **62**(2): 315-323.

Cai, T. T., C. L. Montague and J. S. Davis (2006). "The maximum power principle: An empirical investigation." Ecological Modelling **190**(3-4): 317-335.

Cankorur-Cetinkaya, A., D. Dikicioglu and S. G. Oliver (2017). "Metabolic modeling to identify engineering targets for *Komagataella phaffii*: The effect of biomass composition on gene target identification." Biotechnology and Bioengineering **114**(11): 2605-2615.

Carlson, R. and F. Srienc (2004). "Fundamental *Escherichia coli* biochemical pathways for biomass and energy production: Creation of overall flux states." Biotechnology and Bioengineering **86**(2): 149-162.

Carlson, R. and F. Srienc (2004). "Fundamental *Escherichia coli* biochemical pathways for biomass and energy production: Identification of reactions." Biotechnology and Bioengineering **85**(1): 1-19.

Carlson, R. P. (2007). "Metabolic systems cost-benefit analysis for interpreting network structure and regulation." Bioinformatics **23**(10): 1258-1264.

Carlson, R. P. (2009). "Decomposition of complex microbial behaviors into resource-based stress responses." Bioinformatics **25**(1): 90-97.

Carlson, R. P., A. E. Beck, P. Phalak, M. W. Fields, T. Gedeon, L. Hanley, W. R. Harcombe, M. A. Henson and J. J. Heys (2018). "Competitive resource allocation to metabolic pathways contributes to overflow metabolisms and emergent properties in cross feeding consortia." Biochemical Society Transactions **In Press.**

Carlson, R. P., O. J. Oshota and R. L. Taffs (2012). Systems analysis of microbial adaptations to simultaneous stresses. Reprogramming Microbial Metabolic Pathways. X. Wang, J. Chen and P. Quinn. Netherlands, Springer**:** 139-157.

Carlson, R. P. and R. L. Taffs (2010). "Molecular-level tradeoffs and metabolic adaptation to simultaneous stressors." Current Opinion in Biotechnology **21**(5): 670-676.

Carlton, R. G. and L. L. Richardson (1995). "Oxygen and sulfide dynamics in a horizontally migrating cyanobacterial mat: black band disease of corals." FEMS Microbiology Ecology **18**(2): 155-162.

Carnicer, M., K. Baumann, I. Toplitz, F. Sanchez-Ferrando, D. Mattanovich, P. Ferrer and J. Albiol (2009). "Macromolecular and elemental composition analysis and extracellular metabolite balances of *Pichia pastoris* growing at different oxygen levels." Microbial Cell Factories **8**.

Caspi, R., R. Billington, L. Ferrer, H. Foerster, C. A. Fulcher, I. M. Keseler, A. Kothari, M. Krummenacker, M. Latendresse, L. A. Mueller, Q. Ong, S. Paley, P. Subhraveti, D. S. Weaver and P. D. Karp (2016). "The MetaCyc database of metabolic pathways and enzymes and the BioCyc collection of pathway/genome databases." Nucleic Acids Research **44**(D1): D471-D480.

Causey, T. B., S. Zhou, K. T. Shanmugam and L. O. Ingram (2003). "Engineering the metabolism of *Escherichia coli* W3110 for the conversion of sugar to redox-neutral and oxidized products: Homoacetate production." Proceedings of the National Academy of Sciences of the United States of America **100**(3): 825-832.

Chaplin, M. F. (1986). Carbohydrate Analysis: A Practical Approach. Washington, D.C., IRL Press.

Cheng, Y. F., J. E. Edwards, G. G. Allison, W.-Y. Zhu and M. K. Theodorou (2009). "Diversity and activity of enriched ruminal cultures of anaerobic fungi and methanogens grown together on lignocellulose in consecutive batch culture." Bioresource technology **100**(20): 4821-4828.

Chun, A. Y., L. Yunxiao, S. Ashok, E. Seol and S. Park (2014). "Elucidation of toxicity of organic acids inhibiting growth of *Escherichia coli* W." Biotechnology and Bioprocess Engineering **19**(5): 858-865.

Cole, J. K., J. R. Hutchison, R. S. Renslow, Y. M. Kim, W. B. Chrisler, H. E. Engelmann, A. C. Dohnalkova, D. H. Hu, T. O. Metz, J. K. Fredrickson and S. R. Lindemann (2014). "Phototrophic biofilm assembly in microbial-mat-derived unicyanobacterial consortia: Model systems for the study of autotroph-heterotroph interactions." Frontiers in Microbiology **5**.

D'Onofrio, A., J. M. Crawford, E. J. Stewart, K. Witt, E. Gavrish, S. Epstein, J. Clardy and K. Lewis (2010). "Siderophores from neighboring organisms promote the growth of uncultured bacteria." Chemistry & biology **17**(3): 254-264.

De Lorenzo, V., J. L. Martínez and C. Asensio (1984). "Microcin-mediated interactions between *Klebsiella pneumoniae* and *Escherichia coli* strains." Microbiology **130**(2): 391-400.

de Mazancourt, C. and M. W. Schwartz (2010). "A resource ratio theory of cooperation." Ecology Letters **13**(3): 349-359.

De Mey, M., G. Lequeux, J. Maertens, S. De Maeseneire, W. Soetaert and E. Vandamme (2006). "Comparison of DNA and RNA quantification methods suitable for parameter estimation in metabolic modeling of microorganisms." Analytical Biochemistry **353**(2): 198-203.

De Roy, K., M. Marzorati, P. Van den Abbeele, T. Van de Wiele and N. Boon (2014). "Synthetic microbial ecosystems: An exciting tool to understand and apply microbial communities." Environmental microbiology **16**(6): 1472-1481.

Decho, A. W., R. S. Norman and P. T. Visscher (2010). "Quorum sensing in natural environments: Emerging views from microbial mats." Trends in microbiology **18**(2): 73-80.

Dekel, E. and U. Alon (2005). "Optimality and evolutionary tuning of the expression level of a protein." Nature **436**(7050): 588.

Del Don, C., K. W. Hanselmann, R. Peduzzi and R. Bachofen (1994). "Biomass composition and methods for the determination of metabolic reserve polymers in phototrophic sulfur." Aquatic Sciences **56**(1): 1-15.

DeLong, J. P. (2008). "The maximum power principle predicts the outcomes of two-species competition experiments." Oikos **117**(9): 1329-1336.

Deutscher, J. (2008). "The mechanisms of carbon catabolite repression in bacteria." Current Opinion in Microbiology **11**(2): 87-93.

Dittrich, C. R., G. N. Bennett and K. Y. San (2005). "Characterization of the acetate-producing pathways in *Escherichia coli*." Biotechnology Progress **21**(4): 1062-1067.

Dobell, C. (1932). Antony van Leeuwenhoek and his "Little Animals." Being some account of the father of protozoology and bacteriology and his multifarious discoveries in these disciplines. London, John Bale, Sons & Danielsson, Ltd.

Doelle, H. W., K. N. Ewings and N. W. Hollywood (1982). Regulation of glucose metabolism in bacterial systems. Microbial Reactions, Springer**:** 1-35.

Downs, T. R. and W. W. Wilfinger (1983). "Fluorometric quantification of DNA in cells and tissue." Analytical Biochemistry **131**(2): 538-547.

Dubois, M., K. A. Gilles, J. K. Hamilton, P. A. Rebers and F. Smith (1956). "Colorimetric method for determination of sugars and related substances." Analytical Chemistry **28**(3): 350-356.

Edwards, J. S., R. U. Ibarra and B. O. Palsson (2001). "In silico predictions of *Escherichia coli* metabolic capabilities are consistent with experimental data." Nature Biotechnology **19**(2): 125-130.

Edwards, J. S., R. Ramakrishna and B. O. Palsson (2002). "Characterizing the metabolic phenotype: A phenotype phase plane analysis." Biotechnology and bioengineering **77**(1): 27-36.

Eisenhut, M., W. Ruth, M. Haimovich, H. Bauwe, A. Kaplan and M. Hagemann (2008). "The photorespiratory glycolate metabolism is essential for cyanobacteria and might have been conveyed endosymbiontically to plants." Proceedings of the National Academy of Sciences of the United States of America **105**(44): 17199-17204.

Eiteman, M. A. and E. Altman (2006). "Overcoming acetate in *Escherichia coli* recombinant protein fermentations." Trends in Biotechnology **24**(11): 530-536.

Eiteman, M. A., S. A. Lee and E. Altman (2008). "A co-fermentation strategy to consume sugar mixtures effectively." Journal of Biological Engineering **2**(1): 3.

Elser, J. J., C. Acquisti and S. Kumar (2011). "Stoichiogenomics: The evolutionary ecology of macromolecular elemental composition." Trends in ecology & evolution **26**(1): 38-44.

Elser, J. J., M. E. S. Bracken, E. E. Cleland, D. S. Gruner, W. S. Harpole, H. Hillebrand, J. T. Ngai, E. W. Seabloom, J. B. Shurin and J. E. Smith (2007). "Global analysis of nitrogen and phosphorus limitation of primary producers in freshwater, marine and terrestrial ecosystems." Ecology Letters **10**(12): 1135-1142.

Enyeart, P. J., Z. B. Simpson and A. D. Ellington (2015). "A microbial model of economic trading and comparative advantage." Journal of theoretical biology **364**: 326-343.

Ernst, D., M. Greer, R. Akmatova, S. Pischke, H. Wedemeyer, H. Heiken, H. Tillmann, R. Schmidt and M. Stoll (2014). "Impact of GB virus C viraemia on clinical outcome in HIV-1-infected patients: A 20-year follow-up study." HIV medicine **15**(4): 245-250.

Espie, G. S. and M. S. Kimber (2011). "Carboxysomes: Cyanobacterial RubisCO comes in small packages." Photosynthesis Research **109**(1-3): 7-20.

Everroad, R. C., H. Otaki, K. Matsuura and S. Haruta (2012). "Diversification of bacterial community composition along a temperature gradient at a thermal spring." Microbes and Environments **27**(4): 374-381.

Fajardo, A. and J. L. Martínez (2008). "Antibiotics as signals that trigger specific bacterial responses." Current opinion in microbiology **11**(2): 161-167.

Falkowski, P. G. and J. A. Raven (2007). Aquatic Photosynthesis. Princeton, NJ, Princeton University Press.

Falony, G. and L. De Vuyst (2009). Ecological interactions of bacteria in the human gut. Prebiotics and Probiotics Science and Technology, Springer**:** 639-679.

Farmer, W. R. and J. C. Liao (1997). "Reduction of aerobic acetate production by *Escherichia coli*." Applied and Environmental Microbiology **63**(8): 3205-3210.

Farrand, S. G., C. W. Jones, J. D. Linton and R. J. Stephenson (1983). "The effect of temperature and pH on the growth efficiency of the thermoacidophilic bacterium *Bacillus acidocaldarius* in continuous culture." Archives of Microbiology **135**(4): 276-283.

Farrand, S. G., J. D. Linton, R. J. Stephenson and W. V. McCarthy (1983). "The use of response surface analysis to study the growth of *Bacillus acidocaldarius* throughout the growth range of temperature and pH." Archives of Microbiology **135**(4): 272-275.

Feist, A. M. and B. O. Palsson (2010). "The biomass objective function." Current Opinion in Microbiology **13**(3): 344-349.

Ferreira, M. T., A. S. Manso, P. Gaspar, M. G. Pinho and A. R. Neves (2013). "Effect of oxygen on glucose metabolism: Utilization of lactate in *Staphylococcus aureus* as revealed by in vivo NMR studies." PLoS ONE **8**(3).

Fischer, E. and U. Sauer (2003). "A novel metabolic cycle catalyzes glucose oxidation and anaplerosis in hungry *Escherichia coli*." Journal of Biological Chemistry **278**(47): 46446-46451.

Flamholz, A., E. Noor, A. Bar-Even, W. Liebermeister and R. Milo (2013). "Glycolytic strategy as a tradeoff between energy yield and protein cost." Proceedings of the National Academy of Sciences **110**(24): 10039-10044.

Flamholz, A., E. Noor, A. Bar-Even and R. Milo (2012). "eQuilibrator-the biochemical thermodynamics calculator." Nucleic Acids Research **40**(D1): D770-D775.

Florey, H. W. (1946). "The use of microorganisms for therapeutic purposes." Yale Journal of Biology and Medicine **19**(1): 101-&.

Folsom, J. P. and R. P. Carlson (2015). "Physiological, biomass elemental composition and proteomic analyses of *Escherichia coli* ammonium-limited chemostat growth, and comparison with iron- and glucose-limited chemostat growth." Microbiology **161**: 1659-1670.

Folsom, J. P., A. E. Parker and R. P. Carlson (2014). "Physiological and proteomic Analysis of *Escherichia coli* iron-limited chemostat growth." Journal of Bacteriology **196**(15): 2748-2761.

Fountoulakis, M. and H. W. Lahm (1998). "Hydrolysis and amino acid composition analysis of proteins." Journal of Chromatography A **826**(2): 109-134.

Fröstl, J. M. and J. Overmann (1998). "Physiology and tactic response of the phototrophic consortium "*Chlorochromatium aggregatum*"." Archives of microbiology **169**(2): 129-135.

Georgianna, D. R. and S. P. Mayfield (2012). "Exploiting diversity and synthetic biology for the production of algal biofuels." Nature **488**(7411): 329-335.

Germerodt, S., K. Bohl, A. Lück, S. Pande, A. Schröter, C. Kaleta, S. Schuster and C. Kost (2016). "Pervasive selection for cooperative cross-feeding in bacterial communities." PLoS computational biology **12**(6): e1004986.

Gerstl, M. P., C. Jungreuthmayer and J. Zanghellini (2015). "tEFMA: Computing thermodynamically feasible elementary flux modes in metabolic networks." Bioinformatics **31**(13): 2232-2234.

Goers, L., P. Freemont and K. M. Polizzi (2014). "Co-culture systems and technologies: Taking synthetic biology to the next level." Journal of The Royal Society Interface **11**(96): 20140065.

Goldberg, I., J. S. Rock, A. Benbassat and R. I. Mateles (1976). "Bacterial yields on methanol, methylamine, formaldehyde, and formate." Biotechnology and Bioengineering **18**(12): 1657-1668.

Gorke, B. and J. Stulke (2008). "Carbon catabolite repression in bacteria: Many ways to make the most out of nutrients." Nature Reviews Microbiology **6**(8): 613-624.

Gorokhova, E. and M. Kyle (2002). "Analysis of nucleic acids in *Daphnia*: Development of methods and ontogenetic variations in RNA-DNA content." Journal of Plankton Research **24**(5): 511-522.

Grimm, V. and C. Wissel (1997). "Babel, or the ecological stability discussions: an inventory and analysis of terminology and a guide for avoiding confusion." Oecologia **109**(3): 323-334.

Großkopf, T. and O. S. Soyer (2014). "Synthetic microbial communities." Current opinion in microbiology **18**: 72-77.

Gubernator, B., R. Bartoszewski, J. Kroliczewski, G. Wildner and A. Szczepaniak (2008). "Ribulose-1,5-bisphosphate carboxylase/oxygenase from thermophilic cyanobacterium *Thermosynechococcus elongatus*." Photosynthesis Research **95**(1): 101-109.

Hall-Stoodley, L., J. W. Costerton and P. Stoodley (2004). "Bacterial biofilms: From the natural environment to infectious diseases." Nature reviews microbiology **2**(2): 95.

Han, K. and O. Levenspiel (1988). "Extended Monod kinetics for substrate, product, and cell inhibition." Biotechnology and Bioengineering **32**(4): 430-437.

Han, K., H. C. Lim and J. Hong (1992). "Acetic acid formation in *Escherichia coli* fermentation." Biotechnology and Bioengineering **39**(6): 663-671.

Hanly, T. J. and M. A. Henson (2011). "Dynamic flux balance modeling of microbial co-cultures for efficient batch fermentation of glucose and xylose mixtures." Biotechnology and bioengineering **108**(2): 376-385.

Hanly, T. J., M. Urello and M. A. Henson (2012). "Dynamic flux balance modeling of *S. cerevisiae* and *E. coli* co-cultures for efficient consumption of glucose/xylose mixtures." Applied microbiology and biotechnology **93**(6): 2529-2541.

Harcombe, W. (2010). "Novel cooperation experimentally evolved between species." Evolution **64**(7): 2166-2172.

Harcombe, W. R., W. J. Riehl, I. Dukovski, B. R. Granger, A. Betts, A. H. Lang, G. Bonilla, A. Kar, N. Leiby and P. Mehta (2014). "Metabolic resource allocation in individual microbes determines ecosystem interactions and spatial dynamics." Cell reports **7**(4): 1104-1115.

Henderson, J. W., R. D. Ricker, B. A. Bidlingmeyer and C. Woodward (2000). Rapid, accurate, sensitive, and reproducible HPLC analysis of amino acids, Agilent Technologies.

Henry, C. S., H. C. Bernstein, P. Weisenhorn, R. C. Taylor, J. Y. Lee, J. Zucker and H. S. Song (2016). "Microbial community metabolic modeling: A community data-driven network reconstruction." Journal of Cellular Physiology **231**(11): 2339-2345.

Hense, B. A., C. Kuttler, J. Müller, M. Rothballer, A. Hartmann and J.-U. Kreft (2007). "Does efficiency sensing unify diffusion and quorum sensing?" Nature Reviews Microbiology **5**(3): 230.

Herbert, D., P. J. Phipps and R. E. Strange (1971). Chemical analysis of microbial cells. Methods in microbiology. J. R. Norris and D. W. Ribbons. New York, Academic Press**:** 209-344.

Herigstad, B., M. Hamilton and J. Heersink (2001). "How to optimize the drop plate method for enumerating bacteria." Journal of Microbiological Methods **44**(2): 121-129.

Hibbing, M. E., C. Fuqua, M. R. Parsek and S. B. Peterson (2010). "Bacterial competition: Surviving and thriving in the microbial jungle." Nature Reviews Microbiology **8**(1): 15.

Hill, J. F. and Govindjee (2014). "The controversy over the minimum quantum requirement for oxygen evolution." Photosynthesis Research **122**(1): 97-112.

Hoiczyk, E. and A. Hansel (2000). "Cyanobacterial cell walls: News from an unusual prokaryotic envelope." Journal of Bacteriology **182**(5): 1191-1199.

Holland, J. N. and D. L. DeAngelis (2009). "Consumer-resource theory predicts dynamic transitions between outcomes of interspecific interactions." Ecology Letters **12**(12): 1357-1366.

Hollywood, N. and H. W. Doelle (1976). "Effect of specific growth rate and glucose concentration on growth and glucose metabolism of *Escherichia coli* K-12." Microbios **17**(67): 23-33.

Holms, H. (1996). "Flux analysis and control of the central metabolic pathways in *Escherichia coli*." FEMS Microbiology Reviews **19**(2): 85-116.

Huege, J., J. Goetze, D. Schwarz, H. Bauwe, M. Hagemann and J. Kopka (2011). "Modulation of the major paths of carbon in photorespiratory mutants of *Synechocystis*." Plos One **6**(1).

Hunt, K. A., R. D. Jennings, W. P. Inskeep and R. P. Carlson (2016). "Stoichiometric modelling of assimilatory and dissimilatory biomass utilisation in a microbial community." Environmental Microbiology **18**(12): 4946-4960.

Hussa, E. A. and H. Goodrich-Blair (2013). "It takes a village: Ecological and fitness impacts of multipartite mutualism." Annual review of microbiology **67**: 161-178.

Hyduke, D. R., N. E. Lewis and B. Ø. Palsson (2013). "Analysis of omics data with genome-scale models of metabolism." Molecular BioSystems **9**(2): 167-174.

Imam, S., S. Yilmaz, U. Sohmen, A. S. Gorzalski, J. L. Reed, D. R. Noguera and T. J. Donohue (2011). "iRsp1095: A genome-scale reconstruction of the *Rhodobacter sphaeroides* metabolic network." BMC Systems Biology **5**.

Inada, T., K. Kimata and H. J. Aiba (1996). "Mechanism responsible for glucose-lactose diauxie in *Escherichia coli*: Challenge to the cAMP model." Genes to Cells **1**(3): 293-301.

Ingledew, W. J. and R. K. Poole (1984). "The respiratory chains of *Escherichia coli*." Microbiological Reviews **48**(3): 222-271.

Ishii, S. i., T. Shimoyama, Y. Hotta and K. Watanabe (2008). "Characterization of a filamentous biofilm community established in a cellulose-fed microbial fuel cell." Bmc Microbiology **8**(1): 6.

Izard, J. and R. J. Limberger (2003). "Rapid screening method for quantitation of bacterial cell lipids from whole cells." Journal of Microbiological Methods **55**(2): 411-418.

Jagmann, N. and B. Philipp (2014). "Reprint of design of synthetic microbial communities for biotechnological production processes." Journal of biotechnology **192**: 293-301.

Janssen, P. H. and P. Hugenholtz (2003). "Fermentation of glycolate by a pure culture of a strictly anaerobic gram-positive bacterium belonging to the family *Lachnospiraceae*." Archives of Microbiology **179**(5): 321-328.

Johns, N. I., T. Blazejewski, A. L. C. Gomes and H. H. Wang (2016). "Principles for designing synthetic microbial communities." Current Opinion in Microbiology **31**: 146-153.

Johnson, D. B., T. Kanao and S. Hedrich (2012). "Redox transformations of iron at extremely low pH: Fundamental and applied aspects." Frontiers in Microbiology **3**.

Jordan, D. B. and W. L. Ogren (1984). "The CO2/O2 specificity of ribulose 1,5-bisphosphate carboxylase oxygenase - Dependence on ribulose-bisphosphate concentration, pH, and temperature." Planta **161**(4): 308-313.

Kanehisa, M., S. Goto, Y. Sato, M. Furumichi and M. Tanabe (2012). "KEGG for integration and interpretation of large-scale molecular data sets." Nucleic Acids Research **40**(D1): D109-D114.

Kawamura, M., M. Mimuro and Y. Fujita (1979). "Quantitative relationship between two reaction centers in the photosynthetic system of blue-green algae." Plant and Cell Physiology **20**(4): 697-705.

Kim, Y. M., S. Nowack, M. T. Olsen, E. D. Becraft, J. M. Wood, V. Thiel, I. Klapper, M. Kuhl, J. K. Fredrickson, D. A. Bryant, D. M. Ward and T. O. Metz (2015). "Diel metabolomics analysis of a hot spring chlorophototrophic microbial mat leads to new hypotheses of community member metabolisms." Frontiers in Microbiology **6**.

Kinnersley, M., J. Wenger, E. Kroll, J. Adams, G. Sherlock and F. Rosenzweig (2014). "Ex uno plures: Clonal reinforcement drives evolution of a simple microbial community." PLoS genetics **10**(6): e1004430.

Kirilovsky, D. (2007). "Photoprotection in cyanobacteria: The orange carotenoid protein (OCP)-related non-photochemical-quenching mechanism." Photosynthesis Research **93**(1-3): 7-16.

Kitano, H. (2010). "Violations of robustness trade-offs." Molecular Systems Biology **6**(1): 384.

Klahn, S. and M. Hagemann (2011). "Compatible solute biosynthesis in cyanobacteria." Environmental Microbiology **13**(3): 551-562.

Klamt, S., J. Saez-Rodriguez and E. D. Gilles (2007). "Structural and functional analysis of cellular networks with CellNetAnalyzer." Bmc Systems Biology **1**.

Klamt, S. and A. von Kamp (2011). "An application programming interface for CellNetAnalyzer." Biosystems **105**(2): 162-168.

Kliphuis, A. M. J., A. J. Klok, D. E. Martens, P. P. Lamers, M. Janssen and R. H. Wijffels (2012). "Metabolic modeling of *Chlamydomonas reinhardtii*: Energy requirements for photoautotrophic growth and maintenance." Journal of Applied Phycology **24**(2): 253-266.

Klitgord, N. and D. Segrè (2010). "Environments that induce synthetic microbial ecosystems." PLoS computational biology **6**(11): e1001002.

Knoop, H., M. Grundel, Y. Zilliges, R. Lehmann, S. Hoffmann, W. Lockau and R. Steuer (2013). "Flux balance analysis of cyanobacterial metabolism: The metabolic network of *Synechocystis* sp PCC 6803." Plos Computational Biology **9**(6).

Konopka, A. (2009). "What is microbial community ecology?" The ISME journal **3**(11): 1223.

Korgaonkar, A., U. Trivedi, K. P. Rumbaugh and M. Whiteley (2013). "Community surveillance enhances *Pseudomonas aeruginosa* virulence during polymicrobial infection." Proceedings of the National Academy of Sciences of the United States of America **110**(3): 1059-1064.

Kühl, M. and B. B. Jørgensen (1992). "Microsensor measurements of sulfate reduction and sulfide oxidation in compact microbial communities of aerobic biofilms." Applied and environmental microbiology **58**(4): 1164-1174.

Kumar, K., R. A. Mella-Herrera and J. W. Golden (2010). "Cyanobacterial heterocysts." Cold Spring Harbor Perspectives in Biology **2**(4).

Kuss, S. K., G. T. Best, C. A. Etheredge, A. J. Pruijssers, J. M. Frierson, L. V. Hooper, T. S. Dermody and J. K. Pfeiffer (2011). "Intestinal microbiota promote enteric virus replication and systemic pathogenesis." Science **334**(6053): 249-252.

Law, R. (1979). "Optimal life histories under age-specific predation." American Naturalist **114**(3): 399-417.

Le Novere, N., A. Finney, M. Hucka, U. S. Bhalla, F. Campagne, J. Collado-Vides, E. J. Crampin, M. Halstead, E. Klipp, P. Mendes, P. Nielsen, H. Sauro, B. Shapiro, J. L. Snoep, H. D. Spence and B. L. Wanner (2005). "Minimum information requested in the annotation of biochemical models (MIRIAM)." Nature Biotechnology **23**(12): 1509-1515.

Lendenmann, U. and T. Egli (1998). "Kinetic models for the growth of *Escherichia coli* with mixtures of sugars under carbon-limited conditions." Biotechnology and Bioengineering **59**(1): 99-107.

Li, G., C. M. Brown, J. A. Jeans, N. A. Donaher, A. McCarthy and D. A. Campbell (2015). "The nitrogen costs of photosynthesis in a diatom under current and future pCO(2)." New Phytologist **205**(2): 533-543.

Li, X., M. J. McInerney, D. A. Stahl and L. R. Krumholz (2011). "Metabolism of H2 by *Desulfovibrio alaskensis* G20 during syntrophic growth on lactate." Microbiology **157**(10): 2912-2921.

Liao, Y. C., T. W. Huang, F. C. Chen, P. Charusanti, J. S. J. Hong, H. Y. Chang, S. F. Tsai, B. O. Palsson and C. A. Hsiung (2011). "An experimentally validated genome-scale metabolic reconstruction of *Klebsiella pneumoniae* MGH 78578, iYL1228." Journal of Bacteriology **193**(7): 1710-1717.

Liu, Z., J. Müller, T. Li, R. M. Alvey, K. Vogl, N.-U. Frigaard, N. C. Rockwell, E. S. Boyd, L. P. Tomsho and S. C. Schuster (2013). "Genomic analysis reveals key aspects of prokaryotic symbiosis in the phototrophic consortium "*Chlorochromatium aggregatum*"." Genome biology **14**(11): R127.

Liu, Z. J., Y. Gao, J. Chen, T. Imanaka, J. Bao and Q. Hua (2013). "Analysis of metabolic fluxes for better understanding of mechanisms related to lipid accumulation in oleaginous yeast *Trichosporon cutaneum*." Bioresource Technology **130**: 144-151.

Llaneras, F. and J. Pico (2008). "Stoichiometric modelling of cell metabolism." Journal of Bioscience and Bioengineering **105**(1): 1-11.

Lloyd, L. (2011). HPLC determination of carbohydrates in food and drink, Agilent Technologies.

Lohman, E. J., R. D. Gardner, L. Halverson, R. E. Macur, B. M. Peyton and R. Gerlach (2013). "An efficient and scalable extraction and quantification method for algal derived biofuel." Journal of Microbiological Methods **94**(3): 235-244.

López-Ferber, M., O. Simón, T. Williams and P. Caballero (2003). "Defective or effective? Mutualistic interactions between virus genotypes." Proceedings of the Royal Society of London B: Biological Sciences **270**(1530): 2249-2255.

Lotka, A. J. (1922). "Contribution to the energetics of evolution." Proceedings of the National Academy of Sciences of the United States of America **8**: 147-151.

Lotka, A. J. (1922). "Natural selection as a physical principle." Proceedings of the National Academy of Sciences of the United States of America **8**: 151-154.

Ludwig, M. and D. A. Bryant (2011). "Transcription profiling of the model cyanobacterium *Synechococcus* sp strain PCC 7002 by Next-Gen (SOLiD (TM)) sequencing of cDNA." Frontiers in Microbiology **2**.

Luttik, M. A. H., R. vanSpanning, D. Schipper, J. P. vanDijken and J. T. Pronk (1997). "The low biomass yields of the acetic acid bacterium *Acetobacter pasteurianus* are due to a low stoichiometry of respiration-coupled proton translocation." Applied and Environmental Microbiology **63**(9): 3345-3351.

Maarleveld, T. R., R. A. Khandelwal, B. G. Olivier, B. Teusink and F. J. Bruggeman (2013). "Basic concepts and principles of stoichiometric modeling of metabolic networks." Biotechnology Journal **8**(9): 997-U952.

Madigan, M. T., J. M. Martinko, K. S. Bender, D. P. Clark, D. P. Buckley and D. A. Stahl (2010). Brock Biology of Microorganisms. San Francisco, Benjamin Cummings.

Mahadevan, R. and M. A. Henson (2012). "Genome-based modeling and design of metabolic interactions in microbial communities." Computational and Structural Biotechnology Journal **3**(4).

Mangan, N. M., A. Flamholz, R. D. Hood, R. Milo and D. F. Savage (2016). "pH determines the energetic efficiency of the cyanobacterial CO2 concentrating mechanism." Proceedings of the National Academy of Sciences of the United States of America **113**(36): E5354-E5362.

Márquez, L. M., R. S. Redman, R. J. Rodriguez and M. J. Roossinck (2007). "A virus in a fungus in a plant: Three-way symbiosis required for thermal tolerance." science **315**(5811): 513-515.

Martyushev, L. M. (2013). "Entropy and entropy production: Old misconceptions and new breakthroughs." Entropy **15**(4): 1152-1170.

Maslova, I. P., E. A. Mouradyan, S. S. Lapina, G. L. Klyachko-Gurvich and D. A. Los (2004). "Lipid fatty acid composition and thermophilicity of cyanobacteria." Russian Journal of Plant Physiology **51**(3): 353-360.

McInerney, M. J., J. R. Sieber and R. P. Gunsalus (2009). "Syntrophy in anaerobic global carbon cycles." Current opinion in biotechnology **20**(6): 623-632.

Mee, M. T., J. J. Collins, G. M. Church and H. H. Wang (2014). "Syntrophic exchange in synthetic microbial communities." Proceedings of the National Academy of Sciences **111**(20): E2149-E2156.

Melnicki, M. R., G. E. Pinchuk, E. A. Hill, L. A. Kucek, S. M. Stolyar, J. K. Fredrickson, A. E. Konopka and A. S. Beliaev (2013). "Feedback-controlled LED photobioreactor for photophysiological studies of cyanobacteria." Bioresource Technology **134**: 127-133.

Meyer, B., J. Kuehl, A. M. Deutschbauer, M. N. Price, A. P. Arkin and D. A. Stahl (2013). "Variation among *Desulfovibrio* species in electron transfer systems used for syntrophic growth." Journal of bacteriology **195**(5): 990-1004.

Mikesková, H., Č. Novotný and K. Svobodová (2012). "Interspecific interactions in mixed microbial cultures in a biodegradation perspective." Applied microbiology and biotechnology **95**(4): 861-870.

Minty, J. J., M. E. Singer, S. A. Scholz, C.-H. Bae, J.-H. Ahn, C. E. Foster, J. C. Liao and X. N. Lin (2013). "Design and characterization of synthetic fungal-bacterial consortia for direct production of isobutanol from cellulosic biomass." Proceedings of the National Academy of Sciences **110**(36): 14592-14597.

Miyairi, S. (1995). "CO2 assimilation in a thermophilic cyanobacterium." Energy Conversion and Management **6-9**: 763-766.

Molenaar, D., R. van Berlo, D. de Ridder and B. Teusink (2009). "Shifts in growth strategies reflect tradeoffs in cellular economics." Molecular Systems Biology **5**.

Momeni, B., K. A. Brileya, M. W. Fields and W. Shou (2013). "Strong inter-population cooperation leads to partner intermixing in microbial communities." Elife **2**.

Mori, M., T. Hwa, O. C. Martin, A. De Martino and E. Marinari (2016). "Constrained allocation flux balance analysis." Plos Computational Biology **12**(6).

Morris, J. J., Z. I. Johnson, M. J. Szul, M. Keller and E. R. Zinser (2011). "Dependence of the cyanobacterium *Prochlorococcus* on hydrogen peroxide scavenging microbes for growth at the ocean's surface." PloS one **6**(2): e16805.

Müller, J. and J. Overmann (2011). "Close interspecies interactions between prokaryotes from sulfureous environments." Frontiers in microbiology **2**: 146.

Muller, S. and G. Nebe-von-Caron (2010). "Functional single-cell analyses: Flow cytometry and cell sorting of microbial populations and communities." Fems Microbiology Reviews **34**(4): 554-587.

Muramatsu, M. and Y. Hihara (2012). "Acclimation to high-light conditions in cyanobacteria: From gene expression to physiological responses." Journal of Plant Research **125**(1): 11-39.

Murphy, C. D., M. S. Roodvoets, E. J. Austen, A. Dolan, A. Barnett and D. A. Campbell (2017). "Photoinactivation of Photosystem II in *Prochlorococcus* and *Synechococcus*." Plos One **12**(1).

Murray, J. L., J. L. Connell, A. Stacy, K. H. Turner and M. Whiteley (2014). "Mechanisms of synergy in polymicrobial infections." Journal of microbiology **52**(3): 188-199.

Nagarajan, H., M. Embree, A.-E. Rotaru, P. M. Shrestha, A. M. Feist, B. Ø. Palsson, D. R. Lovley and K. Zengler (2013). "Characterization and modelling of interspecies electron transfer mechanisms and microbial community dynamics of a syntrophic association." Nature communications **4**: ncomms3809.

Nagpal, S., S. Chuichulcherm, A. Livingston and L. Peeva (2000). "Ethanol utilization by sulfate-reducing bacteria: An experimental and modeling study." Biotechnology and Bioengineering **70**(5): 533-543.

Nakamura, Y., T. Kaneko, S. Sato, M. Ikeuchi, H. Katoh, S. Sasamoto, A. Watanabe, M. Iriguchi, K. Kawashima, T. Kimura, Y. Kishida, C. Kiyokawa, M. Kohara, M. Matsumoto, A. Matsuno, N. Nakazaki, S. Shimpo, M. Sugimoto, C. Takeuchi, M. Yamada and S. Tabata (2002). "Complete genome structure of the thermophilic cyanobacterium *Thermosynechococcus elongatus* BP-1." DNA Research **9**(4): 123-130.

Neidhardt, F. C., J. L. Ingraham and M. Schaechter (1990). Physiology of the bacterial cell: A molecular approach. Sunderland, MA, Sinauer Associates.

Noble, J. E. and M. J. A. Bailey (2009). Quantitation of protein. Guide to Protein Purification, Second Edition. R. R. Burgess and M. P. Deutscher. **463:** 73-95.

Noble, J. E., A. E. Knight, A. J. Reason, A. Di Matola and M. J. A. Bailey (2007). "A comparison of protein quantitation assays for biopharmaceutical applications." Molecular Biotechnology **37**(2): 99-111.

Nogales, J., S. Gudmundsson, E. M. Knight, B. O. Palsson and I. Thiele (2012). "Detailing the optimality of photosynthesis in cyanobacteria through systems biology analysis." Proceedings of the National Academy of Sciences of the United States of America **109**(7): 2678-2683.

Noor, E., A. Bar-Even, A. Flamholz, Y. Lubling, D. Davidi and R. Milo (2012). "An integrated open framework for thermodynamics of reactions that combines accuracy and coverage." Bioinformatics **28**(15): 2037-2044.

Nystrom, T. and F. C. Neidhardt (1993). "Isolation and properties of a mutant of *Escherichia coli* with an insertional inactivation of the *uspA* gene, which encodes a universal stress protein." Journal of Bacteriology **175**(13): 3949-3956.

Offre, P., A. Spang and C. Schleper (2013). "Archaea in biogeochemical cycles." Annual Review of Microbiology **67**.

Oh, Y. G., D. Y. Lee, S. Y. Lee and S. Park (2009). "Multiobjective flux balancing using the NISE method for metabolic network analysis." Biotechnology progress **25**(4): 999-1008.

Oldstone, M. (1988). "Prevention of type I diabetes in nonobese diabetic mice by virus infection." Science **239**(4839): 500-502.

Oliver, J. W. K. and S. Atsumi (2014). "Metabolic design for cyanobacterial chemical synthesis." Photosynthesis Research **120**(3): 249-261.

Orth, J. D., I. Thiele and B. O. Palsson (2010). "What is flux balance analysis?" Nature Biotechnology **28**(3): 245-248.

Ortiz-Marquez, J. C. F., M. Do Nascimento, J. P. Zehr and L. Curatti (2013). "Genetic engineering of multispecies microbial cell factories as an alternative for bioenergy production." Trends in biotechnology **31**(9): 521-529.

Overmann, J. (2010). The phototrophic consortium "*Chlorochromatium aggregatum*"–A model for bacterial heterologous multicellularity. Recent Advances in Phototrophic Prokaryotes, Springer**:** 15-29.

Overmann, J., C. Tuschak, J. M. Fröstl, H. Sass and J. Fröstl (1998). "The ecological niche of the consortium "*Pelochromatium roseum*"." Archives of microbiology **169**(2): 120-128.

Paerl, H. W. and J. L. Pinckney (1996). "A mini-review of microbial consortia: Their roles in aquatic production and biogeochemical cycling." Microbial Ecology **31**(3): 225-247.

Paerl, H. W., J. L. Pinckney and T. F. Steppe (2000). "Cyanobacterial-bacterial mat consortia: Examining the functional unit of microbial survival and growth in extreme environments." Environmental Microbiology **2**(1): 11-26.

Pande, G. S. J., F. M. I. Natrah, P. Sorgeloos, P. Bossier and T. Defoirdt (2013). "The *Vibrio campbellii* quorum sensing signals have a different impact on virulence of the bacterium towards different crustacean hosts." Veterinary microbiology **167**(3-4): 540-545.

Pandhal, J. and J. Noirel (2014). "Synthetic microbial ecosystems for biotechnology." Biotechnology letters **36**(6): 1141-1151.

Passarge, J., S. Hol, M. Escher and J. Huisman (2006). "Competition for nutrients and light: Stable coexistence, alternative stable states, or competitive exclusion?" Ecological Monographs **76**(1): 57-72.

Pasteur, L. and J. Joubert (1877). "Charbon et septicemie." Comptes Rendus del Academie des Sciences **85**: 101-105.

Peres, S., M. Jolicoeur, C. Moulin, P. Dague and S. Schuster (2017). "How important is thermodynamics for identifying elementary flux modes?" Plos One **12**(2).

Perez-Garcia, O., G. Lear and N. Singhal (2016). "Metabolic network modeling of microbial interactions in natural and engineered environmental systems." Frontiers in Microbiology **7**.

Petroutsos, D., S. Amiar, H. Abida, L. J. Dolch, O. Bastien, F. Rebeille, J. Jouhet, D. Falconet, M. A. Block, G. I. McFadden, C. Bowler, C. Botte and E. Marechal (2014). "Evolution of galactoglycerolipid biosynthetic pathways - From cyanobacteria to primary plastids and from primary to secondary plastids." Progress in Lipid Research **54**: 68-85.

Pfeffer, C., S. Larsen, J. Song, M. Dong, F. Besenbacher, R. L. Meyer, K. U. Kjeldsen, L. Schreiber, Y. A. Gorby and M. Y. El-Naggar (2012). "Filamentous bacteria transport electrons over centimetre distances." Nature **491**(7423): 218.

Pfeiffer, T. and S. Bonhoeffer (2004). "Evolution of cross-feeding in microbial populations." American Naturalist **163**(6): E126-E135.

Phelan, V. V., W.-T. Liu, K. Pogliano and P. C. Dorrestein (2012). "Microbial metabolic exchange—The chemotype-to-phenotype link." Nature chemical biology **8**(1): 26.

Pimm, S. L. (1984). "The complexity and stability of ecosystems." Nature **307**(5949): 321.

Pirbadian, S., S. E. Barchinger, K. M. Leung, H. S. Byun, Y. Jangir, R. A. Bouhenni, S. B. Reed, M. F. Romine, D. A. Saffarini and L. Shi (2014). "*Shewanella oneidensis* MR-1 nanowires are outer membrane and periplasmic extensions of the extracellular electron transport components." Proceedings of the National Academy of Sciences **111**(35): 12883-12888.

Poltak, S. R. and V. S. Cooper (2011). "Ecological succession in long-term experimentally evolved biofilms produces synergistic communities." The ISME journal **5**(3): 369.

Portnoy, V. A., D. A. Scott, N. E. Lewis, Y. Tarasova, A. L. Osterman and B. O. Palsson (2010). "Deletion of genes encoding cytochrome oxidases and quinol monooxygenase blocks the aerobic-anaerobic shift in *Escherichia coli* K-12 MG1655." Applied and Environmental Microbiology **76**(19): 6529-6540.

Pramanik, J. and J. D. Keasling (1997). "Stoichiometric model of *Escherichia coli* metabolism: Incorporation of growth-rate dependent biomass composition and mechanistic energy requirements." Biotechnology and Bioengineering **56**(4): 398-421.

Prosser, J. I., B. J. Bohannan, T. P. Curtis, R. J. Ellis, M. K. Firestone, R. P. Freckleton, J. L. Green, L. E. Green, K. Killham and J. J. Lennon (2007). "The role of ecological theory in microbial ecology." Nature Reviews Microbiology **5**(5): 384.

Rae, B. D., B. M. Long, L. F. Whitehead, B. Forster, M. R. Badger and G. D. Price (2013). "Cyanobacterial carboxysomes: Microcompartments that facilitate CO2 fixation." Journal of Molecular Microbiology and Biotechnology **23**(4-5): 300-307.

Raven, J. A. (2011). "The cost of photoinhibition." Physiologia Plantarum **142**(1): 87-104.

Raven, J. A., M. C. W. Evans and R. E. Korb (1999). "The role of trace metals in photosynthetic electron transport in O-2-evolving organisms." Photosynthesis Research **60**(2-3): 111-149.

Ravikrishnan, A. and K. Raman (2015). "Critical assessment of genome-scale metabolic networks: The need for a unified standard." Briefings in Bioinformatics **16**(6): 1057-1068.

Reiling, H. E., H. Laurila and A. Fiechter (1985). "Mass culture of *Escherichia coli*: Medium development for low and high density cultivation of *Escherichia coli* B/r in minimal and complex media." Journal of Biotechnology **2**(3-4): 191-206.

Repaske, D. R. and J. Adler (1981). "Change in intracellular pH of *Escherichia coli* mediates the chemotactic response to certain attractants and repellents." Journal of Bacteriology **145**(3): 1196-1208.

Rochaix, J. D. (2011). "Regulation of photosynthetic electron transport." Biochimica Et Biophysica Acta-Bioenergetics **1807**(3): 375-383.

Rodionova, I. A., X. Li, A. E. Plymale, K. Motamedchaboki, A. E. Konopka, M. F. Romine, J. K. Fredrickson, A. L. Osterman and D. A. Rodionov (2015). "Genomic distribution of B-vitamin auxotrophy and uptake transporters in environmental bacteria from the *Chloroflexi* phylum." Environmental microbiology reports **7**(2): 204-210.

Roe, A. J., C. O'Byrne, D. McLaggan and I. R. Booth (2002). "Inhibition of *Escherichia coli* growth by acetic acid: A problem with methionine biosynthesis and homocysteine toxicity." Microbiology **148**: 2215-2222.

Roels, J. A. (1980). "Application of macroscopic principles to microbial metabolism." Biotechnology and Bioengineering **22**(12): 2457-2514.

Roels, J. A. (1983). Energetics and kinetics in biotechnology, Elsevier Biomedical Press.

Rojo, F. (2010). "Carbon catabolite repression in *Pseudomonas*: optimizing metabolic versatility and interactions with the environment." FEMS Microbiology Reviews **34**(5): 658-684.

Romero-Rodriguez, A., D. Rocha, B. Ruiz-Villafan, S. Guzman-Trampe, N. Maldonado-Carmona, M. Vazquez-Hernandez, A. Zelarayan, R. Rodriguez-Sanoja and S. Sanchez (2017). "Carbon catabolite regulation in *Streptomyces*: New insights and lessons learned." World Journal of Microbiology & Biotechnology **33**(9).

Romine, M. F., D. A. Rodionov, Y. Maezato, A. L. Osterman and W. C. Nelson (2017). "Underlying mechanisms for syntrophic metabolism of essential enzyme cofactors in microbial communities." Isme Journal **11**(6): 1434-1446.

Roossinck, M. J. (2011). "The good viruses: Viral mutualistic symbioses." Nature Reviews Microbiology **9**(2): 99-108.

Rosenzweig, R. F., R. Sharp, D. S. Treves and J. Adams (1994). "Microbial evolution in a simple unstructured environment: Genetic differentiation in *Escherichia coli*." Genetics **137**(4): 903-917.

Rousseaux, C. S. and W. W. Gregg (2014). "Interannual variation in phytoplankton primary production at a global scale." Remote Sensing **6**(1): 1-19.

Rykiel, E. J. (1985). "Towards a definition of ecological disturbance." Austral Ecology **10**(3): 361-365.

Sabra, W., D. Dietz, D. Tjahjasari and A. P. Zeng (2010). "Biosystems analysis and engineering of microbial consortia for industrial biotechnology." Engineering in Life Sciences **10**(5): 407-421.

Sandaa, R. A., L. Gómez-Consarnau, J. Pinhassi, L. Riemann, A. Malits, M. G. Weinbauer, J. M. Gasol and T. F. Thingstad (2009). "Viral control of bacterial biodiversity–Evidence from a nutrient-enriched marine mesocosm experiment." Environmental microbiology **11**(10): 2585-2597.

Sander, R. (2015). "Compilation of Henry's law constants (version 4.0) for water as solvent." Atmospheric Chemistry and Physics **15**(8): 4399-4981.

Sattler, L. and F. W. Zerban (1948). "The Dreywood anthrone reaction as affected by carbohydrate structure." Science **108**(2800): 207-207.

Savir, Y., E. Noor, R. Milo and T. Tlusty (2010). "Cross-species analysis traces adaptation of Rubisco toward optimality in a low-dimensional landscape." Proceedings of the National Academy of Sciences of the United States of America **107**(8): 3475-3480.

Schimel, J., T. C. Balser and M. Wallenstein (2007). "Microbial stress-response physiology and its implications for ecosystem function." Ecology **88**(6): 1386-1394.

Schink, B. (1997). "Energetics of syntrophic cooperation in methanogenic degradation." Microbiology and molecular biology reviews **61**(2): 262-280.

Schomburg, I., A. Chang, S. Placzek, C. Sohngen, M. Rother, M. Lang, C. Munaretto, S. Ulas, M. Stelzer, A. Grote, M. Scheer and D. Schomburg (2013). "BRENDA in 2013: Integrated reactions, kinetic data, enzyme function data, improved disease classification: New options and contents in BRENDA." Nucleic Acids Research **41**(D1): D764-D772.

Schuetz, R., N. Zamboni, M. Zampieri, M. Heinemann and U. Sauer (2012). "Multidimensional optimality of microbial metabolism." Science **336**(6081): 601-604.

Schuster, S. and C. Hilgetag (1994). "On elementary flux modes in biochemical reaction systems at steady state." Journal of Biological Systems **2**(2): 165-182.

Sciubba, E. (2011). "What did Lotka really say? A critical reassessment of the "maximum power principle"." Ecological Modelling **222**(8): 1347-1353.

Seifritz, C., J. M. Frostl, H. L. Drake and S. L. Daniel (1999). "Glycolate as a metabolic substrate for the acetogen *Moorella thermoacetica*." Fems Microbiology Letters **170**(2): 399-405.

Senger, R. S. (2010). "Biofuel production improvement with genome-scale models: The role of cell composition." Biotechnology Journal **5**(7): 671-685.

Shade, A., H. Peter, S. D. Allison, D. Baho, M. Berga, H. Bürgmann, D. H. Huber, S. Langenheder, J. T. Lennon and J. B. Martiny (2012). "Fundamentals of microbial community resistance and resilience." Frontiers in microbiology **3**: 417.

Sheng, J., R. Vannela and B. E. Rittmann (2012). "Disruption of *Synechocystis* PCC 6803 for lipid extraction." Water Science and Technology **65**(3): 567-573.

Sheng, J., R. Vannela and B. E. Rittrnann (2011). "Evaluation of methods to extract and quantify lipids from *Synechocystis* PCC 6803." Bioresource Technology **102**(2): 1697-1703.

Shibata, K., A. A. Benson and M. Calvin (1954). "The absorption spectra of suspensions of living microorganisms." Biochimica Et Biophysica Acta **15**(4): 461-470.

Shikanai, T., Y. Munekage and K. Kimura (2002). "Regulation of proton-to-electron stoichiometry in photosynthetic electron transport: physiological function in photoprotection." Journal of Plant Research **115**(1117): 3-10.

Shong, J., M. R. J. Diaz and C. H. Collins (2012). "Towards synthetic microbial consortia for bioprocessing." Current Opinion in Biotechnology **23**(5): 798-802.

Shoval, O., H. Sheftel, G. Shinar, Y. Hart, O. Ramote, A. Mayo, E. Dekel, K. Kavanagh and U. Alon (2012). "Evolutionary trade-offs, Pareto optimality, and the geometry of phenotype space." Science: 1217405.

Sieber, J. R., M. J. McInerney and R. P. Gunsalus (2012). "Genomic insights into syntrophy: The paradigm for anaerobic metabolic cooperation." Annual review of microbiology **66**: 429-452.

Sigma-Aldrich DNA Quantitation Kit, Fluorescence Assay: Technical Bulletin. St. Louis, MO, Sigma-Aldrich.

Singh, S., B. N. Kate and U. C. Banerjee (2005). "Bioactive compounds from cyanobacteria and microalgae: An overview." Critical Reviews in Biotechnology **25**(3): 73-95.

Smid, E. J. and C. Lacroix (2013). "Microbe–microbe interactions in mixed culture food fermentations." Current opinion in biotechnology **24**(2): 148-154.

Song, H.-S., W. R. Cannon, A. S. Beliaev and A. Konopka (2014). "Mathematical modeling of microbial community dynamics: A methodological review." Processes **2**(4): 711-752.

Song, H., M.-Z. Ding, X.-Q. Jia, Q. Ma and Y.-J. Yuan (2014). "Synthetic microbial consortia: From systematic analysis to construction and applications." Chemical Society Reviews **43**(20): 6954-6981.

Sonoike, K., Y. Hihara and M. Ikeuchi (2001). "Physiological significance of the regulation of photosystem stoichiometry upon high light acclimation of *Synechocystis* sp PCC 6803." Plant and Cell Physiology **42**(4): 379-384.

Spijkerman, E. (2007). "Is there really insufficient support for Tilman's R* concept? A comment on Miller et al."

Stams, A. J. and C. M. Plugge (2009). "Electron transfer in syntrophic communities of anaerobic bacteria and archaea." Nature Reviews Microbiology **7**(8): 568.

Stanier, R. Y., R. Kunisawa, M. Mandel and Cohenbaz.G (1971). "Purification and properties of unicellular blue-green algae (order *Chroococcales*)." Bacteriological Reviews **35**(2): 171-&.

Stenuit, B. and S. N. Agathos (2015). "Deciphering microbial community robustness through synthetic ecology and molecular systems synecology." Current Opinion in Biotechnology **33**: 305-317.

Sterner, R. W. and J. J. Elser (2002). Ecological stoichiometry: The biology of elements from molecules to the biosphere. Princeton, NJ, Princeton University Press.

Stevens, S. E., C. O. Patterson and J. Myers (1973). "Production of hydrogen peroxide by blue-green algae - Survey." Journal of Phycology **9**(4): 427-430.

Stolyar, S., S. Van Dien, K. L. Hillesland, N. Pinel, T. J. Lie, J. A. Leigh and D. A. Stahl (2007). "Metabolic modeling of a mutualistic microbial community." Molecular systems biology **3**(1): 92.

Stomp, M., J. Huisman, F. De Jongh, A. J. Veraart, D. Gerla, M. Rijkeboer, B. W. Ibelings, U. I. Wollenzien and L. J. Stal (2004). "Adaptive divergence in pigment composition promotes phytoplankton biodiversity." Nature **432**(7013): 104.

Stoodley, P., K. Sauer, D. G. Davies and J. W. Costerton (2002). "Biofilms as complex differentiated communities." Annual Reviews in Microbiology **56**(1): 187-209.

Subashchandrabose, S. R., B. Ramakrishnan, M. Megharaj, K. Venkateswarlu and R. Naidu (2011). "Consortia of cyanobacteria/microalgae and bacteria: Biotechnological potential." Biotechnology advances **29**(6): 896-907.

Taffs, R., J. E. Aston, K. Brileya, Z. Jay, C. G. Klatt, S. McGlynn, N. Mallette, S. Montross, R. Gerlach, W. P. Inskeep, D. M. Ward and R. P. Carlson (2009). "In silico approaches to study mass and energy flows in microbial consortia: A syntrophic case study." Bmc Systems Biology **3**.

Tamime, A. Y. and R. K. Robinson (1999). Yoghurt: Science and Technology. Cambridge, Woodhead.

Tan, C. H., K. S. Koh, C. Xie, M. Tay, Y. Zhou, R. Williams, W. J. Ng, S. A. Rice and S. Kjelleberg (2014). "The role of quorum sensing signalling in EPS production and the assembly of a sludge community into aerobic granules." The ISME journal **8**(6): 1186.

Taylor, K. (1995). "A modification of the phenol sulfuric-acid assay for total carbohydrates giving more comparable absorbances." Applied Biochemistry and Biotechnology **53**(3): 207-214.

Taylor, P. and P. L. Williams (1975). "Theoretical studies on the coexistence of competing species under continuous-flow conditions." Canadian Journal of Microbiology **21**(1): 90-98.

Tcherkez, G. G. B., G. D. Farquhar and T. J. Andrews (2006). "Despite slow catalysis and confused substrate specificity, all ribulose bisphosphate carboxylases may be nearly perfectly optimized." Proceedings of the National Academy of Sciences of the United States of America **103**(19): 7246-7251.

Tepper, N., E. Noor, D. Amador-Noguez, H. S. Haraldsdóttir, R. Milo, J. Rabinowitz, W. Liebermeister and T. Shlomi (2013). "Steady-state metabolite concentrations reflect a balance between maximizing enzyme efficiency and minimizing total metabolite load." PloS one **8**(9): e75370.

Terzer, M. and J. Stelling (2008). "Large-scale computation of elementary flux modes with bit pattern trees." Bioinformatics **24**(19): 2229-2235.

Thauer, R. K., A.-K. Kaster, H. Seedorf, W. Buckel and R. Hedderich (2008). "Methanogenic archaea: Ecologically relevant differences in energy conservation." Nature Reviews Microbiology **6**(8): 579.

Thiele, I., A. Heinken and R. M. Fleming (2013). "A systems biology approach to studying the role of microbes in human health." Current opinion in biotechnology **24**(1): 4-12.

Tillmann, H. L., H. Heiken, A. Knapik-Botor, S. Heringlake, J. Ockenga, J. C. Wilber, B. Goergen, J. Detmer, M. McMorrow and M. Stoll (2001). "Infection with GB virus C and reduced mortality among HIV-infected patients." New England Journal of Medicine **345**(10): 715-724.

Tilman, D. (1980). "Resources - A graphical-mechanistic approach to competition and predation." American Naturalist **116**(3): 362-393.

Tilman, D. (1981). "Tests of resource competition theory using four species of Lake Michigan algae." Ecology **62**(3): 802-815.

Tilman, D. (1982). Resource competition and community structure. Princeton, Princeton University Press.

Trevelyan, W. E. and J. S. Harrison (1952). "Studies on yeast metabolism. 1. Fractionation and microdetermination of cell carbohydrates." Biochemical Journal **50**(3): 298-303.

Treves, D. S., S. Manning and J. Adams (1998). "Repeated evolution of an acetate-crossfeeding polymorphism in long-term populations of *Escherichia coli*." Molecular biology and evolution **15**(7): 789-797.

Trinh, C. T., A. Wlaschin and F. Srienc (2009). "Elementary mode analysis: A useful metabolic pathway analysis tool for characterizing cellular metabolism." Applied Microbiology and Biotechnology **81**(5): 813-826.

Valenzuela, J., A. Mazurie, R. P. Carlson, R. Gerlach, K. E. Cooksey, B. M. Peyton and M. W. Fields (2012). "Potential role of multiple carbon fixation pathways during lipid accumulation in *Phaeodactylum tricornutum*." Biotechnology for biofuels **5**(1): 40.

Valgepea, K., K. Adamberg, R. Nahku, P. J. Lahtvee, L. Arike and R. Vilu (2010). "Systems biology approach reveals that overflow metabolism of acetate in *Escherichia coli* is triggered by carbon catabolite repression of acetyl-CoA synthetase." BMC Systems Biology **4**.

Van Handel, E. (1985). "Rapid determination of glycogen and sugars in mosquitos." Journal of the American Mosquito Control Association **1**(3): 299-301.

Vanveen, J. A. and E. A. Paul (1979). "Conversion of bio-volume measurements of soil organisms, grown under various moisture tensions, to biomass and their nutrient content." Applied and Environmental Microbiology **37**(4): 686-692.

Vasilikiotis, C. and A. Melis (1994). "Photosystem-II reaction-center damage and repair cycle - Chloroplast acclimation strategy to irradiance stress." Proceedings of the National Academy of Sciences of the United States of America **91**(15): 7222-7226.

Vier, B., G. Rogge and B. Voigt (1992). "Production of lipids from a thermoacidophilic *Bacillus* strain. 1. Lipids from *Bacillus acidocaldarius* ZIMET-11274." Acta Biotechnologica **12**(1): 37-40.

Vogl, K., J. Glaeser, K. R. Pfannes, G. Wanner and J. Overmann (2006). "*Chlorobium chlorochromatii* sp. nov., a symbiotic green sulfur bacterium isolated from the phototrophic consortium "*Chlorochromatium aggregatum*"." Archives of microbiology **185**(5): 363-372.

Vrede, T., D. R. Dobberfuhl, S. Kooijman and J. J. Elser (2004). "Fundamental connections among organism C : N : P stoichiometry, macromolecular composition, and growth." Ecology **85**(5): 1217-1229.

Vu, T. T., E. A. Hill, L. A. Kucek, A. E. Konopka, A. S. Beliaev and J. L. Reed (2013). "Computational evaluation of *Synechococcus* sp PCC 7002 metabolism for chemical production." Biotechnology Journal **8**(5): 619-630.

Vu, T. T., S. M. Stolyar, G. E. Pinchuk, E. A. Hill, L. A. Kucek, R. N. Brown, M. S. Lipton, A. Osterman, J. K. Fredrickson, A. E. Konopka, A. S. Beliaev and J. L. Reed (2012). "Genome-Scale Modeling of Light-Driven Reductant Partitioning and Carbon Fluxes in Diazotrophic Unicellular Cyanobacterium *Cyanothece* sp ATCC 51142." Plos Computational Biology **8**(4).

Waide, R., M. Willig, C. Steiner, G. Mittelbach, L. Gough, S. Dodson, G. Juday and R. Parmenter (1999). "The relationship between productivity and species richness." Annual review of Ecology and Systematics **30**(1): 257-300.

Walker, C. B., A. M. Redding-Johanson, E. E. Baidoo, L. Rajeev, Z. He, E. L. Hendrickson, M. P. Joachimiak, S. Stolyar, A. P. Arkin and J. A. Leigh (2012). "Functional responses of methanogenic archaea to syntrophic growth." The ISME journal **6**(11): 2045.

Wanner, G., K. Vogl and J. Overmann (2008). "Ultrastructural characterization of the prokaryotic symbiosis in "*Chlorochromatium aggregatum*"." Journal of bacteriology **190**(10): 3721-3730.

Ward, D. M., M. M. Bateson, M. J. Ferris, M. Kuhl, A. Wieland, A. Koeppel and F. M. Cohan (2006). "Cyanobacterial ecotypes in the microbial mat community of Mushroom Spring (Yellowstone National Park, Wyoming) as species-like units linking microbial community composition, structure and function." Philosophical Transactions of the Royal Society B-Biological Sciences **361**(1475): 1997-2008.

Warnecke, T. and R. T. Gill (2005). "Organic acid toxicity, tolerance, and production in *Escherichia coli* biorefining applications." Microbial Cell Factories **4**.

Waters, C. M. and B. L. Bassler (2005). "Quorum sensing: cell-to-cell communication in bacteria." Annu. Rev. Cell Dev. Biol. **21**: 319-346.

White, D., J. Drummond and C. Fuqua (2012). The Physiology and Biochemistry of Prokaryotes. New York, Oxford University Press.

Whyte, J. N. C. (1987). "Biochemical composition and energy content of 6 species of phytoplankton used in mariculture of bivalves." Aquaculture **60**(3-4): 231-241.

Wintermute, E. H. and P. A. Silver (2010). "Emergent cooperation in microbial metabolism." Molecular systems biology **6**(1): 407.

Wolfe, A. J. (2005). "The acetate switch." Microbiology and Molecular Biology Reviews **69**(1): 12-+.

Yamaoka, T., K. Satoh and S. Katoh (1978). "Photosynthetic activities of a thermophilic blue-green alga." Plant and Cell Physiology **19**(6): 943-954.

Yokota, A., T. Iwaki, K. Miura, A. Wadano and S. Kitaoka (1987). "Series on glycolate metabolism in *Euglena gracius* 21. Model for the relationships between CO2-concentrating mechanism, CO2 fixation, and glycolate synthesis during photosynthesis in *Chlamydomonas reinhardtii*." Plant and Cell Physiology **28**(8): 1363-1376.

Yu, Z., S. Krause, D. A. Beck and L. Chistoserdova (2016). "A synthetic ecology perspective: How well does behavior of model organisms in the laboratory predict microbial activities in natural habitats?" Frontiers in microbiology **7**: 946.

Zelezniak, A., S. Andrejev, O. Ponomarova, D. R. Mende, P. Bork and K. R. Patil (2015). "Metabolic dependencies drive species co-occurrence in diverse microbial communities." Proceedings of the National Academy of Sciences of the United States of America **112**(20): 6449-6454.

Zhang, C. C., S. Laurent, S. Sakr, L. Peng and S. Bédu (2006). "Heterocyst differentiation and pattern formation in cyanobacteria: A chorus of signals." Molecular microbiology **59**(2): 367-375.

Zhou, Y., A. Vazquez, A. Wise, T. Warita, K. Warita, Z. Bar-Joseph and Z. N. Oltvai (2013). "Carbon catabolite repression correlates with the maintenance of near invariant molecular crowding in proliferating *E. coli* cells." BMC Systems Biology **7**.

Zinn, M., B. Witholt and T. Egli (2004). "Dual nutrient limited growth: Models, experimental observations, and applications." Journal of biotechnology **113**(1-3): 263-279.

Zomorrodi, A. R., M. M. Islam and C. D. Maranas (2014). "d-OptCom: Dynamic multi-level and multi-objective metabolic modeling of microbial communities." ACS synthetic biology **3**(4): 247-257.

Zomorrodi, A. R. and C. D. Maranas (2012). "OptCom: A multi-level optimization framework for the metabolic modeling and analysis of microbial communities." PLoS computational biology **8**(2): e1002363.

Zuroff, T. R. and W. R. Curtis (2012). "Developing symbiotic consortia for lignocellulosic biofuel production." Applied microbiology and biotechnology **93**(4): 1423-1435.